Stochastic Modelling of Hygrothermal Performance of Highly Insulated Wood Framed Envelopes

Lin Wang

A Thesis
In the Department
of
Building, Civil and Environmental Engineering

Presented in Partial Fulfillment of the Requirements
For the Degree of
Doctor of Philosophy (Building Engineering) at
Concordia University
Montreal, Quebec, Canada

May, 2018

CONCORDIA UNIVERSITY

School of Graduate Studies

This is to certify that the thesis prepared

By: Lin Wang

Entitled: Stochastic Modelling of Hygrothermal Performance of Highly Insulated Wood Framed Envelopes

and submitted in partial fulfillment of the requirements for the degree of

Doctor of Philosophy (Building Engineering)

complies with the regulations of the University and meets the accepted standards with respects to originality and quality.

Signed by the final Examining Committee:

_____ Chair
Dr. Sudhir Mudur

_____ External Examiner
Dr. Girma Bitsuamlak

_____ External to Program
Dr. Yong Zeng

_____ Examiner
Dr. Zhi Chen

_____ Examiner
Dr. Radu Zmeureanu

_____ Thesis Supervisor
Dr. Hua Ge

Approved by

_____
Dr. Fariborz Haghighat, Graduate Program Director

June 14 2018 _____
Dr. Amir Asif, Dean, Faculty of Engineering and Computer Science

ABSTRACT

Stochastic modelling of hygrothermal performance of highly insulated wood framed envelopes

Lin Wang, Ph.D.

Concordia University, 2018

Wood-framed construction is one of the main building types for residential buildings in North America because of their features such as light-weight, easily built and environmental friendly. However, prolonged exposure to moisture during construction and in service is a durability concern for wood framed envelopes. As building energy consumption has gained increasing attention in recent years, the majority of building codes in North America require higher insulation levels in building envelopes to improve the building energy efficiency. However, the highly insulated wood framed envelopes may have higher risk of moisture problems such as mold growth and wood decay depending on their configurations. Hygrothermal simulation programs have been widely used for evaluating hygrothermal performance of wood framed envelopes. However, the uncertainties of the input parameters may result in a discrepancy between simulation results and the real performance of the wood framed envelopes, thereafter, unable to reveal the actual risks of moisture problems. Stochastic modelling has been used to investigate the uncertainties of the input parameters and their influence, however, the stochastic parameters were only limited to material properties and boundary conditions in previous studies without considering the moisture loads such as air leakage and rain leakage.

This thesis focuses on developing a methodology to evaluate the hygrothermal performance of wood framed envelopes under various moisture loads using stochastic approach. A stochastic modelling framework is developed based on a well-developed hygrothermal simulation program- DELPHIN and a robust programming platform- MATLAB. Latin Hypercube Sampling technique and Factorial Design Experiment are combined to organize the stochastic material properties, boundary conditions and moisture loads, and generate stochastic models. Uncertainty and

sensitivity analysis are performed based on the stochastic input parameters and results to evaluate the moisture content level and mold growth risk, as well as the sensitivity of the moisture performance to each influential factor.

The developed stochastic modelling framework is applied to analyze the hygrothermal performance of Cross Laminated Timber (CLT) wall assemblies and compared with parametric study to demonstrate the advantages of stochastic approach. Then, the hygrothermal performance of the highly insulated wood framed walls (deep cavity walls and exterior insulated walls) are analyzed using the stochastic modelling framework. It is found that the exterior insulated walls have lower mold growth risk than deep cavity walls, and the wall with high permeance exterior insulation (mineral wool) is safer than that with low permeance exterior insulation (polyisocyanurate) in terms of mold growth. The moisture performance of the walls is more sensitive to moisture loads than to material properties, and the significance of the moisture loads (air leakage and rain leakage) depends on climate condition. The thresholds of air leakage rate and rain deposition factor are obtained for the highly insulated wood framed walls to avoid mold growth risk. The design guidelines are formulated for energy efficient and durable wood framed envelopes. The developed stochastic modelling framework can be also applied to other moisture damage risk analysis such as wood decay and the damage caused by freeze/thaw cycles.

Acknowledgement

I would like to express my great thanks to my supervisor Dr. Hua Ge, for her seasoned and patient guidance. I have always been inspired by her profound knowledge in Building Physics and encouraged by her enthusiasm for research. This thesis cannot be completed without her constructive advices.

I would also like to thank the members of my thesis committee, for their precious comments and suggestions, which are not only valuable in polishing this thesis but also treasures for my future research.

I would like to thank Uli Ruisinger and Heiko Fechner at Dresden University of Technology for their detailed technical support of DELPHIN.

Finally, I would like to express my special thanks to my families. Their encouragement and support are essential for me to pursue my Ph.D.

Table of Contents

List of Figures ix

List of Tables xii

Nomenclature xiii

Chapter 1. Introduction 1

1.1 Problem statement 1

1.2 Objectives and scope 3

1.3 Outline of the thesis 4

Chapter 2. Literature review 6

2.1 Hygrothermal simulation 6

2.1.1 Moisture storage mechanisms 6

2.1.2 Moisture transport mechanisms 10

2.1.3 Heat and moisture balance equations 14

2.1.4 Hygrothermal simulation programs 17

2.2 Uncertainty and sensitivity analysis methods 18

2.2.1 Risk assessment 18

2.2.2 Uncertainty analysis 19

2.2.3 Sensitivity analysis 20

2.3 Uncertainties of HAM modelling 25

2.4 Hygrothermal performance of highly insulated wood framed walls 27

2.5 Summary 29

Chapter 3. Development of stochastic modelling methodology 30

3.1 Comparison between WUFI and DELPHIN 30

3.2 Stochastic variables 35

3.2.1 Material properties 35

3.2.2 Boundary conditions 36

3.2.3 Moisture loads 37

3.3 Stochastic case generation 41
3.3.1 Sampling technique for stochastic variables 41
3.3.2 Factorial design for scenario variables 42
3.4 Stochastic modelling framework design 43
3.5 Stochastic hygrothermal analysis tool 45
3.6 Summary 46
Chapter 4 Hygrothermal model validation and parametric study of CLT wall assemblies 47
4.1 Experimental setup 48
4.2 Hygrothermal model setup 50
4.2.1 Unification of material properties 52
4.2.2 Unification of WDR calculation 53
4.3 Comparison between simulation results and measurements 54
4.4 Sensitivity analysis method 55
4.4.1 One factor at a time method 55
4.4.2 Material properties 55
4.4.3 Boundary conditions 57
4.5 Results and analysis 58
4.5.1 Influence of material properties 58
4.5.2 Influence of boundary conditions 60
4.6 Summary 66
Chapter 5 Air leakage simulation methods 68
5.1 Introduction 68
5.2 Experimental setup 70
5.3 Hygrothermal model setup 75
5.3.1 Material properties 75
5.3.2 Boundary conditions and climatic conditions 76
5.3.3 Air leakage modelling methods 80
5.4 Results and analysis 84
5.4.1 Comparison between modeling and measurements 84

5.4.2 Performance evaluation 91
5.5 Summary 99
Chapter 6 Application of stochastic approach to two case studies 101
6.1 Case study 1: CLT wall assemblies 101
6.1.1 Stochastic variables 101
6.1.2 Scenario variables 104
6.1.3 Results and analysis 105
6.1.4 Conclusions for case study 1 117
6.2 Case study 2: highly insulated walls 119
6.2.1 Stochastic variables 119
6.2.2 Scenario variables 120
6.2.3 Results and analysis 122
6.2.4 Conclusions for case study 2 166
Chapter 7 Conclusions and future work 169
7.1 Conclusions 169
7.1.1 Conclusions regarding stochastic simulation methodology 169
7.1.2 Conclusions regarding hygrothermal performance and design strategies for CLT walls and highly insulated wood framed walls 170
7.2 Future work 171
References 173
Appendices 189
Appendix 1 Amount of rain leakage deposited at OSB sheathing for Waterloo and Vancouver 189
Appendix 2 Comparison of indoor RH, temperature and moisture excess between low and high internal moisture load 192
Appendix 3 Condensation rate calculated at the interior surface of OSB of the highly insulated walls 194
Appendix 4 Annual condensation amount at interior surfaced of OSB caused by air leakage 200

List of Figures

Figure 2.1 Moisture storage curve (left) and moisture retention cueve (right) (Zhao, 2012)..... 7
Figure 2.2 The variation of vapour permeability with relative humidity (Wu, 2007) 11
Figure 2.3 Moisture content profiles in the calcium silicate plate subjected to the water absorption test and the corresponding Boltzmann transformed data (Carmeliet et al., 2004)..... 13
Figure 2.4 Thermal conductivity of mineral wool and foam glass granules as a function of volume related moisture content and the temperature (Ochs and Muller-Steinhagen, 2005) 16
Figure 2.5 Procedure of calculating PRCC (Marino et al., 2008)..... 24
Figure 3.1 Stochastic cases generation 43
Figure 3.2 Stochastic simulation procedure..... 44
Figure 3.3 Structure of stochastic hygrothermal analysis tool..... 45
Figure 4.1 CLT wall assembly (McClung et al., 2014) 49
Figure 4.2 Typical sensor layout in CLT wall assemblies (McClung et al., 2014) 49
Figure 4.3 Initial moisture content profiles of the CLT panels..... 52
Figure 4.4 Comparison of wind-driven rain on east façade between WUFI and DELPHIN 53
Figure 4.5 Comparison between simulation results and measurements 54
Figure 4.6 RMSD between simulation results and measurements 55
Figure 4.7 Influence of material properties..... 59
Figure 4.8 RMSD in MCs between high and low values of each material property 60
Figure 4.9 Influence of rain deposition factor (RL-Rain Leakage, E-East, W-West) 62
Figure 4.10 Influence of cladding cavity ventilation rate (RL-Rain Leakage, E-East, W-West). 64
Figure 4.11 RMSD in MCs between high and low values of rain deposition factor and cladding cavity ventilation rate..... 65
Figure 5.1 Locations of test walls (Fox, 2014) 72
Figure 5.2 Air leakage test setup (Fox, 2014)..... 72
Figure 5.3 Plan view of the air leakage test setup..... 73
Figure 5.4 Cross sectional diagram of typical test panel configuration with sensor locations (Fox, 2014) 74
Figure 5.5 Moisture storage function of OSB and Cellulose fiber 78
Figure 5.6 Monitored weather data 79

Figure 5.7 1 mm air layer locations. 81
Figure 5.8 Connection of models for different test periods. 82
Figure 5.9 Moisture source strength at the interior surface of OSB sheathing calculated for the air injection period 84
Figure 5.10 Comparison in moisture content of OSB between simulations and measruements .. 86
Figure 5.11 Comparison between simulations with different L_{cd} and measurements from different locations 88
Figure 5.12 Comparison in MC of OSB between simulations and measurements 89
Figure 5.13 Comparison in MC of OSB between the air convection method and the air infiltration method for two-year simulation period 93
Figure 5.14 Sensitivity analysis of mold growth index for I-joist wall with cellulose insulation and baseline wall with fiberglass insulation 96
Figure 5.15 Mold growth index for I-joist wall and baseline wall with fiberglass insulation (North orientation) 98
Figure 6.1 Material property functions of CLT panel 103
Figure 6.2 Stochastic results of B1 (low permeance WRB) 106
Figure 6.3 Stochastic results of B2 (high permeance WRB) 107
Figure 6.4 PCCs for B1 (low permeance WRB) 109
Figure 6.5 PCCs for B2 (high permeance WRB) 110
Figure 6.6 Sensitivity analysis for initial moisture content 112
Figure 6.7 Root mean square of the PCCs (E-East, W-West, RL-Rain Leakage) 115
Figure 6.8 Stochastic results of MC with variation of material properties_Waterloo 123
Figure 6.9 Stochastic results of MC with variation of material properties and air leakage rates_low load_Waterloo 126
Figure 6.10 Stochastic results of MC with variation of material properties and air leakage rates_high load_Waterloo 128
Figure 6.11 Stochastic results of MC with variation of material properties and rain deposition factors_south_Waterloo 130
Figure 6.12 Stochastic results of MC with variation of material properties, air leakage rates (high load_south) and rain deposition factors (south)_Waterloo 131

Figure 6.13 Mold growth index with air leakage _north_Waterloo 133
Figure 6.14 Probability density functions of highest mold growth index _ Waterloo..... 135
Figure 6.15 PCCs of material properties to MC 138
Figure 6.16 PCCs of material properties and air leakage rates to MC_ north 140
Figure 6.17 PCCs of material properties and air leakage rates to mold growth index_north..... 143
Figure 6.18 Relationship between air leakage rate and highest mold growth index _ Waterloo 146
Figure 6.19 PCCs of air leakage rates (high load_south) and rain deposition factors (south) _Waterloo..... 147
Figure 6.20 Relationship between air leakage rates, rain deposition factor and highest mold growth index with air leakage (high load_south) and rain leakage (south) _Waterloo 149
Figure 6.21 Stochastic results of MC with variation of material properties _ Vancouver 151
Figure 6.22 Stochastic results of MC with variation of material properties and air leakage rates_low load_Vancouver 152
Figure 6.23 Stochastic results of MC with variation of material properties and air leakage rate_high load_Vancouver 154
Figure 6.24 Stochastic results of MC with variation of material properties and rain deposition factors (1% of wind-driven rain)_Vancouver 155
Figure 6.25 Stochastic results of MC with variation of material properties and rain deposition factors (0.1% of wind-driven rain)_east_Vancouver..... 156
Figure 6.26 Stochastic results of MC with variation of material properties, air leakage rates (high load_east) and rain deposition factor (east)_Vancouver..... 157
Figure 6.27 Probability density functions of the highest mold growth index _Vancouver 159
Figure 6.28 Relationship between rain deposition factor and highest mold growth index_east_Vancouver 163
Figure 6.29 Relationship between air leakage rate and highest mold growth index under high load_Vancouver 164
Figure 6.30 Relationship between air leakage rate, rain deposition factor and highest mold growth index with air leakage (high load_east) and rain leakage (east)_Vancouver..... 165

List of Tables

Table 3.1 Comparison of moisture storage parameters between WUFI and DELPHIN 31
Table 3.2 Comparison of moisture transport properties between WUFI and DELPHIN 32
Table 4.1 Components of the selected wall assemblies 50
Table 4.2 Material properties of the CLT wall components 50
Table 4.3 Boundary conditions 51
Table 4.4 Moisture storage function 56
Table 4.5 Vapour resistance factor as a function of relative humidity 57
Table 4.6 Range of material properties 57
Table 5.1 Summary of the test walls 70
Table 5.2 Wall components details for Figure 5.4 (Fox, 2014) 74
Table 5.3 Material properties for I-joist wall (Type 2), baseline wall (Type 3) and polyisocyanurate exterior insulated wall (Type 5) 76
Table 5.4 Boundary conditions 76
Table 5.5 Initial moisture content 78
Table 5.6 Condensation hours at the interior surface of OSB sheathing calculated for the entire simulation period 84
Table 5.7 Best matched models and the highest MC difference with measurements 90
Table 5.8 Parameters for equation 5-3 and equation 5-5 (Ojanen et al., 2010) 95
Table 6.1 Statistical figures of stochastic variables 102
Table 6.2 Factorial design of scenario variables 104
Table 6.3 Parameters of the best and worst matched cases 105
Table 6.4 Stochastic variables of hygric properties 119
Table 6.5 Factorial design of scenario variables of highly insulated wood framed walls 120
Table 6.6 The uncertainties caused by different factors- Waterloo 136
Table 6.7 The uncertainties caused by different factors- Vancouver 160
Table 6.8 Mold growth risks of the walls under different moisture loads and climatic conditions 167
Table 6.9 Threshold of air leakage rates and rain deposition factors under different moisture loads and climatic conditions 168

Nomenclature

Symbol	Parameter	Unit
A	Water absorption coefficient	$kg/m^2 \cdot s^{0.5}$
c	Specific heat capacity of dry material	J/kg·K
c_{in}	Water vapour concentration of indoor air	kg/m^3
$c_{sat.p}$	Water vapour saturation concentration at condensation plane	kg/m^3
c_{pl}	Specific heat capacity of liquid water	J/kg·K
c_{pv}	Specific heat capacity of vapour	J/kg·K
D_w	Moisture diffusivity	m^2/s
D_{ww}	Moisture diffusivity at saturation state	m^2/s
F_D	Rain deposition factor	-
F_E	Rain exposure factor	-
F_L	Empirical constant	$kg \cdot s/(m^3 \cdot m)$
g_l	Liquid flux	$kg/m^2 \cdot s$
g_v	Vapour flux	$kg/m^2 \cdot s$
g_{vc}	Convective vapour flux	$kg/m^2 \cdot s$
g_{vd}	Diffusive vapour flux	$kg/m^2 \cdot s$
h_l	Enthalpy of liquid water	J/kg
h_v	Enthalpy of water vapour	J/kg
$h_{v.e}$	Latent heat of evaporation	J/kg
K_l	Liquid water conductivity	kg/m·s·Pa

L_{cd}	Stud cavity depth starting from interior of OSB sheathing	m
p_c	Capillary pressure	Pa
p_s	Saturation vapour pressure	Pa
p_v	Vapour pressure	Pa
q_{CL}	Air leakage flux	$m^3/m^2 \cdot s$
q_{cond}	Conductive heat flux	W/m^2
q_{conv}	Convective heat flux	W/m^2
r_h	Horizontal rain intensity	mm/h
r_{bv}	Rain deposition on vertical wall	$kg/m^2 \cdot h$
S_w	Moisture source strength	$kg/m^2 \cdot s$
T	Temperature	K or ℃
U	Hourly average wind speed at 10 m	m/s
v	Air velocity	m/s
Vr	Cladding ventilation rate	1/h (ACH)
w	Moisture content	kg/m^3
w_f	Saturation water content	kg/m^3
w_l	Liquid water content	kg/m^3
w_v	Water vapour content	kg/m^3
w_{lim}	Limit moisture content that divides hygroscopic region and capillary region	kg/m^3

Greek symbols

α_l	Long-wave radiation emissivity	-
α_s	Short-wave radiation absorptivity	-

α_{ex}	Exterior heat transfer coefficient	$W/m^2 \cdot K$
α_{in}	Interior heat transfer coefficient	$W/m^2 \cdot K$
β_{ex}	Exterior vapour transfer coefficient	s/m
β_{in}	Interior vapour transfer coefficient	s/m
δ	Vapour permeability	kg/m·s·Pa
δ_a	Vapour permeability in air	kg/m·s·Pa
θ_l	Partial volume fraction	-
θ_{por}	Porosity	-
λ	Heat conductivity	W/m·K
λ_d	Heat conductivity of dry material	W/m·K
λ_w	Heat conductivity of wet material	W/m·K
μ	Vapour diffusion resistance factor	-
μ_{Dry}	Vapour diffusion resistance factor at dry state	-
ρ	Bulk density of materials	kg/m^3
ρ_v	Water vapour density	kg/m^3
φ	Relative humidity	%

Abbreviations

ACH	Air change per hour
AFR	Adhering Fraction of Rain
CLT	Cross Laminated Timber
HAM	Heat, air and moisture
MD	Moisture diffusivity
MC	Moisture content

MEW	Vapour diffusion resistance factor
MSF	Moisture storage function
NVP	Non-vapour permeable
OFAT	One factor at a time
PCC	Partial correlation coefficient
PRCC	Partial ranked correlation coefficient
RH	Relative humidity
RMSD	Root mean square of the differences
SRC	Standardized regression coefficient
SRRC	Standardized ranked regression coefficient
VP	Vapour permeable
WDR	Wind-driven rain
WRB	Water resistive barrier

Chapter 1. Introduction

1.1 Problem statement

Wood-framed buildings are the dominant building type for low-rise buildings in North America because of their features such as light-weight, easily built and environmental friendly. Due to these advantages, there are renewed interests in using engineered wood products as the structural, load bearing element in tall wood buildings. For example, the feasibility of a 20 storey wood building using cross laminated timber (CLT) as the main structural component in North Vancouver, a place with high wind-driven rain and seismic loads, was thoroughly evaluated including architectural, structural, fire safety, buildability and durability (FPInnovation and NEWBuilds, 2014). An 18 storey tall wood building with mass timber is used as the main structural component was constructed in University of British Columbia (UBC), Vancouver. The floor plate slabs and façade of this building are made by CLT and prefabricated high-pressure laminated timber separately (Chan, 2016). However, prolonged exposure to moisture during construction and in service is a durability concern for most wood products. As building energy consumption has gained increasing attention in recent years, the majority of building codes require higher insulation level to improve the building energy efficiency (Finch et al., 2013).

There are different design strategies to achieve the higher insulation level of the wood framed building envelope, such as widening the stud cavity to adapt a thicker insulation material or adding an exterior insulation while keeping the depth of stud cavity the same as traditional walls. However, the highly insulated walls may lead to a higher risk of moisture problems. For example, deep cavity walls have a lower temperature on the colder side of the insulation layer, thereby increases the risk of interstitial condensation caused by vapour diffusion or air leakage (Janssens and Hens, 2003). Although the exterior insulated walls have less possibility of interstitial condensation than those without exterior insulation (Maref et al., 2010), the wood sheathing may have a lower drying potential if the exterior insulation has a low permeance (Gibson, 2010). The moisture loads such as wind driven rain leakage and air leakage on the highly insulated wall also increase the potential of moisture problems such as mold growth and wood decay (Rousseau, 1999; Maref et al., 2007), which dramatically reduce the durability performance of the building envelope and affect the health of occupants (EPA, 2013).

Therefore, many research projects have been conducted to investigate the hygrothermal performance of the highly insulated walls (Maref et al., 2010; Arena et al., 2013; Parsons and Lieburn, 2013; Smegal et al., 2013; Craven and Garber-Slaght, 2014; Glass et al., 2015). Most of the researches are based on the combination of experimental study and hygrothermal modelling. By field measurement, the hygrothermal performance of the investigated wall assemblies can be monitored under specific period and location. The hygrothermal models can be created based on the wall configurations under investigation, and the simulation results from the hygrothermal models can be compared with monitored data from field measurement for validation. Then the validated hygrothermal models can be used to evaluate the wall performance under other climate conditions. Generally, the hygrothermal models are deterministic models, in which the deterministic values are used for the input parameters. However, the factors influencing the hygrothermal responses are stochastic in nature such as the variability of material properties, boundary conditions, as well as the moisture loads. The uncertainties of the input parameters may lead to a deviation between the simulation results and the actual performance of the envelope assemblies, consequently, may lead to faulty designs.

Many uncertainty and sensitivity analysis methods have been applied in building performance simulation to investigate the uncertainties of input parameters and their influence (Tian, 2013). The stochastic approach is applied to the field of building physics for uncertainty and sensitivity analysis because of the following advantages: 1)By performing stochastic analysis, the influential parameters are varied simultaneously so that the interaction between the parameters can be taken into account (J. Lomas and Eppel, 1992); 2) The stochastic sensitivity analysis can obtain more accurate estimates of sensitivity indicators and 3) The stochastic analysis can be applied to dynamic nonlinear situation (Irving, 1992).

In general, the standard stochastic analysis procedure can be summarized into the following four steps (Salonvaara et al., 2001; Holm and Kunzel, 2002; Zhao et al., 2011; Defraeye et al., 2013):

1) Random number generation: The influential parameters are considered as stochastic variables and assigned with probability distributions. The random numbers will be generated from the probability distribution for each stochastic variable.

2) Sampling: The generated random numbers for each parameter are selected according to a proper sampling technique, and they are combined randomly to form a stochastic case.

3) Simulation: The simulation is performed for each stochastic case to obtain the stochastic results.

4) Uncertainty and sensitivity analysis: The uncertainty of the stochastic results can be evaluated by statistical figures such as mean value and standard deviation. The relationship between the inputs and outputs can be analyzed by a sensitivity indicators such as standardized regression coefficient or partial correlation coefficient.

Most of the previous stochastic analysis were focused on the influence of material properties and boundary conditions (Holm and Kunzel, 2002; Zhao et al., 2011; Defraeye et al., 2013). The moisture loads, such as the air leakage and rain leakage, also have significant influence on the hygrothermal performance, especially for the highly insulated wood framed walls. Although the influence of air leakage and rain leakage was investigated through hygrothermal modelling (Saber et al., 2011; Ojanen and Kumaran, 1996; Karagiozis and Kunzel, 2009; Hagentoft and Harderup, 1996), the average values of the air leakage and rain leakage rate are commonly used for simulation, which cannot reveal the moisture problem risks caused by the uncertainties of the moisture loads. Therefore, it is necessary to take the moisture loads and their uncertainties into account to evaluate the moisture problem risks of the highly insulated wood framed envelopes.

1.2 Objectives and scope

As discussed above, although the hygrothermal performance of the highly insulated wood framed envelopes has been investigated by many researchers, there may be still moisture problem risks which cannot be revealed by experimental study and traditional hygrothermal simulation because of the uncertainties of the material properties, boundary conditions and moisture loads. The stochastic approach has been applied for hygrothermal analysis of conventional wood framed walls, however the stochastic variables are only limited to material properties and boundary conditions, without consideration of the uncertainties of moisture loads.

Therefore, this thesis focuses on developing a stochastic methodology based on one-dimensional hygrothermal modelling to provide reliable durability assessment of highly insulated wood framed walls, revealing the moisture problem risks caused by the uncertainties of material properties, boundary conditions and moisture loads. The specific objectives of this thesis are to:

- Develop a stochastic methodology, which includes a hygrothermal simulation program, stochastic uncertainty and sensitivity analysis methods, and factorial design method.
- Evaluate the reliability of the hygrothermal simulation programs by comparing the simulation results with field measurements and inter-program comparison.
- Develop an one-dimensional air leakage modelling method for creating the reliable models to simulate the impact of air leakage on the wood framed walls.
- Evaluate the mold growth risks of different design strategies of highly insulated wood framed walls.
- Identify the important factors that influence the hygrothermal performance of the highly insulated wood framed walls, ranking the significance of the influential factors.
- Provide design suggestions of highly insulated wood framed walls in different climatic conditions.

1.3 Outline of the thesis

Chapter 2 reports a comprehensive literature review, which includes the hygrothermal modelling methods, risk assessment methods, uncertainty and sensitivity analysis methods, and the current research status of hygrothermal performance of highly insulated walls and the application of stochastic approach on hygrothermal analysis. Based on the comprehensive literature review, this chapter identifies the detailed knowledge gaps.

Chapter 3 develops a stochastic analysis methodology targeting the knowledge gaps presented in chapter 2. This chapter compares the most commonly used hygrothermal simulation programs - WUFI and DELPHIN to select a proper program for stochastic modelling, reviews factors that influence the simulation results to design a framework for generating stochastic models, and constructs a software platform to perform stochastic simulation, uncertainty and sensitivity analysis.

Chapter 4 evaluates the reliability of the selected hygrothermal simulation program. The evaluation is based on the experimental study of Cross Laminated Timber (CLT) wall assemblies, which was conducted by McClung (2014). One-factor-at-a-time (OFAT) sensitivity analysis is performed to provide a preliminary insight of uncertainties of the moisture content in CLT panels and the significance of the influential factors.

Chapter 5 develops an one-dimensional air leakage modelling method based on the experimental study of highly insulated wood framed walls conducted by Fox (2014). This chapter compares two simplified air leakage modelling methods - air convection method and air infiltration method, and trial-and-error method is used to create the reliable hygrothermal model for investigating the impact of air leakage on wood framed walls.

Chapter 6 applies the developed stochastic approach to two case studies - CLT wall assemblies and highly insulated wood framed wall assemblies for durability performance assessment. This chapter performs stochastic simulations to investigate the uncertainties of the moisture content of CLT wall assemblies, and rank the significance of the influential factors. And stochastic simulations are also performed for highly insulated wood framed walls to investigate the mold growth risks and develop design strategies.

Chapter 7 summarizes the contributions and conclusions of this thesis. This chapter provides the design guidelines of highly insulated wood framed walls in cold and mild/humid climate zones, and discusses future works.

Chapter 2. Literature review

2.1 Hygrothermal simulation

The theories of heat, air and moisture transfer through porous building materials are the basis of most hygrothermal simulation tools. The HAM (heat, air and moisture) models have been fully developed in the past few decades. There are different ways to classify the HAM models (steady-state or transient-state, one-dimensional or two-dimensional, different driving potentials). A comprehensive review of the HAM models can be found in literature (Hens, 1996). This thesis focuses on one-dimensional, transient state HAM model. The driving potential of moisture transport used in the HAM model determines the input parameters of the simulation tool. This section mainly reviews two ways of describing moisture storage and transport processes as the main topic of this thesis is related to moisture problems. The basic equations of heat transfer through building envelopes are also provided, but the air transfer equations are not included because they are not involved in the air leakage simulation method discussed in this thesis.

2.1.1 Moisture storage mechanisms

Porous building materials are capable of absorbing moisture from their environment. The process of moisture transfer in porous materials can be categorized into three regions, which are named as hygroscopic region, capillary region and over-capillary region. In the hygroscopic region, which starts from dry state, the moisture transfer is characterized by vapour diffusion. With the increase of relative humidity, the vapour molecules will be bounded on the pore surface. The moisture content increases gradually in the hygroscopic region. When the surface tension cannot bound the moisture molecules, the moisture moves into pores and the moisture transfer falls into the capillary region. Although the critical relative humidity is generally assumed as around 95% (Kunzel, 1995), it is dependent on material property so it is not accurate enough to use a certain relative humidity as the threshold between hygroscopic and capillary region for all materials (Carmeliet and Roels, 2002). In the capillary region, some of the pores are filled with liquid water and the moisture transfer mechanism could be both of vapour diffusion and liquid conduction, which result in a dramatic increase of moisture content. The over-capillary region begins with the relative humidity reaching 100% when all the pores are filled with water, and moisture content are reaching free water saturation. The moisture transfer mechanism in the over-capillary region is liquid conduction

and gravity flow. In the field of building physics, the moisture activity in material rarely reaches the over-capillary region. The moisture storage characteristics can be described by using the moisture storage curves the variation of moisture content with relative humidity or capillary pressure. In the hygroscopic region, the relationship between moisture content and relative humidity can be observed clearly, therefore, moisture storage curve can be used in this region. The moisture content increases steeply at high relative humidity (greater than 95%), so the relationship between moisture content and relative humidity cannot be interpreted clearly by moisture storage curve. Therefore, the moisture storage property is described by the moisture retention curve, which shows the relationship between moisture content and capillary pressure. The moisture storage curve and moisture retention curve are presented in Figure 2.1.

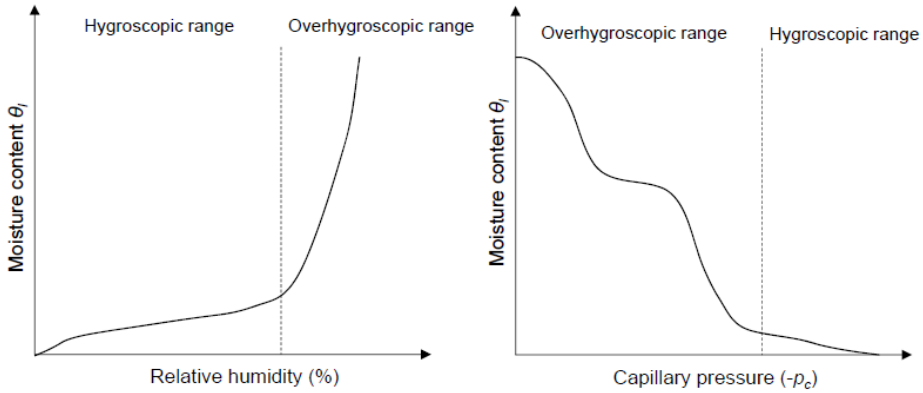

Figure 2.1 Moisture storage curve (left) and moisture retention cueve (right) (Zhao, 2012)

For the hygrothermal modelling purpose, the moisture storage curve and retention curve can be expressed by analytical equations, which can be established by different ways.

Analytical equation for moisture storage curve (sorption isotherm)

The analytical equation of sorption isotherm describes the moisture content as a function of relative humidity. A simple sorption isotherm formula was suggested by Kunzel (1995).

$$w(\varphi; b) = w_f \frac{(b-1)\varphi}{b-\varphi} \tag{2-1}$$

where

w- moisture content (kg/m^3)

w_f- free water saturation (kg/m^3)

φ- relative humidity (%)

b- fitting factor

By using this equation, only the moisture contents at relative humidity 80% (reference moisture content) and 100% (free water saturation) are needed to estimate the fitting factor. Then, the moisture content at any relative humidity level can be calculated by this equation. Kunzel (1995) compared the moisture storage function estimated by equation 2-1 with the measured sorption isotherm for four materials: lime silica brick, cellular concrete, clay brick and gypsum board, and the estimated storage functions show a good agreement with the measured values. However, this formula is not accurate enough for all materials, some materials (e.g. some kinds of concrete) cannot be estimated by this equation. Another analytical equation was used by Burch (1997) for developing MOIST- a hygrothermal software.

$$w(\varphi; a; b; c) = \frac{\varphi}{a\varphi^2+b\varphi+c} \quad (2\text{-}2)$$

where

w- moisture content (kg/m^3)

φ- relative humidity(%)

a, b, c- fitting factor

There are three fitting factors that need to be determined, which means at least three test points are needed to generate the moisture storage curve.

Analytical equation of moisture retention curve

The sorption isotherm equations, which describe moisture content as the function of relative humidity, are only applicable in the hygroscopic range but not in the capillary region (Carmeliet and Roels, 2002). It is necessary to establish the relationship between moisture content and the capillary pressure when considering the moisture transfer in the capillary region.

The analytical equation of moisture retention curve describes the moisture content as a function of the capillary pressure. Moisture retention curve was originally used in soil science to model the

transient water and solute transport in the vadose zone. The relationship between the moisture content in soil and the capillary pressure can be expressed by analytical functions, and the parameters can be obtained by fitting the function to experimental water content and conductivity data (van Genuchten, 1980). Based on van Genuchten's equation (1980), Durner (1994) developed an unimodal curve that can be used in the field of building physics:

$$w(p_c; a, n, m) = w_f[1 + (ap_c)^n]^{-m} \quad (2\text{-}3)$$

where

p_c- capillary pressure (Pa)

w_f- free water satureation (kg/m^3)

α- scalling factor determining the position of the pore volume maximum

n,m- deimensionless curve-shape parameters

Carmeliet and Roels (2002) developed bimodal equation based on unimodal equation and they compared the unimodal and bimodal equations by simulating the wetting process of ceramic brick and calcium silicate. They found that bimodal equation is preferable for describing the wetting curve. They also developed a mixed equation, which describes moisture content by both relative humidity and capillary pressure:

$$w(\varphi, p_c;\ w_{lim}, \alpha, n, m) = w_{lim}\varphi^n + (w_{cap} - w_{lim})\ [1 + (\alpha p_c)^m]^{-(1-(1/m))} \quad (2\text{-}4)$$

where

w_{lim}- the limit moisture content that divides the hygroscopic region and capillary region (kg/m^3)

w_{cap} – free water saturation (kg/m^3)

The mixed equation performs comparable (ceramic brick) or slightly inferior (calcium silicate) to the bimodal equation according to the comparison conducted by Carmeliet and Roels (2002). A more complicated equation was suggested by Grunewald et al. (2003).

$$\theta_l(p_c) = \sum_{I=0}^{N} \frac{\theta_i}{\sqrt{2}}\left(1 + \mathrm{erf}\left(\frac{p_{ci} - p_c}{\sqrt{2}s_I}\right)\right) \quad (2\text{-}5)$$

where

p_c- the capillary pressure (Pa)

θ_l- the partial volume fraction

S_l- the deviation parameter describing the width of the pore volume distribution

In this equation, more information, such as the pore structure and pore radii, is needed for obtaining the moisture retention curve. It's too complicated for engineering application purpose, although it shows the highest accuracy (the errors between the calculated values and the measured data were less than 3% for a new insulation mortar) based on the comparison of different equations performed by Zhong et al. (2010).

2.1.2 Moisture transport mechanisms

Moisture transport in porous materials includes different mechanisms from the hygroscopic region to the over-capillary region. In the hygroscopic region with low relative humidity, the dominated moisture transport mechanism is vapour diffusion. With the increase of relative humidity, the moisture molecule is accumulated on the pore surface and capillary condensation will occur. With the accumulation of liquid water, both vapour diffusion and liquid diffusion are involved in moisture transport process. The moisture content increases steeply under the combined effect of vapour diffusion and liquid diffusion. The mixed transport mechanism is dominated in the end of hygroscopic region and the beginning of capillary region. When the pores are fully filled with liquid water, which means moisture transport comes into the over-capillary region, moisture cannot be transported through the material by vapour diffusion and the transport mechanism is dominated by the liquid conduction. The relationship between moisture content and relative humidity is hard to be observed in this region.

Vapour Transport

Vapour transport in porous material can be categorized into vapour diffusion and vapour convection. Vapour diffusion is driven by vapour pressure gradient. The diffusive vapour flow can be calculated according to Fick's law as follows:

$$g_{vd} = -\delta \nabla p_v \tag{2-6}$$

where

δ- vapour permeability (kg/m·s·pa)

p_v- vapour pressure (Pa)

g_{vd}- diffusive vapour flow (kg/m·s)

The vapour permeability is largely dependent on moisture content. In the hygroscopic region with lower relative humidity, the moisture transfer mechanism is dominated by vapour diffusion, and the vapour permeability mainly reflects the capability of vapour diffusion. The vapour molecule will be accumulated on the pore surface as the increase of moisture content. The surface diffusion will occur when the surface tension cannot bound the vapour particles, and liquid flow will be involved. Therefore, the permeability in hygroscopic region with higher relative humidity reflects the mixed effect of vapour diffusion and liquid diffusion, and it is greater than that in the region of lower relative humidity. A typical variation of vapour permeability with moisture content is presented in Figure 2.2.

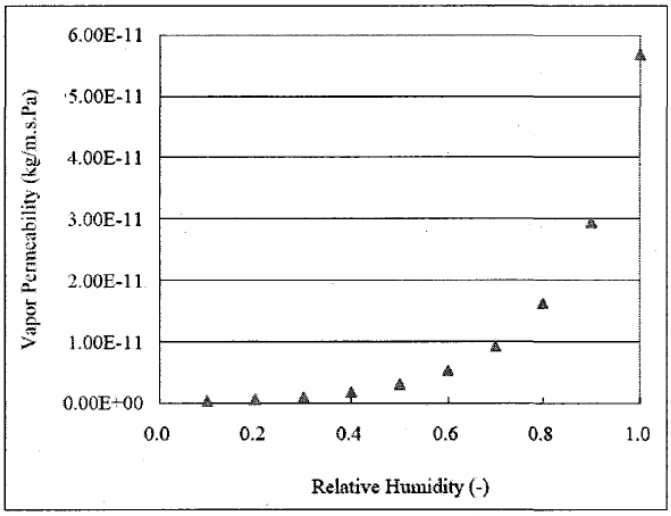

Figure 2.2 The variation of vapour permeability with relative humidity (Wu, 2007)

As the vapour diffusion in porous building materials is impeded by the absorption effect of the pore wall and the complicated pore path, the diffusion flow in porous building materials is less than that in the air. Therefore, vapour diffusion resistance factor is also introduced to calculate the vapour flow:

$$g_{vd} = -\frac{\delta_a}{\mu}\nabla p \tag{2-7}$$

where

δ_a- vapour permeability in the air (kg/m·s·pa)

μ- vapour diffusion resistance factor

Vapour convection is caused by air movement, which can be led by buoyancy force, wind-induced pressure and mechanical force. The vapour convection is only taken into account when the air flow, such as infiltration or exfiltration, is considered in the HAM model (Li, 2008). The vapour convection can be expressed by the following equation:

$$g_{vc} = v\rho_v \tag{2-8}$$

where

v- air velocity (m/s)

ρ_v- water vapour density (kg/m^3), it is dependent on temperature and relative humidity.

Liquid transport

The liquid transport can be described by moisture diffusivity method or liquid conductivity method, depending on which parameter is used as the driving potential. If moisture content is used as the driving potential, the liquid transport coefficient should be moisture diffusivity; if capillary pressure is used as the driving potential, the liquid transport coefficient should be liquid conductivity. When capillary pressure is used as the driving potential, the liquid transport equation can be written as follows:

$$g_l = K_l \nabla p_c \tag{2-9}$$

where

K_l-liquid conductivity (kg/m·s·pa)

p_c- capillary pressure (Pa)

With moisture content as the driving potential, the liquid transport equation can be written as follows：

$$g_l = -D_w \nabla w \tag{2-10}$$

where

D_w- moisture diffusivity (m^2/s)

w- moisture content (kg/m^3)

Generally, the moisture diffusivity is determined by moisture content profile, which can be obtained from water absorption test. By performing this test, one surface of the specimen is in contact with water. The distribution of moisture within the specimen is determined as a function of time at various intervals until the moving moisture front advances to half of the specimen. As long as the moisture content profile is obtained, the moisture diffusivity can be calculated according to Boltzmann transformation (Janz, 1997). A typical moisture content profile is presented in Figure 2.3.

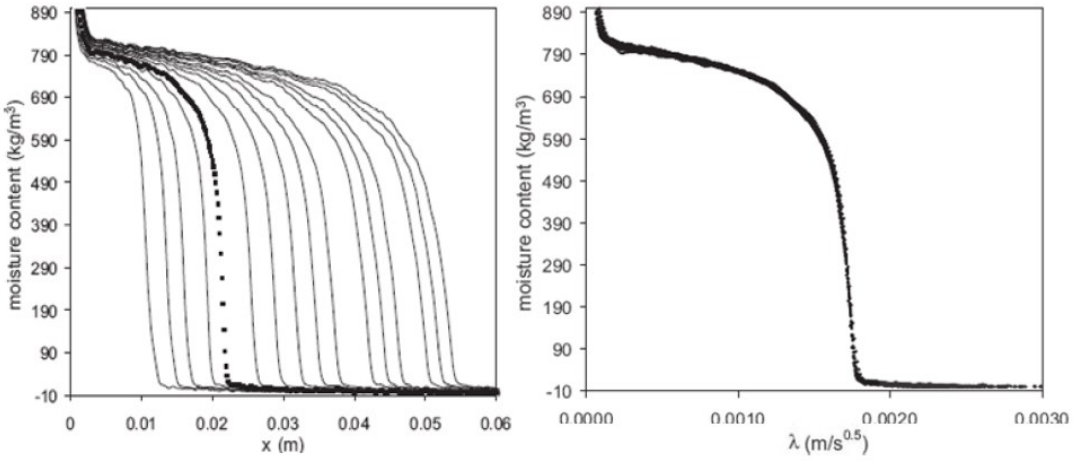

Figure 2.3 Moisture content profiles in the calcium silicate plate subjected to the water absorption test and the corresponding Boltzmann transformed data (Carmeliet et al., 2004).

The moisture diffusivity can be calculated using the following equation:

$$D(w) = -\frac{1}{2}\frac{d\lambda}{dw}\int_{w_0}^{w_1}\lambda dw_f \qquad (2\text{-}11)$$

where

w_f- the free water saturation (kg/m^3)

w_0- the initial moisture content (kg/m^3)

$\lambda = \frac{x}{\sqrt{t}}$

λ- Boltzmann variable

x- thickness of material (m)

t- time (s)

The measurement of moisture profile is usually performed based on nuclear-magnetic resonance or γ radiography (Gummerson et al., 1979; Nelson, 1972), which are time-consuming and cost-intensive (Krus and Holm, 1999). Many researchers investigated other simple methods to determine the moisture diffusivity (Kunzel, 1995; Pel, 1995; Krus and Holm, 1999; Haupl and Fechner, 2003; Carmeliet et al., 2004). A typical function used by WUFI is presented as follows:

$$D_w = 3.8 \cdot (A/w_f)^2 \cdot 1000^{(\frac{w}{w_f}-1)} \quad (2\text{-}12)$$

where

A- water absorption coefficient ($kg/m^2 \cdot s^{0.5}$)

w_f- free water saturation (kg/m^3)

The A-value is also obtained from water absorption test, by which the mass increase is recorded as a function of time. Then, the A-value can be defined as the slope of the line of mass increase against the square root of time divided by the area of the surface in contact with water. Kumaran (1999) compared the moisture diffusivity calculated using A-value with that obtained based on moisture content profile for spruce. The moisture diffusivity obtained from the two methods agreed at higher moisture content range, but they did not match well at low moisture content range.

2.1.3 Heat and moisture balance equations

Moisture Balance Equation

Based on the mass conservation law, the rate of moisture change in time at a given control volume should be equal to the sum of all the incoming and outgoing fluxes together with the source production rate. Combining the vapour transfer and liquid transfer, the moisture balance equation can be written as follows:

$$\frac{\partial w}{\partial t} = -\nabla(g_v + g_l) = \nabla(\delta \nabla p_v + D_w \nabla w) + Q_m \quad (2\text{-}13)$$

or

$$\frac{\partial w}{\partial t} = -\nabla(g_v + g_l) = \nabla(\delta \nabla p_v - K_l \nabla p_c) + Q_m \quad (2\text{-}14)$$

where

Q_m- moisture source (kg/m^3)

Heat Balance Equation

The heat transport in building envelope includes heat conduction and heat convection. Based on Fourier's law, the heat conduction can be described by the following equation:

$$q_{cond} = -\lambda \nabla T \quad (2\text{-}15)$$

where

λ- heat conductivity (W/m·K)

q_{cond}- conductive heat flux (W/m^2)

T- temperature (K)

The heat conductivity is dependent on temperature and moisture content. Normally, the influence of temperature can be neglected, while the influence of moisture content is more important. According to Kunzel (1995), the thermal conductivity of building materials can be described as a function of moisture content:

$$\lambda(w) = \lambda_w + (\lambda_d - \lambda_w)\frac{w_f - w}{w_f} \quad (2\text{-}16)$$

where,

λ_w- heat conductivity of wet material (W/m·K)

λ_d- heat conductivity of dry material (W/m·K)

w_f- saturation moisture content (kg/m^3)

w- moisture content (kg/m^3)

Also, the relationship between heat conductivity and moisture content can be found by experiment. A typical curve that describes the heat conductivity as a function of moisture content is presented in Figure 2.4.

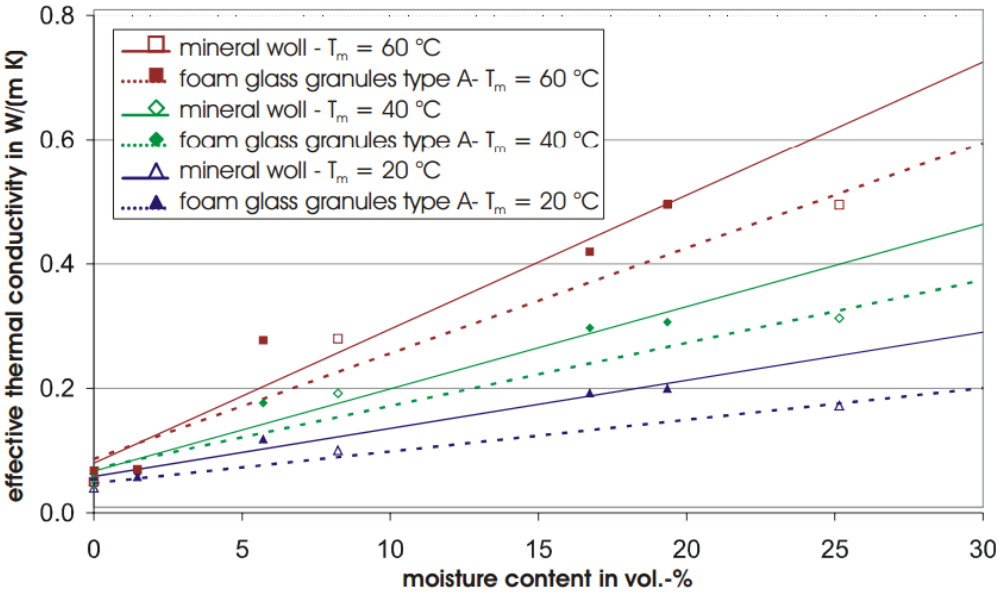

Figure 2.4 Thermal conductivity of mineral wool and foam glass granules as a function of volume related moisture content and the temperature (Ochs and Muller-Steinhagen, 2005)

Ignoring the air leakage, the convective heat can be divided into latent heat and sensible heat. The convective heat is carried by the moisture that passes through the building envelope. Then the convective heat can be described by the following equation:

$$q_{conv} = g_v h_v + g_l h_l \quad (2\text{-}17)$$

where

h_v- the enthalpy of water vapour (J/kg)

h_l- the enthalpy of liquid water (J/kg)

The heat that the building envelope component holds at a certain time can be written as follows:

$$H = \rho c T + h_v w_v + h_l w_l \quad (2\text{-}18)$$

where

ρ- bulk density (kg/m^3)

c- specific heat capacity of dry material (J/kg·K)

w_v- water vapour content (kg/m^3)

w_l- liquid water content (kg/m^3)

Base on the energy conservation law, the heat balance equation can be written as follows:

$$\frac{\partial}{\partial t}(\rho c T + h_v w_v + h_l w_l) = -\nabla(-\lambda \nabla T + g_v h_v + g_l h_l) \quad (2\text{-}19)$$

Assuming the latent heat of evaporation and the specific heat of building materials and liquid water are constants, and considering $h_v=h_{v.e}+c_{pv}T$, $h_l=c_{pl}T$, where $h_{v.e}$ is the latent heat of evaporation, c_{pv} is the specific heat capacity of vapour, c_{pl} is the specific heat capacity of liquid water, the heat balance equation can be re-written as follows:

$$(\rho c + w c_{pl})\frac{\partial T}{\partial t} = \nabla(\lambda \nabla T) + h_{v.e}\nabla[\delta(\varphi \frac{dP_s}{dT}\nabla T + P_s \nabla \varphi)] \quad (2\text{-}20)$$

where

P_s- saturation vapour pressure, which is φP_v (Pa)

2.1.4 Hygrothermal simulation programs

Many hygrothermal simulation tools are developed based on the heat and moisture transfer models (Rode, 1990; Kunzel, 1995; Hens, 1996; Burch, 1997; Kalagasidis, 2004; Hagentoft, 2002ab; Salonvaara, 2004; Janssen et al., 2007), and the successful applications of these tools can also be found in literature (Kunzel, 1998; Beaulieu et al., 2001). A comprehensive review of the hygrothermal simulation programs can be found in Delgado (2013).

In general, the reliability of the hygrothermal simulation tools has to be evaluated before they are widely used. There are many differences among the hygrothermal simulation tools, such as the different methods of describing moisture storage and transport mechanisms, different ways of dealing with material properties or rain loads and different numerical methods. The evaluation of the hygrothermal simulation tools should be based on standardized procedure to obtain objective conclusions. To unify the reliability evaluation method, five benchmarking cases, which covered various climatic conditions, material combinations and moisture transport mechanisms have been

proposed in HAMSTAD project (Hagentoft et al., 2004). Many developers validated their hygrothermal simulation tools based on the five benchmarking cases (Kalagasidis, 2004; Li, 2008).

Sometimes, the validation works are conducted based on the field measurement results from experimental facilities or actual houses. These validation works are based on specific wall constructions and environmental conditions, thereby the parameters of the validated models can be varied for uncertainty and sensitivity analysis. Mundt-Petersen (2013) performed the validation work based on five different wood-frame houses. The hygrothermal models were created according to the actual wall components and environmental conditions in WUFI. The simulated relative humidity and temperature of the walls were compared with the measurement results, and the simulation results generally showed a good agreement with measured results. Alev et al. (2014) conducted a measurement study based on a test wood frame house with consideration of air leakage. The measured relative humidity and temperature of the inner surface of the wall were compared with the hygrothermal simulation results obtained from WUFI, and there was a good agreement between the measured results and simulated results. However, to establish a confidence of a hygrothermal model, the validation work is not only limited to comparing the simulation results with measured results, it is also necessary to compare the simulation results among different simulation programs (Cornick et al. 2009).

2.2 Uncertainty and sensitivity analysis methods

2.2.1 Risk assessment

Risk is defined as the probability of a consequence at a certain scenario. A consequence may be referred to as an unwanted outcome i.e. the moisture damage of the building envelope, which is a possible combination of the influencing parameters (Kaplan and Garrick, 1981; Shahriari, 2011). The risk assessment methods can be categorized into qualitative and quantitative methods. Qualitative methods focus on factor identification and organization. Factor identification is to map out all of the related parameters that influence the outcome of the analysis, and the purpose of factor organization is to establish all of the relations between the parameters and outcomes (Janssen et al., 2013). There are various methods for factor identification and organization, and the most commonly used are Fault Tree and Event Tree analysis (FTA and ETA) (Bedford and Cooke, 2001), Failure Modes Effects Analysis (FMEA) (Nielsen, 2002), Variation Mode and Effect

Analysis (VMEA) (Chakhunashvili et al., 2004), Hazard and Operability study (HAZOP) (Shahriari, 2011). Quantitative approaches calculate the probability distribution of the outcome and quantify the risk based on uncertainty analysis. Therefore, quantitative approaches involve uncertainty analysis and sensitivity analysis and they are more pertinent to the target problem in this thesis.

2.2.2 Uncertainty analysis

Uncertainty analysis is to investigate how much variation in the output is due to the variation in the input. There are two types of uncertainty quantification: forward uncertainty propagation and inverse uncertainty quantification (Wikipedia, 2015). Forward uncertainty propagation is the quantification of uncertainties in system outputs propagated from uncertain inputs. It focuses on the influence on the outputs from the parametric variations. The purpose of forward uncertainty propagation is to calculate the low-order moments of outputs, i.e. mean and variance, to evaluate the reliability of outputs and to assess the probability distribution of outputs. Inverse uncertainty quantification estimates the discrepancy between experiment and mathematical model and estimates the values of unknown parameters in the model if there is any. Therefore, the purposes of inverse uncertainty quantification are bias correction, which quantifies the model inadequacy, and parameter calibration, which estimates the unknown parameters.

Uncertainty analysis for risk assessment is a typical example of forward uncertainty propagation. The methodologies of forward uncertainty analysis can be categorized into probabilistic approaches and non-probabilistic approaches. As the probabilistic approaches are based on the calculation of probability density functions for sampling statistics and are consistent with the theory of decision analysis, they are considered as the most rigorous approaches to uncertainty analysis in engineering design (Arnaut, 2008).

There are several types of probabilistic approaches, such as FORM and SORM methods (first order and second order reliability method), Monte Carlo method (Lee and Chen, 2008). If the number of uncertainty variables is not too high, the FORM and SORM methods have similar efficiency as Monte Carlo method. However, FORM and SORM methods are only suitable for continuous variables. Moreover, FORM and SORM methods are typically used to estimate the probability density function at a certain point, which cannot represent the uncertainty through the entire range

(Janssen et al., 2013). Although the application of FORM and SORM methods in building physics can be found in literature (Pietrzyk and Hagentoft, 2008), they are not widely used due to their limitations. In comparison, Monte Carlo method is based on sampling techniques, which is suitable for both continuous and discrete variables. Monte Carlo method is able to build entire probability density function to assess global uncertainty and sensitivity. Therefore, Monte Carlo method is often used in the field of building physics. The only drawback of Monte Carlo method is that it requires a large number of simulations to guarantee the reliability of the results, which makes the computational cost high (Janssen et al., 2013).

2.2.3 Sensitivity analysis

Sensitivity analysis is the study of how the uncertainty in the output of a mathematical model can be apportioned to different sources of the inputs uncertainty. By performing the sensitivity analysis, the relationship between input and output variables can be investigated and the most influential input parameter to the output can be identified. There are several methods of performing the sensitivity analysis. In general, the sensitivity analysis methods can be categorized into local method and global method. Local method examines the influence of the input parameter in a small range around a certain point, while global method investigates the sensitivity of the input parameter through the entire parameter distribution (Hamby, 1995).

2.2.3.1 Differential sensitivity analysis method-local method

Differential sensitivity analysis is based on the partial differentiation of the model in aggregated form. It can be thought as the propagation of input uncertainties (Cunningham et al., 1980). A model including the input variables $X= (x_1, x_2,\ldots,x_n)$ and output variable Y is:

$$Y = f(X) \tag{2-21}$$

The model can be rewritten as a first-order Taylor series approximation. Then the variance of Y at a certain point X_0 can be calculated using the general error propagation equation (Helton, 1993):

$$V(Y) = \sum_{i=1}^{n} \left(\frac{\partial f(X_0)}{\partial X_i}\right)^2 V(x_i) \tag{2-22}$$

The variance of Y can be used as a measure of uncertainty of output at X_0. Then the sensitivity of x_i to Y at point X_0 can be calculated using the following formula (Helton, 1993):

$$s_i = \frac{\left[\frac{\partial f(X_0)}{\partial X_i}\right]^2 V(x_i)}{V(Y)} \quad (2\text{-}23)$$

where

s_i- sensitivity indicator of x_i

This method is considered as a direct method and the backbone of almost all other sensitivity analysis method and it is computationally efficient (Hamby, 1995). However, this method is only suitable for linear problem and is valid only for small parameter uncertainties (Koda et al., 1979). Furthermore, this method can only examine the sensitivity of the input parameters in a small range around a certain point and it cannot investigate the influence of the parameters through their entire range. Thirdly, this method cannot consider the interaction between the input parameters (Tian, 2013).

2.2.3.2 Screening based methods-global method

The simplest screening-based method is one at a time experiment (OAT). This method changes the examined parameter into two extreme values with keeping other parameters to be constant and only one parameter is examined at each time. The difference between the results from the two extreme cases can be used as the sensitivity indicator (Saltelli et al., 2000). Morris method, which is proposed by Morris (1991), is an advanced OAT method and it examines the effect of parameter in more detail (Saltelli et al., 2004). By performing this method, the range of the examined parameter is divided into N intervals with equal differential element. Then the element effect of each interval is calculated, and the overall effect of this parameter is evaluated by using the mean and variance of the element effect distribution. The procedure of Morris method is:

Step 1: Calculate a reference case (the case with a random selected value from the range of an examined input $x_j(1)$)

Step 2: Split the range of the input into N intervals with equal differential element Δ

Step 3: Calculate the element effect around the selected value using the following equation

$$d\big(x\,(1)\big) = \frac{y\big(x_1(1),\cdots x_{j-1}(1),x_j(1)+\Delta,\cdots,x_k(1)\big)-y(x(1))}{\Delta} \quad (2\text{-}24)$$

Step 4: Let x(2) be the new vector$(x_1(1), \cdots x_{j-1}(1), x_j(1) + \Delta, \cdots, x_k(1))$, repeat step 3, calculate the element effect d(x(2)). The same procedure is performed to calculate d(x(3))…d(x(n)), which constitutes F_j, the finite distribution of element effect.

Step 5: Calculate the mean μ and variance σ of F_j to evaluate the importance of x_j.

The Morris method can be considered as a global sensitivity analysis method because the examined parameter changes in every step and the final sensitivity measures are calculated by averaging at different points of the input space (Tian, 2013). However, if the F_i contains negative elements, which indicates the model is non-monotonic, the effects of the examined parameters may be underestimated by adding the negative values to the positive values. To overcome this drawback, Compolongo and Rossi (2002) proposed that the absolute values of the elementary effects should be considered to evaluate the influence of the examined parameter reasonably. Although this method is a global method, it belongs to one at a time experiment (OAT), which still cannot examine the interaction between the parameters. In addition, Morris method cannot quantify the variance of the output so it cannot provide uncertainty analysis.

2.2.3.3 Regression based methods-global method

Regression methods are based on the linear regression between input and output because they investigate the relationship between the output and input variables by linear model. By performing regression sensitivity analysis, the input and output variables are standardized and the influence of units are removed so that all the coefficients are in a comparable level (Iman and Helton, 1991). For equation 2-21, the input variables can be assigned as random values, which are sampled from their possible range according to the sampling techniques. Then each input variable can be considered as a vector, which contains the random values, and the random output values can be calculated accordingly. Therefore, equation 2-21 can be rewritten as a linear regression equation:

$$Y = f(X_1, X_2, \cdots X_n) \tag{2-25}$$

$$y_i = b_0 + \sum_j b_j x_{ij} + \varepsilon_i \quad i = 1,2, \ \cdots m, \ j = 1,2, \cdots n$$

where

$$Y = (y_1, y_2, \cdots, y_m)$$

$$X_1 = (x_{11}, x_{21}, \cdots, x_{m1})$$
$$X_2 = (x_{12}, x_{22}, \cdots, x_{m2})$$
$$\vdots$$
$$X_n = (x_{1n}, x_{2n}, \cdots x_{mn})$$

b_j - regression coefficient

Based on such a model, the standardized regression coefficient (SRC) can be calculated according to the following equation:

$$SRC = b_j \frac{s_y}{s_{xj}} \tag{2-26}$$

where

s_y - corrected standard deviation of Y

s_{xj} - corrected standard deviation of x_j

If the input variables are independent, the absolute value of SRC provides a measure of variable's importance, the input parameter with larger SRC has a higher importance than that with smaller SRC. The sign of the SRC indicates whether the output variable increase (positive SRC) or decrease (negative SRC) with the corresponding input variable (Helton and Davis, 2002). Another indicator to measure the relationship between input and output variable is correlation coefficient $r_{x,y}$, it is also calculated based on equation 2-27.

$$r_{x,y} = \frac{\sum_i^N (x_{ij} - \bar{x}_j)(y_i - \bar{y})}{[\sum_{i=1}^N (x_{ij} - \bar{x}_j)^2]^{1/2} [\sum_{i=1}^N (y_i - \bar{y})^2]^{1/2}} \tag{2-27}$$

The partial correlation coefficient (PCC) can be calculated based on correlation coefficient (Helton, 1993). PCC indicates the linear relationship between x_j and y after the linear effects of remaining input variables on y are removed. To calculate PCC, another two regression models should be built first:

$$\hat{x} = c_0 + \sum_{\substack{p=1 \\ p \neq j}}^{k} c_p \, x_p \tag{2-28}$$

$$\hat{y} = b_0 + \sum_{\substack{p=1 \\ p \neq j}}^{k} b_p \, x_p \tag{2-29}$$

Then the PCC is the correlation coefficient between two residuals $(x_j - \hat{x_j})$ and $(y - \hat{y})$ (Helton, 1993). The PCC and SRC produce the same ranking when the input variables are uncorrelated to each other. The reliability of the PCC and SRC relies on the linearity of the model. If the relations between input and output are nonlinear but monotonic, the partial ranked correlation coefficient (PRCC) and standardized ranked regression coefficient (SRRC) should be used to improve the linear relationship between the input and output (Helton and Davis, 2002). By performing SRRC or PRCC calculation, the input and output variables are assigned with values in their ranking order. For example, the smallest value is assigned as 1, the next smallest value is assigned as 2, etc. Then the SRC or PCC between ranked input variable and output variable is calculated as the sensitivity index. An example of calculating PRCC is shown in Figure 2.5

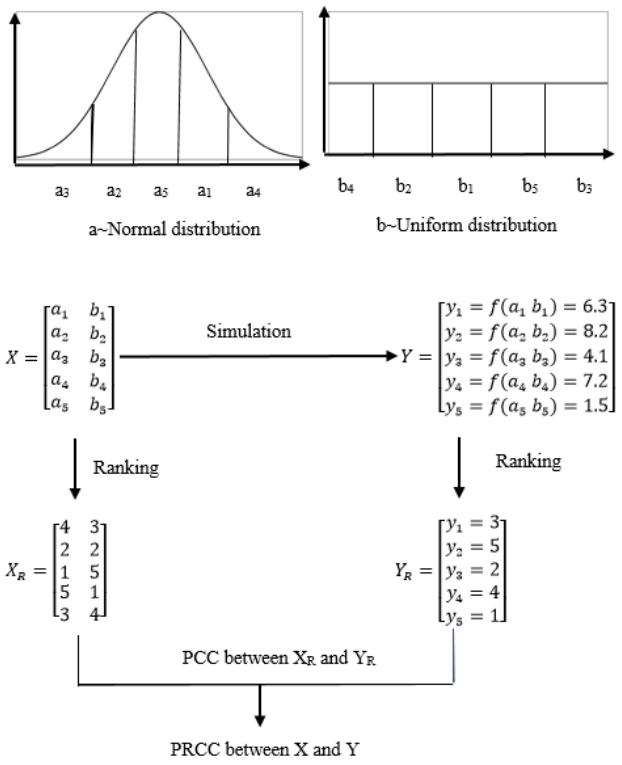

Figure 2.5 Procedure of calculating PRCC (Marino et al., 2008)

The PRCC and SRRC are in the range between -1.0 and +1.0. A value close to ±1.0 indicates significant monotonic relationship between inputs and output, while a value close to zero indicates a non-significant relationship between the inputs and output (Iman and Helton, 1991). As the

random values of the input parameter are sampled from their actual range, the regression sensitivity analysis can be considered as a global method. There are a number of sensitivity indicators that can be selected depending on different situations (linear, non-linear, correlated or un-correlated input parameters), the regression method is more flexible than screening-based method.

2.3 Uncertainties of HAM modelling

Although the HAM models have been well developed and commonly used for evaluating the hygrothermal performance of the building envelope, there are always discrepancies between the simulation results and the real hygrothermal performance. The factors that cause the discrepancies are the uncertainties of the HAM modelling, which can be categorized into four types: 1) enclosure uncertainty, 2) scenario uncertainty, 3) modelling uncertainty and 4) numerical uncertainty (De Wit, 2001; Macdonald, 2002; Moon, 2005; Zhao, 2012).

- Enclosure uncertainty is the uncertainties related to the building envelope itself, e.g., the uncertainties of material properties and material dimensions.
- Scenario uncertainty refers to all the external uncertainties in the simulation that do not come from the enclosure itself. For example, the uncertainties of climatic conditions and boundary conditions can be considered as scenario uncertainty.
- Modelling uncertainty is derived from the difference between physical phenomena and simplified mathematical description. For instance, the sorption and desorption curve is usually not differentiated in current HAM models.
- Numerical uncertainty is the errors introduced by the different numerical methods such as implicit methods, explicit methods, discretization strategies as well as convergence criteria.

This thesis mainly focuses on the enclosure uncertainty and scenario uncertainty, the modelling uncertainty and numerical uncertainty are not within the scope of this thesis.

In the field of building performance simulation, the influence of the input uncertainties are investigated by various uncertainty and sensitivity analysis methods (Macdonald, 2002; De Wit, 2001; Corrado and Mechri, 2009). As to hygrothermal simulations, the uncertainty and sensitivity analysis were also carried out to investigate the influence of material properties, boundary conditions as well as climatic conditions (Holm and Kunzel, 2001; Salonvaara et al., 2001; Zhao et al., 2011; Cornick et al., 2009; Pallin, 2013)

Holm and Kunzel (2001) applied one-factor-at-a-time (OFAT) sensitivity analysis to investigate the influence of material properties. An AAC flat roof model, which used the best estimated parameters, was set up as the base case. Then the examined parameters were changed from P to P+ΔP and from P to P-ΔP, where P was the value used in the base case and ΔP is the mean deviation for each parameter, and one parameter was changed at a time to generate a new case. The simulation was performed for each model with the changed parameter to calculate the amount of the moisture change after one year. The uncertainty of moisture change was investigated and the moisture influential parameters were identified. However, the OFAT analysis method changes one parameter at a time and does not consider the interaction among various parameters.

To take into account the interaction among various parameters, Salonvaara et al. (2001) performed stochastic modelling to study the uncertainties of material properties and their influence on the hygrothermal performance. The stochastic method employed by Salonvaara et al. (2001) is Monte-Carlo method. The material parameters were assumed to follow normal distribution based on their uncertainties, and all the parameters were changed simultaneously so that the interaction among the parameters can be considered. However, Salonvaara et al. (2001) only analyzed the moisture content range of the wall, the sensitivity of the moisture content to each material parameter was not studied. Zhao et al. (2011) extended the Monte Carlo stochastic method to take boundary conditions into consideration. The relationship between input and output was analyzed by partial correlation coefficient (PCC) and the important influential parameters, including the material properties and boundary conditions, were identified. They found that the PCCs, which represent the sensitivity of the moisture content to each influential parameter, were not constant and varied with time. In fact, the PCCs of the influential parameters are dependent on climatic conditions instead of time, therefore, the influence of the climatic conditions on the wall should be investigated as well. The moisture loads such as rain leakage and air leakage were not taken into account in Zhao's (2011) study.

For climatic conditions, the influence of uncertainty in rain data was investigated by Cornick et al. (2009). Ten locations representative of Canadian climate types were selected for analysis. The rain data of the coldest year for each location was selected as the basis for sensitivity analysis. Parametric study was performed by increasing or decreasing the base rain load by 20%, which was determined based on the general error between the measured rain data and the estimated rain data.

The moisture content and mold growth index of a typical wood frame wall was simulated over one year to evaluate the influence of the uncertainty of the rain data. The main conclusion of this study was that the variation of the rain data only caused a small change of the hygrothermal response of the wall for most climatic conditions. However, this conclusion was based on an ideal condition without considering rain leakage, which may significantly influence the hygrothermal performance of the wall.

In terms of indoor conditions, Pallin et al. (2011) developed a stochastic methodology to quantify the uncertainty of indoor moisture generation of different room types. The methodology was used for the hygrothermal risk assessment (Pallin, 2013). The assessment procedure was divided into qualitative risk evaluation and quantitative risk evaluation. Although the failure events such as air leakage or rain leakage were taken into account, they were only included in the qualitative risk evaluation, which was based on event tree analysis (ETA), fault tree analysis (FTA) or variation mode and effect analysis (VMEA) methods. These methods are different forms of organizing the failure events or influencing factors, they cannot quantify the uncertainty of the hygrothermal performance derived from the failure events.

The uncertainty and sensitivity analysis methods that have been used in the field of building physics are summarized by Janssen et al. (2013), and a probability assessment framework was established by Kalagasidis et al. (2013). However, there is a lack of systematical methodology to quantify the uncertainty of the hygrothermal performance caused by moisture loads. And the highly insulated walls were not investigated using stochastic approach.

2.4 Hygrothermal performance of highly insulated wood framed walls

NRC-IRC researchers investigated the hygrothermal performance of two types of exterior insulated wood framed walls- XPS and semi-rigid mineral fiber insulation by field experimental study, and compared their performance with conventional 2x6 wood framed wall with fiber glass installed in the stud cavity (Maref et al., 2010). The temperature, relative humidity at most layers of the wall assemblies, and the moisture content of wood-based materials were monitored from fall 2007 to summer 2008 in Ottawa, the cold climate zone. The measured results showed that adding external insulation reduces the potential of interstitial condensation, and air leakage is a significant factor that transports moisture into wall assemblies. Similar conclusion was also

obtained by Smegal et al. (2013), who compared XPS exterior insulation wall with the conventional 2x6 wood framed wall in mild-humid climate zone. It was found that the wall with external XPS insulation has lower moisture durability risks than conventional 2x6 wall. However, the wall without external insulation has a higher drying rate than external insulated wall after rain events.

In terms of deep cavity wall, Arena et al. (2013) conducted field measurement study for R-40 double stud wall with cellulose fiber was installed for stud insulation. The hygrothermal performance of the investigated wall was monitored from July 2012 to mid-April 2013 under climate zone 5A, and the measured data was compared with hygrothermal modelling results from WUFI. There was a reasonable agreement between the measured results and simulation results, the results showed that the investigated walls were failed according to ASHRAE Standard 160 - 30 days criterion for mold growth. The condensation potential was investigated by comparing the monitored and simulated temperature with the dew point of the condensation surface, and it was found there was a high condensation potential.

Fox (2014) conducted field experimental study to investigate the hygorthermal performance of highly insulated wood framed walls and the impact of air leakage. The hygrothermal performance of two types of deep cavity walls (double stud wall and I-joist wall) and three types of exterior insulated walls (polyisocyanurate wall, XPS wall and mineral wool wall) were monitored from Oct. 2012 to Jun. 2013 under cold climatic condition with controlled air leakage rate. It was found that the exterior insulated wall performs better than the deep cavity wall in terms of reducing condensation potential and mold growth risk. The hygrothermal models were created based on the tested walls, and calibrated by comparing the measured results and simulation results. Although the calibrated models can be used to investigate the walls under other climate conditions, the uncertainties of the material properties and moisture loads may result in the moisture problem risks, which cannot be revealed by the deterministic models.

2.5 Summary

Many hygrothermal simulation tools are developed based on the HAM models and became powerful tools for predicting the hygrothermal performance of wood framed walls. The reliability of the simulation programs are generally evaluated by comparing the simulation results and the experiment results before they are widely used for hygrothermal performance evaluation.

Discrepancies are always found between the simulation results and the measurement results. Stochastic uncertainty and sensitivity analysis methods have been used to investigate the factors that influence the simulation results, and the moisture problem risks. However, the impact of the moisture loads, such as air leakage and rain leakage, were not taken into account in previous studies.

The investigations of highly insulated wood framed walls have confirmed exterior insulated walls have lower risk of interstitial condensation and mold growth than deep cavity walls, and air leakage is a significant factor that influences the moisture performance. However, the variability of air leakage may result in a higher moisture content level of the wood sheathings than those observed in experimental study and deterministic hygrothermal modelling. Additionally, the impact of rain leakage was not well investigated in previous studies.

This thesis aims to address the knowledge gaps identified and to develop a stochastic modelling framework to analyze the moisture performance of wood framed building envelopes under various moisture loads such as air leakage and rain leakage. And the sensitivity of the moisture performance to each influential factor is evaluated as well.

Chapter 3. Development of stochastic modelling methodology

To fulfill the knowledge gaps stated in section 2.5, a stochastic modelling methodology is developed in this chapter. The developed methodology should have the following features to solve the targeted problems:

- Include a reliable hygrothermal modelling program that is able to simulate the transient heat and moisture transports in wood frame walls, and the hygrothermal model file can be accessed and modified repeatedly to generate stochastic cases.
- The probability distribution of the stochastic variables is well defined. An advanced sampling technique is applied to generate stochastic cases, which are composed of the stochastic parameters.
- The influential factors, including the material properties and moisture loads, are well organized to observe the uncertainty of the hygrothermal performance and the significance of stochastic variables at different moisture load levels.

3.1 Comparison between WUFI and DELPHIN

As stated in section 2.1.1, there are two ways to describe the moisture storage property: moisture storage curve and moisture retention curve. Most of the hygrothermal modeling programs are developed based on these two methods. The most commonly used commercial hygrothermal modeling programs are WUFI, which is developed based on moisture storage curve, and DELPHIN, which is developed based on moisture retention curve. WUFI is developed by Fraunhofer Institute for Building Physics, the main theories behind WUFI is from Kunzel (1995). DLPHIN is developed by Dresden University of Technology, the most relating theories about DELPHIN can be found in Scheffler (2008). Both WUFI and DELPHIN have been fully developed, and can be applied in hygrothermal analysis. The differences in material properties between WUFI and DELPHIN are presented in Table 3.1 and Table 3.2.

Table 3.1 Comparison of moisture storage parameters between WUFI and DELPHIN

WUFI	DELPHIN
1. Open Porosity (-): Open porosity can be used to determine the maximum moisture content.	1. Open Porosity (-): Open porosity can be used to determine the maximum moisture content. It is the same as defined in WUFI.
2. Free saturation (kg/m^3): A capillary active material in contact with water will take up this water until it reaches its free saturation.	2. Effective saturation moisture content (m^3/m^3): The effective saturation moisture content is a long term saturation. It is greater than or equal to the capillary saturation moisture content
	3. Capillary saturation moisture content (m^3/m^3): The capillary saturation moisture content is the mean moisture content of a sample obtained in the water uptake experiment at the end of the first water uptake period.
3. Reference moisture content (kg/m^3): Reference moisture content is the moisture content at RH-80%. It can be used to approximate the moisture storage function.	4. Moisture content at RH-80% (m^3/m^3): Hygroscopic moisture content at RH-80% obtained in a hygroscopic absorption experiment. It should match the absorption isotherm at RH-80%.
	5. Limitation hygroscopic moisture content (m^3/m^3): Limitation hygroscopic moisture content for those materials that must not get wet. May be used as indicator for materials that shall be subjected to hygroscopic moisture loads only, such as most insulation materials.

Table 3.2 Comparison of moisture transport properties between WUFI and DELPHIN

WUFI	DELPHIN
1.Vapour diffusion resistance factor (-): It is the factor by which the vapour diffusion in the material is impeded, as compared to diffusion in air.	1.Vapour permeability (kg/s·m·Pa) : $g_{vd} = -\delta \nabla p$ where δ- vapour permeability(kg/m·s·Pa) ∇p- vapour gradient 2. Vapour diffusion resistance factor (-) : Same as WUFI
2. Water absorption coefficient (kg/m^2·s$^{0.5}$): The water absorption coefficient is the slope of the line of mass increase against the square root of time divided by the area of the surface in contact with water.	3.Water absorption coefficient (kg/m^2·s$^{0.5}$) : Same as WUFI
3. Moisture diffusivity (m^2/s): $g_l = -D_w \nabla w$ where D_w- moisture diffusivity (m^2/s) ∇w- moisture content gradient	4. Liquid conductivity (kg/m·s·Pa): $g_l = K_l \nabla p_c$ where K_l-liquid conductivity (kg/m·s·Pa) ∇p_c- capillary pressure gradient

The parameters used in WUFI are based on the moisture storage curve method, and those used in DELPHIN are based on the moisture retention curve method. However DELPHIN allows user input moisture storage function and moisture diffusivity to describe the moisture storage and liquid transport properties, and it is able to convert such parameters into moisture retention curve and liquid conductivity for calculation.

In terms of boundary conditions, there is no difference in heat and vapour exchange coefficients, short and long wave radiation coefficients between WUFI and DELPHIN. However, the rain factor are different between WUFI and DELPHIN because they use different wind-driven rain model to calculate the wind driven rain. In WUFI, there are two methods to calculate the wind-driven rain. Firstly, the wind-driven rain load can be calculated by the following equation:

$$r_{bv} = r_h \cdot (R_1 + R_2 \cdot U \cdot \cos\theta) \quad (3\text{-}1)$$

where

R_1 & R_2 – Rain factor. They are strongly dependent on the specific location on the building façade. For vertical surfaces, R_1 is zero. R_2 is about 0.2 s/m for free standing locations without influence from surrounding buildings; it is markedly less in the center of façade; it is greater at exposed locations of a building. Users can define R_2.

U - hourly average wind speed at 10m (m/s)

θ - angle between wind direction and normal to the wall

r_h - rainfall intensity, horizontal surface (mm/h)

r_{bv} - rain deposition on vertical wall ($kg/m^2 \cdot h$)

Alternatively, the wind-driven rain load on a vertical wall can be estimated using the method by ASHRAE Standard 160 (2016):

$$r_{bv} = F_E \cdot F_D \cdot F_L \cdot U \cdot \cos\theta \cdot r_h \quad (3\text{-}2)$$

where

F_E - rain exposure factor

F_D - rain deposition factor

F_L - empirical constant, 0.2 ($kg \cdot s/m^3 \cdot mm$)

U - hourly average wind speed at 10m (m/s)

θ - angle between wind direction and normal to the wall

r_h - rainfall intensity, horizontal surface (mm/h)

r_{bv} - rain deposition on vertical wall (kg/m^2·h)

In DELPHIN, the wind-driven rain can be calculated by using the following equation:

$$j_{rain\_nor} = k_{wind} \cdot k_{rain} \cdot j_{rain\_hor} \quad (3\text{-}3)$$

where

k_{wind} - wind coefficient

k_{rain} - rain exposure coefficient

$j_{rain.hor}$ - rain flux density on a horizontal plane, (kg/m^2·s)

$j_{rain.nor}$ - rain flux density normal to the wall surface (wind-driven rain), (kg/m^2·s)

The wind coefficient can be calculated by the following equation:

$$k_{wind} = \begin{cases} 0 & \text{if} \left(\beta_{wind} \geq \frac{\pi}{2}\right) \text{or} (v_{wind} \leq 0) \\ \frac{\cos(\beta_{wind})}{\sqrt{1+1141 \cdot \sqrt{\frac{3600 \cdot j_{rain.hor}}{v_{wind}^4}}}} \cdot \exp\left(-\frac{12}{5 \cdot \sqrt{3600 \cdot j_{rian.hor}}}\right) \end{cases} \quad (3\text{-}4)$$

$$\beta_{wind} = \begin{cases} |\alpha_{wall} - \alpha_{wind}| & \text{if } |\alpha_{wall} - \alpha_{wind}| \leq \pi \\ \text{else} & 2\pi - |\alpha_{wall} - \alpha_{wind}| \end{cases} \quad (3\text{-}5)$$

where

α_{wall} - wall orientation, (Deg)

α_{wind} - wind direction, (Deg)

v_{wind} - wind velocity, (m/s)

The hourly wind-driven rain calculated outside of DELPHIN can be directly imposed on the exterior surface of the wall as imposed water flux. Therefore, users can calculate the wind-driven rain by using the model other than the built-in rain model in DELPHIN.

The climatic parameters including temperature, relative humidity, direct solar radiation, diffuse solar radiation, wind speed, wind direction and horizontal rain data, required by WUFI is the same as those by DELPHIN. In WUFI, there is a built-in climate database, which includes most cities in Europe and North America, and the customized weather data can also be used. However, there

is no built-in climate database in DELPHIN, users can only define the customized weather data according to the data format that is accepted by DELPHIN.

The calculation model in WUFI includes heat and moisture balance equations. The moisture balance equation is based on moisture storage curve method with the relative humidity being used as the driving potential. The calculation model in DLEPHIN includes heat and moisture balance equations and air flow model. The moisture balance equation is based on moisture retention curve method with the capillary pressure is used as the driving potential. As shown in Figure 2.1, for moisture storage curve, the relationship between moisture content and relative humidity cannot be well interpreted in the high relative humidity region because the curve becomes dramatically steep in this region. The moisture retention curve is more proper to describe the moisture storage property in the high relative humidity region.

The stochastic simulation needs the hygrothermal simulations with the random parameters to be carried out repeatedly. Therefore, the hygrothermal model file should be accessed and modified in other programing environment such as Python and MATLAB, and the calculation engine should be called outside the hygrothermal program. WUFI project files cannot be accessed outside the program and the simulation has to be performed inside the program, while DELPHIN project files and calculation engine can be accessed in other programing environment, therefore, DELPHIN is more suitable for stochastic analysis.

3.2 Stochastic variables

In the hygrothermal simulation tools, the input parameters are assigned with deterministic values, which are the mean values determined from lab measurements or empirical correlations. In the stochastic framework, the input parameters should be assigned with stochastic values, which are generated from the probability distribution of the parameter based on the statistical figures such as mean value and standard deviation.

3.2.1 Material properties

The uncertainty of material properties is inevitable due to their inhomogeneous nature, the workmanship quality during manufacture process, and the different measurement procedures. The material properties collected from different laboratories may have large variances (Roels et al., 2004). The variances can also be observed even the properties are obtained from the same

laboratory with standard test procedure (Bomberg et al., 2005; Kumaran et al., 2006). In general, the material properties measured in laboratory are reported with the mean value and standard deviation, which can be used for defining the probability distribution of the material properties. They are generally assumed as a normal distribution. The stochastic values of the parameter can be generated based on the probability distribution. The material property functions, such as the moisture storage function, moisture diffusivity as a function of moisture content, and vapour resistance factor as a function of moisture content, can be scaled by multiplying a coefficient: parameter_stochastic/parameter_mean.

Due to the cost and time required by laboratory tests, typically there are only a few test points available to generate the material property function. For example, there are only three test points of sorption isotherm of OSB to form the moisture storage function from relative humidity 50% to 93% (Kumaran et al., 2002), but the hygrothermal simulation needs the moisture storage function to cover the whole RH range from 0% to 100%. The pressure plate method can be used to obtain the moisture retention curve, which describes the relationship between moisture content and capillary pressure at high RH level. And the capillary pressure can be converted to RH to complement the moisture storage function at RH level higher than 93%. Zhao (2012) proposed a method of completing moisture storage data based on cluster and regression methods. However, a large number of material samples need to be tested for cluster and regression analysis. Alternatively, the data can be completed based on the analytical equations, which are proposed by Kunzel (1995). It can also be completed by interpolation. The analytical equation or interpolation method is easier to implement in hygrothermal modelling.

3.2.2 Boundary conditions

The uncertainties of the boundary conditions is derived from the environmental conditions, surface properties, such as the roughness and color, and design strategies. For example, the deposition rain factor is dependent on the type of the roof, height of the building, and the surrounding terrain (ASHRAE, 2016). The deposition rain factor is generally assumed from 0.35 to 1, the values between 0.35 and 1 is assumed to have the same probability when the design information of the building is not completed. Therefore, the deposition rain factor can be considered as a uniform distribution. Other boundary conditions such as heat exchange coefficient, vapour exchange

coefficient, long-wave and short-wave radiation coefficient can be assigned as a normal distribution. It was found that the uncertainties of surface exchange coefficients have insignificant influence on moisture performance of the wood framed walls (Zhao, 2012), therefore they are not considered as stochastic variable in this thesis.

3.2.3 Moisture loads

The moisture loads of wood framed building envelope can be from four primary sources, 1) liquid water from precipitation; 2) water vapour, from exterior and from activities and process within the building; 3) liquid and vapour from the soil adjoining the building; 4) built-in moisture from construction materials or moisture brought in with goods and people (Straube, 2002). This thesis mainly focuses on water vapour from indoor environment and the liquid water from precipitation. The water vapour can be transported by vapour diffusion and vapour convection, which is brought by the air penetrated into the wall assembly. The amount of water vapour transported into the wall assembly depends on the indoor moisture load and air leakage rate. The liquid water from precipitation is described by wind-driven rain, which is deposited on the exterior wall surface. Considering the defects of the rain defense layers, the rain water can penetrate into the wall assembly and is directly deposited on the wood sheathing. Therefore, the rain leakage rate is a critical parameter describing the amount of the wind-driven rain that is penetrated into the wall assembly. The following sections discuss the uncertainties of the internal moisture load, air leakage rate, wind-driven rain and rain leakage rate.

Internal moisture load

Moisture excess, which is defined as the difference between indoor and outdoor moisture concentration, is commonly used as an indicator of internal moisture load level. However, it cannot be used as an input parameter in hygrothermal simulation programs. The hygrothermal simulation programs use indoor temperature and relative humidity to describe the indoor condition.

There are many research projects collecting the data of indoor temperature and relative humidity from different rooms or buildings, which aim to establish stochastic inputs for hygrothermal simulations (M.M.Ramos and Grunewald, 2015). In Canada, a research project investigating the indoor temperature and relative humidity was conducted by Tariku and Simpson (2014). The indoor temperature and relative humidity of four suites (suite A, B, C, D) in a multi-unit residential

building in Vancouver were monitored from May 2010 to Oct. 2011. The selected four suits represent different occupant density, floor area and physical orientations. The monitored data was statistically analyzed to obtain the internal moisture load level. It was concluded that the seasonal average moisture excess distributions in the four suites can be classified into low level (suite A and D, which have 3 and 2 occupants respectively) and high level (suite B and C, which have 4 and 6 occupants respectively). The rooms with the same function have similar moisture excess, e.g. the kitchen generally has the highest moisture excess, while the living rooms and bedrooms generally have a lower moisture excess. The seasonal standard deviation of the moisture excess in different rooms is ranging from 0.8 g/m^3 to 1.2 g/m^3 except for suite A, which has a standard deviation of 3.8 g/m^3 in winter time, and such significant fluctuation is caused by the usage of portable humidifier. However, the seasonal standard deviation describes the periodical variation of moisture excess, it does not reflect the uncertainty of the moisture excess among different rooms or suites, which depends on the usage pattern, such as the occupancy density and moisture generation rate. The data collected by Tariku and Simpson (2014) is valuable to categorize typical moisture load level, but cannot be used as stochastic inputs.

Alternatively, there are different empirical models to define indoor temperature and relative humidity at different moisture load level (EN13788, EN15026, ASHRAE 160). In Europe, the EN13788 and EN15026 define indoor RH/T based on outdoor climatic condition and indoor moisture excess level. In North America, ASHRAE 160 (2016) provides three methods to define indoor design relative humidity: simplified method, intermediate method and full parametric calculation. In simplified method, the indoor relative humidity is determined based on daily average outdoor relative humidity. The intermediate method involves more factors to define indoor relative humidity, such as air conditioning type (heating-only, AC with or without dehumidification), number of occupant and air change rate. The full parametric calculation requires a comprehensive hygrothermal model that considers heat and moisture balance between interior surface and indoor air including the moisture buffering effects of interior finishes and furniture. The information required by full parametric calculation method is almost equivalent to hygrothermal simulation. The intermediate method considers more factors than simplified method and it is easier to implement than full parametric method, therefore, this method is adopted by WUFI to define the indoor temperature and relative humidity. Different combinations of the

influential factors give different moisture excess level, and the indoor temperature and relative humidity are generated accordingly. This thesis takes occupants number as the scenario variable to obtain representative moisture load levels.

Air leakage rate

Air leakage is one of the important moisture loads that may increase the risk of moisture problems of wood framed walls (Janssens and Hens, 2003; TenWolde and Rose, 1996). The potential moisture damage caused by air leakage in conventional light wood framed walls installed with low water vapour permeable exterior insulation has been identified (Armstrong et al., 2010), the moist indoor air can exfiltrate through wall assemblies and condense at surfaces below its dew point, such as wood sheathing. In ANNEX 55, the airtightness level of residential buildings is widely investigated and eight European countries reported their collected data, which can be used as stochastic inputs. Chen et al. (2012) summarized the air leakage database for five countries: Czech Republic, France, Germany, UK and USA. The air leakage data reported in the database is measured by standardized procedure, generally fan pressurization test (ASTM, 2010) for residential building or air-handling equipment test (CGSB, 1996) for commercial building. The air leakage data measured from fan pressurization test is generally reported as air change rate (ACH, 1/h) or air leakage rate (m^3/h), which is based on the whole building. To investigate the air leakage through a wall, the total air leakage rate has to be averaged to each side of the wall assemblies. Emmerich and Persily (2014) developed the air leakage database for commercial building envelope in United State to support sustainable building design. This database also includes the 5-side and 6-side averaged air leakage rate through a wall assembly ($m^3/h{\cdot}m^2$). The air leakage rates of two groups of buildings were reported: 79 buildings with air barrier and 290 buildings without specifically indicating having an air barrier. It was found that the air leakage rate of the 79 buildings with air barrier (5.0 ± 3.7 $m^3/h{\cdot}m^2$) is almost 70% less than the 290 buildings without specifically indicating having an air barrier (15.6 ± 11.9 $m^3/h{\cdot}m^2$). The reported data is tested under 75 Pa pressure difference between indoor and outdoor. These data can be converted to the values under 5Pa, which represents natural condition, to be used as the stochastic inputs. Although Emmerich and Persily's air leakage database mainly focuses on commercial buildings, the data averaged to single wall assembly is also applicable to wood framed residential building (ASHRAE Fundamental, 2013).

Beside the uncertainty in air leakage rate, the impact of air leakage is also influenced by air path and the amount of air reaching the condensation plane. To consider such uncertainties, chapter 5 develops a method based on one-dimensional hygrothermal simulation to investigate the impact of air leakage.

Rain leakage rate

For a given climatic condition, the amount of rainwater deposited on the wall assembly is dependent on the topography surroundings the building and the structure of the building itself such as the type of the roof, the installation of overhang (ASHRAE 160, 2016). Considering the defects of the rain defense layers, such as the wall cladding, air cavity and water resistive barrier, the rain leakage rate is a critical parameter describing the amount of wind-driven rain that is penetrated into the wall assembly. There are few studies investigate the amount of the rainwater penetrating into the wall assembly. ASHRAE 160 (2016) proposed that 1% of the rain water reaching the exterior cladding surface can be deposited on the exterior surface of water resistive barrier to simulate the rain leakage. Kunzel and Zirkelbach (2012) applied ASHRAE 160 method on External Thermal Insulation Composite System (ETICS) to simulate moisture performance under rain leakage. Simulations were performed for five selected locations, where the amount of wind-driven rain in the most exposed orientations are ranging from 112 $l/m^2 \cdot a$ to 193 $l/m^2 \cdot a$. The moisture sources of 1%, 2%, 3% and 4% wind-driven rain were deposited evenly on the OSB sheathing. It was found that the 1% and 2% of rain leakage does not result in any moisture issue, the 3% and 4% of rain leakage lead to a risky moisture content (higher than 20%) of OSB sheathing. However, the uncertainty of rain deposition factor, which reflects the topography surroundings and the structure of the building and thereafter influence the amount of wind-driven rain, was not taken into account. Ott et al. (2015) also evaluated the ASHRAE 160 method by depositing 1% wind-driven rain on two positions: the exterior surface of WRB and the exterior surface of insulation, which is behind the WRB. It was found that depositing the rain leakage on the exterior surface of WRB does not give the satisfying results since the defect of the WRB is not taken into account. While, depositing the rain leakage behind the WRB increases the moisture content of insulation and adjacent layer by factor of 20-30, which is abnormally high. However, the amount of annual wind-driven rain, which significantly influences the moisture content level, was not clearly specified.

The conclusions of the impact of rain leakage may be different under different circumstances, e.g. the amount of precipitation, the deposition factor, which influences the amount of wind-driven rain. For a given climatic condition, the rain deposition factor can be considered as a stochastic variable to reflect the variation of the wind-driven rain. The amount of rain leakage (percentage of wind-driven rain) is still disputable between the magnitude of 0.1% and 1%. Since there are not enough experimental studies to prove the range of rain leakage, this thesis performs two sets of simulations with different levels of rain leakage (0.1% and 1% of wind-driven rain) to establish a threshold that may result in moisture problem.

3.3 Stochastic case generation

As stated in section in section 2.3, this thesis mainly focuses on enclosure uncertainties and scenario uncertainties. Therefore, the input parameters are also categorized into enclosure parameters, which describe the material properties of the building envelope, and scenario parameters, which are related to moisture loads. The parameters that describe material properties can be considered as stochastic variables because every value falls into the range of the parameter that is possible to occur. The parameters that describe moisture load levels such as air leakage rate and rain leakage rate can be considered as stochastic variables as well. Standard stochastic analysis procedure can be performed to obtain the stochastic results of moisture content or mold growth index, which are used to evaluate the moisture damage risks, and sensitivity indexes, which are used to evaluate the influence of material properties and moisture loads. The sensitivity indexes obtained from regression analysis only reflect the significance of the relationships between input and output variables, but they cannot reflect how much uncertainty is caused by a specific variable. To evaluate the impact of moisture loads, it is necessary to know the increment of the results' uncertainty under a specific type of moisture load. Therefore, the type of moisture load is considered as scenario variable with only two states "happen" or "not happen", thereby the hygrothermal performance of the wood framed wall can be observed under different types of moisture loads.

3.3.1 Sampling technique for stochastic variables

The simplest sampling technique is random sampling. The random sampling technique takes all the generated random values from the probability distribution into hygrothermal simulation. The

random values of different parameters are combined randomly to generate the stochastic cases. The random sampling technique is a computationally expensive and time consuming method because the simulation has to be performed for hundreds of times to guarantee the sampling convergence (Janssen, 2013).

Latin Hypercube Sampling technique is a high efficiency sampling technique. By using the Latin Hypercube Sampling technique, the probability distribution is divided into n intervals with equal probability. Then the random value from each interval can only be selected once to ensure that there is no overlapping. The number of simulations required can be reduced using this method. With the consideration of sampling convergence and efficiency, Latin Hypercube Sampling technique will be used in the stochastic modelling framework.

3.3.2 Factorial design for scenario variables

For scenario variables, which reflect the types of moisture loads, factorial design can be applied to examine the impact of each type of moisture load and their combinations. Each scenario variable can be assigned with two values "+" (on) or "-" (off). The combinations of the scenario variables represent different scenarios. For each scenario, the stochastic cases, including the stochastic variables of material properties and moisture loads will be generated using the LHS method. The procedure of stochastic cases generation is presented in Figure 3.1.

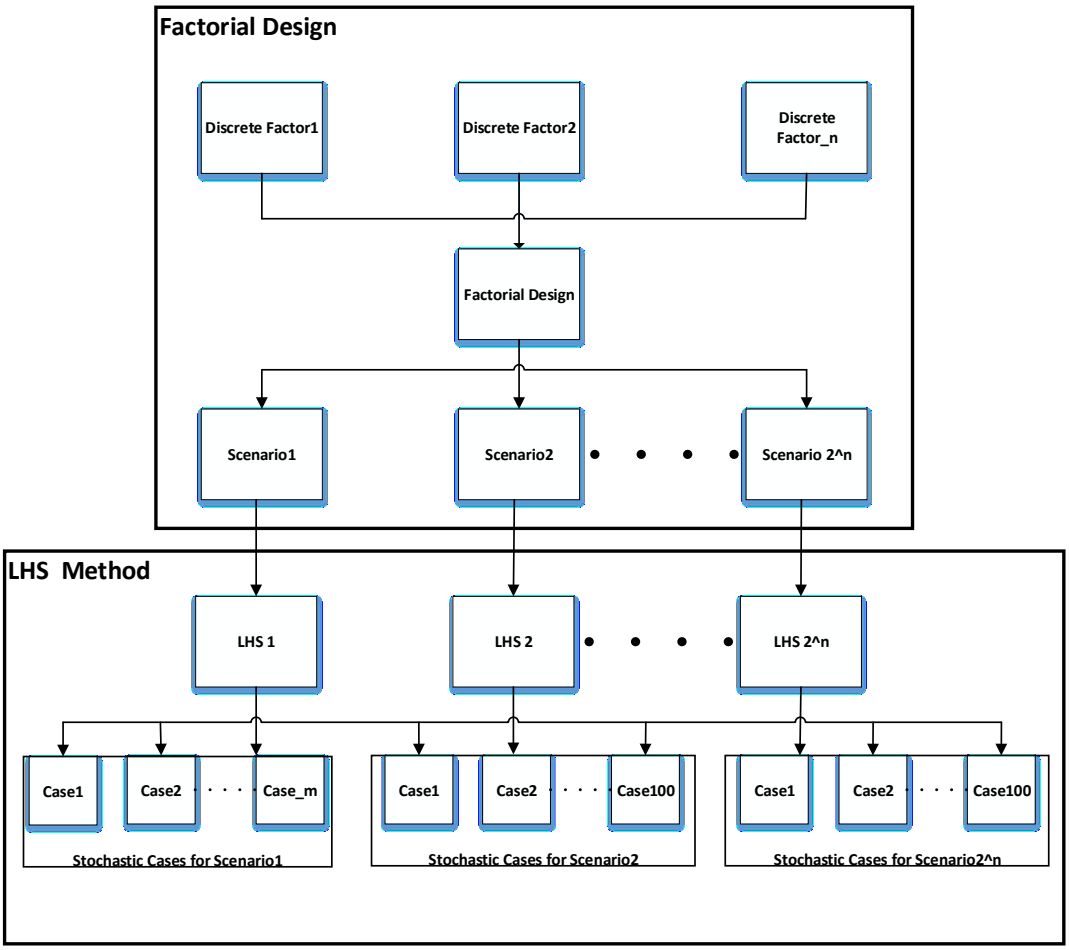

Figure 3.1 Stochastic cases generation

3.4 Stochastic modelling framework design

The stochastic modelling framework will be based on DELPHIN, the validated hygrothermal simulation program and MATLAB, the programing environment that is able to access DELPHIN project file and simulation engine. The stochastic simulation will be performed according to the following steps:

1) The hygrothermal model using mean values will be created in DELPHIN as a base case.

2) The base case will be imported into stochastic parameter generator to generate the stochastic cases.

3) The simulation engine will be called in MATLAB to run the simulations for the stochastic cases repeatedly.

4) The uncertainty and sensitivity analysis will be performed based on the stochastic results to investigate the probability of moisture problem and the influence of the parameters.

The stochastic procedure is presented in Figure 3.2:

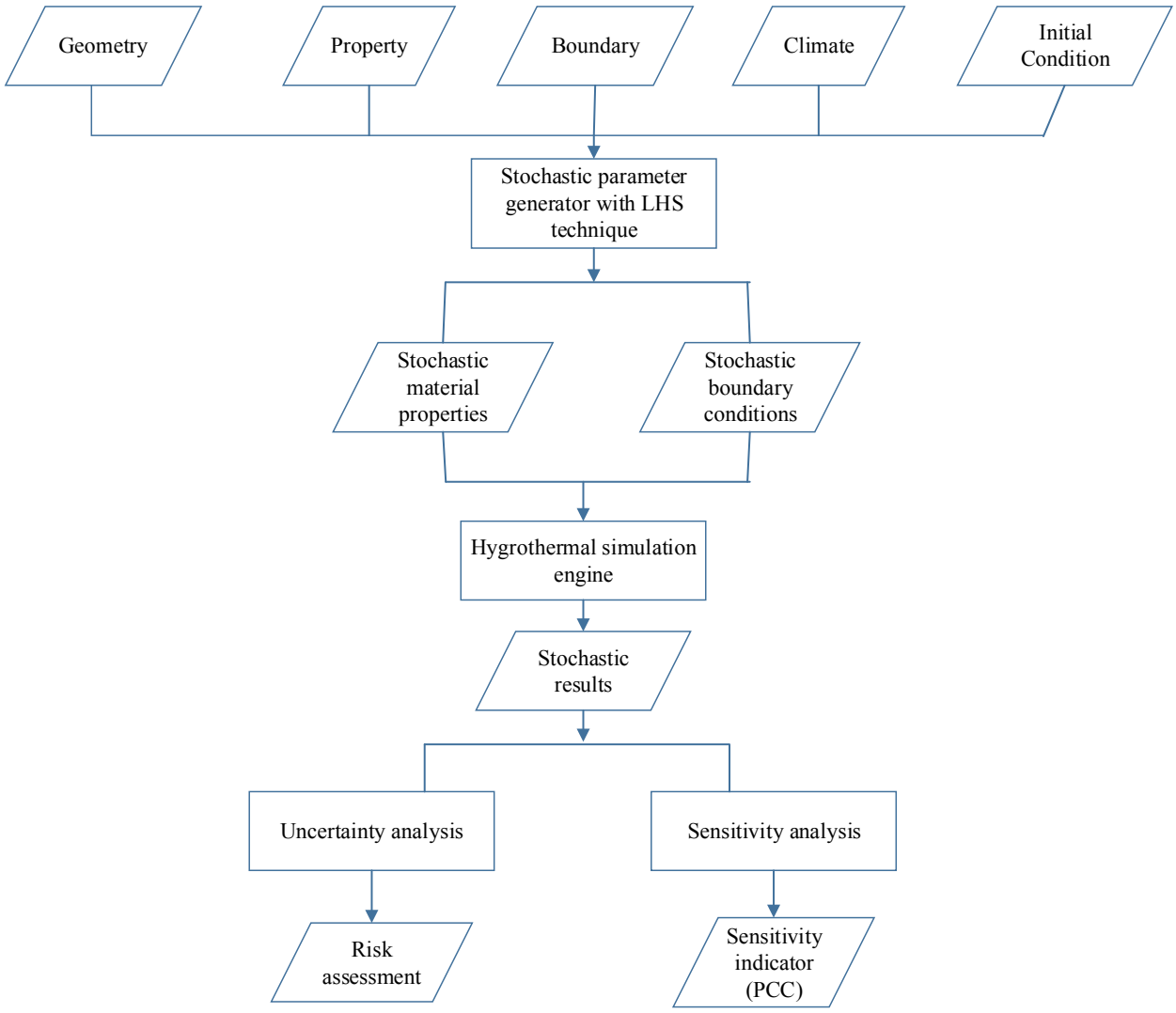

Figure 3.2 Stochastic simulation procedure

The stochastic modelling procedure will be performed for each scenario that is represented by the combination of the moisture loads. Combining Figure 3.1 with Figure 3.2, the stochastic modelling framework is established. Then the moisture problem risks can be evaluated under different moisture loads by comparing the uncertainty of the hygrothermal performance for each scenario.

3.5 Stochastic hygrothermal analysis tool

Based on the stochastic modelling framework introduced above, a stochastic hygrothermal analysis tool can be developed based on DELPHIN and MATLAB, and it will be able to perform the stochastic hygrothermal analysis of wood framed walls. The structure of the stochastic analysis tool is presented in Figure 3.3.

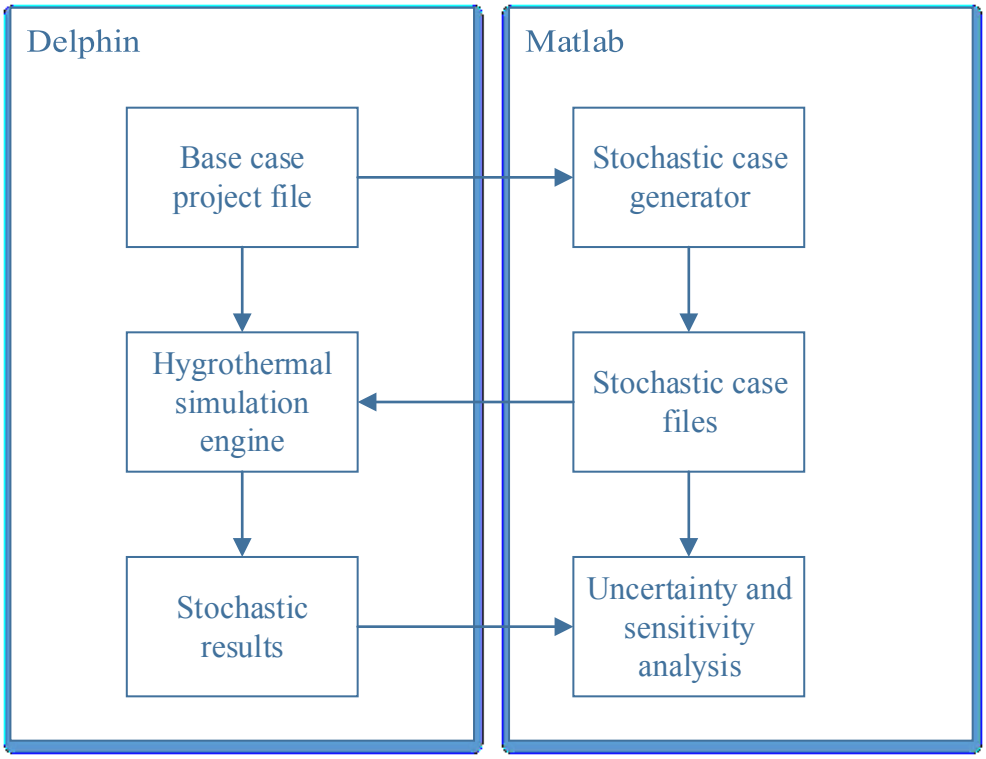

Figure 3.3 Structure of stochastic hygrothermal analysis tool

3.6 Summary

This chapter develops a stochastic modelling methodology, which can be used to evaluate the hygrothermal performance of the wood framed walls under different moisture loads. The main works of this chapter are:

- The most commonly used commercial hygrothermal simulation programs – WUFI and DELPHIN are compared from input parameters and simulation methods.
- A comprehensive survey is conducted to determine the range of the stochastic variables including the material properties, air leakage rate and rain deposition factor.
- The influential factors are categorized into stochastic variables and scenario variables, Latin Hypercube Sampling technique and Factorial Design can be combined to generate the stochastic cases under different moisture loads.
- A stochastic modelling tool, which is based on DELPHIN and MATLAB, is developed to implement stochastic simulation.

Chapter 4 Hygrothermal model validation and parametric study of CLT wall assemblies

This chapter presents the validation and inter-program verification of the hygrothermal models of cross-laminated timber (CLT) wall assemblies. The validated models are used for uncertainty and sensitivity analysis using one-factor-at-a-time method.

CLT panels have a potential market in North America for building mid-rise or even taller structures due to their good structural and fire safety performance, carbon storage capacity, light weight, and prefabricated nature (Gagnon and Pirvu, 2011; Karacabeyli and Douglas, 2013). There were several studies that focused on the wetting and drying behavior of wood products including CLT panels. Some of these studies were based on hygrothermal simulation using WUFI (Haglund, 2011; Goto et al., 2011; Kalamees and Vinha, 2003; Hameury et al., 2005). Although WUFI has been widely used in hygrothermal modeling, there are known difficulties and limitations in modeling the hygrothermal behavior of wood products by only using a Fickian model, particularly under high relative humidity and transient conditions (Hakansson, 1998; Peuhkuri, 2003; Wang et al., 2014; Wadso, 1994). Other studies were focused on measurements, including laboratory (Lepage, 2012) and field measurements (McClung et al., 2014). However, such experiments can only investigate the hygrothermal performance under specific environmental conditions with specific material properties. Laboratory measurements have shown significant uncertainties in material properties. Such uncertainties may lead to moisture risks, which may not be revealed under experimental conditions. Therefore, the uncertainties of material properties should be taken into account when evaluating the hygrothermal performance of CLT panels. The influence of various environmental loads and the uncertainties of material properties can only be comprehensively evaluated by a reliable hygrothermal model, which should be validated first.

The hygrothermal performance of sixteen CLT wall assemblies with various design configurations were tested in a building envelope test facility by McClung et al. (2014). Discrepancies between simulation results from WUFI and measurements were observed in the previous study. To further investigate the discrepancies between simulation results and measurements, the uncertainties in simulations caused by the uncertainties in input parameters including material properties and boundary conditions under different environmental loads are studied through sensitivity analyses.

In this chapter, one-factor-at-a-time (OFAT) method is employed for the sensitivity analysis and applied in two commercial hygrothermal simulation programs, WUFI and DELPHIN. Simulation results from both DELPHIN and WUFI are compared with measurements for validation. The validated models are used for sensitivity analyses to evaluate the influence material properties and boundary conditions.

4.1 Experimental setup

The hygrothermal performance of sixteen 0.6 m by 0.6 m CLT panels made of five different wood species (or species groups) and four different wall configurations was monitored over a two-year period under the climatic conditions of Waterloo, Ontario (McClung et al., 2014) . Two main parameters studied in this experiment were wood species of CLT panels and wall configurations in terms of the combined vapour permeance of exterior insulation with water resistive barrier outboard of the CLT panels.

In general, the configuration of each test wall included a structural CLT panel on the interior, followed by a rainwater and air control layer, i.e. the water resistive barrier (WRB), exterior insulation, and rain-screen fibre cement panel with a 19 mm air cavity behind the cladding created by plywood furring spaced at 400 mm. There are two types of self-adhesive WRB on the outside of the CLT panels, a vapour permeable (VP) WRB and a non-vapour permeable (NVP) WRB. In combination with two types of exterior insulations, four categories of wall assemblies with three levels of vapour permeance were created: 1) Low exterior permeance - NVP membrane and mineral wool insulation (with a combined permeance of 1.6 ng/Pa·s·m^2); 2) High exterior permeance - VP membrane and mineral wool insulation (with a combined permeance of 975 ng/Pa·s·m^2); 3) Medium exterior permeance - VP membrane and expanded polystyrene (EPS) insulation (with a combined permeance of 64.4 ng/Pa·s·m^2); and 4) Low interior permeance with medium exterior permeance - VP membrane and EPS insulation (with a combined permeance of 64.4 ng/Pa·s·m^2), plus 0.15 mm polyethylene sheet on the interior (3 ng/Pa·s·m^2). On the interior side of the CLT, each assembly included an interior air space built with light wood frame and gypsum drywall. Figure 4.1 shows a typical wall section.

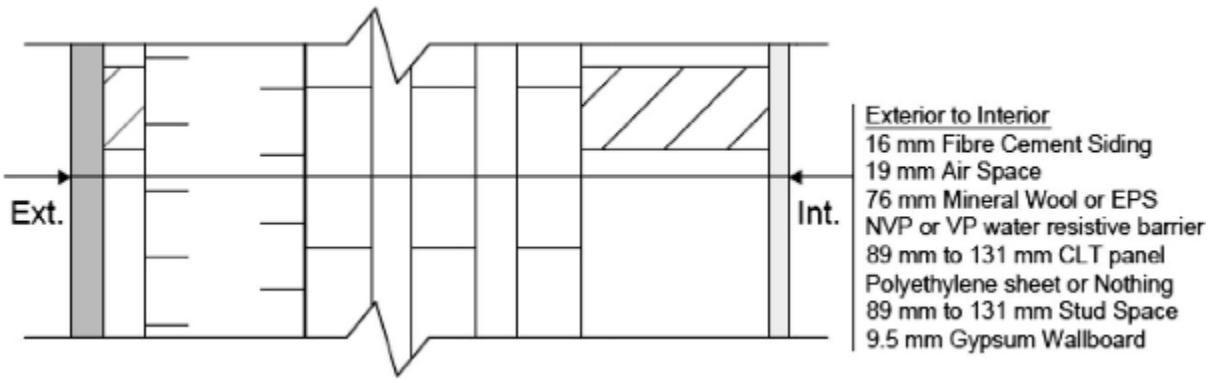

Figure 4.1 CLT wall assembly (McClung et al., 2014)

The CLT panels were initially wetted with the moisture content (MC) in the surface layers approaching or exceeding 30%. MC pins made of ceramic-coated stainless steel nails, thermistors, and RH sensors were installed across the wall assemblies to monitor the hygrothermal behavior of the CLT panels. Figure 4.2 shows the typical sensor layout and notation for the test assemblies.

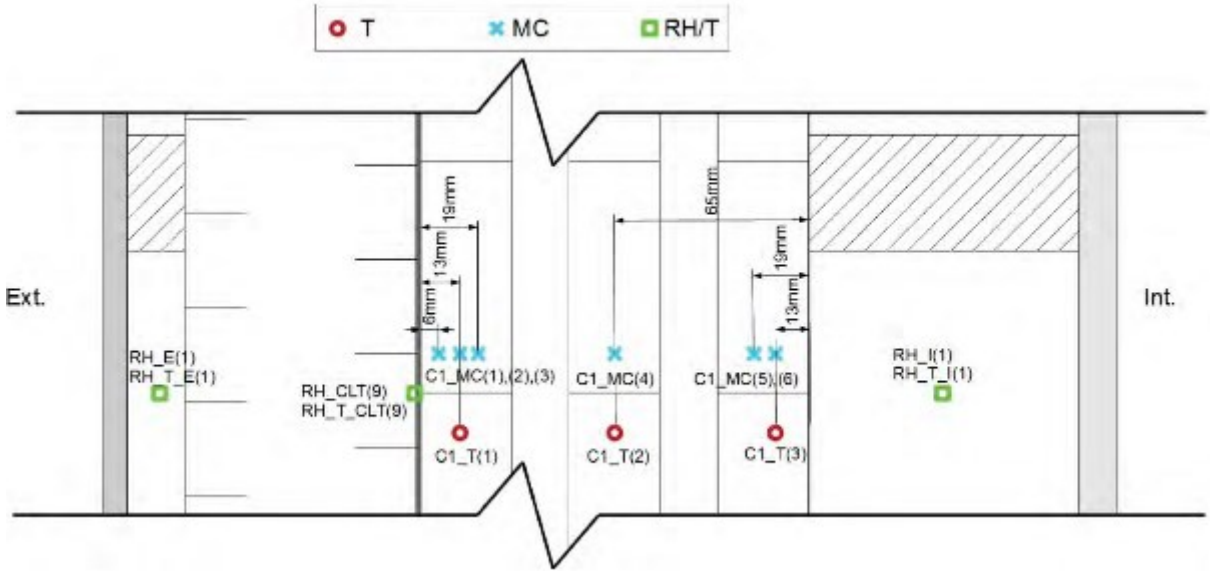

Figure 4.2 Typical sensor layout in CLT wall assemblies (McClung et al., 2014)

The test wall was located on the east side of the building envelope test facility. The exterior weather conditions were monitored on the roof of this field test facility. Measurements were taken every hour including temperature, RH, global solar radiation, rainfall, wind speed, and wind direction. The interior of the facility was maintained at 21℃±1℃ and 50% ±3%RH to represent a typical

indoor moisture load for the summer but a high interior moisture load scenario in the winter. More detailed information on the experimental setup can be found in McClung et al. (2014).

4.2 Hygrothermal model setup

The wall assemblies that used Quebec black spruce with low permeance WRB (B1) and high permeance WRB (B2) are selected for analysis in this paper. Table 4.1 shows a detailed description of the selected wall assemblies and Table 4.2 lists the basic material properties of each component. The basic material properties and material functions of CLT panel, including moisture storage function, vapour resistance factor as a function of relative humidity and moisture diffusivity as a function of moisture content, were determined based on the laboratory water uptake tests conducted by Lepage (2012) and the physical characterization tests conducted by Alsayegh et al. (2013). The basic properties of other materials are taken from WUFI's material database. Table 4.3 lists the boundary conditions set in the hygrothermal models, which are the same for both DELPHIN and WUFI.

Table 4.1 Components of the selected wall assemblies

Wall assemblies	**Cladding**	**Insulation**	**WRB**	**CLT panel species type**	**Interior layer**	
B1	16 mm Fibre cement board with 19 mm Ventilated cavity	76 mm Mineral wool	Low permeance-NVP membrane	102 mm Quebec black spruce	89 mm air space	9.5 mm gypsum board
B2			High permeance-VP membrane			

Table 4.2 Material properties of the CLT wall components

	ρ (kg/m^3)	**θ_{por} -**	**W_f (kg/m^3)**	**μ_{Dry} -**	**D_{ww} (m^2/s)**	**c (J/kg·K)**	**λ (W/m·K)**
Cement board	1130	0.48	350	28	5.17E-9	840	0.255
Air gap	1.3	1	-	0.56	-	1000	0.13
Mineral wool	96	0.95	0.5	1.1	-	850	0.032

NVP WRB (B1)	130	0.001	0.9	50000	-	2300	2.3
VP WRB (B2)	100	0.001	0.9	49.7	-	1500	2.4
CLT panel	536	0.73	630	1876	100	2500	0.12
Gypsum board	625	0.706	430	7.03	3.9E-7	870	0.16

Table 4.3 Boundary conditions

α_{in} (W/m²·K)	α_{ex} (W/m²·K)	β_{in} (s/m)	β_{ex} (s/m)	α_s -	α_l -	F_E -	F_D -	AFR -	V_r (1/h)
8	17	2.2E-8	8.0E-7	0.6	0.9	1.0	0.35	0.7	50

The rain factors were determined based on the wind-driven rain (WDR) model in ASHRAE 160 (2016). The test building is located in a medium terrain with a sloped roof. As suggested by ASHRAE 160, a rain exposure factor of 1.0 and a deposition factor of 0.35 are assumed in the simulation model.

The initial moisture content profile was created with intermittent changes based on the initial moisture content reading measured at each moisture content monitor location when the data collection was started. Figure 4.3 shows the initial moisture content profiles of the CLT panel in B1 and B2 wall assemblies. The initial moisture content of B1 is higher than B2 in the first 20mm.

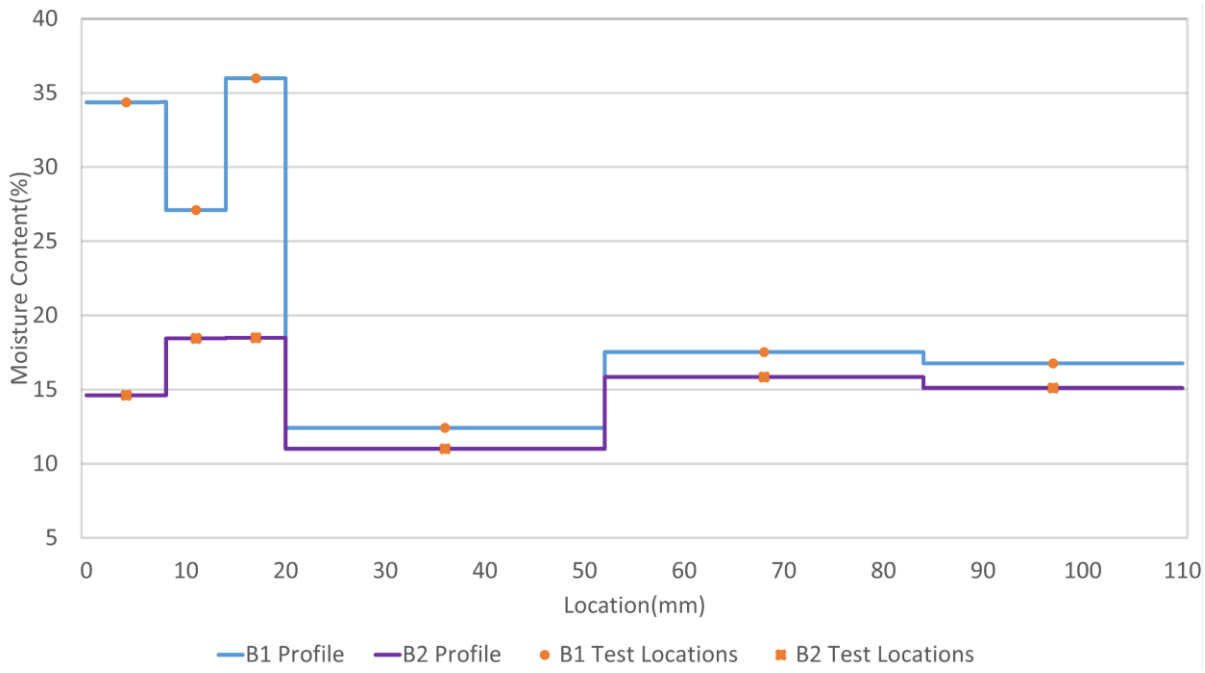

Figure 4.3 Initial moisture content profiles of the CLT panels

The initial moisture content and temperature of other materials are set at 50% RH and 20ºC, which are close to the measured relative humidity and temperature at RH/T sensors locations.

The on-site weather data were collected from Aug. 2011 to Aug. 2013. The simulations are performed for the same period. The moisture content of the exterior layer of the CLT panel, CLT_MC (1) located 6mm from the exterior face as shown in Figure 4.2, is used for analysis.

4.2.1 Unification of material properties

As stated in section 3.1.1, WUFI and DELPHIN use different methods to perform simulation. To have the same material property inputs, moisture storage function is used as the input in both WUFI and DELPHIN given that DELPHIN is able to automatically convert the moisture storage function to moisture retention curve.

In WUFI, the liquid transport is described by moisture diffusivity, while liquid conductivity is used in DELPHIN by default. The moisture diffusivity method can also be chosen in DELPHIN to describe liquid transport property. The moisture diffusivity in WUFI includes moisture diffusivity for suction and moisture diffusivity for redistribution, while DELPHIN does not differentiate moisture diffusivity for suction and redistribution. In WUFI, moisture diffusivity for suction and

redistribution are used, while only moisture diffusivity for redistribution is used in DELPHIN. WUFI uses vapour resistance factor to describe the vapour transport property, while DELPHIN can use both vapour permeability and vapour resistance factor. The vapour resistance factor or vapour permeability is considered as a function of relative humidity. The value (vapour resistance factor or vapour permeability) at dry state is used to scale the material function. In this thesis, vapour resistance factor is used for both DELPHIN and WUFI.

4.2.2 Unification of WDR calculation

To compare the WDR amount impinged on façade as climatic loads in WUFI and DELPHIN, the on-site wind and rain data collected over the two-year period are used to calculate WDR on the east façade as an example. ASHRAE 160 model is used to calculate WDR in WUFI with a rain deposition factor (F_D) of 0.35 and the rain exposure factor (F_E) of 1.0. The wind-driven rain calculated by DELPHIN follows the standard rain model in DELPHIN with a rain factor (K_{rain}) of 0.35. As shown in Figure 4.4, the WDR calculated by WUFI and DELPHIN have a similar pattern, however, there is a significant difference in quantity. The WDR model used in WUFI gives a much higher amount of WDR than that obtained from DELPHIN. To compare the hygrothermal model between WUFI and DELPHIN, the WDR load on the exterior wall surface should be the same. Therefore, the WDR calculated by ASHRAE 160 model in WUFI is applied to the exterior wall surface in DELPHIN instead.

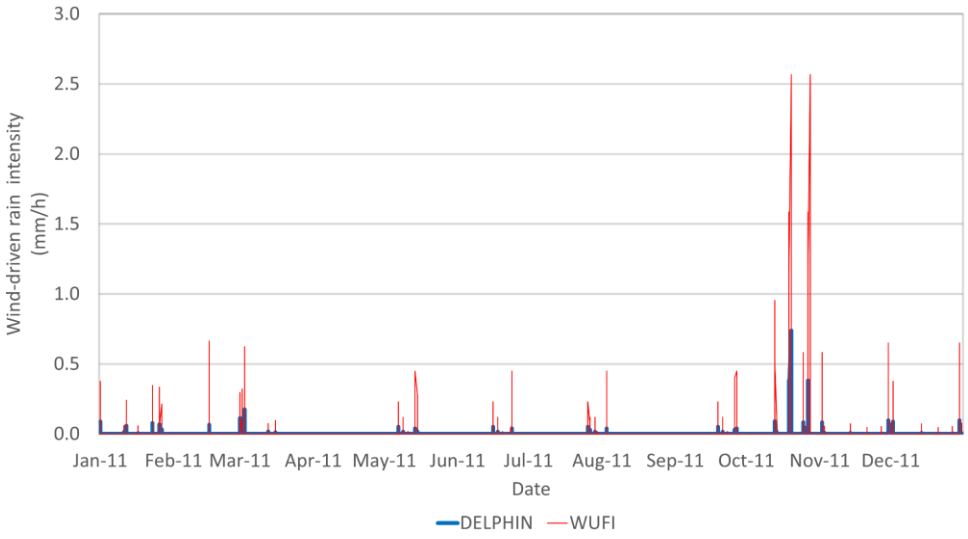

Figure 4.4 Comparison of wind-driven rain on east façade between WUFI and DELPHIN

4.3 Comparison between simulation results and measurements

Figure 4.5 shows the comparison between simulation results obtained from WUFI and DELPHIN and measurements for wall assembly B1 with low permeance WRB and wall assembly B2 with high permeance WRB. Simulation results from both WUFI and DELPHIN have the similar trend with field measurements. For B1, WUFI's results overestimate the MCs of CLT during the whole simulation period, while DELPHIN's results are very close to measurements, within 0.5%. The discrepancy is almost stable during the examined period-from Aug. 2011 to Aug. 2013. For B2, these two programs give very similar results and both WUFI and DELPHIN overestimate the MCs of CLT.

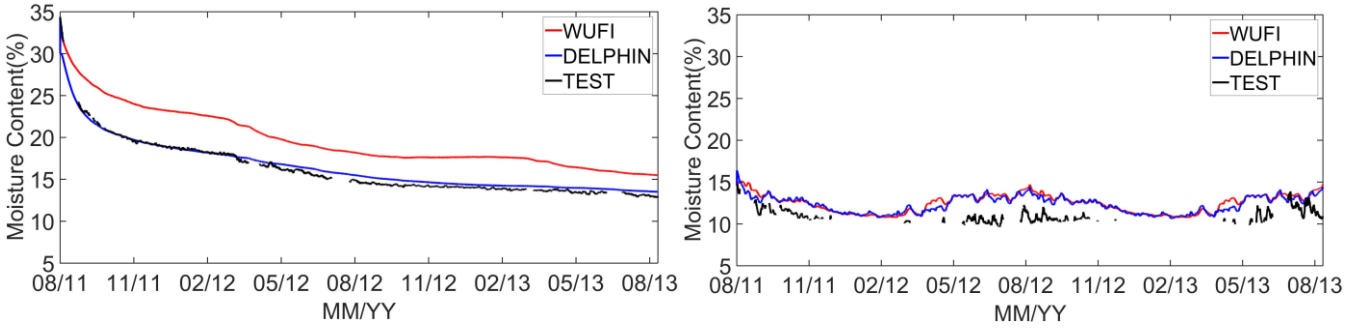

a) B1- low exterior permeance b) B2- High exterior permeance

Figure 4.5 Comparison between simulation results and measurements

To quantify the discrepancy between simulations and measurements, the root mean square of the differences (RMSD) between simulation results and measurements through the entire simulation period is calculated. As shown in Figure 4.6, the RMSD is 3.6% between WUFI and TEST and 0.5% between DELPHIN and TEST for B1. For B2, the RMSD is 2.3% between WUFI and TEST and 2.1% between DELPHIN and TEST. In general, DELPHIN's results are closer to measurements than WUFI's results.

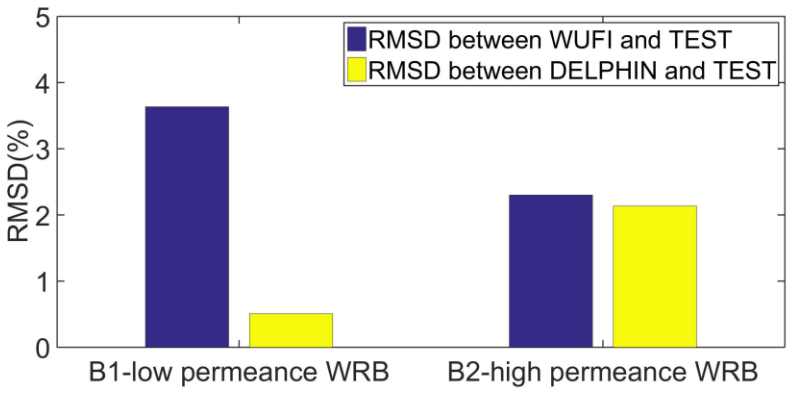

Figure 4.6 RMSD between simulation results and measurements

4.4 Sensitivity analysis method

4.4.1 One factor at a time method

One-factor-at-a-time method (OFAT) is used to investigate the influence of material properties and boundary conditions. Using this method, the examined parameter will be changed into two extreme values while keeping other parameters constant. The difference between the results from the two extreme cases can be used as the sensitivity indicator. The RMSD between the two extreme results through the entire simulation period is used as the sensitivity index. The RMSD can be calculated using equation 4-1:

$$\text{RMSD}=\sqrt{\frac{\sum_{i=1}^{n}(X_{higher\_i}-X_{lower\_i})^2}{n}} \quad (4\text{-}1)$$

where

X_{higher_i} - the simulation result with higher parameter at time i

X_{lower_i} - the simulation result with lower parameter at time i

RMSD - The root mean square of difference between the results with high value and that with low value through the entire simulation period.

4.4.2 Material properties

Given that the moisture content of CLT is mainly influenced by its hygric properties, moisture storage function (MSF), moisture diffusivity (MD) and vapour diffusion resistance factor (MEW) of CLT panel are selected as influencing factors for the sensitivity analysis. These material

properties are generally determined by laboratory tests. Typically, only a few test points are available because of the complexity and duration of the tests. Values between two test points are generally generated by linear interpolation when performing hygrothermal simulations. The material functions can be scaled by basic material parameters, i.e. saturation water content, moisture diffusivity at saturation water content, and vapour resistance at dry state. The uncertainties of each test point can be found in literatures (Alsayegh et al., 2013; Kumaran et al., 2002; Wu, 2007). The range of the basic parameters is determined based on the uncertainties reported in literatures. Table 4.4 and Table 4.5 present the moisture storage function and vapour resistance factor as a function of relative humidity. Moisture diffusivity for suction in WUFI is automatically generated from the water absorption coefficient, A-value, determined based on the laboratory water uptake tests (Lepage, 2012). Moisture diffusivity for redistribution was set to 2×10^{-10} m^2/s at normalized moisture content of 30%, 1×10^{-4} m^2/s at normalized moisture content of 68% and 100 m^2/s at normalized moisture content of 70% (Lepage, 2012). The extreme values of each parameter are determined by the range of each parameter (Table 4.6). The basic parameters of material properties are changed once at a time.

Table 4.4 Moisture storage function

RH (%)	**MC (kg/m^3)**
0	0
10	43.7
30	53.1
50	62.6
70	75.6
80	86.2
90	105
93	116
95	126
99	188
99.5	218
99.9	296
99.95	332

99.99	410
100	630

Table 4.5 Vapour resistance factor as a function of relative humidity

RH(%)	Vapour resistance factor
0	1876
25	469
35	208
45	187
75	46.9
85	28.8
95	18.8

Table 4.6 Range of material properties

Parameter	Range
Moisture Storage Function (MSF)	-20% to +10%
Moisture Diffusivity (MD)	-50% to +50%
Vapour resistance factor (MEW)	-25% to +25%

4.4.3 Boundary conditions

The boundary conditions investigated include the rain factor and cladding ventilation rate. The range of rain deposition factor is set from 0.35 to 1 according to ASHRAE 160 (2016), and the cladding ventilation rate is set from 0 1/h to 100 1/h. Considering various scenarios, it is necessary to investigate the west orientation, which receives the highest amount of WDR at this test site. The rain leakage is also taken into account, in which a 1% wind-driven rain is assumed to be deposited on the exterior layer of the CLT panel for the cases with rain leakage.

4.5 Results and analysis

4.5.1 Influence of material properties

Figure 4.7 shows the simulation results from WUFI and DELPHIN with the extreme values of the three hygric properties. Similar trends are observed in simulation results obtained from these two programs. For B1, the cases with low vapour permeance WRB, the moisture storage function has a negative influence (higher MSF value, lower moisture content) at the beginning when MC is above 20%. When the MC gets below 20%, the influence of the moisture storage function becomes positive (higher MSF value, higher moisture content). The initial MC of CLT at the exterior layer of B1 assembly was about 35%. At the initial drying stage, higher moisture storage function leads to a higher moisture diffusivity, which facilitates the moisture redistribution, therefore, a higher MSF results in a faster drying and lower MC. When the moisture content gets below 20%, the moisture diffusivity decreases dramatically and the redistribution process becomes slower. In the meantime, a higher moisture storage function means the material is able to hold more moisture at the same relative humidity level, therefore moisture storage function has a positive influence on the moisture content (Figure 4.7a). Figure 4.7c shows that in WUFI simulation results, the higher the vapour resistance factor, the higher the MC of CLT and this positive influence is slightly more obvious when the MC gets below 20%. Below 20% MC, the moisture transport is a mixture of both liquid and vapour and a higher vapour resistance may limit the moisture redistribution in the vapour form, which results in higher MCs. In DELPHIN simulation results, the influence of vapour resistance factor is negligible. In general, the influence of moisture diffusivity is negative (the higher MD, the lower MC) throughout the entire simulation period for DELPHIN although the influence of moisture diffusivity is insignificant when the MC gets below 20% in WUFI simulation results (Figure 4.7e). The cases with higher moisture transport coefficients (vapour permeability and moisture diffusivity) have lower moisture content since moisture transport including vapour transport and liquid transport facilitates the drying process.

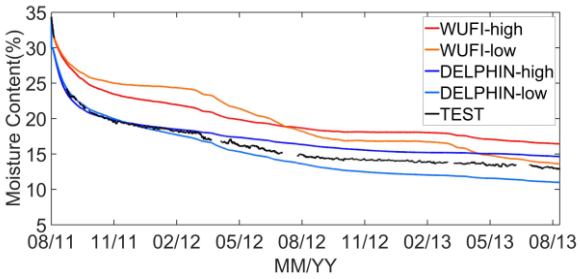

a) Influence of MSF - B1

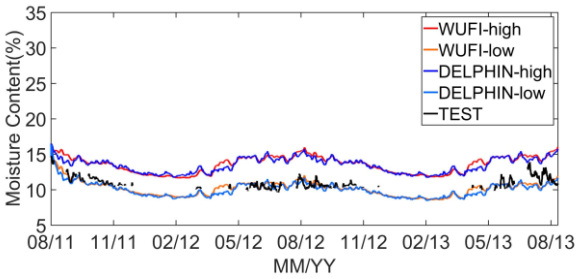

b) Influence of MSF - B2

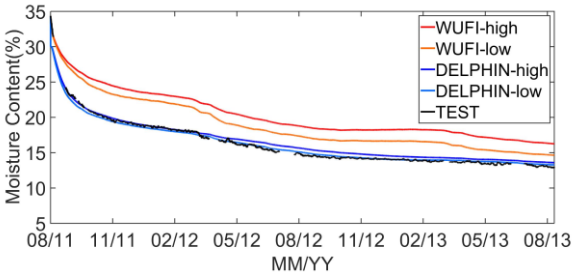

c) Influence of MEW - B1

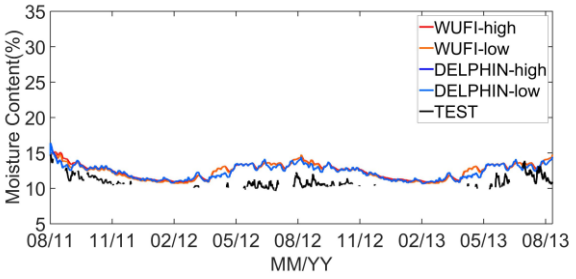

d) Influence of MEW - B2

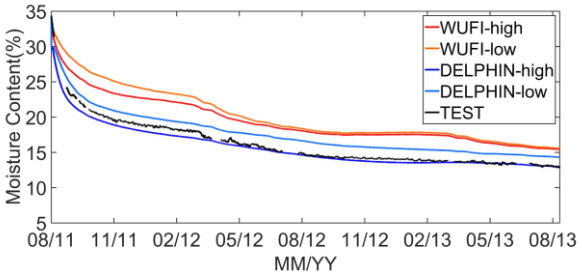

e) Influence of MD - B1

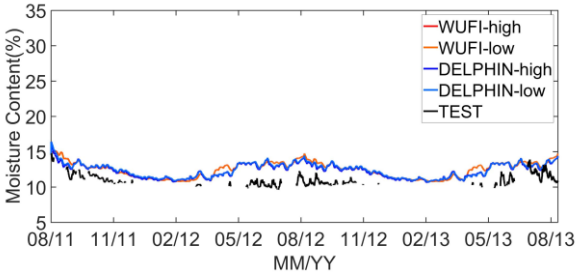

f) Influence of MD - B2

Figure 4.7 Influence of material properties

MSF: Moisture Storage Function, MEW: Vapour Resistance Factor, MD: Moisture Diffusivity

For B2, the cases with high vapour permeance WRB, the moisture storage function has a positive influence (the higher MSF, the lower MC) throughout the entire simulation period (Figure 4.7b), which is similar to what is observed in B1 for MC level below 20%. As explained earlier, a higher moisture storage function means the material is able to hold more moisture at the same relative humidity level, therefore moisture storage function results in higher MC. The simulation results with a lower MSF value are closer to measurements. The influence of moisture transport

coefficients (vapour resistance factor and moisture diffusivity) is negligible, as shown in Figure 4.7d and Figure 4.7f.

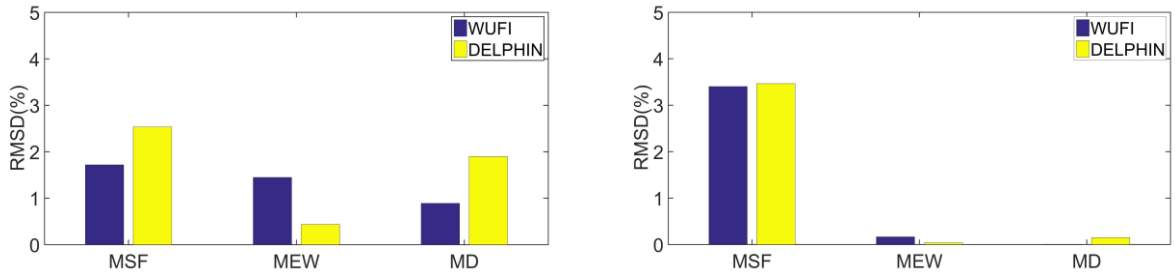

a) B1 – low vapour permeance b) B2 – high vapour permeance

Figure 4.8 RMSD in MCs between high and low values of each material property

The RMSD in MCs between high and low values is calculated for each material property (Figure 4.8). For wall assembly B1 (Figure 4.8a), in WUFI simulation results, a 30% change in MSF of CLT results in about 1.8% MC change and the influence of MSF is the most significant followed by the vapour resistance factor (RMSD in MC change of 1.6%) and moisture diffusivity (RMSD in MC change of 1.0%). In DELPHIN simulation results, a 30% change in MSF of CLT results in about 2.5% MC change and the influence of MSF is the most significant followed by the moisture diffusivity (RMSD in MC change of 2.0%) and the vapour resistance factor (RMSD in MC change of 0.4%). The influence of vapour resistance factor is insignificant. For wall assembly B2, where MC level is below 15%, a 30% change in MSF results in about 3.5% MC change, while the influence of vapour resistance factor and moisture diffusivity is less than 0.2% in MC change. In summary, the influence of moisture storage function is more significant for B2 than B1, while the influence of moisture transport coefficients (vapour resistance factor and moisture diffusivity) are more significant for B1 than B2. For both B1 and B2, the moisture storage function plays a more important role than moisture transport coefficients.

4.5.2 Influence of boundary conditions

Figure 4.9 shows the influence of rain factor for two different orientations with and without rain leakage. Similar simulation results are obtained from WUFI and DELPHIN.

For wall assembly B1 with low vapour permeance WRB, the change in rain deposition factor does not have any influence on the MCs of CLT when no rain leakage is considered (Figure 4.9a and

Figure 4.9c). The change of rain deposition factor influences the WDR amount deposited on the façade, thus the moisture absorbed by the fiber cement cladding. However, the low vapour permeance WRB in B1 restricts the interaction between CLT panel with the exterior ambient environment and the change in moisture content of the cladding does not influence the MCs in CLT. The influence of rain deposition factor becomes noticeable when the rain leakage is introduced as shown in Figure 4.9b and Figure 4.9d, and this influence is more significant for the west orientation, where the cladding receives a higher amount of wind-driven rain. When rain leakage is assumed, the CLT panel is wetted and the low vapour permeance WRB limits the drying of CLT panel towards exterior, therefore, there is a moisture accumulation in CLT panels. The MC levels increase with the increase of rain deposition factor and the peaks of MC response to the rain events. The trends are similar for the East and West orientation. Typically, DELPHIN simulation results are lower than those obtained from WUFI. The moisture content is above 20% during the entire simulation period, especially for the west orientation with a higher amount of WDR in WUFI results. For DELPHIN results the MC level remains also above 20% most of the time.

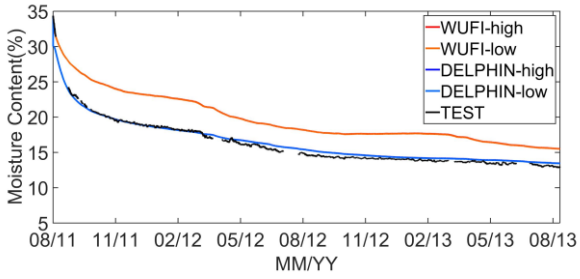

a) B1-No RL, E

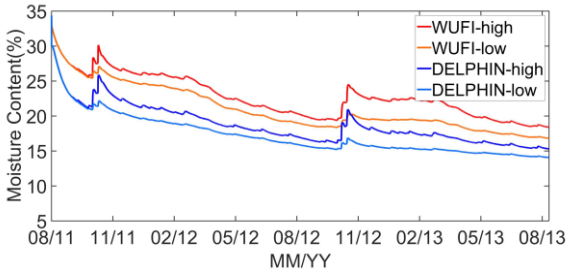

b) B1-RL, E

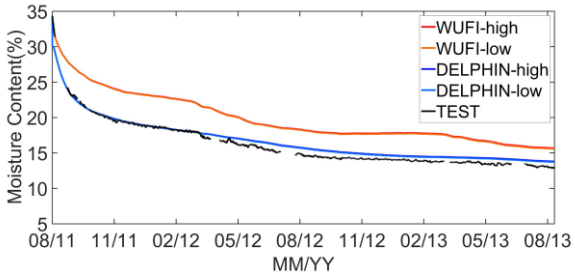

c) B1-No RL, W

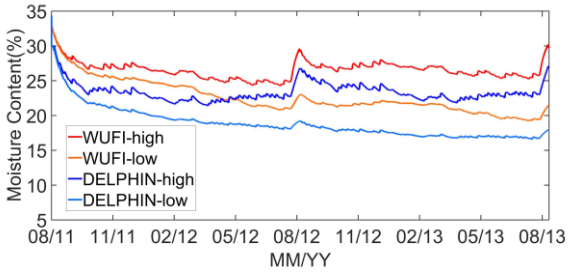

d) B1-RL, W

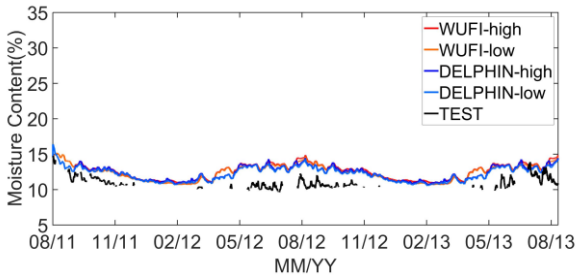

e) B2-No RL, E

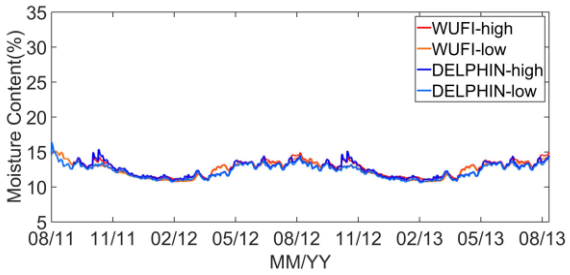

f) B2-RL, E

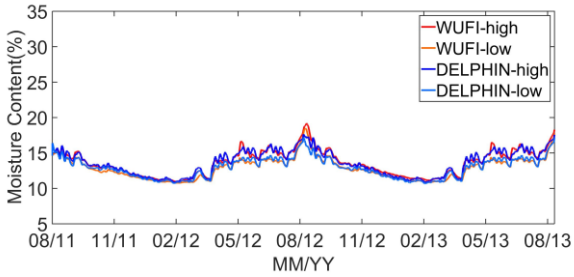

g) B2-No RL, W

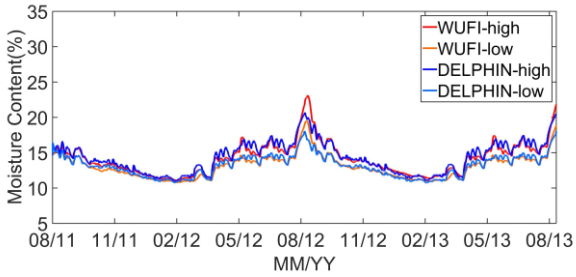

h) B2-RL, W

Figure 4.9 Influence of rain deposition factor (RL-Rain Leakage, E-East, W-West)

For B2, the cases with high vapour permeance WRB, the change in rain deposition factor does not have any influence on the MCs of CLT for the east orientation with or without rain leakage, as shown in Figure 4.9e and Figure 4.9f. For the west orientation, the increase of rain deposition factor increases the MCs of CLT for both the cases with and without rain leakage due to a higher WDR amount received on the west façade. The MC of CLT is below 20% most of the time with a short period of MC peaked at above 20% with rain leakage on the west orientation, which means that the vapour permeable WRB allows enough drying towards exterior and the CLT walls with vapour permeable WRB is able to handle the amount of incidental rain leaked through the WRB. Therefore, there is no moisture problem risk for B2 cases even under the worst condition, i.e. west orientation with 1% rain leakage. Although the peak value of the moisture content is still able to reach around 25%, it is able to decrease to around 15% quickly after a heavy rain event. The risk of moisture problem due to rain penetration in B2 is much lower than that in B1.

Figure 4.10 shows the influence of cladding cavity ventilation rates for two different orientations with and without rain leakage. As shown in Figure 4.10a to Figure 4.10d, the change in cladding ventilation rate does not have influence on the MCs of CLT for wall assembly B1 given that the

low vapour permeance WRB restricts the interaction between CLT panel and its exterior ambient environment. For wall assembly B2, the high vapour permeance WRB allows the interaction of CLT panel with its ambient environment and the increase of cladding cavity ventilation has a slight and similar influence on the MCs of CLT for the east orientation with and without rain leakage (Figure 4.10e and Figure 4.10f). The influence of cladding cavity ventilation becomes more significant for the west orientation where a higher WDR is received on the façade (Figure 4.10g and Figure 4.10h). Without cavity ventilation, the MC of CLT peaks above 20% during rain events and the provision of cavity ventilation helps the removal of moisture from CLT wetted by rain leakage. The drying effect of cavity ventilation is more significant for the west orientation than for the east orientation.

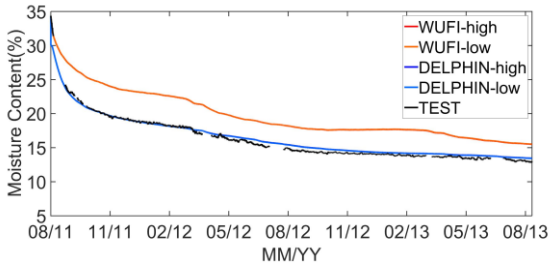

a) B1-No RL, E

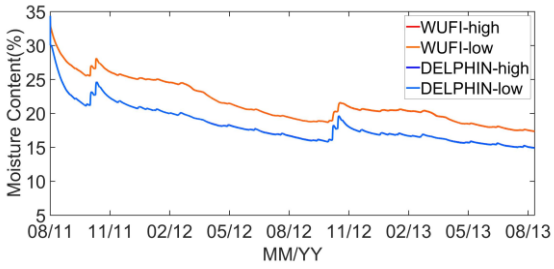

b) B1-RL, E

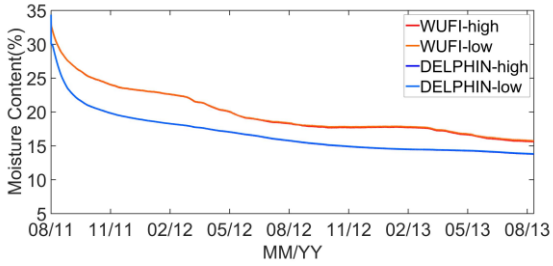

c) B1-No RL, W

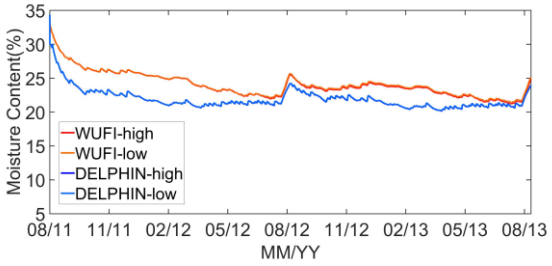

d) B1-RL, W

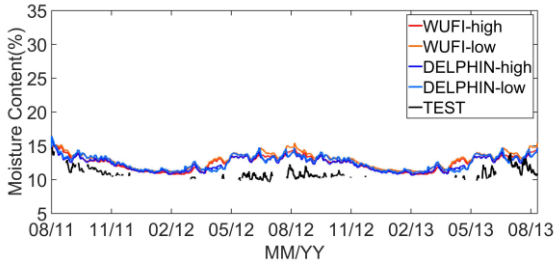

e) B2-No RL, E

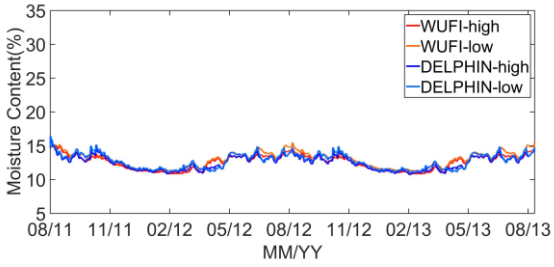

f) B2-RL, E

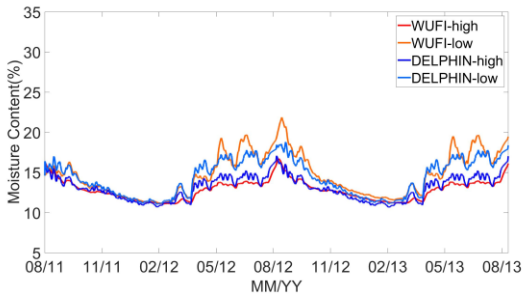

g) B2-No RL, W

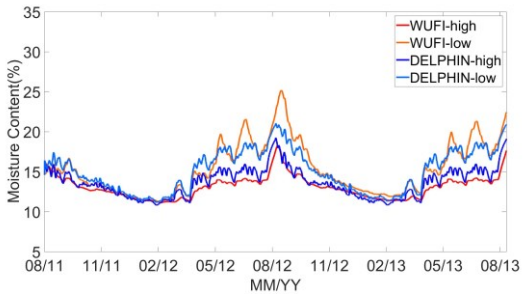

h) B2-RL, W

Figure 4.10 Influence of cladding cavity ventilation rate (RL-Rain Leakage, E-East, W-West)

The RMSD in MCs between high and low values is calculated for rain deposition factor (Figure 4.11a and Figure 4.11b) and cladding cavity ventilation rate (Figure 4.11c and Figure 4.11d). As discussed earlier, for wall assembly B1, the change in rain deposition factor only influences the cases with rain leakage and the change of rain deposition factor from 0.35 to 1 results in a MC change of about 2% for the east orientation and about 4-5% for the west orientation, respectively (Figure 4.11a). Compared to wall assembly B1, for wall assembly B2, the influence of rain deposition factor increases for the cases without rain leakage but decreases for the cases with rain leakage. The influence of rain deposition factor is greater for the west orientation and for the cases with rain leakage. A change of rain deposition factor from 0.35 to 1 results in a MC change less than 0.5% for the east orientation for cases with and without rain leakage, while for the west orientation the change of rain deposition factor results in a MC change of 0.8% without rain leakage and 1.4% with rain leakage (Figure 4.11b).

As shown in Figure 4.11c and Figure 4.11d, cladding cavity ventilation only influences wall assembly B2 and the influence is more significant for the west orientation. A change of cladding cavity ventilation rate from 0 to 100ACH results in a MC change less than 0.5% for both cases with and without rain leakage for the east orientation. For the west orientation, the cladding cavity ventilation rate change results in 1% MC change in DELPHIN results and 2-2.5% in WUFI results and the influence is slightly higher for the case with rain leakage.

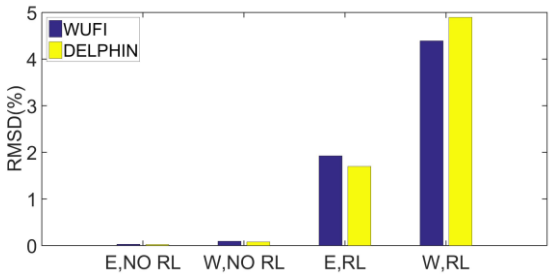

a) Rain deposition factor – B1

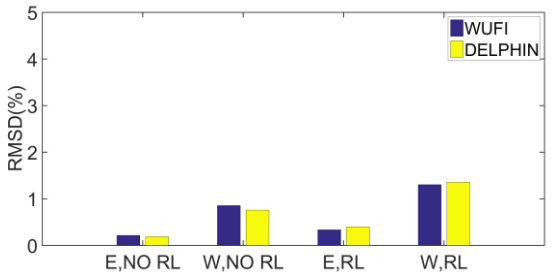

b) Rain deposition factor – B2

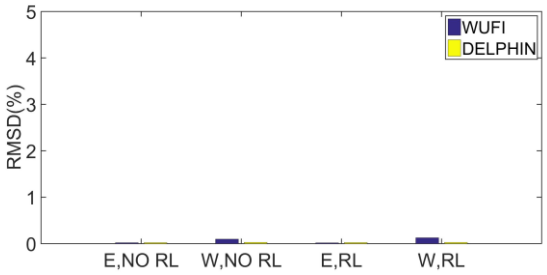

c) Cladding cavity ventilation rate – B1

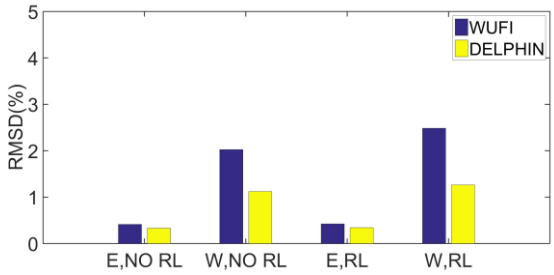

d) Cladding cavity ventilation rate – B2

Figure 4.11 RMSD in MCs between high and low values of rain deposition factor and cladding cavity ventilation rate

In summary, the significance of influence of material properties and boundary conditions depends on the configuration of wall assemblies and the environmental loads. For B1 with low vapour permeance WRB, the MC of the CLT panel is influenced mainly by hygric properties and the rain leakage amount. The change of material properties between two extreme values, namely moisture storage function, vapour resistance factor and moisture diffusivity, results in a MC change of 1-2.5% in the exterior layer of the CLT panel, while the change in rain deposition factor can result in a MC change of 2% for the east orientation and 5% for the west orientation. Cladding cavity ventilation does not have any influence at all. Therefore, it is important to ensure a good wall design to minimize the risk of rainwater penetration for wall assemblies with low vapour permeance WRB. For wall assembly B2 with high vapour permeance WRB, the MC of the CLT panel is mainly influenced by the moisture storage function among the three hygric properties investigated, which can result in 3.5% MC change in the exterior layer of the CLT. Both rain deposition factor and cladding cavity ventilation have noticeable influence, however, the influence of these two boundary conditions are less than the influence of moisture storage function.

4.6 Summary

In this chapter, two commercial hygrothermal simulation programs, namely WUFI and DELPHIN, are used to investigate the hygrothermal performance of CLT wall assemblies. The two CLT wall assemblies investigated has black spruce CLT panel with the same wall configuration except for the WRB, one with low vapour permeance and the other with high vapour permeance. The hygrothermal models are validated by comparing simulation results with measurements. The sensitivity analysis is then performed using the validated models to investigate the influence of hygric material properties and boundary conditions under different environmental loads. The main conclusions of this study are:

- In general, both WUFI and DELPHIN simulation results have a good agreement with field measurements. Both programs tend to overestimate the MCs of the CLT panels. For wall assembly with low vapour permeance WRB, B1, the MCs obtained from WUFI are about 3.5% higher than measurements, while MCs obtained from DELPHIN are within 0.5% compared to measurements. For wall assembly with high vapour permeance WRB, B2, these two programs give very similar results. The MCs from simulations are about 2.5% higher than the measurements.
- The moisture storage function is the most influential hgric material property. At MC level above 20%, the higher the moisture storage function the lower the MC, while at MC level below 20%, the higher the moisture storage function the higher the MC. The moisture transport coefficients (vapour permeability and moisture diffusivity) negatively influence the moisture content of CLT for B1, but less significant than moisture storage function. For B2, the moisture transport coefficients have no influence on moisture content of CLT.
- For wall assembly with low permeance WRB, B1, the influence of rain deposition factor only becomes important for the cases with rain leakage since the low vapour permeability of WRB restricts the interaction between CLT panel with its exterior ambient environment and limits drying to exterior. For wall assembly with high permeance WRB, B2, the influence of rain deposition factor is more important for west orientation than east orientation because the west façade receives higher amount of wind-driven rain. The high vapour permeability of WRB in B2 allows the interaction between CLT panel with its exterior ambient environment and facilities drying to exterior.

- For wall assembly with low permeance WRB, B1, cladding cavity ventilation rate does not have any influence on the MCs of CLT. For B2, cladding cavity ventilation helps the removal of moisture accumulation in CLT, especially for the cases with rain leakage. The influence of cladding cavity ventilation is slightly more significant than rain deposition factor.

Chapter 5 Air leakage simulation methods

5.1 Introduction

The influence of air leakage on wood framed walls have been investigated by experimental studies (Desmarais, 2000; Derome, 2005; Langmans et al., 2012; Alev et al., 2014), hygrothermal simulations (Ojanen and Kumaran, 1996; Karagiozis and Kunzel, 2009; Saber et al., 2011; Hagentoft and Harderup, 1996) and the combination of experiments and simulations (Kalamees and Kurnitski, 2010; Saber and Maref, 2015; Pallin et al., 2016; Svoboda, 2007; Younes and Shdid, 2013; Shdid and Younes, 2015; Belleudy et al., 2015). Desmarais (2000) conducted an experimental study for the conventional 89 mm fiberglass insulated wall (2×4) and the conventional wall with additional rigid insulation on exterior and interior sides. The hygrothermal performance of these three types of walls with three air leakage paths, i.e. long air exfiltration path, concentrated air exfiltration path and distributed exfiltration path, were monitored under simulated climatic conditions from the beginning of the winter to late spring. Derome (2005) performed measurements for two flat roof assemblies filled with cellulose insulation through a wetting and drying cycle from winter to summer under different air leakage paths. It was found that wood-frame constructions with cellulose insulation have the benefit of distributing moisture over a large volume of material, but cellulose may reach very high moisture contents and prolong the presence of moisture within wood-frame assemblies when exposed to moisture sources.

In terms of hygrothermal modelling, Ojanen and Kumaran (1996) investigated the relationship between the moisture accumulation in stud cavity and the air leakage rate by steady-state calculation and transient two-dimensional heat, air, and moisture (HAM) modeling. Karagiozis and Kunzel (2009) studied the drying and wetting effect caused by airflow through the EIFS-Clad wall by introducing an airflow path into the hygrothermal model. Saber et al. (2011) developed a 3-D heat and air transport model to investigate the effect of air leakage rate on the apparent R-value for different wall assemblies. Hagentoft and Harderup (1996) investigated the wall insulated by cellulose fiber with and without vapour retarder and air leakage. It was found that the moisture level of a wall strongly depends on vapour retarder, air leakage, and indoor moisture supply.

The combination of experiment and simulation improves the reliability of the simulation models. Kalamees and Kurnitski (2010) studied a joint of an external wall and attic floor with the presence

of air leakage by both laboratory tests and 2-D simulations. They concluded that mineral wool sheathing with SBPO film outperformed wood fiberboard sheathing because of its higher thermal resistance and vapour permeability. Saber and Maref (2015) further investigated the exterior insulated walls with and without structural sheathing (OSB). They found that the exterior insulated walls with structural sheathing has lower risk of mold growth than those without structural sheathing. Pallin et al. (2016) investigated different air leakage patterns and provided calibration method for 1-D simulation through theoretical equations to study 2-D dimensional effects. There are also studies using CFD approach to model air flow patterns and temperature distribution within the constructions to investigate the effect of air leakage (Svoboda, 2007; Younes and Shdid, 2013; Shdid and Younes, 2015). Belleudy et al. (2015) investigated the air leakage effect on the hygrothermal field in a ceiling section insulated with cellulose using a HAM model developed based on COMSOL. The model is capable of calculating the 2-D hygrothermal field in the presence of air flow. The simulation results showed a good agreement with measurements and the HAM model is considered as validated and can be used for predicting the hygrothermal performance of wood constructions with air leakage.

Although the 2-D, 3-D model and CFD approach can be used to investigate the effect of air leakage, these methods are complicated to be used for engineering practices. Kunzel (2012) proposed two simplified methods to simulate the effect of air leakage, which are air convection method (adding a ventilated air layer) and air infiltration method (adding condensed moisture source). These two methods were applied to a typical flat roof assembly and it was found that the air infiltration method tends to give higher moisture contents than the air convection method. However, the applicability of these two methods for different types of wood frame walls has not been well investigated. The randomness of the leaking air distribution within wall assemblies may lead to discrepancies between simulation and real performance of walls, therefore, it is necessary to calibrate the specific model by adjusting relevant parameters such as the position of the air layer or the amount of the air reaching the condensation plane before it can be widely used.

This chapter investigates the effect of air leakage on the hygrothermal performance of three wood-framed walls, one baseline and two highly insulated walls. Two simplified air leakage modelling methods, air convection method and air infiltration method, are implemented in a transient HAM simulation program, DELPHIN, which is able to simulate the hygrothermal performance of porous

building materials by solving coupled heat and moisture balance equations with consideration of heat and moisture sources in the wall assemblies. Although DELPHIN has built-in air balance equation, the convective air flow is considered separately from heat and moisture transport (DELPHIN, 2015). Therefore, it is worthwhile to investigate how well the simplified methods can model the effect of air leakage on the hygrothermal performance of wall assemblies. The specific hygrothermal models created by the two methods are calibrated by adjusting the critical parameters, i.e. the position of the air layer in the air convection method and the amount of air reaching the condensation plane in the air infiltration method to match the measured moisture content of OSB sheathing. The applicability of these two methods for each type of wall is evaluated based on the comparison between simulation results and measurements. The air infiltration method, which tends to overestimate the moisture content of OSB sheathing, as a more conservative approach, is used for the long-term hygrothermal performance evaluation. Four levels of airtightness, i.e. tight, average, leaky and extreme are investigated. Mold growth index is used as an indicator to evaluate the long-term hygrothermal performance. To be consistent with the original reference (Kunzel, 2012), the term "air infiltration model" is used throughout this thesis. However, note that the air leakage modeled in this thesis is air exfiltration through the wall assembly instead.

5.2 Experimental setup

To investigate the air leakage effect on the hygrothermal performance of wood framed walls, thirteen test walls were built and installed on the Building Envelope Test Facility located in Southern Ontario Canada (Fox, 2014). The measurements obtained from this study are used to validate the hygrothermal models and study the impact of air leakage. The investigated walls can be categorized into baseline wall with 140 mm fiberglass insulation, deep cavity wall, and exterior insulated wall. Table 5.1 shows the details about the framing and insulation of the test walls.

Table 5.1 Summary of the test walls

Wall types	**Wall ID**	**Wall framing**	**Insulation**	**RSI $K \cdot m^2/W$**
Baseline wall	3	140 mm framing	140 mm fiber glass	3.9
	1	284 mm double stud	284 mm cellulose fiber	6.8

Deep cavity wall	2	241 mm I-joist	241 mm cellulose fiber	5.8
	4	184 mm framing	152 mm closed cell spray polyurethane foam (ccSPF)	6.4
Exterior insulated wall	5	140 mm framing	140 mm fiber glass; 50 mm exterior polyisocyanurate insulation	6.1
	6	140 mm framing	140 mm fiber glass; 64 mm exterior XPS insulation	6.1
	7	140 mm framing	140 mm fiber glass; 76 mm exterior mineral wool insulation	6.0

These walls were installed on the north and south elevations of the Building Envelope Test Facility. A weather station installed on the rooftop of the facility is used to monitor on-site hourly weather data including temperature, relative humidity, global solar radiation, rainfall, wind speed and direction. The Vaisala™ HUMICAP^{R} HMP 35C shielded from solar radiation and precipitation is used to measure the relative humidity and temperature. The accuracy of the RH sensor is ±2% RH from 0 to 90% RH and ±3% RH from 90 to 100% RH at 20°C, and the accuracy of temperature sensor is ±0.4 °C from −24 °C to 48 °C. The solar radiation is monitored by a Kipp & Zonen pyranometer, which is mounted in an unobstructed, horizontal position. The accuracy of the pyranometer is ±10 W/m^2 with a sensitivity to temperature dependence of <1% from −10 °C to +40 °C. Wind speed and direction is monitored using the RM Young Wind Sentry 03002-10A anemometer, which has an operating range of 0–50 m/s with an accuracy of ±0.5 m/s. The balanced wind direction vane uses a 10 k Ω transducer that operates with 1% linearity and an accuracy of ±5°. The precipitation is measured with a 0.1 mm/count tipping bucket rain gauge. The temperature, relative humidity, wind speed and direction were monitored from a height of 10 m above grade. The pyranometer was located lower on the instrumentation mast at roof height with the tipping bucket rain gauge. The indoor conditions including temperature and relative humidity are also monitored. The monitored data is used for hygrothermal modelling. Figure 5.1 shows the installation of the test walls and weather station located on the roof of the Building Envelope Test Facility.

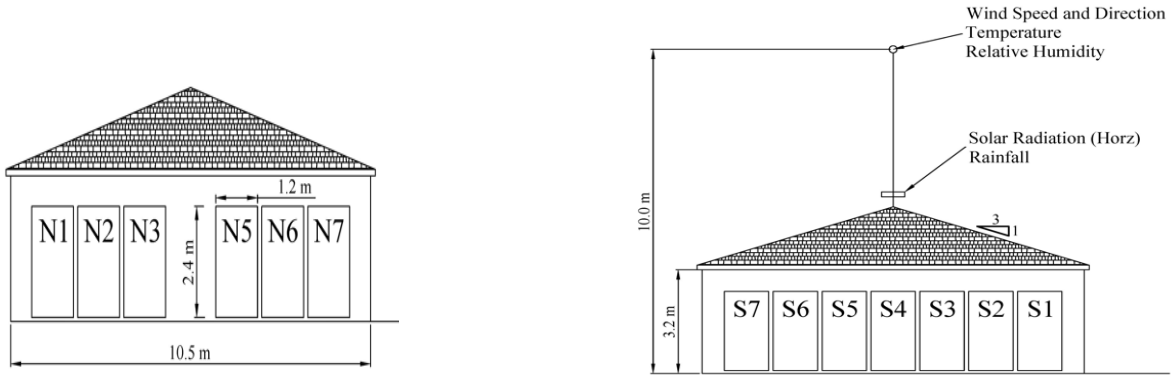

a) North elevation b) South elevation

Figure 5.1 Locations of test walls (Fox, 2014)

Air leakage was simulated by injecting room air into the stud cavity of test walls. The air leakage test was administered through the lower access port in the test walls as shown in Figure 5.2. The air was piped from a centralized location through 25 mm polyethylene tubing to a flow meter placed at each wall. The air pump is shown in Figure 5.2a and a typical wall connection is shown in Figure 5.2b. The exhaust port in the upper plate was accessed with a 25mm drill bit through the interior drywall and 6-mil polyethylene to allow the injected air to leave the wall cavity and return to the interior of the Building Envelope Test Facility. Figure 5.3 shows the plan view of the air leakage test setup.

c

a) central air pump used for air injection b) air injection port

Figure 5.2 Air leakage test setup (Fox, 2014)

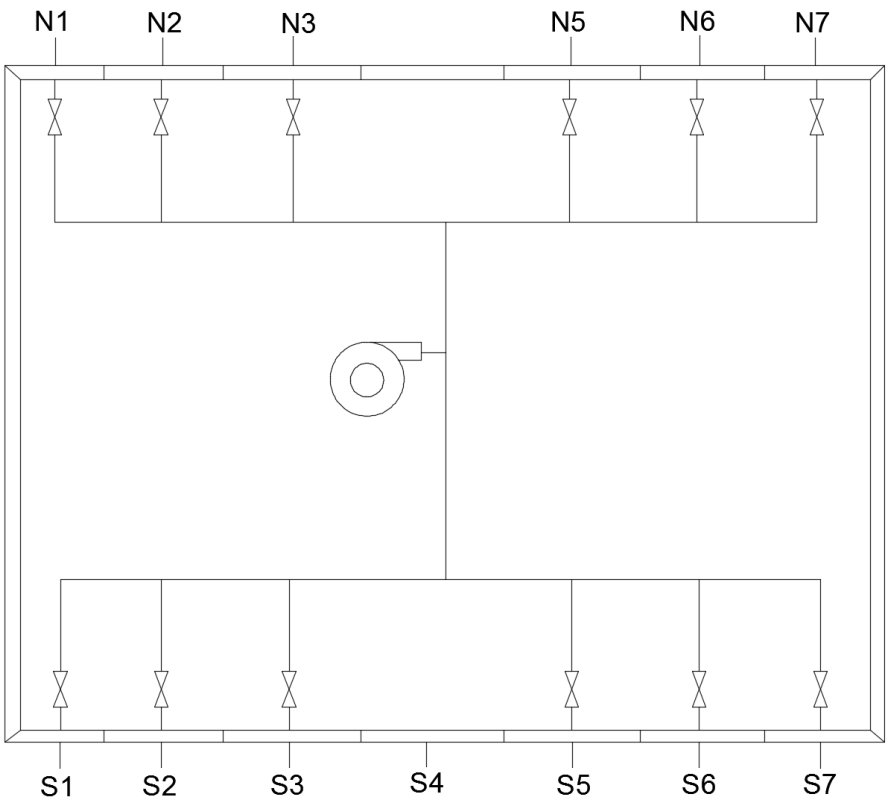

Figure 5.3 Plan view of the air leakage test setup

The air injection system maintained a 0.315 L/s flow rate through each of the test walls to represent an average level of air tightness of wall assemblies under 5 Pa natural pressure differential that typically occurs across wall assemblies in the absence of an elevated stack effect or high wind velocity.

The moisture and temperature sensors were installed on the OSB sheathing and bottom and top plates and RH sensors were installed in air cavity and stud cavity to monitor the hygrothermal conditions across the wall assemblies. Figure 5.4 shows the general wall assembly cross-section with sensor locations. Three pairs of moisture content (MC) sensors were installed at the lower, middle and upper location of the OSB sheathing to monitor the vertical MC profile. MC pins are made of ceramic coated stainless steel nails and electronically insulated along the shaft except for the tip. They were inserted at a depth of 5 mm into the OSB sheathing. Thermistors were installed along with the MC pins and these temperature readings were used for compensating the effect of temperature on MC readings. MC readings were also corrected for species. More details about the

sensors and experimental setup can be found in Fox (2014). The detailed wall components of a typical wall are listed in Table 5.2.

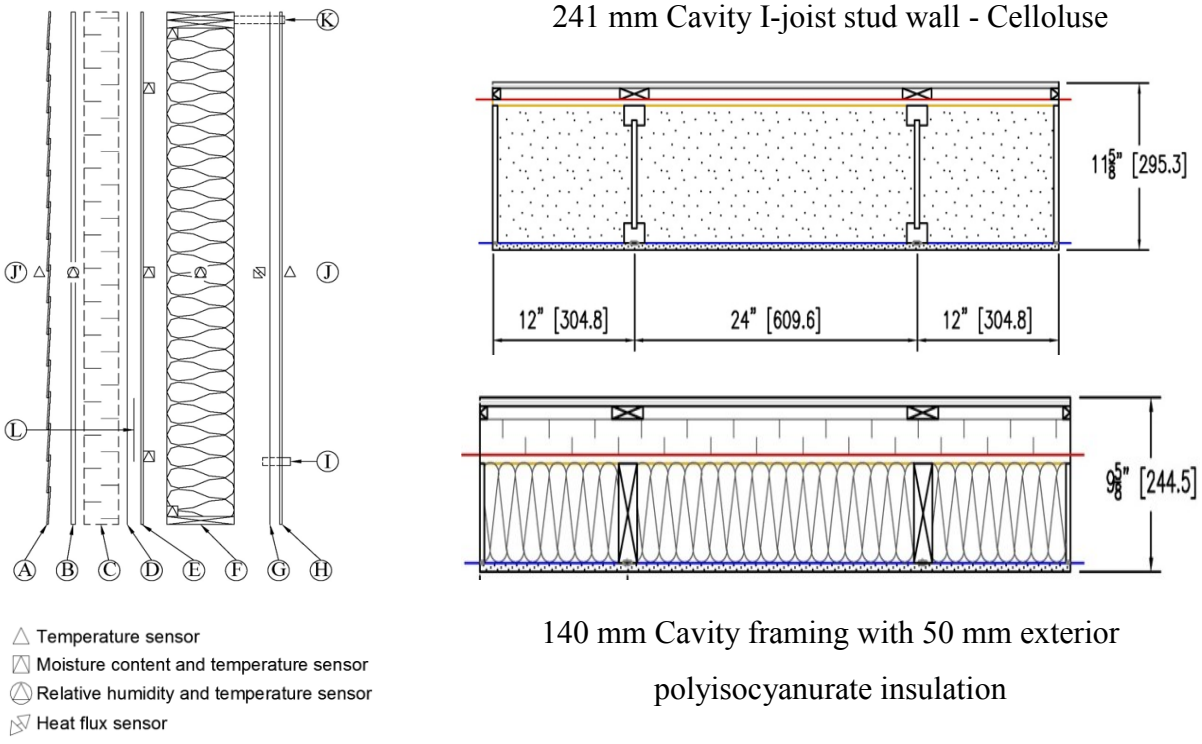

a) General side view

b) Top view of I-joist wall and exterior polyisocyanurate insulated wall

Figure 5.4 Cross sectional diagram of typical test panel configuration with sensor locations (Fox, 2014)

The data collected from November 2012 to June 2013 were used for analysis. The analyzed period was divided into three distinct intervals: 1) a fall/winter baseline period from November 2012 to mid-February 2013; 2) a wintertime air leakage test from mid-February to early April 2013; and 3) a springtime drying period extending from early April to early June 2013.

Table 5.2 Wall components details for Figure 5.4 (Fox, 2014)

ID	Wall component
A	11 mm Fibre cement siding
B	19 mm strapping / drainage space

C	Exterior Insulation (if installed)
D	SBPO air barrier and water resistive layer
E	11 mm OSB Sheathing
F	140, 184 or 241 mm framing as required
G	6-mil polyethylene (not installed in polyisocyanurate and XPS exterior insulated walls)
H	12.5 mm drywall
I	Air injection port
J'-J	Sensors through wall insulation cavity
K	Air exhaust port
L	Exterior water injection wetting sheet

5.3 Hygrothermal model setup

The hygrothermal models are created in DELPHIN, a simulation program for coupled heat, air, and moisture and transport in porous building materials. DELPHIN version 5.8.3 (released on January 2015) is used for hygrothermal modelling.

5.3.1 Material properties

To represent different types of highly insulated walls, the I-joist wall (deep cavity wall) and polyisocyanurate exterior insulated wall are selected for simulations. The baseline wall (38 mm by 140 mm stud wall) is used as the reference. The measured moisture content of OSB is used for validating the hygrothermal models. The material properties of these walls are determined from several sources (Kumaran et al., 2002; Mukhopadhyaya et al., 2007) and listed in Table 5.3.

Table 5.3 Material properties for I-joist wall (Type 2), baseline wall (Type 3) and polyisocyanurate exterior insulated wall (Type 5)

	ρ (kg/m^3)	θ_{por} (m^3/m^3)	W_f (kg/m^3)	μ_{Dry} -	D_{ww} (m^2/s)	c (J/kg·K)	λ (W/m·K)
Cement Board	1130	0.479	152	905	2.16E-8	840	0.24
Air Gap	1.3	0.999	-	0.56	-	1000	0.13
Polyisocyanurate	33.57	0.99	19.17	1622	-	1470	0.023
Water Resistive Barrier	400	0.001	0.9	328	-	1500	2.4
OSB	650	0.9	377	994	1.29E-10	1880	0.1
Cellulose fiber	68	0.95	500	1.86	-	2500	0.042
Fiberglass	30	0.99	208	1.35	-	840	0.036
Gypsum Board	625	0.706	430.625	172	3.47E-11	870	0.16

5.3.2 Boundary conditions and climatic conditions

The boundary conditions assigned for the hygrothermal model are listed in Table 5.4.

Table 5.4 Boundary conditions

α_{in} ($W/m^2·K$)	α_{ex} ($W/m^2·K$)	β_{in} (s/m)	β_{ex} (s/m)	α_s -	α_l -	F_E -	F_D -
8	17	5.6E-8	1.19E-7	0.6	0.9	1.0	0.35

The rain factors are determined according to the wind driven rain model in ASHRAE 160 (2016). DELPHIN does not have this model built-in, therefore, the hourly wind-driven rain data is calculated following AHSRAE 160 (2016) and imported into DELPHIN and directly imposed on the exterior surface of the wall.

The monitored on-site weather data (shown in Figure 5.6) was used to generate the customized weather files for DELPHIN. The indoor climate file is also generated based on the monitored indoor temperature and relative humidity, which was maintained at 20°C and 40% RH.

The initial MC of OSB is determined based on the measured MC at the beginning of the monitoring. The initial MC of insulation is determined based on the measured RH at the beginning of the

monitoring. The measured initial RH of the cellulose fiber is about 50% for south orientation and 56% for north orientation. According to sorption isotherm of cellulose fiber (Figure 5.5b), the moisture content at 50% RH is about 8.9 kg/m3, which is set as the initial MC in the model. However, we notice that the initial MC of the cellulose fiber installed in the north orientation is much higher than that obtained from the corresponding 56% RH due to the higher MC level built-in during the storage period. Therefore, the initial MC of cellulose in the north orientation is calibrated by comparing the simulated and measured MC of OSB in the baseline period. The initial MC of fiber cement board is assumed based on the initial outdoor environmental conditions at 10°C and 90% RH. The initial MC of gypsum board is assumed based on indoor conditions at 20°C and 40% RH. The isotherm sorption curves obtained from ref. (Kumaran et al., 2002; Mukhopadhyaya et al., 2007) for OSB and cellulose fiber are shown in Figure 5.5. The initial MC assigned for each material is listed in Table 5.5.

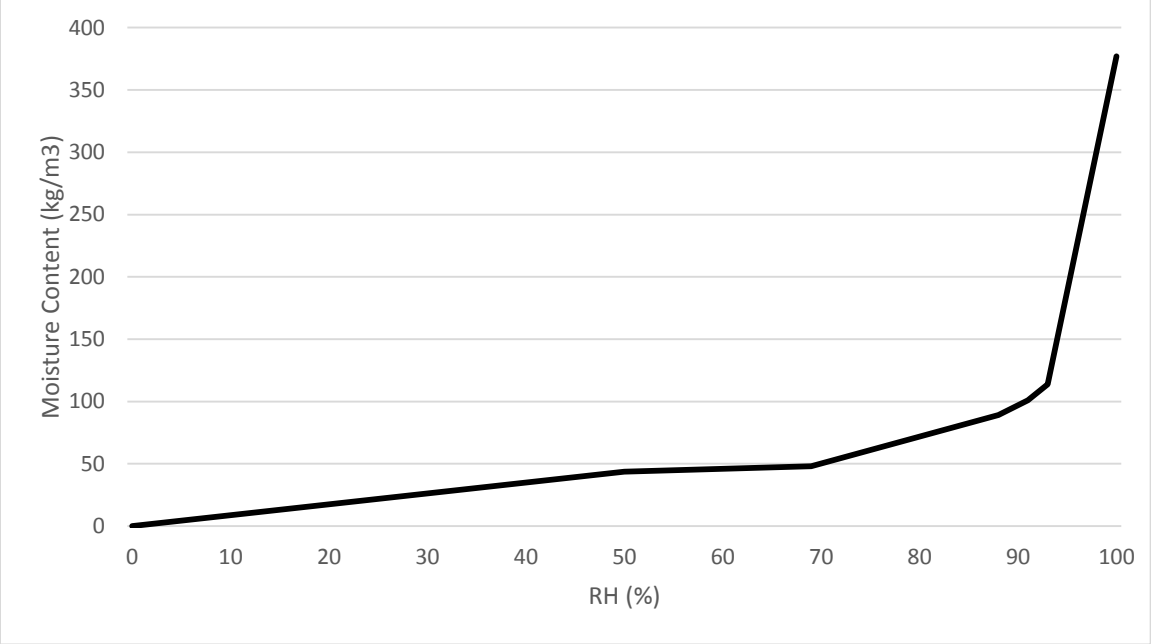

a) Isotherm sorption curve of OSB

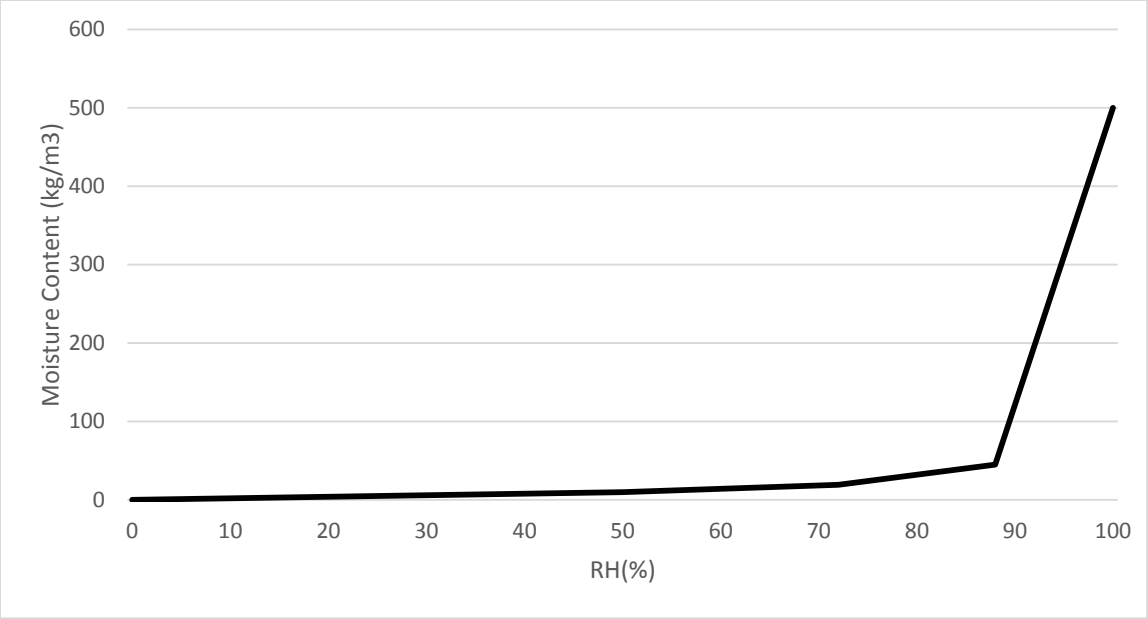

b) Isotherm sorption curve of cellulose fiber

Figure 5.5 Moisture storage function of OSB and Cellulose fiber

Table 5.5 Initial moisture content

Material	**Water content (kg/m^3)**
Fiber cement board	23.6
OSB	32.5
Cellulose fiber	8.9 (South)
	45 (North)
Fiberglass	0.32
Gypsum board	3.44

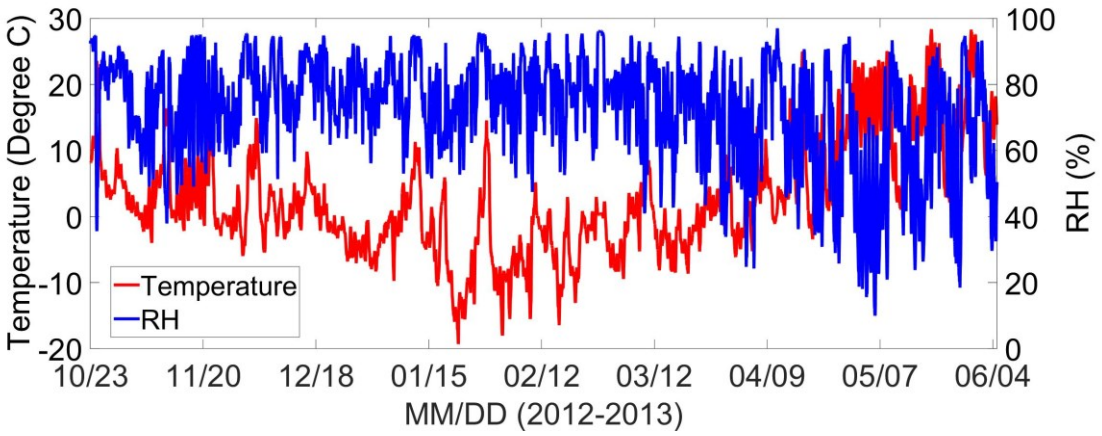

a) Temperature (ºC) and RH (%)

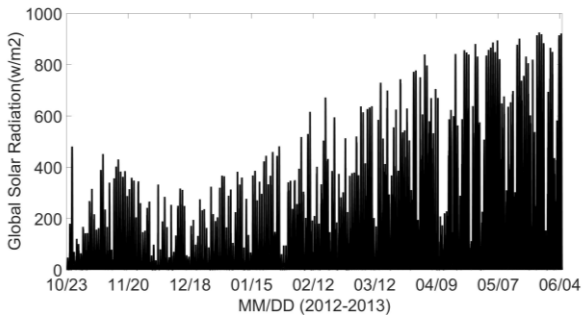

b) Global solar radiation (W/m^2)

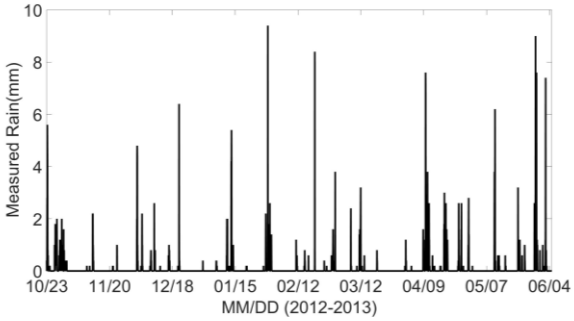

c) Horizontal rain fall (mm)

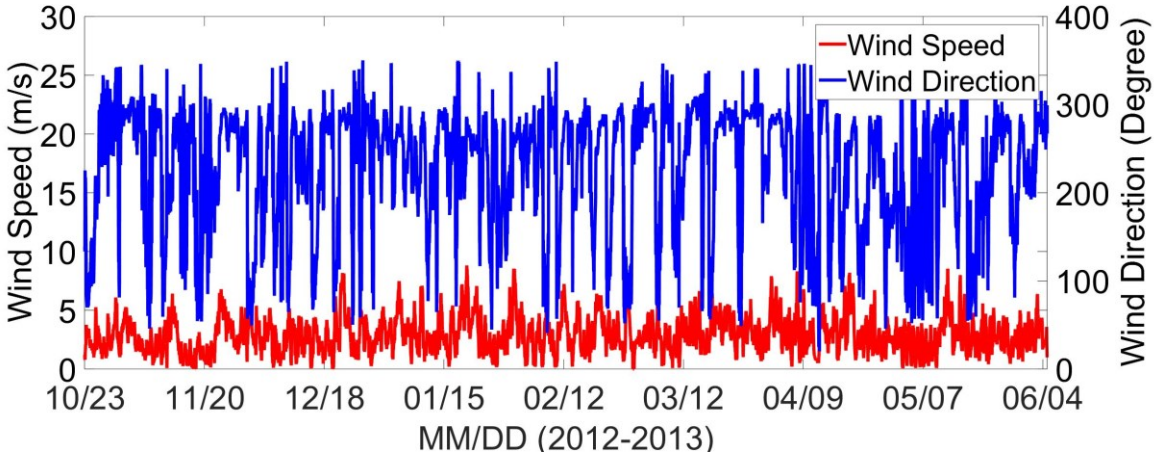

d) Wind speed (m/s) and wind direction (Degree)

Figure 5.6 Monitored weather data

5.3.3 Air leakage modelling methods

5.3.3.1 Air convection model

The air convection model is originally used to simulate the ventilated air cavity behind the exterior cladding by adding a heat and a moisture source to the air layer (Karagiozis and Kunzel, 2009). There are three steps to be followed: firstly, an air layer with the same thickness as the ventilated cavity is created behind the exterior cladding; secondly, an air change source from outdoor is specified for the air layer; and finally, the air exchange rate, which is influenced by wind pressure, thermal buoyancy and moisture concentration buoyancy, is assigned to the air layer to make the stagnant air layer a ventilated air layer. The amount of heat and moisture added to the cavity air layer is calculated based on the outdoor temperature, water vapour content, and the air exchange rate. The source terms are integrated into the energy and mass balance equations. This method can also be employed to simulate the indoor air leakage through a flat roof assembly (Kunzel, 2012). This simulation was based on the assumption that there was a constant indoor air flow between exterior sheathing and roof membrane due to the wind induced pumping effect when the membrane was only mechanically attached. Therefore, a very small air layer (1 mm) with indoor temperature and relative humidity and a constant air change rate was created between exterior sheathing and roof membrane to simulate the indoor air leakage.

In the cases of highly insulated walls, the indoor air was intentionally injected into the stud cavity with a constant air flow rate. To apply the air convection method to this situation, an air layer with indoor air property and constant air change rate is created in the stud cavity, where the insulation layer is located. The thickness of the air layer is set as 1 mm virtually as there is no actual air cavity in the insulation layer. The air change rate of the 1 mm air layer is determined based on the air flow rate injected through the air injection port.

The actual air flow path within the stud cavity is influenced by the type of cavity insulation and its air permeability and difficult to predict. Trial-and-error approach is used to locate this 1 mm air layer to best represent the effect of the injected air on the MC of OSB sheathing. The air layer location is designated as a percentage of cavity depth (L_{cd}) starting from the interior face of the OSB sheathing (0%) to the exterior side of the 6-mil polyethylene (100%). The simulations are performed with the air layer located at 0%, 25%, 50% and 75% of the cavity depth, as shown in

Figure 5.7. The air layer location that best represents the effect of the injected air is determined by comparing the simulated MC of OSB to measurements.

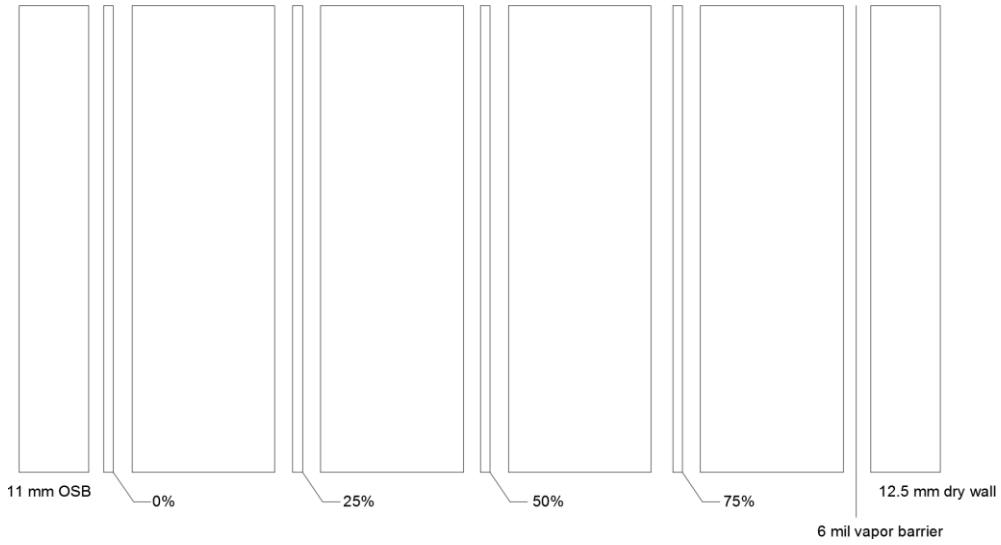

Figure 5.7 1 mm air layer locations.

To implement the air convective method, the hygrothermal models for the three test periods (baseline period, air leakage test period, and drying period) are created separately. The baseline period model does not include this 1 mm air layer in the insulation as there was no air leakage during this period. For the air leakage test period, four models were created with the 1 mm air layer located at 0%, 25%, 50% and 75% of the cavity depth. The initial conditions of all wall components in the air leakage period models are set as the conditions at the end of the baseline period. There are also four models for the drying period corresponding to the four models for the air leakage test period. Figure 5.8 shows the combination of the models for different test periods. The simulation results (MC of OSB) for each period are connected to make up the results for the entire simulation period.

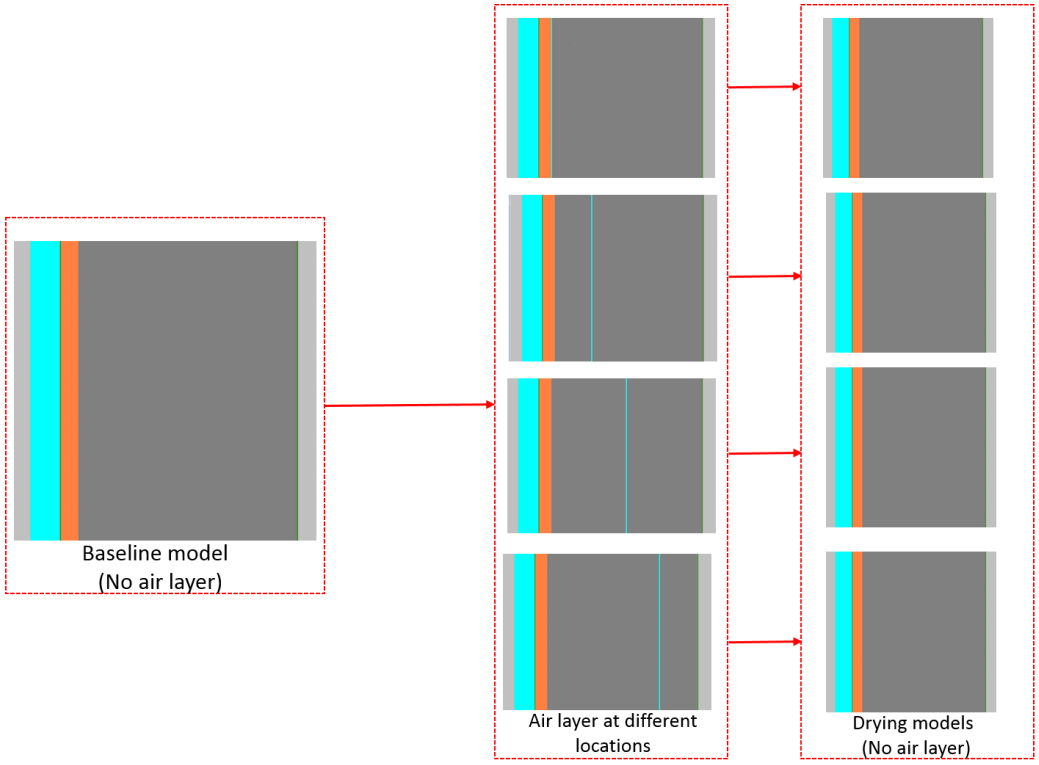

Figure 5.8 Connection of models for different test periods.

5.3.3.2 Air infiltration model

Proposed by Kunzel (2012), the air infiltration model calculates the amount of condensed moisture, which is brought from the air exfiltrates from indoor. The condensed moisture is treated as a moisture source and deposited on the condensation plane, which is generally considered as the interface between wood sheathing and insulation. The amount of condensed moisture can be calculated using equation 5-1:

$$S_w = q_{CL} \cdot (c_{in} - c_{sat.p}) \quad (5\text{-}1)$$

S_w - Moisture source strength kg/m^2·s.

q_{CL} - Air flow through the moisture leaks of the envelope component, m^3/(m^2·s).

c_{in} - Water vapour concentration of indoor air, kg/m^3.

$c_{sat,p}$ - Water vapour saturation concentration at condensation plane, kg/m^3.

This method is based on the assumption that the heat effect of the penetrating air is neglected. The air flow rate (q_{CL}) is typically determined based on the air pressure difference between indoor and outdoor in practice, while the q_{CL} is set as a constant value since a constant airflow rate was maintained through the air injection port. The indoor air vapour concentration is determined based on indoor temperature and relative humidity and the saturation vapour concentration at the condensation plane is determined based on the temperature of the condensation plane under the condition without air leakage. The moisture source strength changes with time since the difference between indoor air vapour concentration and saturation water vapour concentration at condensation plane is not constant. Therefore, a moisture source file that contains the hourly moisture source strength during the air leakage test period is generated according to equation 5-1, and the moisture source is deposited on the condensation plane.

Figure 5.9 shows the calculated moisture source strength of the three types of walls facing north and south orientations. It can be observed that the moisture source strength of I-joist wall is similar to the baseline wall for north orientation. For south orientation, the moisture source strength of I-joist wall is slightly higher than the baseline wall. For the exterior insulated wall, the moisture source strength is zero for the whole examined period, which means there is no condensation at the condensation plane. Table 5.6 shows the condensation hours, the total hours that the condensation will occur during the entire simulation period, for the three types of walls. The I-joist wall has a higher number of condensation hour than the baseline wall because it has colder surface temperature at the condensation plane due to the deeper insulation cavity. There is no condensation hour for the exterior insulated wall as the exterior insulation increases the temperature of the OSB above the dew-point of the indoor air.

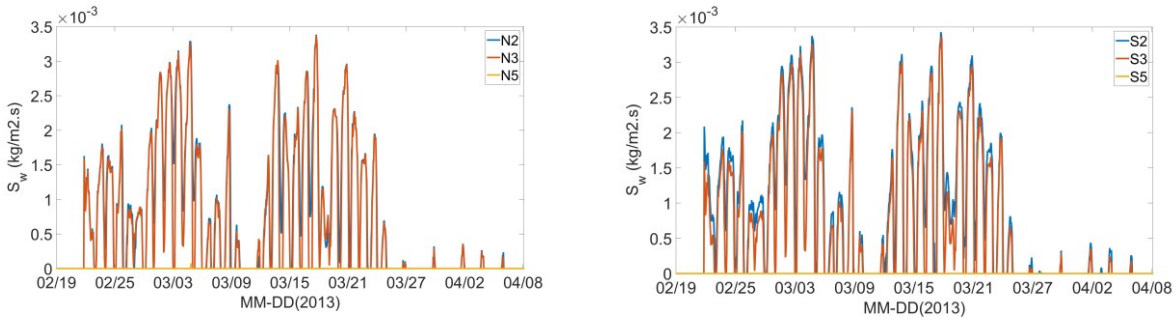

a) North orientation

b) South orientation

Figure 5.9 Moisture source strength at the interior surface of OSB sheathing calculated for the air injection period

Table 5.6 Condensation hours at the interior surface of OSB sheathing calculated for the entire simulation period

	I-joist wall	**Baseline wall**	**Exterior insulated wall**
North	618	550	0
South	633	550	0

The calculated moisture source strength is based on the assumption that all the injected air is able to reach the condensation plane. However, as discussed earlier, the distribution of the injected air in the stud cavity depends on the type of insulation and its air permeability, therefore, the amount of air that can reach the condensation plane differs for each test wall and is less than the total amount of air injected before it exits from the exhaust port located at the top plate. Therefore, simulations are performed for 100%, 75%, 50% and 25% of the total amount of the injected air to determine the air flow rate that can best approximate the effect of injected air on the MC of the OSB sheathing.

5.4 Results and analysis

5.4.1 Comparison between modeling and measurements

As discussed in section 5.2, three pairs of MC sensors were installed at the lower, middle and upper location of the OSB sheathing to monitor the vertical MC profile. Depending on the type of wall assemblies, the MC levels vary while simulated air leakage was introduced. The MC

measurements at the middle location are used for the comparison between measurements and modeling results given the following considerations: 1) depending on the type of cavity insulation, i.e. the air permeability and hygric properties, the difference in MC measurements at the three locations varies. In general, the MC at the middle location falls between the MC measured at the bottom and top locations. 2) Although the inlet and outlet of the air injection is provided, the actual air leakage path is uncertain and may differ in the stud cavity of different wall assemblies depending on the type of insulation. In general, it can be reasonably assumed that after the injected air entries the stud cavity for a while reaching the middle location, the injected air is able to sufficiently mix with the stud cavity air and the airflow is stabilized, therefore, the effect of the injected air on the MC of OSB at this middle point can better represent the response of the wall to the simulated air exfiltration than the MCs measured at the upper and lower locations.

5.4.1.1Air convection method

Figure 5.10 shows the comparison between the simulation results obtained at different air layer locations and the measurements. The simulation results have the similar trend as the measurements and the influence of the 1 mm air layer location is more significant for the north-oriented walls than that for the south-oriented walls. Among the three types of walls, the I-joist wall with cellulose fiber insulation is the most sensitive to the location of the 1 mm air layer as the difference between the results from 0% L_{cd} air layer model and 75% L_{cd} air layer model is the greatest for the north-oriented test wall, followed by the baseline wall with fiberglass insulation and the exterior insulated wall with polyisocyanurate.

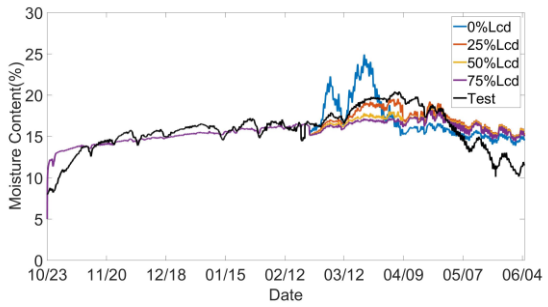

a) I-joist wall: N2

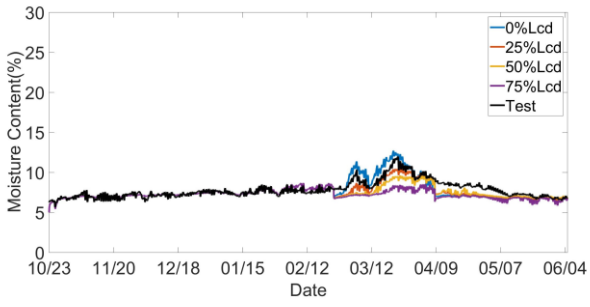

b) I-joist wall: S2

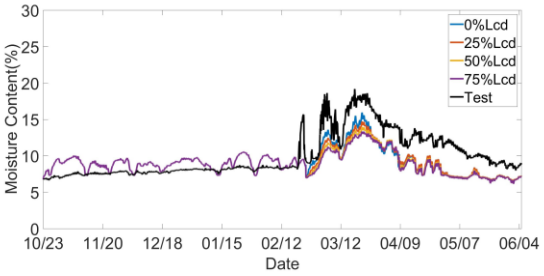

c) Baseline wall: N3

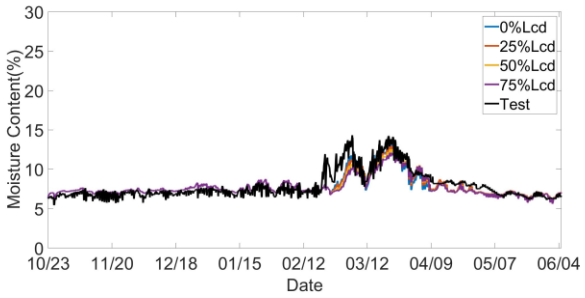

d) Baseline wall: S3

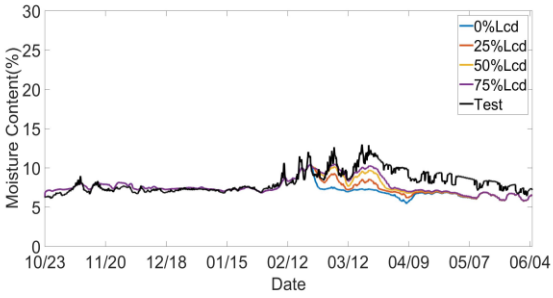

e) Exterior polyisocyanurate: N5

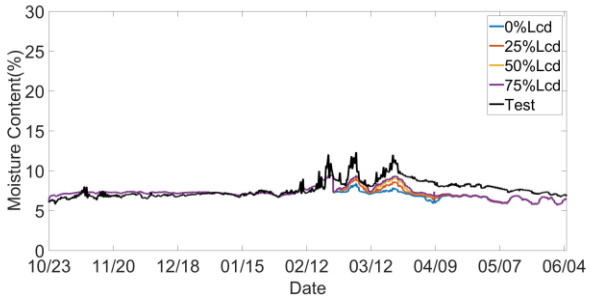

f) Exterior polyisocyanurate: S5

Figure 5.10 Comparison in moisture content of OSB between simulations and measruements

L_{cd}: The cavity depth starting from the interior of OSB

For the I-joist wall in north orientation, the highest MC difference in simulated results between 0% L_{cd} model and 75% L_{cd} model is about 8%. The 25% L_{cd} model has the best agreement with measurements. The highest MC difference between the best matched model and measurement is about 2% during the air leakage period. For the south orientation, the highest MC difference in simulated results between 0% L_{cd} model and 75% model is about 4%. The highest MC difference between the 25% L_{cd} model and measurement is about 2%.

For the baseline wall in north orientation, the highest MC difference between 0% L_{cd} model and 75% L_{cd} model is about 3%. The 0% L_{cd} model has the best agreement with the measurement with a maximum of about 3% difference in MC. For south orientation, the difference among the different air leakage models is small and all of the models have simulation results very close to measurements with only about a maximum of 2% difference in MC.

For the exterior insulated wall, the highest MC difference between 0% Lcd model and 75% Lcd model is about 3% for the north orientation and 2% for the south orientation, respectively. The best matched model has the air layer located at 75% Lcd with about a maximum of 3% MC difference between simulation results and measurements for both north and south orientations. It can also be observed that the cases with air layer closer to OSB have higher MC for the I-joist wall and baseline wall, however, the cases with air layer closer to OSB have lower MC for the exterior insulated wall. To further investigate this phenomenon, the simulated MCs from the models with different L_{cd} are compared with the measured MCs from different locations as shown in Figure 5.11. It can be seen that the simulated MC of the model with 0% L_{cd} has a better agreement with the measured MC at the bottom location, and the simulated MC of the model with 75% L_{cd} has a better agreement with the measured MC at the middle location. The model with air layer in the 0% L_{cd} position reflects the MC response of the bottom location, where the indoor air directly reaches the OSB without mixing with the air in the stud cavity. As shown in Figure 5.11, both simulation results and measurements indicate that MC at the bottom location does not change over the period of air injection and remains the same as before the air injection period. That may be explained by the fact that the warm indoor air approaching the OSB surface without mixing with the stud cavity air increases the air temperature at the bottom of the OSB, therefore, lowers the OSB surface RH, which counter-balances the moisture brought into the stud cavity by the indoor air, as a result, the OSB surface RH at the bottom location remains more or less the same as before the air injection. The model with air layer in the 75% L_{cd} reflects the MC response of the middle location, where the indoor air has sufficiently mixed with the air in the stud cavity.

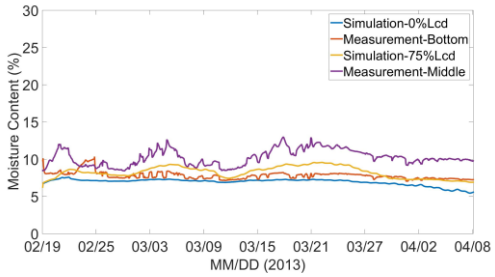

a) Exterior polyisocyanurate: N5

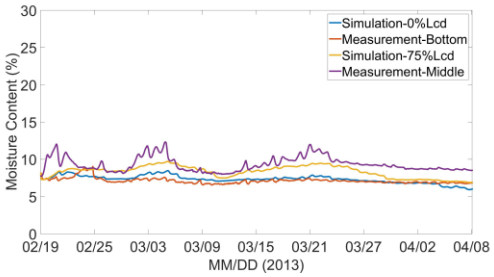

b) Exterior polyisocyanurate: S5

Figure 5.11 Comparison between simulations with different L_{cd} and measurements from different locations

5.4.1.2. Air infiltration method

Figure 5.12 shows the comparison between the simulated MCs of OSB with different q_{CL} and the measurements. The simulation results generally have the similar trend as measurements. In general, the q_{CL} has a positive influence on the MC of OSB, i.e. higher q_{CL} leading to a higher MC of OSB. The baseline wall has the highest MC difference between 100% q_{CL} and 25% q_{CL}, which means it is the most sensitive to the amount of moisture brought by the indoor air deposited on the condensation plane. Since the exterior insulated wall has no condensation hour, the amount of q_{CL} does not influence the MC of OSB. As observed in Figure 5.12e and f, there is no difference between 100% q_{CL} and 25% q_{CL}.

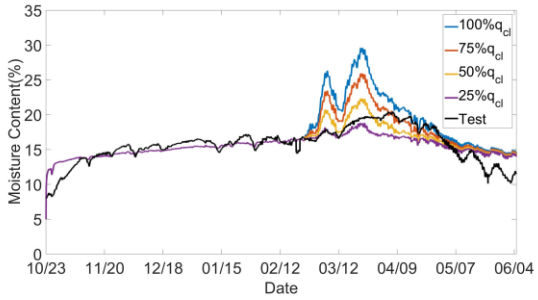

a) I-joist wall: N2

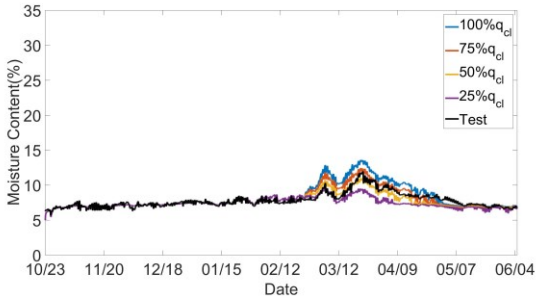

b) I-joist wall: S2

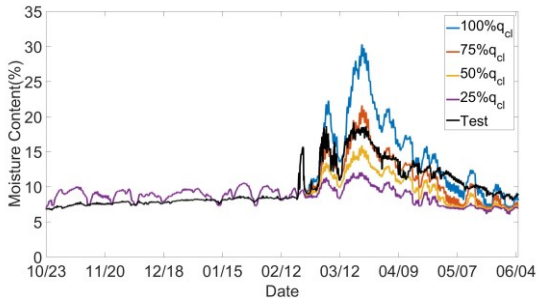

c) Baseline wall: N3

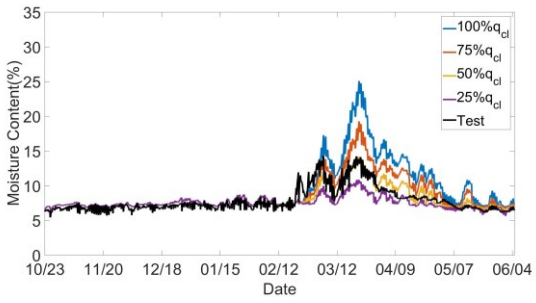

d) Baseline wall: S3

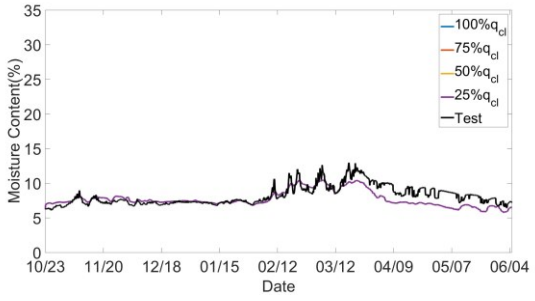

e) Exterior polyisocyanurate: N5

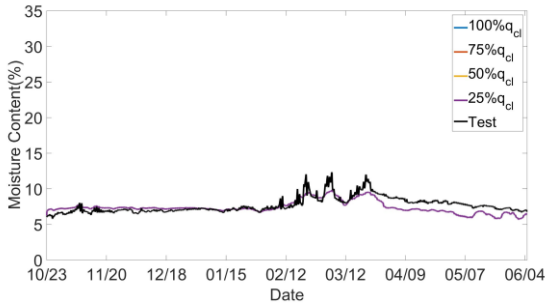

f) Exterior polyisocyanurate: S5

Figure 5.12 Comparison in MC of OSB between simulations and measurements

q_{CL}: The total amount of injected indoor air

For the I-joist wall in the north orientation, the highest MC difference between the model with 100% q_{CL} and 25% q_{CL} is about 10%. The model with 25% q_{CL} has the best agreement with measurements with a maximum of about 3% difference. The influence of airflow amount is less sensitive for the south-oriented I-joist wall. The highest MC difference among the models is about 5%. The model with 50% q_{CL} has the best agreement with measurements. For the baseline wall in north orientation, the highest MC difference between 100% q_{CL} model and 25% q_{CL} model is about 18%, and the 75% q_{CL} model has the best agreement with measurements. For south orientation, the influence of the airflow amount is slightly less than the north-oriented baseline wall. The highest MC difference between 100% q_{CL} model and 25% q_{CL}model is about 15%, and the 50% q_{CL} model has the best agreement with measurements. The simulation results of the exterior insulated wall have a reasonably good agreement with measurements and the highest MC difference is about 2% for both south and north orientated walls.

5.4.1.3. Discussion

Both air convection method and air infiltration methods can obtain simulation results that are very close to measurements as long as the relevant parameters, the location of the air layer and the amount of the air reaching on the condensation plane, are selected properly.

The applicability of the two methods to each type of wall can be evaluated by observing the models that best approximate the MC of OSB. Table 5.7 shows the best models and the highest MC difference between simulations and measurements for each wall.

Table 5.7 Best matched models and the highest MC difference with measurements

Method	**Adjusted parameters**	**N2**	**S2**	**N3**	**S3**	**N5**	**S5**
		I-joist wall with cellulose fiber		**Baseline wall with fiberglass**		**Exterior insulated with polyisocyanurate**	
Air convection method	% of L_{cd} of the best model	25%	25%	0%	0%	75%	75%
	highest MC difference with measurement	2%	2%	3%	2%	3%	3%
Air infiltration method	% of q_{CL} of the best model	25%	50%	75%	50%	*0%	*0%
	highest MC difference with measurement	3%	2%	2%	2%	2%	2%

*Note: For exterior insulated wall, the % of q_{CL} does not influence the result.

As shown in Table 5.7, both methods generate good simulation results with a maximum difference in MC of OSB of 2–3% between simulations and measurements. Given that cellulose fiber insulation has high moisture storage capacity and lower air permeability with dense packed cellulose compared to fiberglass insulation, the amount of moisture carried by the injected air that reached the OSB surface in I-joist wall would be lower than that in the baseline wall with fiberglass insulation. Therefore, the equivalent effect of the injected air on the MC of OSB can be best represented by locating a 1 mm air layer at 25% stud cavity depth for I-joist wall compared to

locating the 1 mm air layer right at the OSB surface for the baseline wall when modeling with air convection method. Similarly, for the air infiltration method, the effect of the injected air on the MC of OSB is equivalent to directly deposit the amount of moisture carried by 25% of the injected air for the I-joist wall, while by 75% of the injected air for the baseline wall. Due to the lower moisture storage capacity and higher air permeability of fiberglass insulation, the air injected into the stud cavity reaches the OSB sheathing surface more easily in the baseline wall compared to that in the I-joist wall with dense packed cellulose fiber. As for the exterior insulated wall, due to surface temperature of the OSB maintained at temperatures above the dew-point of indoor air, no condensation occurs at the OSB surface, therefore, the effect on the MC of OSB is equivalent to 0% air injection for the air infiltration method and a 1 mm air layer located at 75% stud cavity depth for the air convection method.

In general, the location of the 1 mm air layer assumed in the air convection method does not have as significant impact on the MC of OSB as the percentage of injected air deposited at the OSB surface in the air infiltration method. The location of the 1 mm air cavity has a more significant influence on the I-joist cellulose fiber insulation wall than the baseline fiberglass insulation wall, and a slightly greater influence on the north orientation than on the south orientation. In comparison, the influence of assumed percentage of injected air directly deposited on the OSB surface has a more significant influence on both I-joist wall and baseline wall, and similar influence on both north and south orientation for the baseline wall with fiberglass insulation.

The air convection method represents the experimental setup, while the air infiltration method models the air leakage effect by assigning an appropriate amount of moisture directly deposited on the OSB, which is equivalent to the effect of the injected air to each particular test wall. Both methods can provide reasonably good simulation results.

5.4.2 Performance evaluation

5.4.2.1 Moisture content

The validated models with parameters (L_{cd} and q_{CL}) listed in Table 5.7 are used for the long-term hygrothermal performance evaluation using both air convection and air infiltration methods. A constant air leakage rate is assumed for the three test walls over a two-year period starting from

Oct. 2012. The monitored one-year weather data is applied to simulations and repeated for the second year. The MC of the interior layer of OSB is used as the performance indicator for evaluation.

Figure 5.13 shows the comparison between air convection method and air infiltration method. In general, the MC obtained from the air infiltration method is higher than that from the air convection method. For the I-joist wall in north orientation, the results from the air convection method are very close to those from the air infiltration method at the beginning from Oct. 2012 to Apr. 2013. The MC simulated using air convection method becomes lower than that by the air infiltration method in the summer 2013. The highest difference between these two methods is about 5%, which occurs in July 2013. In the summer time, the indoor air has a drying effect on OSB because the moisture concentration of indoor air is lower than that of OSB. The air convection method has taken this drying effect into account, while the air infiltration method assumes the condensation rate is zero when the indoor air is dryer than OSB.

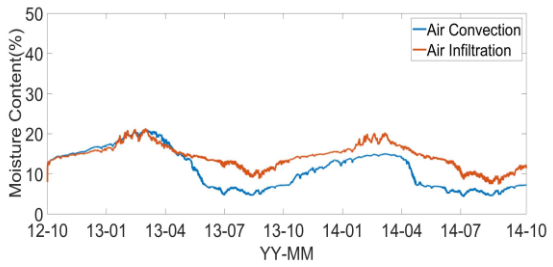

a) I-joist wall: N2

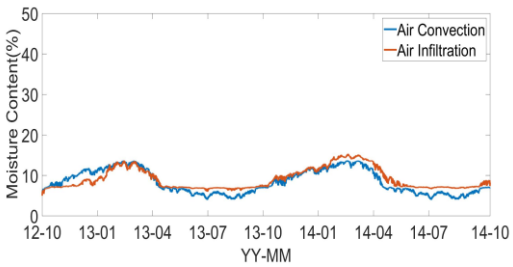

b) I-joist wall: S2

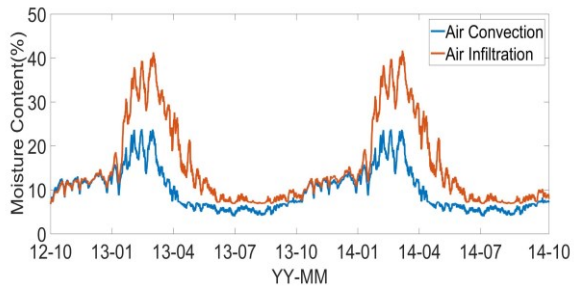

c) Baseline wall: N3

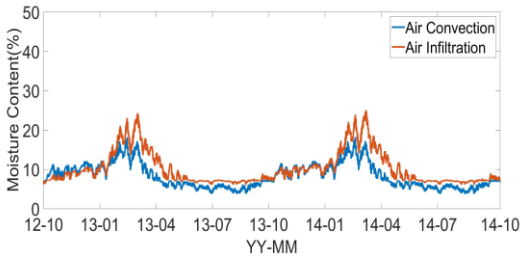

d) Baseline wall: S3

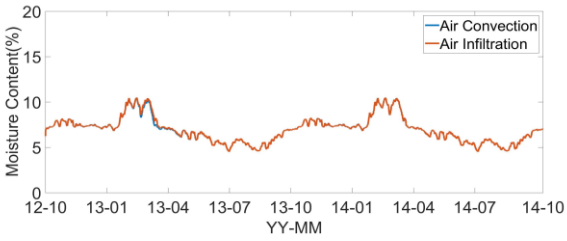

e) Exterior polyisocyanurate: N5

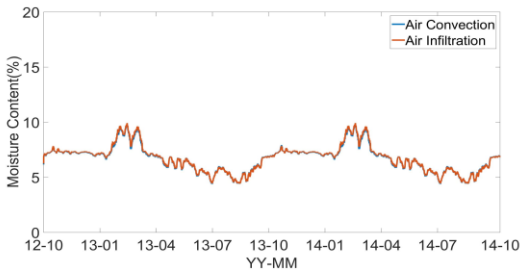

f) Exterior polyisocyanurate: S5

Figure 5.13 Comparison in MC of OSB between the air convection method and the air infiltration method for two-year simulation period.

The difference between air convection method and air infiltration method is more significant for the baseline wall than the I-joist wall in north orientation in winter time and the highest difference between these two methods is about 20%. As shown in Figure 5.10c, the air convection method underestimates the peak MC of OSB, while the air infiltration method overestimates the peak MC of OSB (Figure 5.12c) for the baseline wall compared to the I-joist wall, for which both methods underestimate the peak MC of OSB (Figure 5.10 a and Figure 5.12a). This difference in model performance probably contributes to the significant difference between I-joist wall and baseline wall as seen in Figure 5.13 a and c.

For the south orientation, the results from the air infiltration method are almost the same as those from the air convection method for the I-joist wall, while slightly higher than those from the air convection method for the baseline wall because south receives more solar radiation, which leads to a higher temperature of OSB than the north orientation. Therefore, the condensation hour and condensation rate is lower than that in the north orientation, which makes the MC of OSB is less sensitive to the modeling methods used. For the exterior insulated wall, since there is no condensation on the interior side of OSB due to its higher temperature, modeling methods do not make any difference.

The air infiltration method tends to produce higher moisture content than the air convection method because of two reasons. Firstly, the air infiltration method does not consider the drying effect of the indoor air in summer time when indoor moisture concentration is lower than that at

the surface of OSB. Secondly, air infiltration method considers condensation effect by assuming the condensation rate as a moisture source on the interior side of OSB, while air convection method excludes the condensation effect. Since the air infiltration method tends to overestimate the MC of OSB, which will be more conservative for mold growth risk analysis, and has a similar performance as the air convection method, the air infiltration method is selected for mold growth risk analysis presented in section 5.4.2.2.

5.4.2.2 Mold growth index

The procedure outlined in ASHRAE 160 addendum e (2016) is followed for the calculation of mold growth index. The mold growth index calculation method is developed by Ojanen et al. (2010). Mold growth index is defined based on the mold visual appearance on the wood sheathing surface. There are six levels of mold growth index from 1 (some growth detected only with microscopy) to 6 (100% visually detected coverage). The mold growth index is calculated using the following equations:

$$M_t = M_{t-1} + \Delta M \tag{5-2}$$

M_t - mold index for the current hour

M_{t-1} - mold index for the previous hour

ΔM - change in mold index calculated for each hour, favorable condition using equation 5-3, unfavorable condition using equation 5-7

$$\Delta M = \frac{k_1 k_2}{168 \times \exp(-0.68 \ln T_s - 13.9 \ln RH_s + 0.14W + 66.02)} \tag{5-3}$$

k_1 - mold growth intensity factor, depends on material sensitivity class and current value of M listed in Table 5.8, sensitive class is used in this paper.

k_2 - mold growth attenuation factor calculated using equation 5-4

W - parameter selected based on material sensitivity class, selected based on Table 5.8

$$k_2 = \max\{1 - \exp[2.3(M - M_{max}], 0\} \tag{5-4}$$

M_{max} - the maximum mold index corresponding to surface temperature and relative humidity at current hour, calculated using equation 5-5

$$M_{max} = A + B\left(\frac{RH_{crit}-RH_s}{RH_{crit}-100}\right) - C\left(\frac{RH_{crit}-RH_s}{RH_{crit}-100}\right)^2 \quad (5\text{-}5)$$

RH_{crit} - the critical RH, which is used for judging the favorable or unfavorable conditions, calculated using equation 5-6

$$RH_{crit} = \begin{cases} -0.00267T_s^3 + 0.16T_s^2 - 3.13T_s + 100 \text{ when } T_s \leq 20℃ \\ 20 \text{ when } T_s > 20℃ \end{cases} \quad (5\text{-}6)$$

$$\Delta M = \begin{cases} -0.00133k_3 \; when \; t_{decl} \leq 6 \\ 0 \; when \; t_{decl} \leq 24 \\ -0.000667k_3 \; when \; t_{decl} > 24 \end{cases} \quad (5\text{-}7)$$

k_3 - mold index decline coefficient specific to the material surface, 0.1 is used in this paper

t_{decl} – number of hours from the moment when conditions for mold growth changed from favorable to unfavorable

Table 5.8 Parameters for equation 5-3 and equation 5-5 (Ojanen et al., 2010)

	k_1					
Sensitivity class	**If M<1**	**If M>1**	**W**	**A**	**B**	**C**
Very sensitive	1	2	0	1	7	2
Sensitive	0.578	0.386	1	0.3	6	1
Medium resistant	0.072	0.097	1	0	5	1.5
Resistant	0.033	0.014	1	0	3	1

The air leakage rate (0.315 L/s) used in the model is for a wall assembly with an average airtightness under 5 Pa indoor and outdoor air pressure difference (Fox, 2014). According to ASHRAE (2013) the air leakage rate under 75 Pa air pressure difference is 0.5 L/s·m^2 for tight envelope, 1.5 L/s·m^2 for average envelope and 3 L/s·m^2 for leaky envelope. The 75Pa air pressure difference is generally produced under test conditions. To investigate the effect of air leakage under normal condition, the air leakage rates under 75Pa pressure difference are converted to those under 5Pa pressure difference according to following equation (ASHRAE, 2013):

$$Q = c(\Delta p)^n \quad (5\text{-}8)$$

Q - airflow through opening m^3/s

c - flow coefficient $m^3/(s.Pa^n)$

n - pressure exponent, dimensionless, a typical value for n is about 0.65

After conversion, the air leakage rate under 5 Pa air pressure difference is 0.09 L/s·m^{2}for tight envelope, 0.27 L/s·m^2 for average envelope and 0.54 L/s·m^2 for leaky envelope. Therefore, additional simulations are performed for the tight and leaky scenarios under 5Pa air pressure difference. An extreme condition with 1.5 L/s·m^2 air leakage rate is also simulated to reflect the air leakage level for an average envelope under 75 Pa indoor and outdoor air pressure difference. The amount of condensed moisture calculated by these air leakage rates is also adjusted by the scaling factors listed in Table 5.7. Mold growth index is calculated for the three walls over two years. Given that there is no mold growth risk for exterior insulated wall, only results for the I-joist wall and the baseline wall are shown in Figure 5.14.

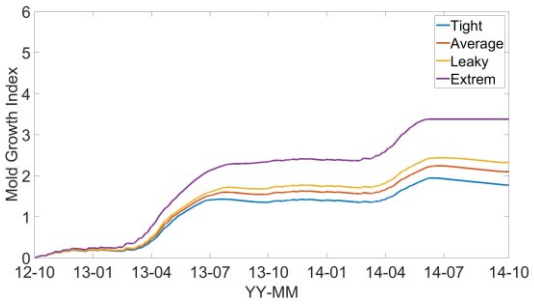

a) I-joist wall: N2

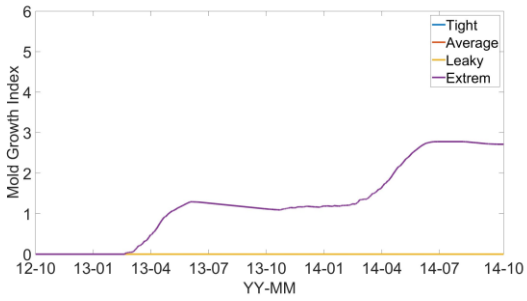

b) I-joist wall: S2

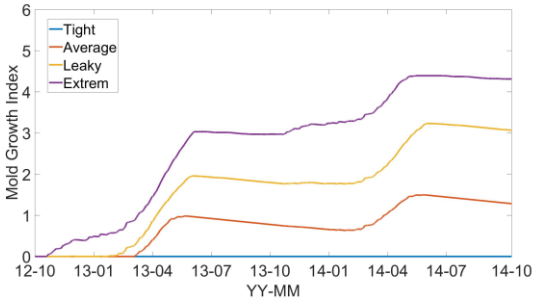

c) Baseline wall: N3

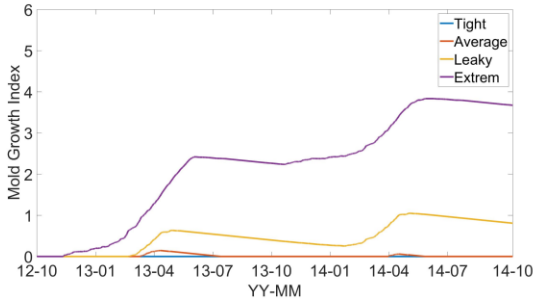

d) Baseline wall: S3

Figure 5.14 Sensitivity analysis of mold growth index for I-joist wall with cellulose insulation and baseline wall with fiberglass insulation

For the I-joist wall in north orientation, at the end of the two-year simulation period, the mold growth index is about 2 for all of the three scenarios (tight, average and leaky), while the mold growth index reaches 3.5 only for the extreme condition. According to ASHRAE 160 (2016), a mold growth index above 3.0 is considered as risk. For the baseline wall in north orientation, at the end of the two-year simulation period, the mold growth index reaches 3.0 with leaky scenario and 4.2 under extreme condition. Therefore, the baseline wall has a slightly higher mold growth risk than the I-joist wall under leaky and extreme conditions.

For the south orientation, the I-joist wall has no mold growth risk even under assumed leaky condition but the mold growth index can reach 3.0 when the wall is under extreme air leakage condition. For the baseline wall, the mold growth index is below 1.0 even under leaky condition, which indicates very low mold growth risk. The highest mold growth index is about 3.8 under extreme air leakage condition, which means the baseline wall has a slightly higher mold growth risk than I-joist wall under such an extreme condition.

The mold growth risk of OSB observed is largely dependent on the insulation materials. The baseline wall with fiberglass insulation has a higher mold growth risk than the I-joist wall with cellulose fiber insulation although the OSB temperature of the I-joist wall is lower than that of the baseline wall. To investigate the performance difference derived by the wall structure (the thickness of insulation), the simulation is also performed for the I-joist wall with fiberglass insulation. The best matched models, which use the scaling factor (75% for both the I-joist wall and the baseline wall with fiberglass insulation) listed in Table 5.7, are used for this investigation. The initial MC of fiberglass in I-joist wall is set as the same as that in the baseline wall (0.32 kg/m^3).

Figure 5.15 shows the mold growth index for the I-joist wall and the baseline wall with fiberglass insulation under different airtightness conditions. It can be found that the mold growth index of I-joist wall is slightly higher than that of the baseline wall. For the tight and average scenarios, both walls do not have mold growth risk according to ASHRAE criteria (2016). The mold growth index is zero over the two years for both the I-joist wall and the baseline wall for the tight scenario. For the average leakage scenario, the maximum mold growth index is 2.1 for the I-joist wall and 1.2 for the baseline wall, respectively. For the leaky and extreme scenarios, both the I-joist wall and the baseline wall have mold growth risks although the difference between these two walls becomes

smaller. For the leaky scenario, the maximum mold growth index is 3.5 for the I-joist wall and 3.1 for the baseline wall, while for the extreme scenario, the maximum mold growth index is 4.4 for the I-joist wall and 4.2 for the baseline wall.

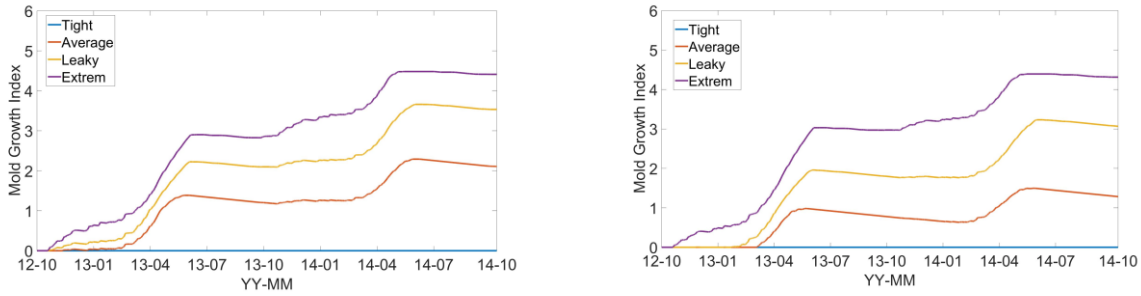

a) I-joist wall: N2 with fiberglass insulation

b) Baseline wall: N3

Figure 5.15 Mold growth index for I-joist wall and baseline wall with fiberglass insulation (North orientation)

5.5 Summary

This chapter investigates the effect of air leakage on the hygrothermal performance of three wood-framed walls, one baseline and two highly insulated walls under cold climatic conditions. Two simplified air leakage modelling methods, air convection method and air infiltration method, are implemented in DLPHIN. The HAM models using the two air leakage modeling methods are calibrated by adjusting the critical parameters, i.e. the position of the air layer in the air convection method and the amount of the indoor air reaching the condensation plane in the air infiltration method, to match the measured MC of OSB sheathing. The applicability of these two air leakage modeling methods is compared. The air infiltration method, which tends to overestimate the moisture content of OSB sheathing, as a more conservative approach, is used for the long-term hygrothermal performance evaluation. Four levels of airtightness, i.e. tight, average, leaky and extreme, are investigated. Mold growth index is calculated following ASHRAE 160 procedure to evaluate the risk of mold growth. Given that the experimental setup modeled a specific air leakage path, i.e. indoor air entering from the interior at the bottom of the stud cavity and returning to the interior at the top of the cavity, the conclusions are generally limited to this specific air leakage pattern. Further investigation of the modeling approach for other air leakage scenarios may be needed.

The main conclusions of this chapter are:

- The simulation results generally have the similar trend with measurements for both air convection method and air infiltration method. The models that best approximate the MC of OSB can be configured by adjusting the position of air layer in the air convection method and the amount of the indoor air reaching the condensation plane in the air infiltration method.
    - Using the air convection method, the models that best approximate the MC of OSB sheathing have the 1 mm air layer located at 25% of cavity depth (L_{cd}) from the interior surface of OSB for the I-joist wall with 240 mm cellulose fiber insulation, at 0% L_{cd}, i.e. at the interior surface of the OSB for the baseline wall with 140 mm fiber glass insulation, and at 75% L_{cd} for the exterior insulated wall, respectively. The indoor air has a drying effect on MC of OSB in summer season.

- Using the air infiltration model, the models that best approximate the MC of OSB sheathing have an equivalent of 25% of the total amount (q_{CL}) of the injected air reaching the condensation plane for the I-joist wall facing north orientation, and 50% of the total amount for the south orientation. For the baseline wall, the best model has an equivalent of 75% q_{CL} for north facing orientation and 50% q_{CL} for the south orientation. For the exterior insulated wall, there is no condensation on the condensation plane.
- In general, south facing walls are less sensitive to the location of air layer and the equivalent amount of indoor air reaching the condensation plane assumed in simulations.

- Given that the air infiltration method takes into account condensation and excludes the drying effect of indoor air, the best matched models using the air infiltration method tend to slightly overestimate the MC of OSB sheathing, while the best matched models using the air convection method tends to slightly underestimate the MC of OSB compared to measurements. Consequently, the air infiltration method results in higher MC of OSB of wood-frame walls investigated for the two-year simulation period with a constant air leakage rate.
- The hgrothermal performance of the baseline 2x6 wall with fiberglass insulation is more sensitive to the change of airtightness level than the I-joist wall with cellulose fiber insulation. For north orientation, the mold growth index increases from zero to 3 when the airtightness changes from tight to leaky and reaches 4 under extreme leaky condition, while the mold growth index of the I-joist wall only reaches 3 under the extreme leaky condition.
- When the I-joist wall is fitted with fiberglass insulation instead, the I-joist wall exhibits higher risk of mold growth than the 2x6 wood frame wall. The mold growth index reaches 3.0 after six months of constant air leakage and reaches 4.5 after 8 months and stabilized at 5 at the end of the two-year simulation period for north facing wall under the extreme leaky levels.
- The exterior insulated wall has no risk of mold growth as the exterior insulation results in a higher OSB temperature and a surface RH staying below the critical RH for mold growth.

Chapter 6 Application of stochastic approach to two case studies

This chapter presents the stochastic hygrothermal analysis of CLT walls and highly insulated wood framed walls. According to Finch et al. (2013), there are three insulation strategies depending on the placement of insulations- interior insulated wall, exterior-insulated wall and split insulated wall.

The CLT wall is selected as a representative of exterior-insulated wall for stochastic analysis. In Chapter 4, the hygrothermal performance of CLT walls with low exterior permeance and high exterior permeance are evaluated under normal condition and rain leakage condition. The uncertainties of the moisture content of CLT panel caused by material properties and rain leakage are investigated through parametric study, which changes one parameter at a time. However, the on-factor-at-a-time method does not consider the combined effects of the parameters on simulation result, and the simulations are only performed for the models with extreme parameters, which cannot evaluate the moisture problem risks. In this chapter, stochastic approach is applied to investigate the uncertainties of the moisture content of CLT panels with the material properties, rain deposition factors and cladding ventilation rate are considered as stochastic variables.

The baseline wall, I-joist wall and polyisocyanurate wall investigated in Chapter 5 are selected as the representatives of interior insulated wall and split-insulated wall. The stochastic simulations are also performed for mineral wool wall, the wall with high permeance exterior insulation, to compare with polyisocyanurate wall, the wall with low permeance exterior insulation. In Chapter 5, the impact of air leakage on hygrothermal performance of highly insulated walls is investigated through different air leakage modelling methods- air infiltration method and air convection method. This chapter further investigates the impact of air leakage through stochastic approach. The impact of other moisture loads such as rain leakage, internal moisture load level are also investigated through the stochastic simulation methodology developed in Chapter 3.

6.1 Case study 1: CLT wall assemblies

6.1.1 Stochastic variables

For material properties, the basic hygric properties including saturation water content (W_f), vapour resistance factor at dry state (μ_{Dry}) and moisture diffusivity at saturation water content (D_{ww}) are considered as stochastic variables. They are assumed to follow a normal distribution. The property

functions-moisture storage function, vapour resistance factor as a function of relative humidity, and moisture diffusivity as a function of normalized water content are scaled based on the basic hygric parameters. The influential boundary conditions such as the rain deposition factor, short-wave radiation absorptivity, and cladding ventilation rate are considered as stochastic variables with a uniform distribution assumed. The range of rain deposition factor is determined according to ASHRAE 160 (2016). The short-wave radiation absorptivity can be varied from 0.4 to 0.9 depending on the exterior material (WUFI Pro 5.3, 2014). A light color fiber cement board was used as cladding in the field study. To investigate the influence of short-wave radiation absorptivity, the range of 0.4–0.9 is chosen. The range of cavity ventilation from 0 ACH to 100 ACH is chosen according to the review of field studies by Simpson (2010). The mean values and standard deviations of the stochastic variables are presented in Table 6.1. Figure 6.1 shows the stochastic material functions, which are generated by multiplying a coefficient: parameter_stochastic / parameter_mean.

Table 6.1 Statistical figures of stochastic variables

	Material properties			**Boundary conditions**		
	W_f	**μ_{Dry}**	**D_{ww}**	**F_D**	**α_s**	**V_r**
	kg/m^3	**-**	**m^2/s**	**-**	**-**	**1/h**
Statistical parameter	630 (42)	1876 (143.8)	100 (16.6)	0.35 to 1	0.4 to 0.9	0 to 100
Distribution	Normal	Normal	Normal	Uniform	Uniform	Uniform

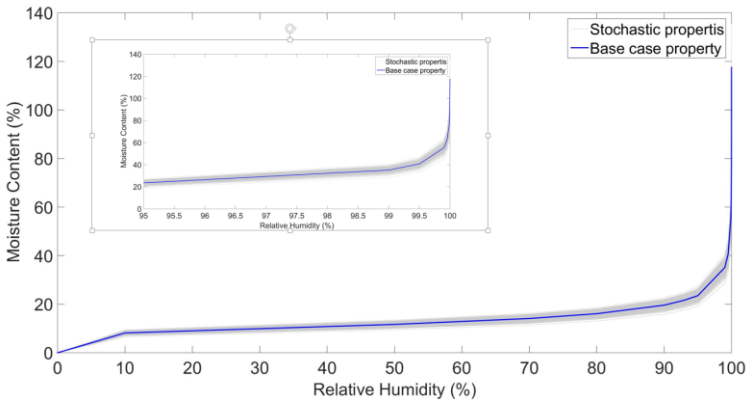

a) Moisture storage function

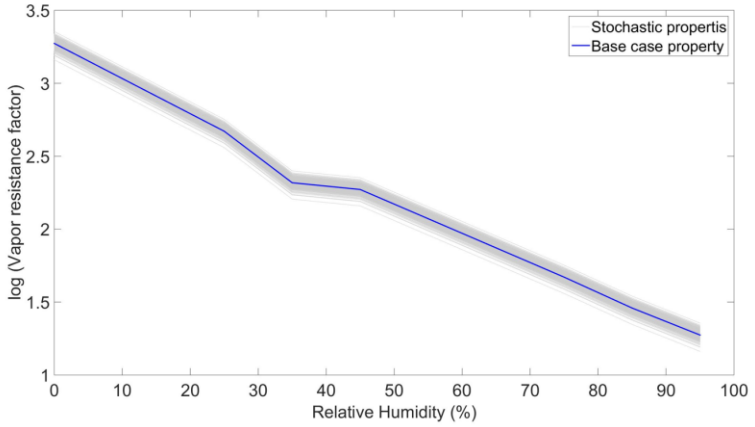

b) Vapour resistance factor as a function of relative humidity

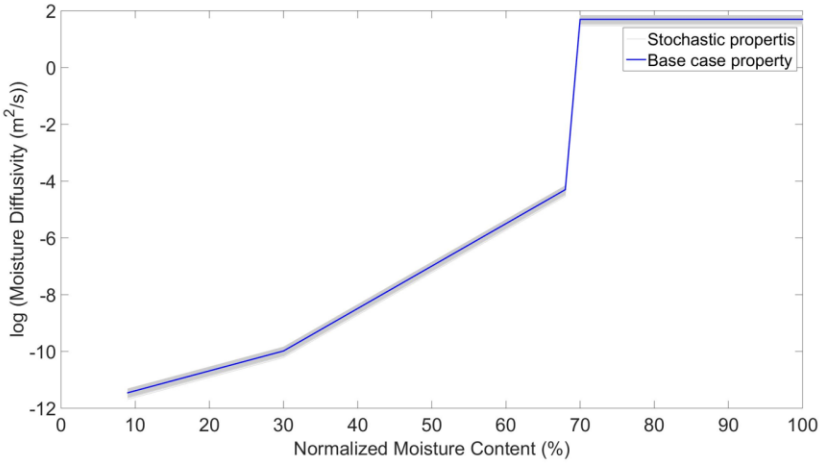

c) Moisture diffusivity as a function of moisture content

Figure 6.1 Material property functions of CLT panel

6.1.2 Scenario variables

The factors that are considered as scenario variables are orientation, rain leakage. The analysis of on-site weather data showed that the west orientation receives the highest amount of wind-driven rain (330mm), the east orientation, which is the test orientation, receives much lower amount of wind-driven rain (135mm). Therefore, east orientation and west orientation are chosen as the two extreme values. The rain leakage is an important moisture load which impacts the moisture performance of the CLT panel, therefore, it is selected as one of the influential factors for analysis. According to ASHRAE 160 (2016), 1% of wind-driven rain is assumed to be deposited on the exterior surface of the CLT panel. The two extreme values of rain leakage are 0% (no rain leakage) and 1%. The two extreme values for the vapour permeance of WRB are these used in the test wall, with a vapour resistance of 49.7 for the high vapour permeance WRB and a vapour resistance of 50000 for the low vapour permeance WRB. For each factor, two extreme values are assigned. Then the scenario variables can be organized by a 3 factor 2 level full factorial design. There will be 2^3=8 combinations of these variables. Table 6.2 shows the combinations of these factors. Each combination represents one scenario, in which the stochastic variables are sampled by the Latin Hypercube Sampling method.

Table 6.2 Factorial design of scenario variables

Factor combination scenarios	**Orientation**	**Rain Leakage**	**Vapour permeance of WRB**
1	East	Without (0%)	Low (μ =50000)
2	West	Without (0%)	Low (μ =50000)
3	East	With (1%)	Low (μ =50000)
4	West	With (1%)	Low (μ =50000)
5	East	Without (0%)	High (μ= 49.7)
6	West	Without (0%)	High (μ =49.7)
7	East	With (1%)	High (μ =49.7)

8	West	With (1%)	High (μ =49.7)

In summary, for each parameter, 100 random values are generated by the Latin Hypercube Sampling method. By taking all the factors into account, 8*100=800 cases were generated.

6.1.3 Results and analysis

6.1.3.1 Uncertainty analysis of moisture content

Figure 6.2 and Figure 6.3 show the stochastic results for wall assembly B1 and B2, respectively. It is obvious that the stochastic results have the same moisture content pattern as the base cases. The moisture content pattern of wall assembly B1 is significantly different than that of B2 due to the difference in the vapour permeance of the WRB and the initial MC level.

Figure 6.2a and Figure 6.3a also show the comparison between measurements and the stochastic results for B1 and B2. It can be seen that the stochastic results have similar trend as the test results. For B1, the test results fall within the stochastic results and agree well with the base case simulation results. For B2, most stochastic results have overestimated the MCs. The largest difference of moisture content between the stochastic results and the test result is about 5% for both B1 and B2. The parameters of the best and worst-matched cases are presented in Table 6.3. Generally, the best-matched case of B1 has similar W_f and D_{ww} with that of the base case. The rain deposition factor is lower than average, and this is also true for solar radiation absorptivity and cladding ventilation rate. The worst-matched case has higher W_f, lower μ_{Dry} and lower D_{ww}. The rain deposition factor is higher than average and the cladding ventilation rate is lower than average, the short-wave radiation absorptivity is equal to the average value. For B2, the best-matched case has a lower W_f, lower D_{ww} and a higher μ_{Dry}. The rain deposition factor is lower than the average, the short-wave radiation absorptivity is about the average, and the cladding ventilation rate is higher than the average.

Table 6.3 Parameters of the best and worst matched cases

Wall assemblies	**Material properties**			**Boundary conditions**		
	W_f (kg/m^3)	**μ_{Dry} -**	**D_{ww} (m^2/s)**	**F_D -**	**α_s -**	**V_r (1/h)**

B1	Best	611.1	1726.6	105	0.47	0.51	42.2
	Worst	726.2	1788.3	75.5	0.75	0.65	27.8
B2	Best	511.7	1925.1	77.6	0.38	0.63	65.5
	Worst	726.2	1788.3	75.5	0.75	0.65	27.8

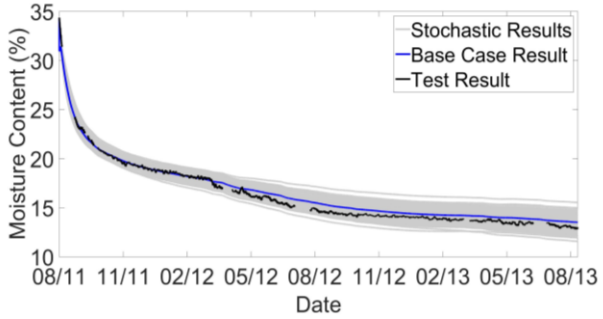

a) Scenario 1- East, without rain leakage

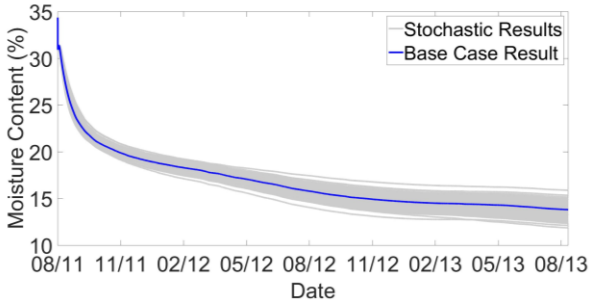

b) Scenario 2 -West, without rain leakage

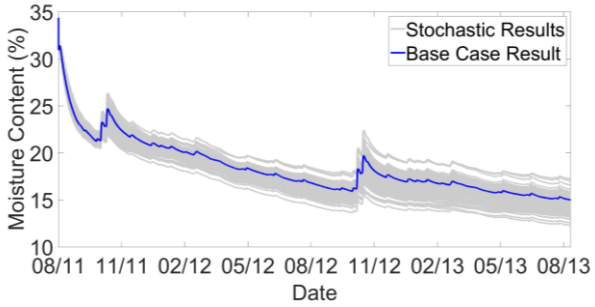

c) Scenario 3 - East, with rain leakage

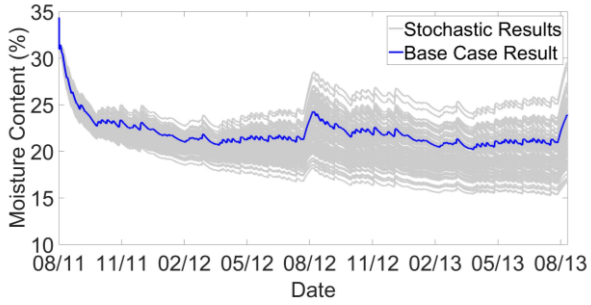

d) Scenario 4 - West, with rain leakage

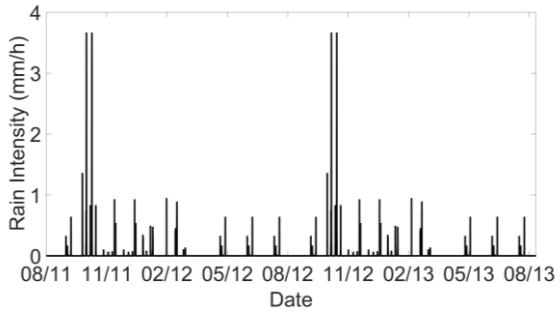

e) Wind-driven rain-East

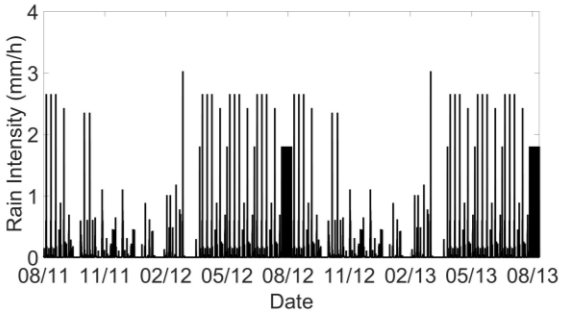

f) Wind-driven rain-West

Figure 6.2 Stochastic results of B1 (low permeance WRB)

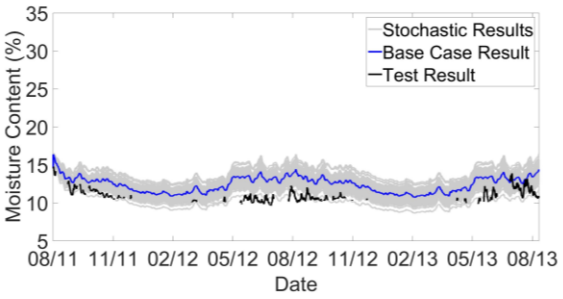

a) Scenario 5 - East, without rain leakage

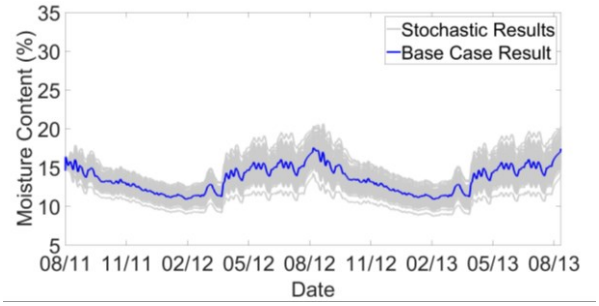

b) Scenario 6 - West, without rain leakage

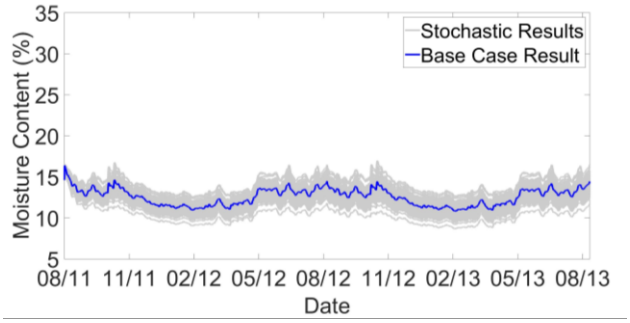

c) Scenario 7 - East, with rain keakage

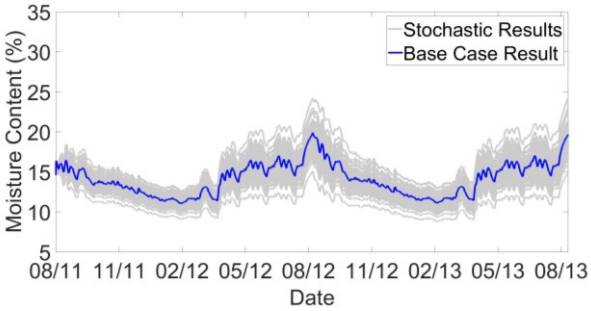

d) Scenario 8 - West, with rain leakage

Figure 6.3 Stochastic results of B2 (high permeance WRB)

B1-low permeance WRB assembly

For B1, the moisture content is not responsive to the variation of environmental conditions. It decreases continuously when there is no rain leakage as shown in Figure 6.2a and Figure 6.2b. For the east orientation without rain leakage (Figure 6.2a), the case with lowest moisture content is able to decrease to below 20% from 35% in about 3 months. The moisture content of the case with the highest moisture content is able to decrease to below 20% after 6 months, and this is also true for the west orientation (Figure 6.2b), which receives a higher amount of wind-driven rain. At the end of the examined period, the spread of the moisture content is about 4% for both scenario 1 (east orientation without rain leakage) and scenario 2 (west orientation without rain leakage). Although the overall trend of the moisture content is still decreasing when the rain leakage is introduced for the east orientation, there are two peaks in Oct. 2011 and Oct. 2012- the periods with the highest rain load (Figure 6.2c). The moisture content decreases to below 20% after 3 months for the case with the lowest MC, and it takes 9 months to dry to below 20% for the case

with the highest MC. Cases with higher MC typically has a much higher rain deposition factor. Since the drying period with higher moisture content becomes longer than those without rain leakage, the risk of the moisture problem will be greater. For the west orientation with rain leakage (Figure 6.2d), only a few cases are able to dry to below 20% because of the higher amount of wind-driven rain deposited on the west façade. The range of the moisture content is expanding with time. At the end of the two-year simulation periods, the range of moisture content between the highest and lowest cases is 5% for the east, and 13% for the west façade, respectively.

B2-high permeance WRB assembly

For B2, the moisture content fluctuates with the variation of rain load as shown in Figure 6.3. For the east orientation, the moisture contents will not exceed 20% during the examined period for both scenarios with (scenario 7) and without (scenario 5) rain leakage. The largest range of MC is 5.0% for the scenario without rain leakage and 5.5% for the scenario with rain leakage. For the west orientation, even without rain leakage there are a few cases with moisture content slightly exceeding 20% when the rain load becomes higher. Such cases have much higher rain deposition factor (close to 1.0), lower short-wave radiation absorptivity, and lower cladding ventilation rate. When rain leakage is introduced (Figure 6.3d), there are more cases with moisture content exceeding 20%. The highest moisture content is about 25%. The largest range of the moisture content is 7.9% for the scenario without rain leakage and 10.1% for scenario with rain leakage, respectively.

6.1.3.2 Sensitivity analysis

Figure 6.4 and Figure 6.5 show the sensitivity index (PCC) for each scenario. It can be seen that the PCCs are changing with time and the variation pattern of the PCCs of B1 is significantly different from B2. For B1, the PCCs of each parameter do not vary much within a short time period, which means they are not influenced by the ambient climatic conditions, while the PCCs for B2 are responsive to the variation of environmental conditions.

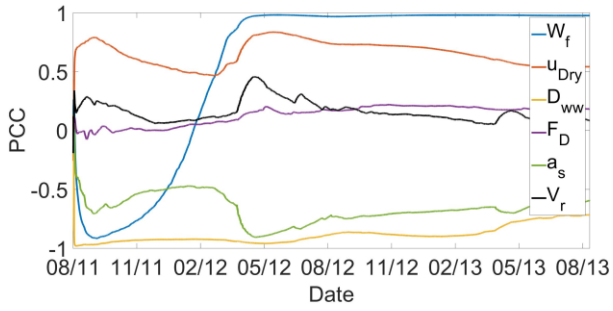

a) Scenario1 - East, without rain leakage

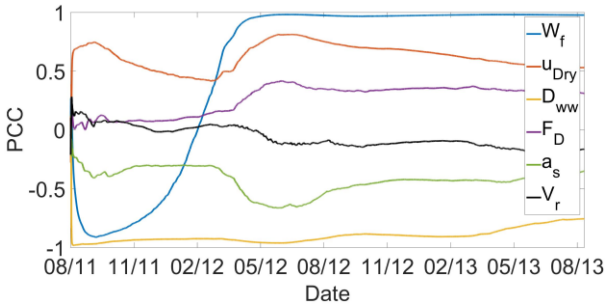

b) Scenario 2 - West, without rain leakage

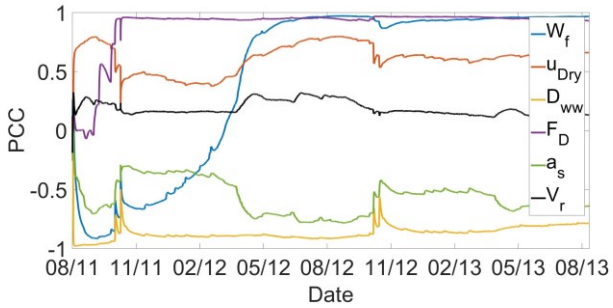

c) Scenario 3 - East, with rain leakage

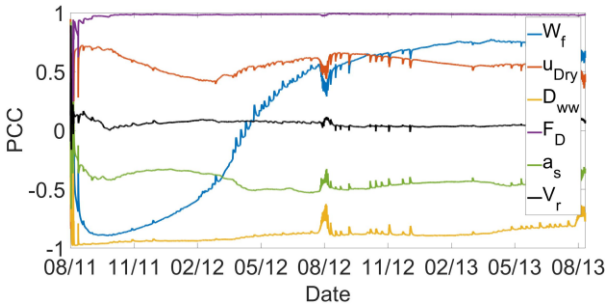

d) Scenario 4 - West, with rain leakage

Figure 6.4 PCCs for B1 (low permeance WRB)

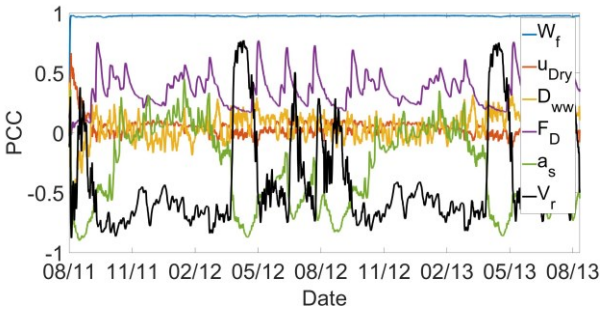

a) Scenario 5 - East, without rain leakage

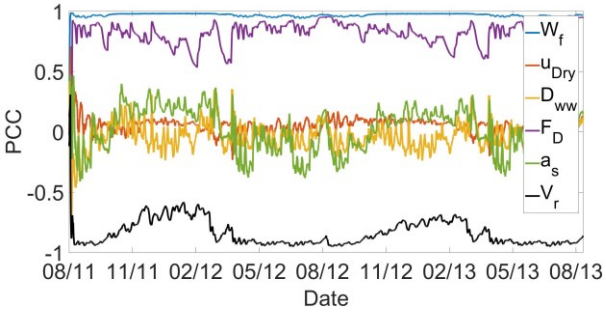

b) Scenario 6 - West, without rain leakage

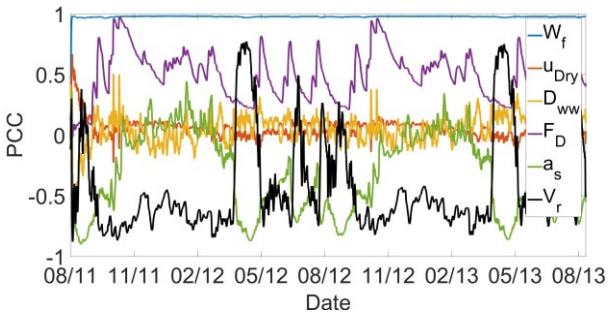

c) Scenario 7 - East, with rain leakage

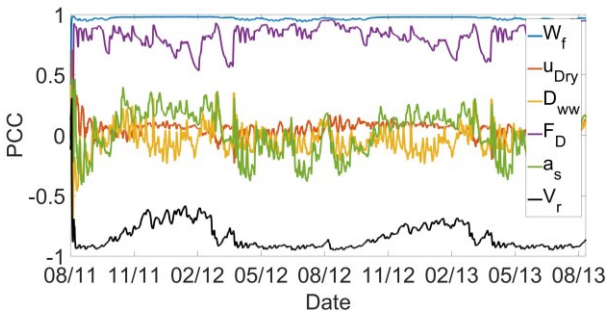

d) Scenario 8 - West, with rain leakage

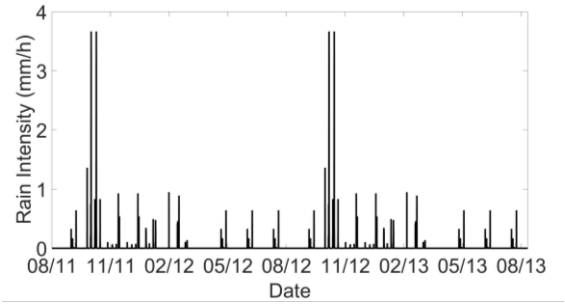

e) Wind-driven rain - East

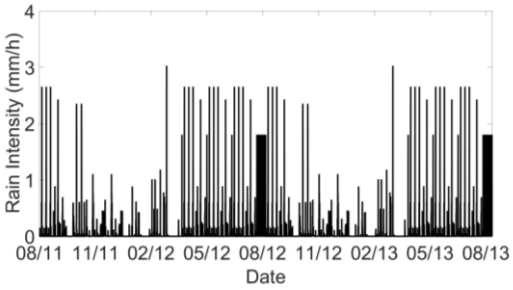

f) Wind-driven rain - West

Figure 6.5 PCCs for B2 (high permeance WRB)

Due to the low vapour permeance of WRB in B1, when no rain leakage is introduced, the MC level of CLT is not influenced much by the environmental conditions, as shown by the insignificant influence of ventilation rate (V_r) and rain deposition factor (F_D) i.e. low absolute value of PCC for F_D and V_r (Figure 6.4 a, b). The influence of vapour resistance factor (μ_{Dry}) is less significant than that of the moisture storage function. Both the short-wave radiation absorptivity ($\boldsymbol{\alpha}_s$) and moisture diffusivity (D_{ww}) have a negative influence, i.e. higher short-wave radiation absorptivity and higher moisture diffusivity, lower MC level, with the influence of moisture diffusivity being more significant. When rain leakage is introduced (Figure 6.4 c,d), the influence of rain deposition factor is increased significantly. The ventilation rate still has an insignificant impact due to the low permeance of WRB. The influence of other parameters is similar to the cases without rain leakage.

The PCCs of parameters in B2 fluctuate significantly during the two-year simulation period except for the moisture storage function, which always has a positive influence on the moisture content with a PCC value close to 1.0. Because of the high vapour permeance of WRB, the MC level of CLT in B2 is more responsive to the ambient environment. Therefore, the influence of boundary

conditions is more significant, while the influence of material properties i.e. vapour resistance factor and moisture diffusivity, becomes less significant. The trend is similar for both cases without (Figure 6.5 a, b) and with (Figure 6.5 c, d) rain leakage. The rain deposition factor and ventilation rate have more significant influences than the short-wave radiation absorptivity. The rain deposition factor has a positive PCC and fluctuates following the occurrence of rain events (shown in Figure 6.5 e, f), while the ventilation rate has a negative PCC most of the time, i.e. higher ventilation rate facilitating drying, and a positive PCC occasionally with peaks during dry periods without rain. Different influence of cavity ventilation is observed for the east and the west orientation. For the east orientation, there are occasions when cavity ventilation increases MC level, i.e. the PCC becomes positive. These occasions occur when solar radiation is low. For the west orientation though (Figure 6.5 b, d), cavity ventilation always has a negative PCC value. Generally, the influence of short-wave radiation absorptivity is less in the west orientation compared to the east. The more detailed discussion on the influence of each parameter is provided in the following sections.

Influence of moisture storage function

For B1, most of the parameters have a more or less stable PCCs except for the saturation water content (W_f), which represents the moisture storage function. For example, for scenario 1 as shown in Figure 6.4 a, at the beginning of the test, the PCC of the moisture storage quickly reached to about -0.9 and then gradually changed from negative to positive and reached close to 1.0 after 6 months when the MC level of CLT reached below 20%. It indicates that the influence of moisture storage depends on the level of moisture content, which is related to the mechanism of moisture storage and transport. At the initial drying stage from above 30% MC to the fiber saturation level, at which all the free water is removed from the cell cavities, typically around 28%, the influence of moisture storage function is significant. When the MC level gradually decreases from the fiber saturation level to 20%, the influence of moisture storage function decreases and changes from negative to positive. Below 20%, the influence of moisture storage function increases and changes to positive and stays at a constant value close to 1.0. This change of PCC in storage function is also observed for the scenarios with rain leakage (Figure 6.4 c, d). It is also noted that for scenario 4 (west orientation with rain leakage, Figure 6.4 d), at higher MC levels the PCC of the storage function is smaller compared to scenario 2-west orientation without rain leakage (Figure 6.4 b).

Therefore, it can be said that at lower MC level, where vapour transport is dominant, storage function has a significant positive influence on the MC level (higher storage function, higher MC level), while at higher MC level greater than 20%, where liquid transport governs, the influence of storage function is less and has a negative impact (higher storage function, lower MC).

Simulations are also carried out for B1 with initially low MC and B2 with initially high MC level. Similar trend is observed (Figure 6.6). The MC level of B1 started from 15% (Figure 6.6c), the PCC of W_f remains positive and is close to 1.0 (Figure 6.6a). Note that the initial increase of MC in B1 is due to the redistribution of moisture from the layer at 13 mm from the exterior, which has a higher initial MC level than the outer layer at 6mm. Although the initial MC level of B2 is high, close to 35% (Figure 6.6 d), the high vapour permeance of the WRB allowed the CLT panel dried quickly to below 20%, the PCC of W_f changed quickly from negative to positive and remains close to 1.0 after the MC reaches below 20% (Figure 6.6 b). Therefore, the influence of moisture storage is governed by the moisture content level and the drying stage.

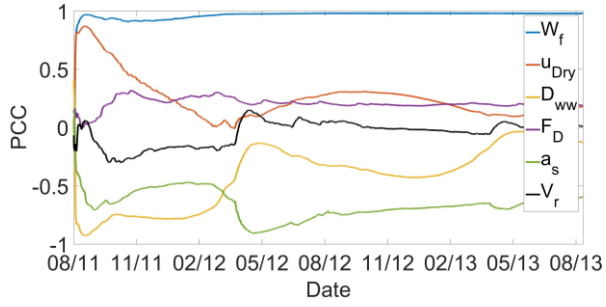

a) PCCs_B1_lower initial MC

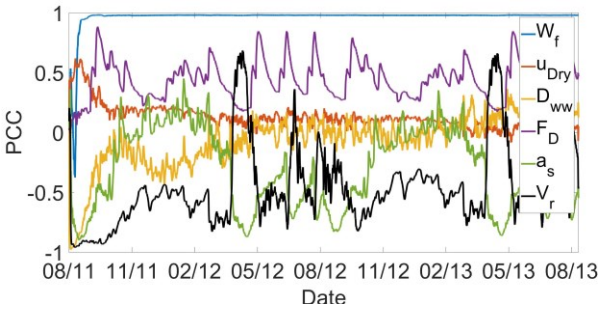

b) PCCs_B2_higher initial MC

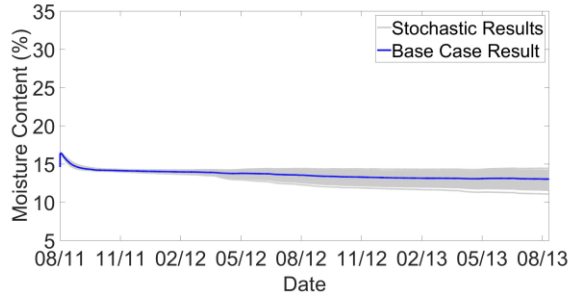

c) Stochastic results_B1_lower initial MC

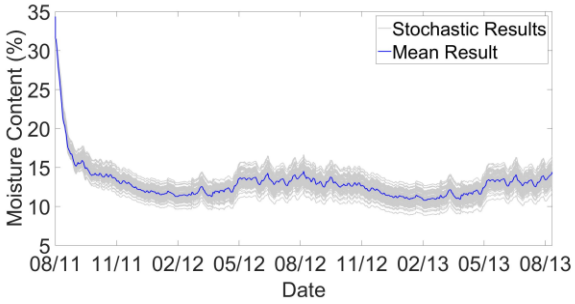

d) Stochastic results_B2_higher initial MC

Figure 6.6 Sensitivity analysis for initial moisture content

Influence of moisture transport properties

For B1, both vapour resistance factor and moisture diffusivity have an influence with the influence of the moisture diffusivity being more significant (Figure 6.4). Although both vapour diffusion and liquid transport facilitate the drying process, liquid transport plays a more important role than vapour diffusion. Because of the low exterior vapour permeance, the moisture can only be removed inward through the CLT panel. For B2, the PCCs for moisture diffusivity and vapour resistance factor fluctuate around zero (Figure 6.5), which means the influence of moisture transport properties becomes insignificant when higher vapour permeance WRB is used. The moisture is able to be removed outward due to the high vapour permeance of WRB and mineral wool insulation.

Influence of rain deposition factor

For B1, wall assembly with low permeance WRB, the PCCs of rain deposition factor do not exceed 0.5 without rain leakage (Figure 6.4 a, b), which means the influence of the rain deposition factor is insignificant, The PCCs of rain deposition factor become close to 1 when the rain leakage is introduced (Figure 6.4 c, d), which means the rain deposition factor has a strong positive influence on the moisture content. For scenario 4, the case facing the west with 1% rain leakage, the influence of rain deposition factor is more significant than the saturation water content W_f (Figure 6.4 d).

For B2, the wall assembly with high permeance WRB, the PCCs of rain deposition factor are higher than B1 without rain leakage but lower than B1 with rain leakage. The PCCs of rain deposition factor fluctuates between 0.3 and 0.8 for the east orientation without rain leakage (Figure 6.5 a), between 0.3 and 1 when the rain leakage is introduced (Figure 6.5 c). The west orientation has higher PCCs, which fluctuate from 0.4 to 0.9 without rain leakage (Figure 6.5 b) and from 0.6 to 1 with rain leakage (Figure 6.5 d). This means that the rain deposition factor has more significant influence on the moisture performance of CLT walls in west orientation than east orientation due to the higher wind-driven rain loads received on the west façade (as shown in Figure 6.5f).

Influence of short-wave radiation absorptivity

The PCCs of short-wave radiation absorptivity are negative for B1 scenarios, which means solar radiation facilitates the drying of CLT panels (Figure 6.4). It can be seen that the influence of solar

radiation is more significant in the east orientation (Figure 6.4 a, c) than the west orientation (Figure 6.4 b, d). This is because the east orientation receives less amount of rain than the west orientation.

For B2 scenarios, the PCCs of short-wave radiation absorptivity fluctuates between positive and negative depending on the occurrence of rain events (Figure 6.5). The solar radiation facilitates drying after a short period of rain, while it increases the moisture content level in CLT during dry periods. Similar to B1 scenarios, the influence of short-wave radiation absorptivity is less for the west orientation (Figure 6.5 b, d) than that for the east orientation (Figure 6.5 a, c).

Influence of cladding ventilation rate

The PCCs of cladding ventilation rate are around 0 for all the scenarios with low permeance WRB (Figure 6.4), which means that the ventilation rate has little influence on the moisture content of B1 assembly.

For B2, the ventilation rate has a significant negative correlation with the moisture content for most of the time in the east orientation, although the influence becomes positive during dry periods without rain (Figure 6.5 a, c). This means that the cavity ventilation is possible to bring moisture from the humid ambient air to the CLT panel during dry periods. The influence of ventilation rate is always negative for the west orientation (Figure 6.5 b, d), and the PCCs of the ventilation rate vary between -0.9 and -0.6, which means the cladding ventilation has an effect of removing the moisture from the CLT panel when there is continuous rain load.

The overall influence of stochastic parameters

To evaluate the overall effect of each stochastic parameter, the root mean square of the PCCs of each parameter over the entire simulation duration is calculated (Figure 6.7).

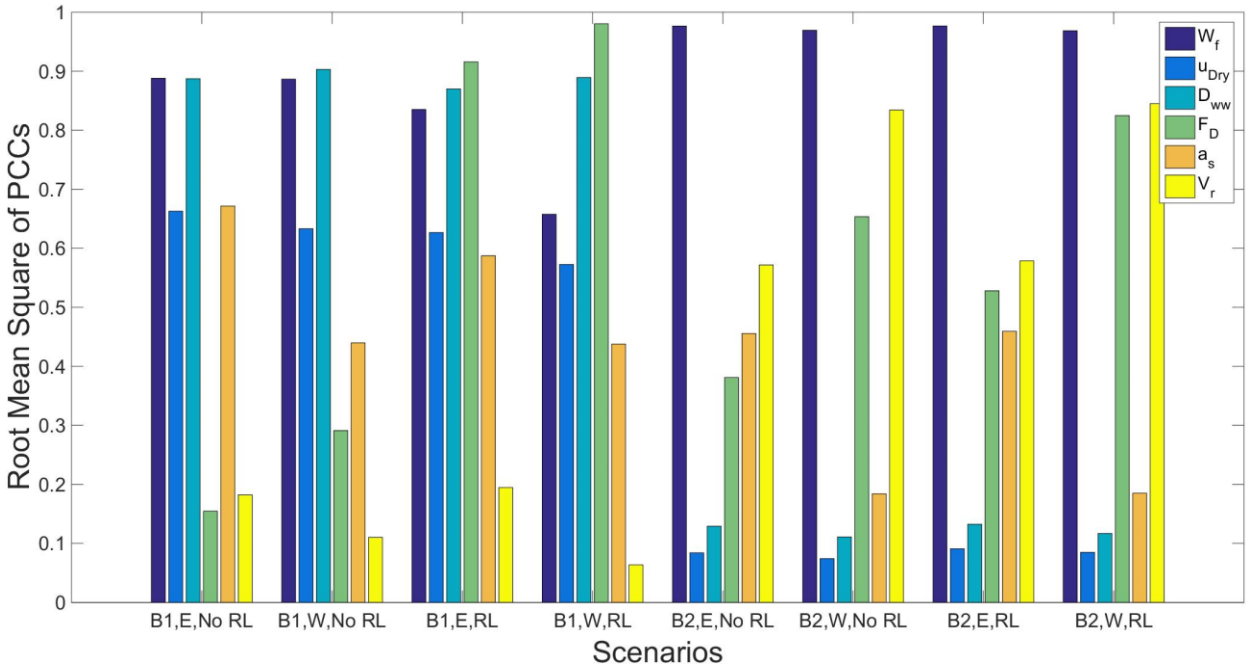

Figure 6.7 Root mean square of the PCCs (E-East, W-West, RL-Rain Leakage)

For B1, without rain leakage, moisture diffusivity (D_{ww}) and moisture storage property represented by the saturation water content (W_f), are the most important factors. With the introduction of rain leakage, the influence of moisture diffusivity becomes more significant than the moisture storage property, especially for the west orientation. The influence of vapour resistance factor (μ_{Dry}) is almost the same for the four scenarios. The rain deposition factor (F_D) has little influence on the moisture content without rain leakage, while it becomes significant when the rain leakage is introduced. The influence of ventilation rate (V_r) is not important for all four scenarios. The effect of short-wave radiation absorptivity ($\boldsymbol{\alpha}_s$) is dependent on the orientation, the PCCs are higher in the east orientation than that in the west orientation.

For B2, the moisture storage property is always the most influential factor, while the influence of transport properties is insignificant. The influence of rain deposition factor and ventilation rate is more significant under conditions with higher rain loads, i.e. cases in the west orientation or cases with rain leakage introduced. Similar to B1, the influence of short-wave radiation absorptivity is more significant in the east orientation than the west orientation.

Comparison between parametric study and stochastic approach

Parametric study (one factor at a time method) provides an information that how much the uncertainty of the result is caused by the variation of a specific parameter, while PCC obtained from stochastic method indicates the significance of linear relationship between the stochastic results and stochastic variables. Take scenario 1 (B1, east, no rain leakage) for example, the RMSD of MSF is higher than that of MD as shown by Figure 4.8, which means the moisture storage function results in a higher MC uncertainty than moisture diffusivity. However, the RMS of PCC of MSF is similar with that of MD as shown by Figure 6.7, which means both moisture storage function and moisture diffusivity have a significant linear relationship with MC. For parametric study with only changing MSF, the MC range at the end of the simulation period is from 11% to 15% (Figure 4.7a), which is similar with that for stochastic simulation (from 12% to 16% as shown by Figure 6.3a). This means the MC uncertainty is mainly caused by the variation of moisture storage function. Although moisture diffusivity has a similar PCC with moisture storage function (Figure 6.7), but the MC uncertainty (from 13% to 14% at the end of simulation period) caused by MD (Figure 4.7e) is smaller than that (from 12% to 16% at the end of simulation period) of the stochastic results (Figure 6.3a).

Parametric study changes one parameter at a time, which cannot reveal the combined effect of the influential parameters on the simulation results. Take scenario 4 (B1, west, with rain leakage) for example, the highest MC uncertainty (from 17% to 29%) of the stochastic simulation (Figure 6.3d) is higher than that (from 18% to 27%) of parametric study which only changes rain deposition factor (Figure 4.9d). Since both moisture storage function and rain deposition factor have strong positive relationship with MC level (Figure 6.4d), the combined effect of these two parameters may increase the uncertainty of the simulation results. Therefore, parametric study may not be able to properly evaluate the moisture damage risks, which may be enlarged by the combined effect of different parameters.

In summary, parametric study can be used to investigate the impact of one parameter when the influences of other parameters are not significant, however, it does not consider the combined effect of the influential parameters on the simulation result. For the moisture damage risk assessment, stochastic approach is more suitable than parametric study because it changes all the

influential parameters simultaneously, which takes the combined effect of the parameters into account.

6.1.4 Conclusions for case study 1

It is noticed that the influence of most parameters on the hygrothermal performance of CLT panels changes with time and climatic conditions. The PCCs of B1 are much more stable than B2. This indicates that the low permeance WRB is able to serve as a weather barrier to reduce the sensitivity of the moisture performance of the CLT panel to the variation of environmental loads. The benefit is the moisture performance of the CLT panel will be relatively stable as long as there is no failure of the WRB. However, the moisture is hard to be removed when there is a rain leakage. Since rain penetration is hard to be completely eliminated as a result of deficiency in design or construction, wall assemblies with low vapour permeance WRB may be more prone to moisture problem and requires more attention for quality control.

For B2, the PCCs of the influential parameters are fluctuating with the environmental loads, especially the rain load, except for the PCCs of saturation water content, which remain stable and close to 1. The high vapour permeance of WRB allows the CLT panels interact with the ambient air and is more sensitive to the variation of environmental conditions than B1. The moisture content of the CLT panel will be increased when the rain load becomes higher, but it is easier to be dried even with a rain leakage. Therefore, the risk of moisture problem of B2 will be relatively lower under the climatic conditions evaluated.

The main conclusions of this case study are:

- The cases with low permeance WRB have higher risk of moisture problem than those with high permeance WRB when scenarios including the orientation with the highest wind-driven rain and the occurrence of rain leakage are considered.
- The orientation will not significantly influence the moisture content for the cases with low vapour permeance WRB, however, the rain leakage has a significant impact on the moisture content and it significantly increases the risk of moisture problem for B1. The influence of rain leakage rate is less significant than the orientation for B2, the wall assembly with high vapour permeance WRB.

- Moisture storage function is an important material property that influences the moisture content of CLT panel for both walls. The influence of moisture storage function is governed by the moisture content level and the drying stage. At lower MC levels, where vapour diffusion dominates, moisture storage function has a significant positive influence; while at higher MC levels greater than 20%, where liquid transport governs, the influence of storage function is less and has a negative influence.
- The moisture transport properties have more significant influences on the moisture content for the wall with low vapour permeance WRB. Both the vapour resistance factor and the moisture diffusivity have an influence with the influence of moisture diffusivity being more significant. The influences of moisture transport properties are insignificant for the wall with high vapour permeance WRB.
- Without rain leakage, the rain deposition factor and short-wave radiation absorptivity have insignificant influence on the moisture content for B1. When rain leakage is introduced, the influence of rain deposition factor is increased significantly, while the influence of short-wave radiation absorptivity is still insignificant. For B2, the rain deposition factor is more significant than the short-wave radiation absorptivity. The influence of rain deposition factor fluctuates with the rain load. Generally, the influence of short-wave radiation absorptivity is lower on the west orientation than on the east orientation for both B1 and B2.
- The influences of cladding ventilation are not significant for the wall with low vapour permeance WRB, while it has a significant effect on the wall with high vapour permeance WRB. Most of the time, the cladding ventilation facilitates drying, especially when the rain load becomes higher. However, during dry periods, cladding ventilation may bring in ambient moisture into the wall.

6.2 Case study 2: highly insulated walls

6.2.1 Stochastic variables

6.2.1.1Material properties and boundary conditions

The hygric properties of OSB and insulations are considered as stochastic variables because the moisture content of OSB is used for performance evaluation. These variables are assumed to follow normal distribution. The mean values and standard deviations are determined from Kumaran et al. (2002) and Mukhopadhyaya et al. (2007). The stochastic variables of the hygric properties are listed in Table 6.4

Table 6.4 Stochastic variables of hygric properties

OSB			**Cellulose fiber**		**Fiberglass**		**Polyisocyanurate**		**Mineral wool**	
W_f	μ_{Dry}	**A**	W_f	μ_{Dry}	W_f	μ_{Dry}	W_f	μ_{Dry}	W_f	μ_{Dry}
kg/m³	**-**	**kg/m²·s$^{0.5}$**	**kg/m³**	**-**	**kg/m³**	**-**	**kg/m³**	**-**	**kg/m³**	**-**
337	994	0.0022	500	1.86	208	1.35	19.7	1622	1.41	1.2
(54)	(38)	(0.00055)	(21)	(0.12)	(14.5)	(0.034)	(1.3)	(151)	(0.094)	(0.08)

The surface transfer coefficients are considered as deterministic parameters since these parameters have no significant influence on hygrohtermal performance of wood framed walls (Zhao et al., 2011). The rain deposition factor is considered as stochastic variable to reflect the variability of rain leakage. The monitored on-site weather data is used to generate the customized weather data files for DELPHIN. The indoor climate file is also generated based on the monitored indoor temperature and relative humidity, which was maintained at 20°C and RH40%.

6.2.1.2 Air leakage and rain leakage

The air leakage impacts on moisture content of OSB in two ways: vapour convection and condensation. Air infiltration method can be used to simulate air leakage for the walls which condensation is more significant than vapour convection. For the walls that have no condensation, the moisture content of OSB is also influenced by the leaking air through vapour convection, therefore, air convection method should be used to simulate the impact of air leakage. The air leakage rate (5.0 ± 3.7 m^3/h·m^2 under 75Pa pressure difference for walls with air barrier) is

assumed to follow normal distribution according to the air leakage database developed by Emmerich and Persily (2014), and converted to those under 5Pa pressure difference. The rain leakage is simulated by depositing 1% of wind-driven rain on façade on the exterior surface of OSB sheathing. For the orientation receives the highest wind-driven rain, simulations are also performed for 0.1% of wind-driven rain penetration. The rain deposition factor is from 0.35 to 1 with a uniform distribution as prescribed in ASHRAE 160 (2016). The amount of rain leakage with F_D-0.35 under different orientation for two climatic conditions- Waterloo and Vancouver are presented in Appendix 1.

6.2.2 Scenario variables

The orientation, air leakage and rain leakage are considered as scenario variables. Table 6.5 shows the states of the scenario variables and their combinations with stochastic variables.

Table 6.5 Factorial design of scenario variables of highly insulated wood framed walls

Factor combination scenarios	**Orientation**	**Rain Leakage**	**Air Leakage**	**Stochastic variables**
1	North	Without (0%)	0	Material properties
2	South	Without (0%)	0	Material properties
3	North	Without (0%)	5.0± 3.7 $m^3/h{\cdot}m^2$	Material properties and air leakage rate
4	South	Without (0%)	5.0± 3.7 $m^3/h{\cdot}m^2$	Material properties and air leakage rate
5	North	With (1%)	0	Material properties and rain deposition factor
6	South	With (1%)	0	Material properties and rain deposition factor

7	North	With (1%)	5.0± 3.7 $m^3/h \cdot m^2$	Material properties, air leakage rate and rain deposition factor
8	South or East	With (1%)	5.0± 3.7 $m^3/h \cdot m^2$	Material properties, air leakage rate and rain deposition factor

To observe the impact of building enclosure itself and different types of moisture loads separately, the scenarios can be categorized into four groups: 1) Scenario1 and Scenario 2, which have no air leakage and rain leakage and only material properties are considered as stochastic variables. 2) Scenarios 3 and Scenario 4, with air leakage but without rain leakage. In this group, the material properties and air leakage rate are considered as stochastic variables. 3) Scenario 5 and Scenario 6, with rain leakage but without air leakage. The material properties and rain deposition factor are considered as stochastic variables. 4) Scenario 7 and Scenario 8, both air leakage and rain leakage are introduced. The material properties, air leakage rate and rain deposition factor are considered as stochastic variables. For each scenario, 100 stochastic models are generated by Latin Hypercube Sampling.

As stated in section 3.2.3, occupant number can be taken as a scenario variable to describe different internal moisture load level. The indoor moisture generation rate can be categorized into four levels based on the occupant number, the indoor RH and temperature can be generated accordingly (ASHRAE 160, 2016). The indoor condition created in field measurement (Fox, 2014) is close to the lowest moisture load level calculated from ASHRAE 160 (2016), therefore, it is used as a lower level of internal moisture load. The higher level of internal load is obtained from the scenario with 4 bedroom and 5 occupants according to ASHRAE 160 (2016). The temperature and relative humidity as well as the moisture excess for two climate conditions (Waterloo and Vancouver) for low load condition and high load condition are presented in Appendix 2.

The internal moisture load impacts on the MC of OSB in the way of vapour diffusion and air leakage. For the walls with vapour barrier, the impact of vapour diffusion is much less significant than air leakage, therefore, air leakage is the dominant way of transporting internal moisture onto OSB sheathing. The internal moisture load level directly determines the condensed moisture

strength caused by air leakage. For the scenarios with air leakage, simulations are also carried out under higher level of internal moisture load. The condensation rate, which is calculated by equation 5-1, for different walls with the average air leakage rate for two climatic conditions: Waterloo and Vancouver are presented in Appendix 3. The comparison of the annual condensation (the total amount of the condensed moisture for one year) caused by air leakage for different walls are presented in Appendix 4.

The condensation rate for each type of walls is calculated using the air leakage rate without reduction. For stochastic simulation, the condensation rate is reduced according to the percentages presented in Table 5.7 to generate the moisture sources, which is deposited on the interior surface of OSB sheathing. In Chapter 5, the cellulose fiber of north facing I-joist wall has a higher initial moisture content than south orientation as shown by Table 5.5, in this chapter, the initial moisture contents of cellulose fiber in north orientation is set as same as south orientation to compare the impact of orientation. The q_{CL} reduction of north facing I-joist wall is set as 50%, which is same as south orientation. The moisture content and mold growth index of the interior surface of OSB is observed for performance evaluation since it is the most vulnerable location for mold growth.

6.2.3 Results and analysis

6.2.3.1 Stochastic analysis for Waterloo

6.2.3.1.1 Stochastic results of moisture content

Scenario group 1: stochastic material properties

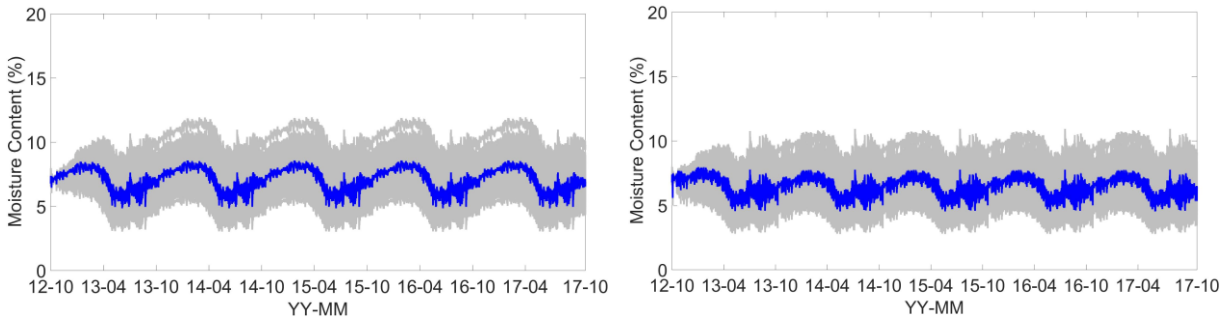

a) Baseline wall _ North

b) Baseline wall _ South

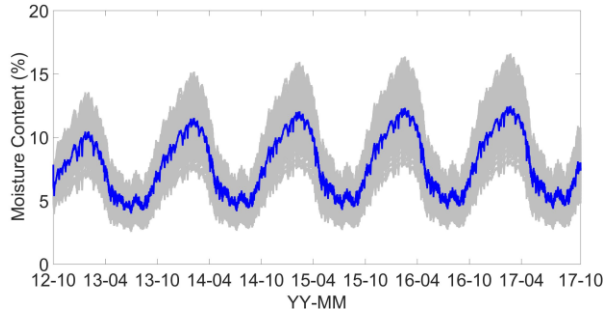

c) I-joist wall _ North

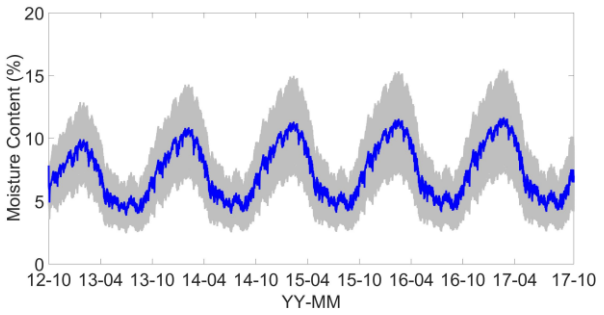

d) I-joist wall _ South

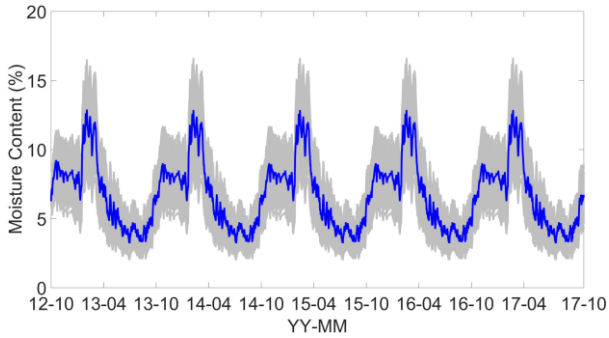

e) Polyisocyanurate wall _ North

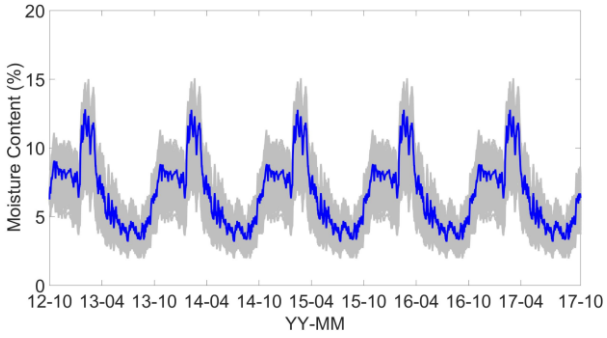

f) Polyisocyanurate wall _ South

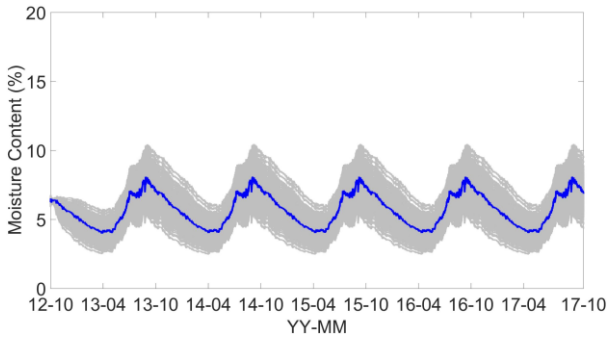

g) Mineral wool wall _ North

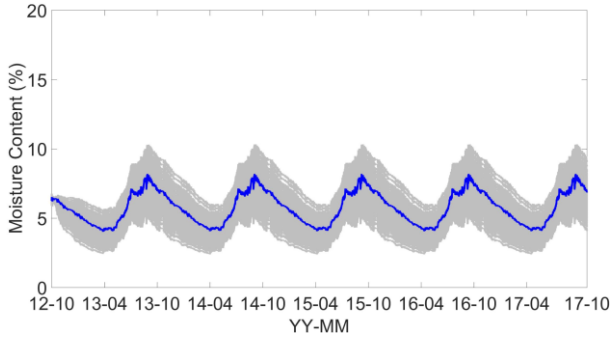

h) Mineral wool wall _ South

Figure 6.8 Stochastic results of MC with variation of material properties_Waterloo

Figure 6.8 shows the stochastic results of OSB moisture content with only the material properties are treated as stochastic variables. The blue curve is the result of base case, which uses the mean values presented in Table 5.3 as the input parameters. The grey curves are the stochastic results with hygric properties listed in Table 6.4 are considered as stochastic variables and other parameters are fixed. The highly insulated walls generally have higher MC level and more significant seasonal variation (increasing in winter and decreasing in summer) than the baseline

wall except for mineral wool exterior insulated wall, which has similar MC level to the baseline wall but different seasonal variations (increasing from spring to summer but decreasing starting from fall to winter). The reasons are for I-joist wall with thicker insulation results in lower OSB temperature and higher OSB surface RH and a 4% higher MC compare to baseline wall, while for polyisocyanurate insulated wall, although the OSB surface temperature is elevated due to its exterior insulation, its low vapour permeability restricts the vapour diffusion, therefore, results in higher MC at OSB sheathing during the wintertime. The high vapour permeability of mineral wool allows inward vapour diffusion from outdoor to OSB, therefore, there is an increase of moisture content of OSB during spring and summer time. The moisture contents of south orientation are slightly lower than north orientation due to higher solar availability, the descriptions below are for north orientation.

For the baseline wall, the moisture content of base case seasonally fluctuates between 5% and 8%. The uncertainty is about $\pm$3% throughout the five years, with the highest MC of the extreme case is about 11%. For I-joist wall, the moisture content of base case gradually increases with a seasonal fluctuation in the first three years. The annual peak value of moisture content increases from 10% in the first year to 12% in the third year, and becomes stable after the third year. The uncertainties of MC are about $\pm$ 2% in summer time and $\pm$4% in winter time. The highest moisture content level of the extreme case is about 16%, which will not result in mold growth issue.

The moisture performance of polyisocyanurate exterior insulated wall is similar with I-joist wall, except that the polyisocyanurate wall has no annual increase of MC. For mineral wool wall, the moisture content level and its seasonal variation are lower than polyisocyanurate wall. The MC of base case varies between 4% and 8%, with uncertainties about $\pm$1.5% in summer time and $\pm$2.5% in winter time, and the highest MC in extreme case is about 10%. The mineral wool wall performs better than polyisocyanurate wall because it has higher exterior permeance so that the moisture is easier to dry outward.

Scenario group 2: stochastic material properties and air leakage rates

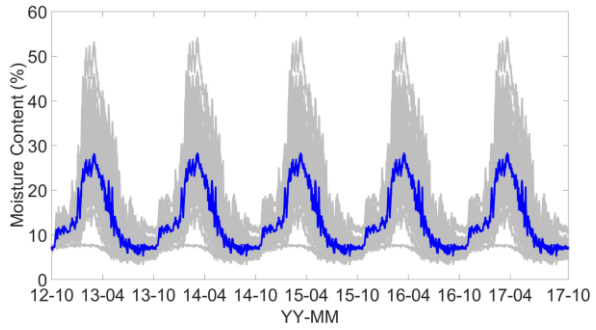

a) Baseline wall _ North

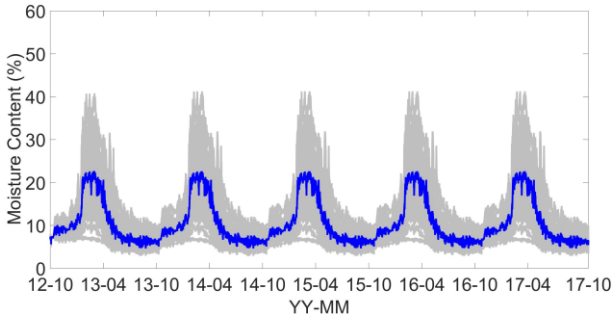

b) Baseline wall _ South

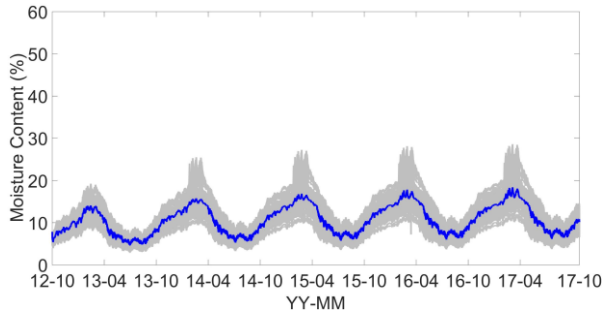

c) I-joist wall _ North

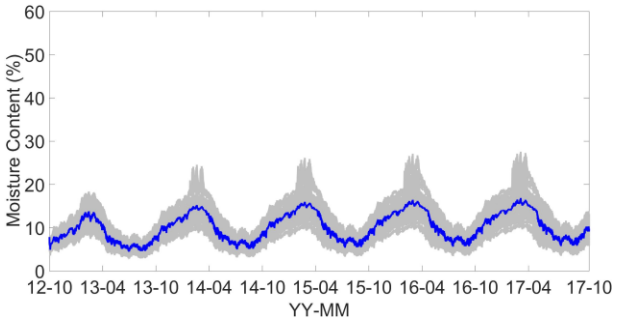

d) I-joist wall _ South

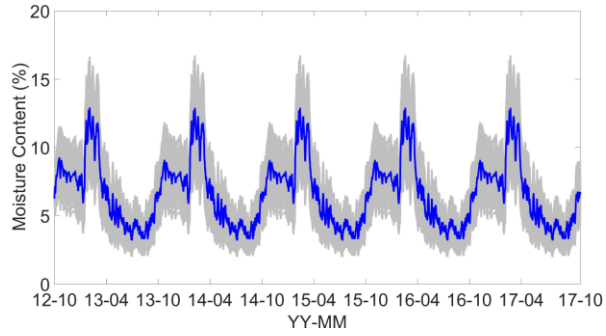

e) Polyisocyanurate wall_North

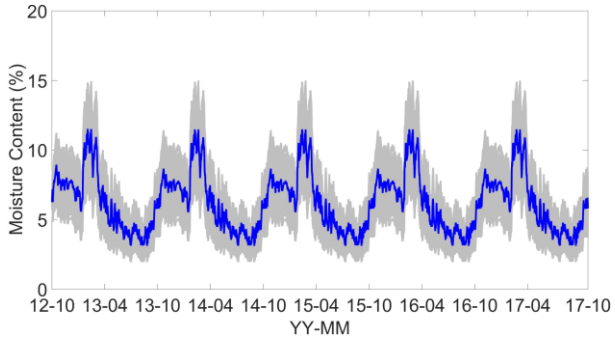

f) Polyisocyanurate wall_South

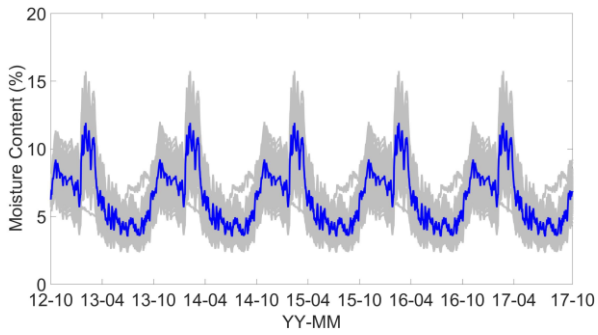

g) Mineral wool wall_North

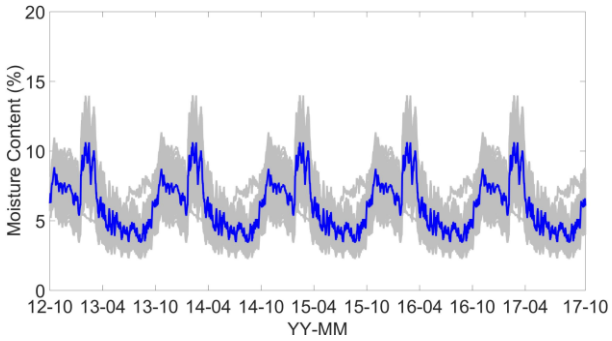

h) Mineral wool wall_South

Figure 6.9 Stochastic results of MC with variation of material properties and air leakage rates_low load_Waterloo

Figure 6.9 shows the simulation results with air leakage under low internal moisture load, which has RH from 20% to 40% (Appendix 2a). When the air leakage is taken into account, the seasonal variation of MC of baseline wall is much more significant than the scenario without air leakage. As shown in Figure 6.9 a, b, the moisture content for north orientation is higher than south orientation because north orientation has 75%q_{CL}, while south orientation has 50%q_{CL}. It can be found that the moisture content level of the base case is lower than the average value. For north orientation, the average value of moisture content fluctuates between 8% and 30%, with uncertainties from ±4% in summer time to ±23% in winter time. The highest moisture content of the extreme case is about 53%. For south orientation, the average moisture content varies between 6% and 28%, with uncertainties from ±4% in summer time to ±18% in winter time.

The I-joist wall has a lower moisture content level than baseline wall and the north orientation is similar with south orientation. The moisture content varies from 4% to 20% with uncertainties from ±2.5% to ±8%. The highest moisture content level of the extreme case is about 28%. The I-joist wall performs better than the baseline wall because the cellulose fiber in I-joist wall has a higher moisture storage capacity than fiberglass in the baseline wall, and the cellulose fiber is able to absorb the moisture carried by the air leakage and reduces the amount of moisture reached the OSB sheathing. The two exterior insulated walls have similar MC level and variation pattern, and the polyisocyanurate wall is slightly higher than mineral wool wall. For polyisocyanurate wall, the moisture content fluctuate between 3% and 13% with uncertainty ±4%. The moisture content of mineral wool wall fluctuate between 3% and 12% with same uncertainty as polyisocyanurate wall.

There is no condensation caused by air leakage for the exterior insulated walls and the OSB MC profiles obtained by air infiltration method are the same as those presented in Figure 6.8 e, f, g, h. However, the air leakage still has impact on the MC of OSB through vapour convection, therefore, air convection method is used to simulate the exterior insulated walls. For polyisocyanurate wall and mineral wool wall, a 1 mm air layer with air change rate 840 1/h is placed in the 75%Lcd to simulate the impact of the air leakage. The air change rate is considered as stochastic variables according to the variation of the air leakage rate. Figure 6.9 e to h are the stochastic results of exterior insulated walls with air convection method are used to simulate the air leakage. It can be seen from Figure 6.9 e and f that the results of polyisocyanurate are similar with those without 1 mm air layer (Figure 6.8 e and f) because polyisocyanurate wall has no vapour barrier and the influence of indoor air for the models without 1 mm air layer is comparable with those with 1 mm air layer. For mineral wool wall, the results from the models with 1 mm air layer (Figure 6.9 g and h) is significantly different from those without 1mm air layer (Figure 6.8 g and h) because of the effect of vapour barrier. It can be seen that the stochastic results with 1 mm air layer are higher than those without 1 mm air layer and the variation pattern is similar with polyisocyanurate wall. The 1 mm air layer significantly influence mineral wool wall because the vapour barrier minimized the influence of indoor air for the models without 1 mm air layer, and the 1 mm air layer which is placed outside of vapour barrier enhanced the impact of indoor air.

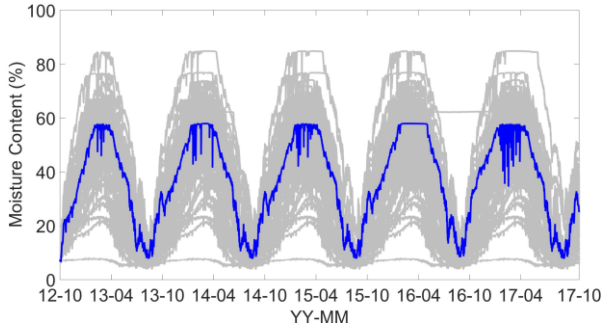

a) Baseline wall _ North

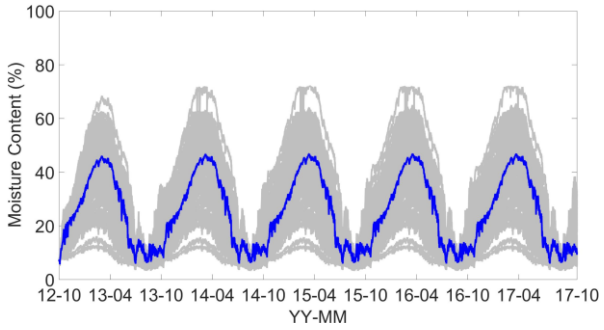

b) Baseline wall _ South

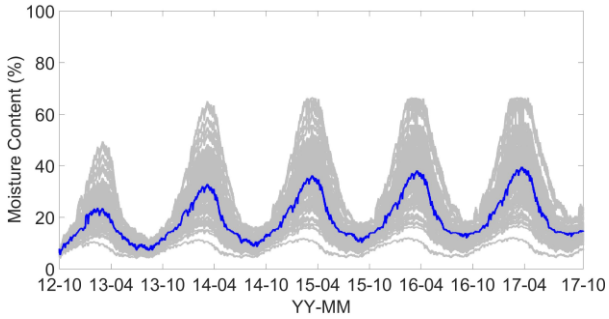

c) I-joist wall _ North

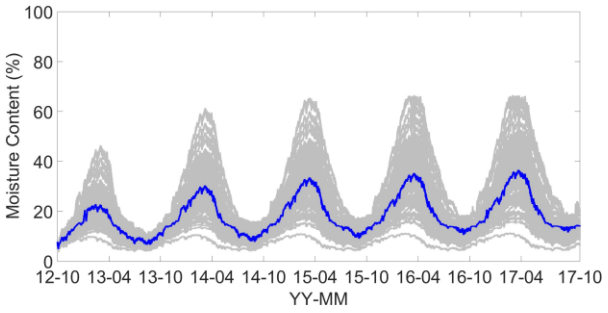

d) I-joist wall _ South

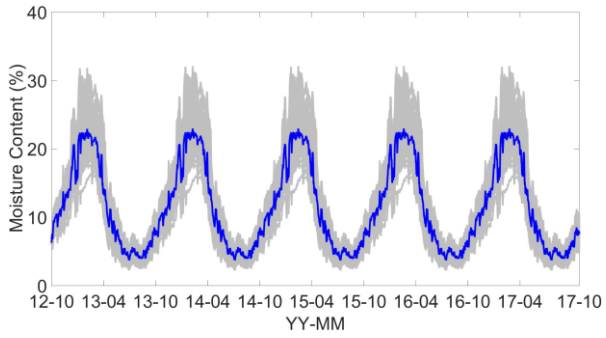

e) Polyisocyanurate wall _ North

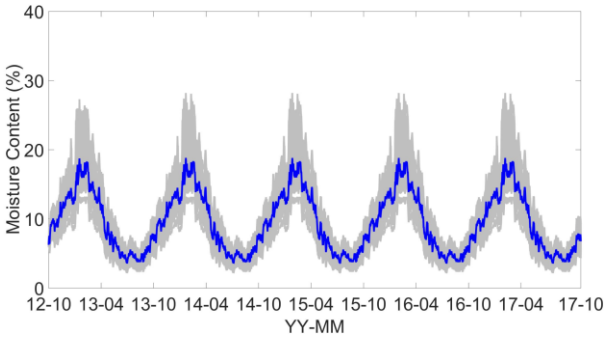

f) Polyisocyanurate wall _ South

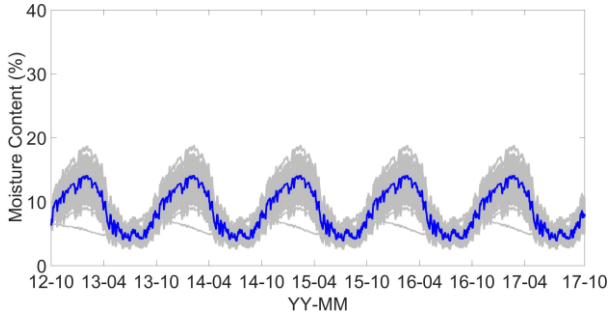

g) Mineral wool wall _ North

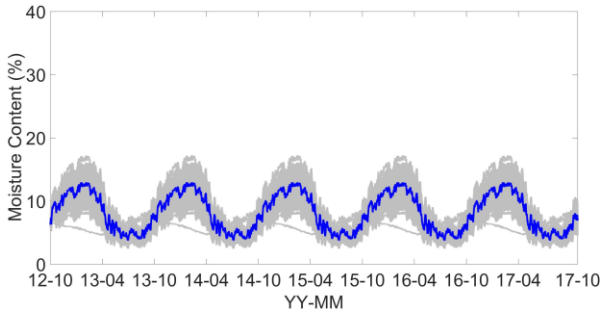

h) Mineral wool wall _ South

Figure 6.10 Stochastic results of MC with variation of material properties and air leakage rates_high load_Waterloo

Figure 6.10 shows the stochastic results under high internal moisture load, under which the RH fluctuates between 30% and 50% (Appendix 2a). It can be seen that the OSB MCs and their uncertainties are much higher than the cases under low moisture load. The baseline wall has the highest MC increment and mineral wool wall has the lowest increment. The MCs variation pattern is similar with that under low internal load.

For baseline wall facing to north orientation the maximum MC is 82%, which is higher than that facing to south orientation (72%). For I-joist wall, the maximum MC is about 66% for both north and south orientation, and the MCs are lower than baseline wall.

For polyisocyanurate wall under high internal moisture load, air infiltration method is used to simulate the influence of air leakage because the moisture brought by condensation is much more than that brought by vapour convection. The q_{CL} is also reduced by same percentage as that applied to baseline wall. The maximum MC is 32% for north orientation and 28% for south orientation. Although there is also condensation potential for mineral wool wall under high load condition, the maximum condensation moisture is less than those brought by vapour convection, therefore, air convection method is used for mineral wool wall. The maximum MC of mineral wool wall is about 17% for both north and south orientation, which is much lower than polyisocyanurate wall. The mineral wool insulated exterior wall can handle the high level of air leakage and has MC level below 19%, while the polyisocyanurate insulated walls has MC of OSB reaches as high as 30%, greater risks than mineral wool, due to the low vapour permeability of polyisocyanurate. With polyethylene vapour barrier removed from the interior side, OSB can be dried towards interior, but only when inward vapour drive potential exists, which in the spring and summer time, therefore, results in much higher MC in OSB during the winter time compared to mineral wool exterior insulated walls.

Scenario group 3: stochastic material properties and rain deposition factors

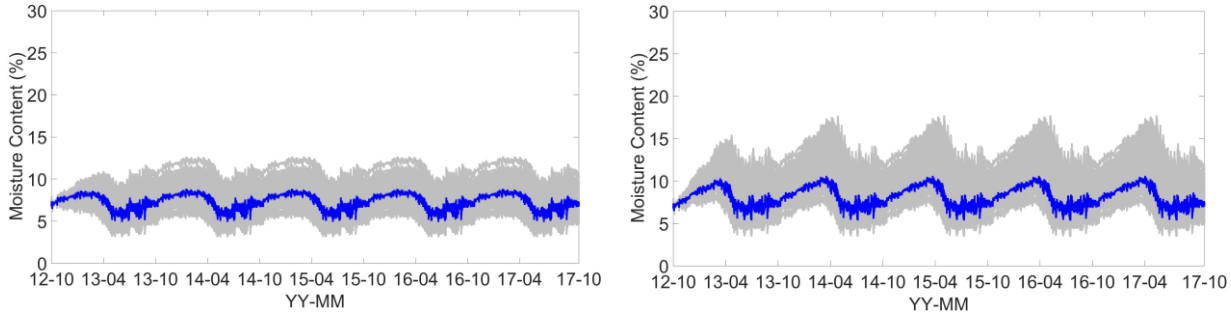

a) Baseline wall _ North

b) Baseline wall _ South

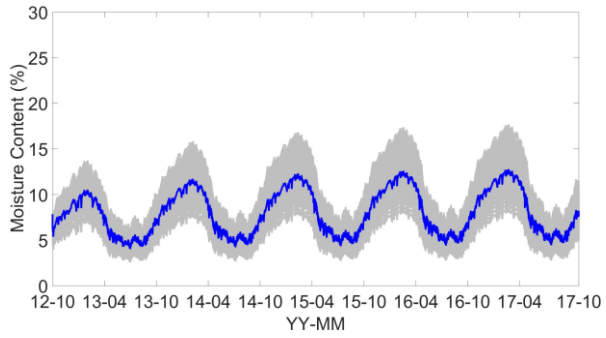

c) I-joist wall _ North

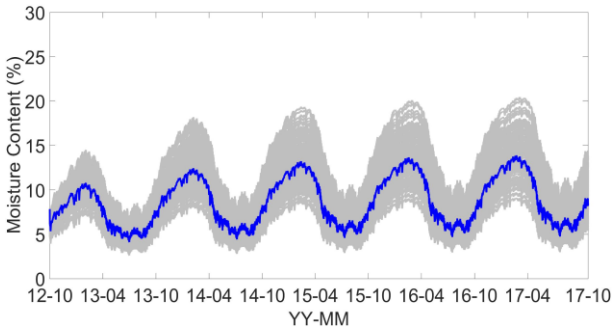

d) I-joist wall _ South

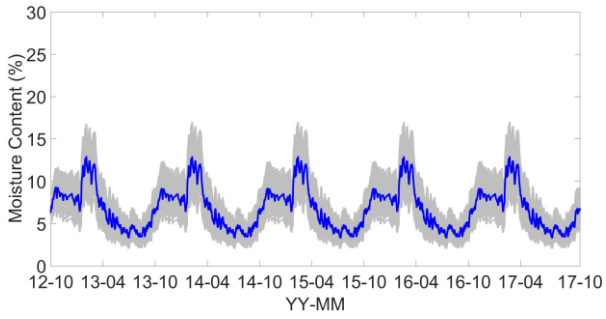

e) Polyisocyanurate wall _ North

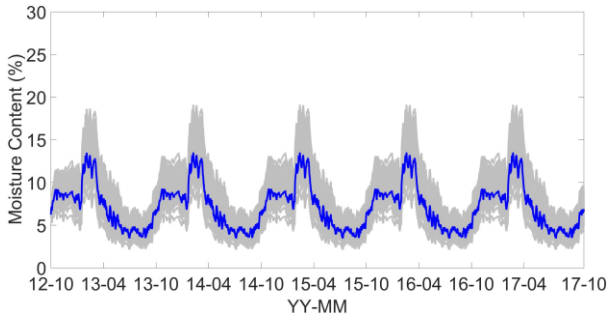

f) Polyisocyanurate wall _ South

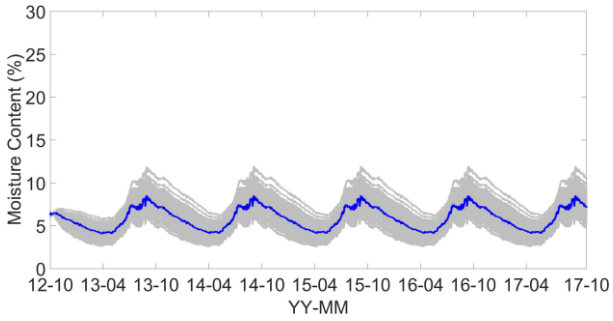

g) Mineral wool wall _ North

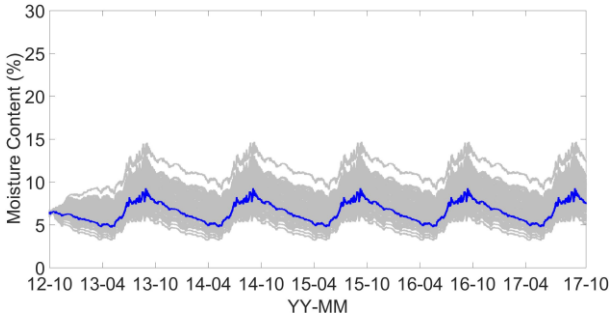

h) Mineral wool wall _ South

Figure 6.11 Stochastic results of MC with variation of material properties and rain deposition factors_south_Waterloo

Figure 6.11 shows the stochastic moisture content of the baseline wall and highly insulated walls with 1% rain leakage. The rain leakage only has slight influence for north orientation, and there is only small increase of MC. The impact of rain leakage is more significant for south orientation than north orientation because south orientation has higher wind-driven rain than north orientation.

The south orientated baseline wall has the MC uncertainties from ±3% in summer time to ±5% in winter time, with the highest value of the extreme case is about 17%. The MC level and their uncertainties are lower than the scenario with air leakage, which means the impact of rain leakage is less significant than air leakage. Similar observation can be found in south orientated I-joist wall, which has moisture content level from 4% to 15%, with uncertainty from ±3% to ±5%.

For exterior insulated walls, the impact of rain leakage is slightly more significant than air leakage with low internal load because the moisture brought by rain leakage is higher than air leakage. The moisture content level of south oriented polyisocyanurate wall is from 5% to 14% with uncertainty from ±2% to ±4%. The moisture content of south oriented mineral wool wall is lower than polyisocyanurate wall because of the higher exterior permeance.

In general, all the walls can handle the 1% rain leakage with MCs of OSB below 20% although slight difference among these walls.

Scenario group 4: Stochastic material properties, air leakage rates and rain deposition factors

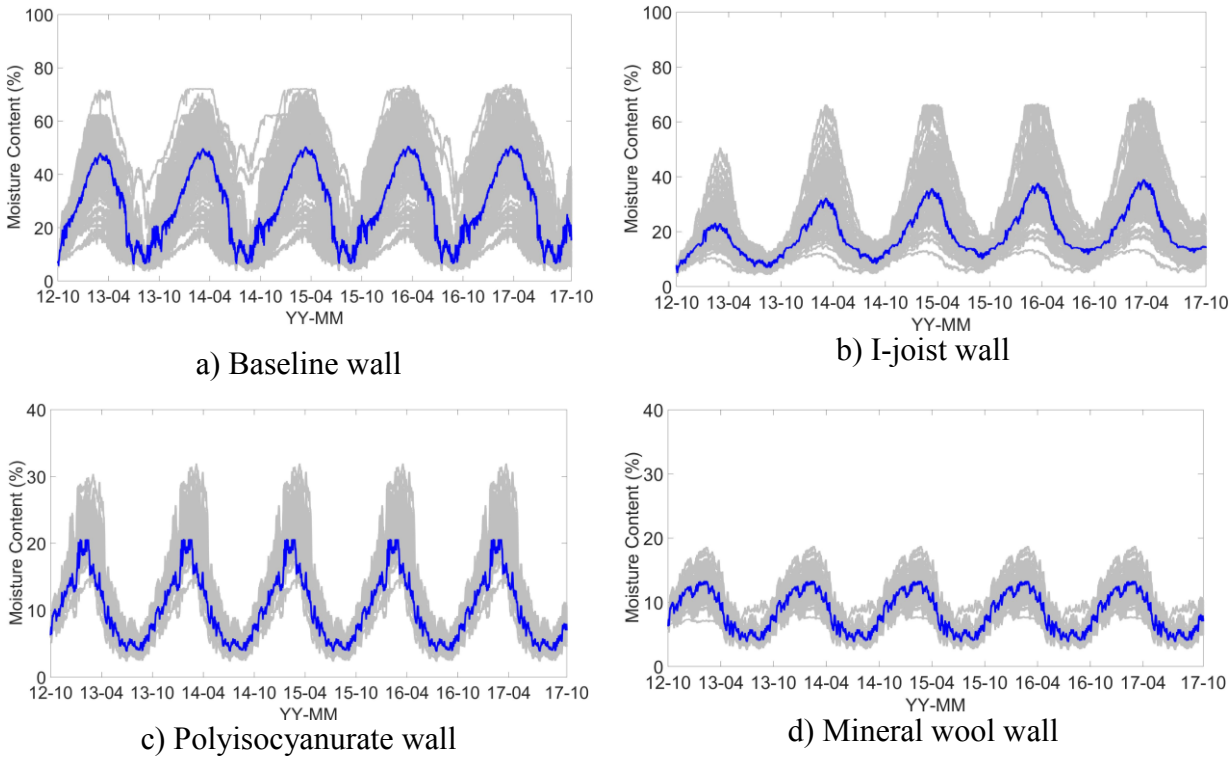

a) Baseline wall

b) I-joist wall

c) Polyisocyanurate wall

d) Mineral wool wall

Figure 6.12 Stochastic results of MC with variation of material properties, air leakage rates (high load_south) and rain deposition factors (south)_Waterloo

Simulations are only performed for south orientation, because the influence of rain leakage is insignificant for north orientation as shown by Figure 6.11 a, c, e, g. The air leakage with high internal load is combined with the rain leakage for south orientation. The MCs increment are within 2% for all the walls compare to the cases facing south orientation with only air leakage is considered. And the moisture content level are lower than the walls facing to north orientation with only air leakage is considered under high internal load. Baseline wall is the worst followed by I-joist wall, polyisocyanurate insulated wall and mineral wool insulated exterior wall performs the best with MC levels stay below 20%. For this climate, air leakage has a greater impact than rain leakage and to have a moisture safe highly insulated walls, air leakage rate needs to be controlled to a low level. In general, exterior insulated walls are safer than interior insulated walls.

6.2.3.1.2 Mold growth risk analysis

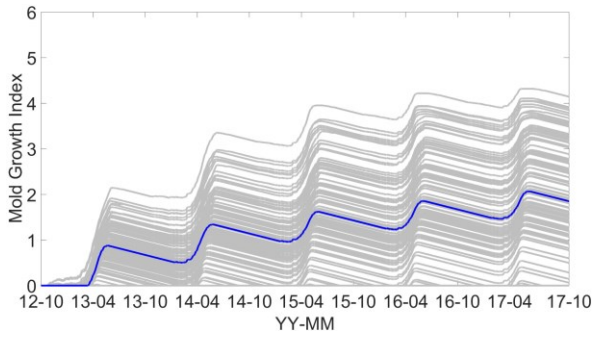

a) Baseline wall _ low load

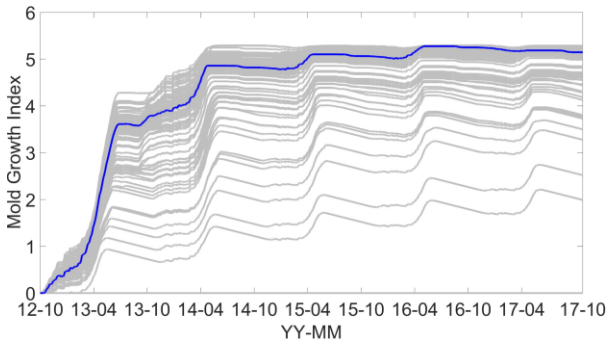

b) Baseline wall _ high load

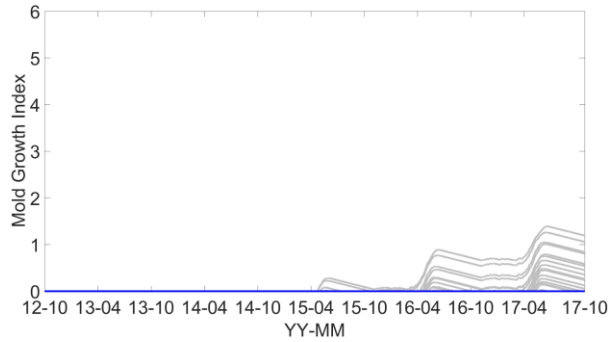

c) I-joist wall _ low load

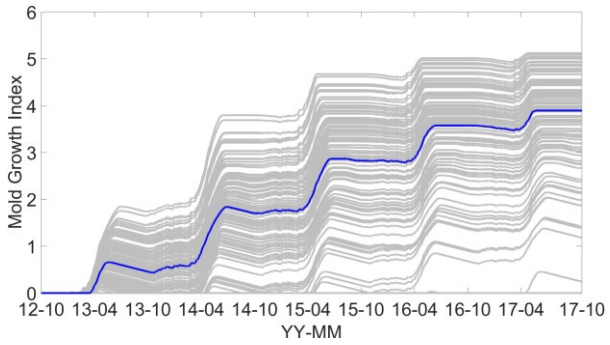

d) I-joist wall _ high load

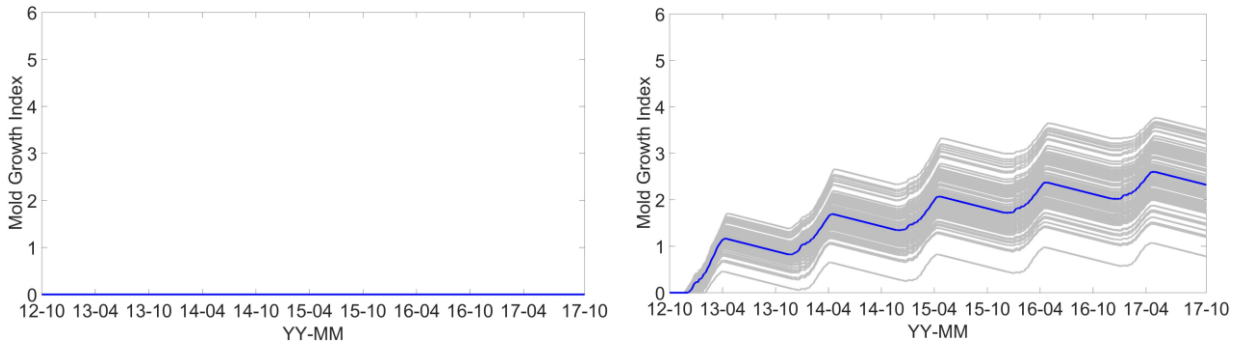

e) Polyisocyanurate wall _ low iload

f) Polyisocyanurate wall_ high load

Figure 6.13 Mold growth index with air leakage _north_Waterloo

Figure 6.13 shows the mold growth index for north facing walls with air leakage under low and high internal loads. The mold growth index for mineral wool wall is zero for both low and high internal load conditions, therefore, mineral wool wall is not presented.

For the baseline wall with low internal load, the mold growth index of based case is in the middle of the stochastic cases, and increases with a seasonal variation (decreasing in summer time and increasing in winter time) from 0 in the first year to 2 in the fifth year. The stochastic cases are evenly distributed around the base case, with a highest value of 4.3 of the extreme case in the fifth year. Under high internal load, the mold growth index of the base case increases steeply in the first two years up to 5, which indicates plenty of mold growth on surface. The stochastic cases are evenly distributed around the base case in the beginning stage (from Oct. 2012 to Apr. 2013), while dispersed from Oct. 2013. Most cases are increasing steeply with a same rate as base case, while few cases increase slowly and become much lower than base case. In the end of the fifth year, most of the stochastic cases are congregated above 4, and few cases are distributed sparsely between 2 and 4.

For I-joist wall with low internal load, the mold growth indexes are zero in the first two years. Only few cases have the mold growth index higher than zero from Apr. 2015, with a maximum value of 1.4 in the fifth year, which indicate there is no mold growth risk. For the scenario with high internal load, the mold growth index of base case is increasing from zero in the first year to 3.9 in the fifth year, and slightly higher than the average level of the stochastic cases. The stochastic

cases above average are more crowded than those below average, the highest mold growth index in the fifth year is 5.1.

For polyisocyanurate wall under low internal load, the mold growth index is zero throughout the five years. Under high internal load, the mold growth index of base case increases from zero in the first year to 2.6 in the fifth year with a seasonal variation (decreasing in summer time and increasing in winter time). The stochastic cases are evenly distributed around the base case with a highest mold growth index 3.7 in the fifth year.

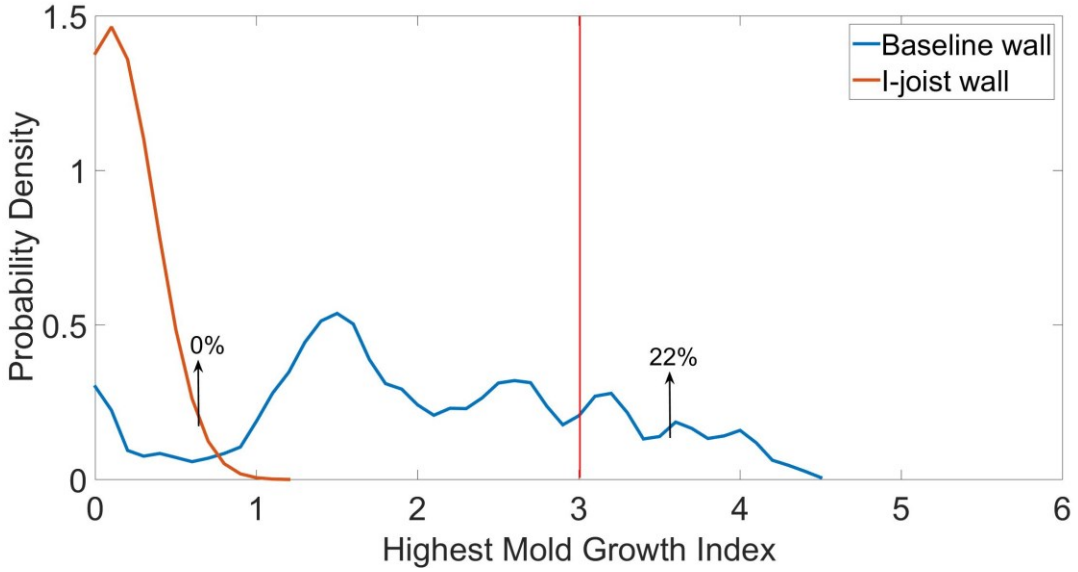

a) With air leakage _ low load _ north

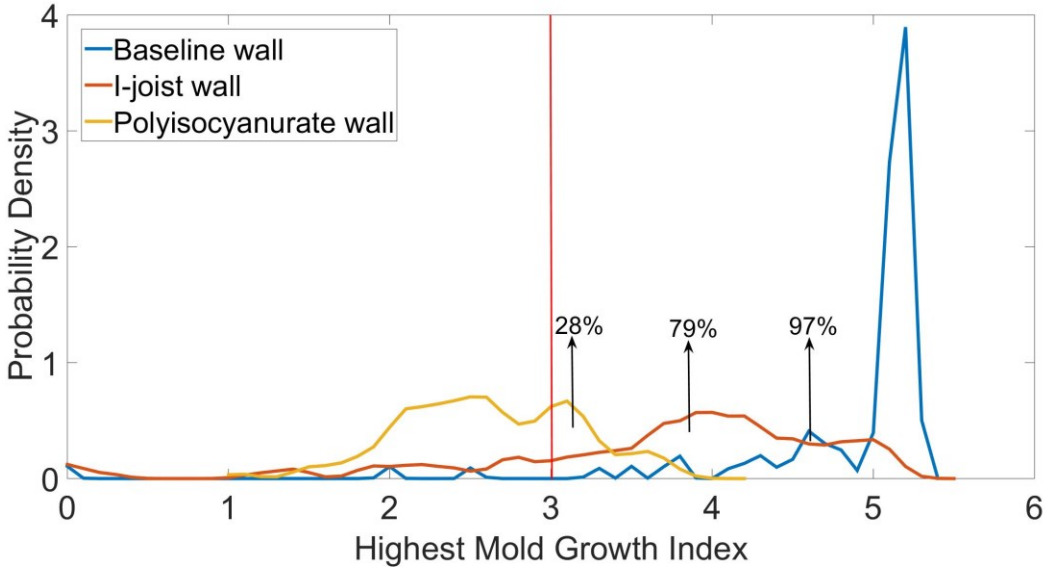

b) With air leakage _ high load _ north

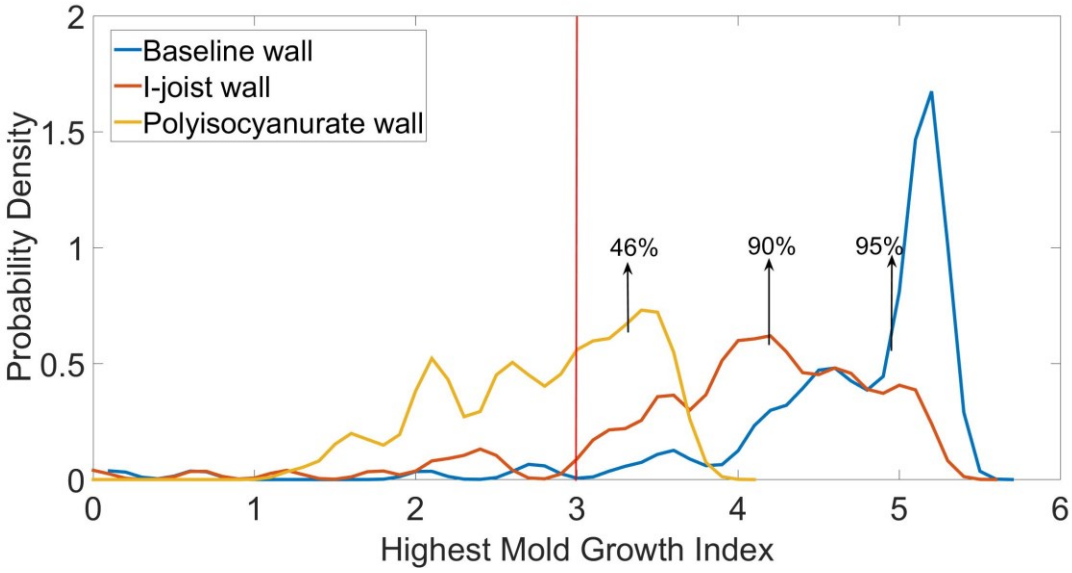

c) With air leakage (high load _ south) and rain leakage (south)

Figure 6.14 Probability density functions of highest mold growth index _ Waterloo

Figure 6.14 shows the probability density function of the highest mold growth index for baseline wall, I-joist wall and polyisocyanurate wall under different scenarios. According to ASHRAE 160 (2016), the mold growth index of the building components surface should not exceed 3 to avoid mold growth problem. It can be found that baseline wall has the highest mold growth risk among

the three types of walls. For the scenario with air leakage and low internal load, there are 22% of stochastic cases for baseline wall have the highest mold growth index higher than 3, which is a threshold of visually detectable mold growth. But the risk of mold growth index higher than 3 is zero for I-joist wall and polyisocyanurate wall. Under high internal load condition, the baseline wall has 97% stochastic cases have the highest mold growth index higher than 3. And this possibility is 79% for I-joist wall, 28% for polyisocyanurate wall. For the scenario with air leakage (high load _ south) and rain leakage (south), the mold growth risks for baseline wall is lower than the scenario with only air leakage (high load _ north), however, the I-joist wall and polyisocyanurate wall have higher mold growth risks than only with air leakage (high load _ north).

6.2.3.1.3 Sensitivity analysis

Table 6.6 lists the highest uncertainty of MC in three scenarios (only material properties are considered as stochastic variables, material properties and air leakage rates are considered as stochastic variables, material properties and rain deposition factors are considered as stochastic variables). It can be seen that the air leakage scenario increases the MC uncertainty of baseline wall and I-joist wall significantly, but has slight influence on exterior insulated walls. The influence of rain leakage is less significant than air leakage for baseline wall and I-joist wall, because the amount of the moisture source caused by rain leakage is less than air leakage. While, for exterior insulated walls, the influence of rain leakage is more significant than air leakage for polyisocyanurate wall with low internal load, but less significant for mineral wool wall because of the higher exterior permeance. Under high internal load, the influence of air leakage is more significant than rain leakage.

Table 6.6 The uncertainties caused by different factors- Waterloo

	Material properties	**Moisture loads**		
	(North)	**Air leakage_Low**	**Air leakage_High**	**Rain leakage**
		North	**North**	**South**
Baseline wall	8±3%	30±23%	46±36%	12±5%
I-joist wall	12±4%	20±8%	39±27%	15±5%
Polyisocyanurate wall	12±4%	13±4%	24±8%	14±5%
Mineral wool wall	8±2.5%	12±4%	14±5%	10±4%

Note: the uncertainties are expressed as absolute errors

Influence of material properties

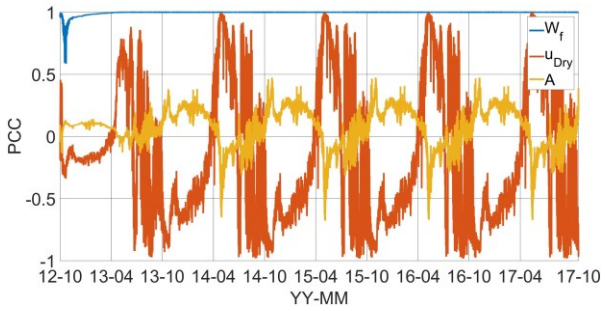

a) Baseline wall _ PCCs of OSB

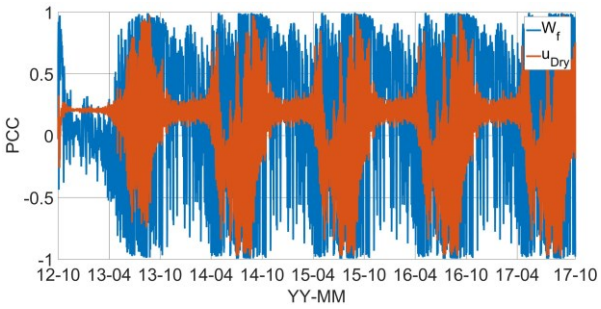

b) Baseline wall _ PCCs of Fiberglass

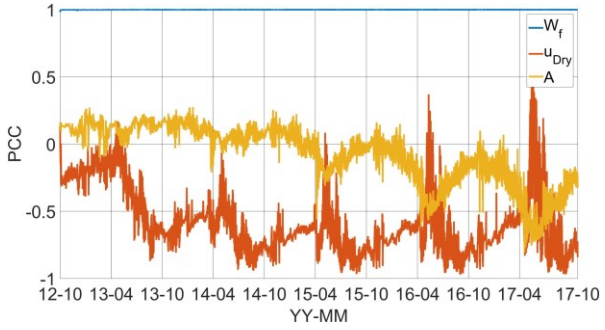

c) I-joist wall _ PCCs of OSB

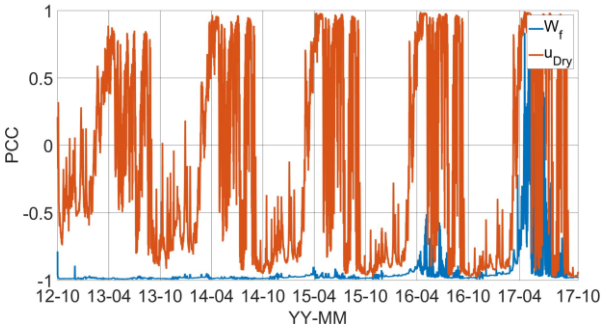

d) I-joist wall _ PCCs of Cellulose Fiber

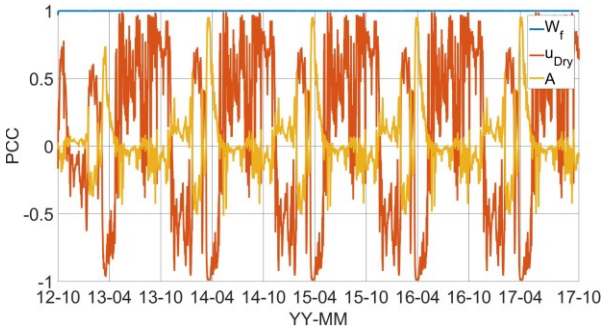

e) Polyisocyanurate wall _ PCCs of OSB

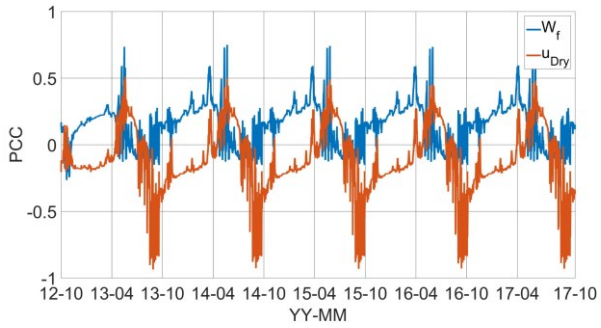

f) Polyisocyanurate wall_PCCs of Polyisocyanurate

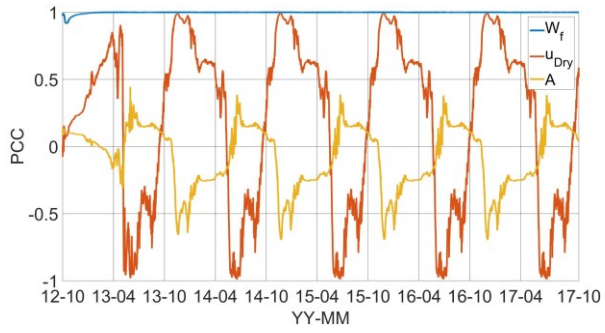

g) Mineral wool wall_ PCCs of OSB

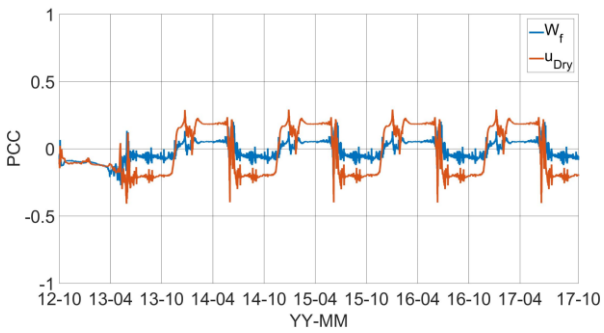

h) Mineral wool wall_ PCCs of Mineral wool

Figure 6.15 PCCs of material properties to MC

Figure 6.15 shows the PCCs of hygric properties of OSB and insulations to moisture content of OSB for the baseline wall and highly insulated walls. It can be seen that the moisture storage function plays the most important role for all the walls. The PCCs of W_f (saturation water content) of OSB are always 1 throughout the 5 years simulation period, which means the MSF has a strong positive influence of OSB moisture content (higher value, higher MC). There are significant fluctuations of transport properties (u-value and A-value). For baseline wall, the u-value (vapour resistance factor) of OSB negatively influence the MC of OSB in winter time, when the MC increases. But the u-value positively influence MC in summer time (higher value, lower MC), when the MC decreases. The influence of A-value, which represent the strength of liquid moisture diffusivity, is less significant than u-value. The A-value positively influence MC of OSB in winter time, but negatively influence MC in summer time. The PCCs of fiberglass fluctuates frequently. Generally, the W_f tends to positively influence MC of OSB in winter time and negatively influence the MC in summer time. The influence of u-value is insignificant in winter time, and becomes significant in summer time (negative influence) and fall time (positive influence).

For I-joist wall the u-value always has a negative influence on MC, because the MC has an upward trend, which means the OSB absorb moisture from ambient, and the higher vapour resistance factor inhibits the absorbing process. The PCC of u-value decreases with a seasonal variation (decreasing in summer time, increasing in winter time), which means the u-value has more significant influence in summer time than in winter time. The influence of A-value is less significant than vapour resistance factor. The PCC of A-value is positive and close to zero in the first three years, which indicates the A-value has almost no influence on MC. While it drops down to below zero

after the third year with a seasonal fluctuation (decreasing in winter, increasing in summer), which means the A-value has a negative influence on MC and the influence is more significant in winter time than in summer time. The PCC of W_f of cellulose fiber has a negative influence on MC of OSB except for the summer time in the last year, higher W_f means higher moisture storage capacity of cellulose fiber, which is able to absorb more moisture from OSB. The u-value of cellulose fiber has a negative influence in winter time and positive influence in most of summer time. Higher vapour resistance factor prevent the vapour transfer from cellulose fiber to OSB in winter time, while the direction of vapour transfer is from outside to inside in summer time, the higher vapour resistance factor inhibits the moisture transfer inward.

For polyisocyanurate wall, the u-value of OSB has negative influence in most time of winter, when the moisture content increases. While it has positive influence in most time of simmer, when the moisture content decreases. The influence of A-value is less significant than u-value, and is opposite to u-value. The u-value of polyisocyanurate insulation has a PCC from -0.2 to -0.1 in winter time. According to statistical test, the absolute PCC values lower than 0.2 get p-value higher than 0.05, which means no significant linear relationship between two variables. The u-value of polyisocyanurate wall has weak positive influence (higher than 0.2 but lower than 0.5) in the beginning of spring time and strong negative influence (lower than -0.5) in the late of summer time. For mineral wool wall, the periodical variation of the PCCs of transport properties is reverse to polyisocyanurate wall because it has a different MC variation pattern (decreasing in winter and increasing in summer). The PCCs of W_f and u-value of mineral wool wall fluctuate between zero, which indicates there is no significant correlation between material properties of mineral wool insulation and MC of OSB.

Influence of air leakage

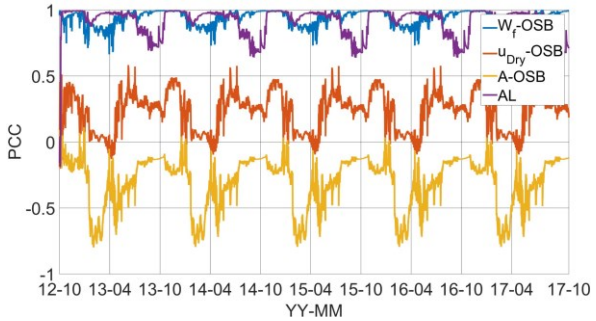

a) Baseline wall _ low load

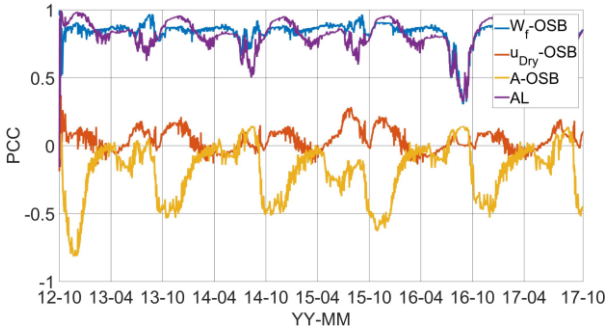

b) Baseline wall _ high load

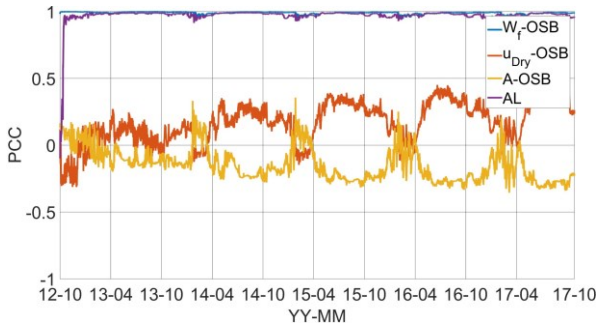

c) I-joist wall _ low load

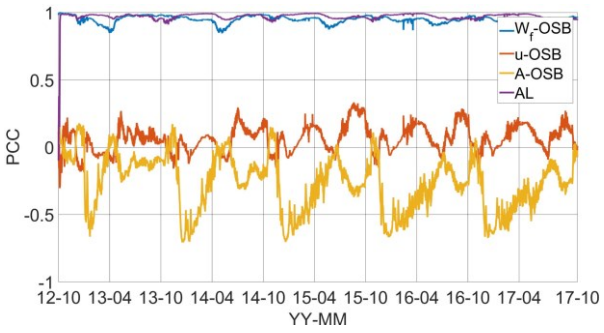

d) I-joist wall _ high load

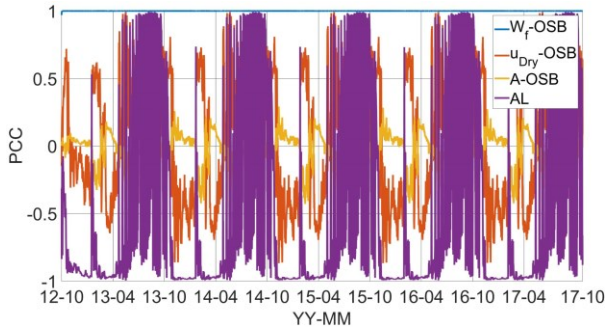

e) Polyisocyanurate wall _ low load

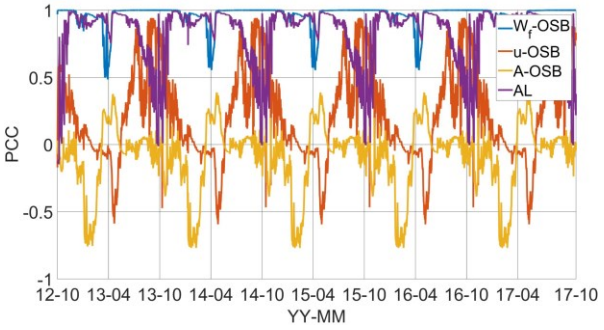

f) Polyisocyanurate wall _ high load

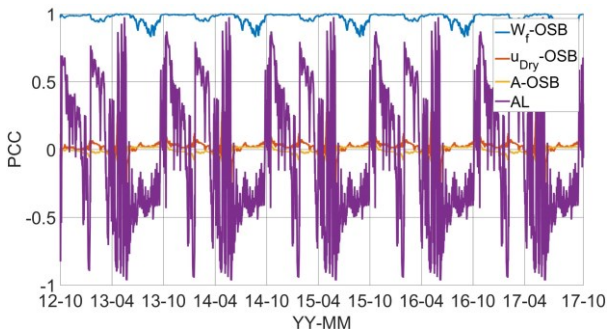

g) Mineral wool wall _ low load

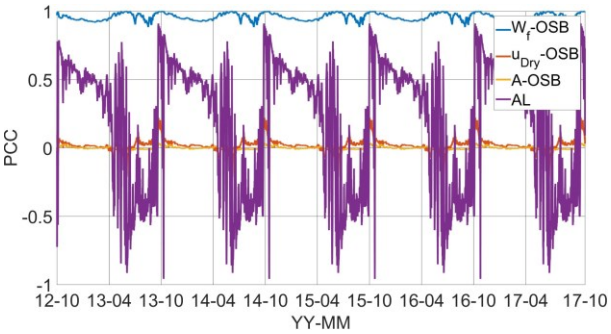

h) Mineral wool wall _ high load

Figure 6.16 PCCs of material properties and air leakage rates to MC_ north

Figure 6.16 shows the PCCs of material properties and air leakage rate for the north facing walls under low internal moisture load and high internal moisture load. It can be seen that the air leakage rate has strong positive influence on MC of OSB for the walls have condensations (baseline wall, I-joist wall, polyisocyanurate wall under high load condition). For the walls have no condensation and using air convection method (polyisocyanurate wall under low load condition and mineral wool wall), the influence of air leakage rate has a periodical variation.

It can be seen from Figure 6.16 a and b that for baseline wall the PCC of air leakage rate is higher in winter time than in summer time, which means the influence of air leakage is more significant in winter time than in summer time. The influence of u-value is less significant than A-value. Although there is a positive PCC for u-value, the PCC is lower than 0.5 in most time, which means the relationship between u-value and MC of OSB is not significant. The A-value has a significant negative influence on MC in winter time, when the PCC of air leakage rate becomes higher. Therefore, the liquid transport is the dominate way of the moisture getting out from the OSB. Under high internal load, the influence of transport properties becomes less significant than those under low internal load.

For I-joist wall, there is no seasonal variation for the PCC of air leakage rate and it always close to 1. The influence of u-value and A-value are not significant in the first year. While the PCC of u-value increases toward positive direction with a seasonal variation (higher in summer and lower in winter) and A-value decreases with an opposite direction (lower in winter higher in summer), which means the vapour and liquid transfer may be helpful to remove the MC from OSB in summer time but this influence is not significant since the absolute value of PCCs are lower than 0.5. Under high load condition, the PCC of u-value is close to zero throughout the five years while the PCC of A-value becomes lower than -0.5 in winter time, which means the liquid transfer has a significant effect of reducing MC of OSB.

For polyisocyanureate wall under low load condition, the influence of transport properties is similar with the scenario without air leakage. The influence of air leakage rate is negative in winter time and positive in most time of summer. The negative influence of air leakage rate is caused by the drying effect of indoor air as analyzed in section 5.4.1.1. Under high load condition, the influence of air leakage is always positive with a seasonal variation (more significant in winter time than in summer time), because the condensation is occurred in wintertime. The u-value has a significant positive influence in summer time and the A-value has a negative influence in winter time, which indicates both vapour and liquid transfer are significantly helpful of reducing MC of OSB while the vapour transfer is more significant in summer time and liquid transfer is more significant in winter time.

For mineral wool wall, there is no condensation under both low load condition and high load condition. The air leakage rate tends to positively influence the MC of OSB in winter time and negatively influence MC in summer time, and this phenomena is more significant under high load condition. The moisture transport properties have no influence on MC of OSB in both low load and high load condition.

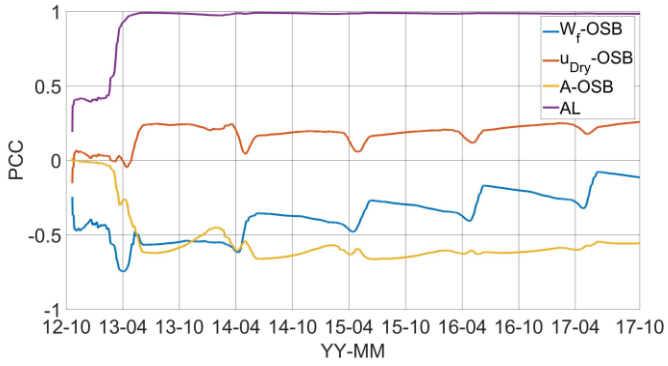

a) Baseline wall _ low load

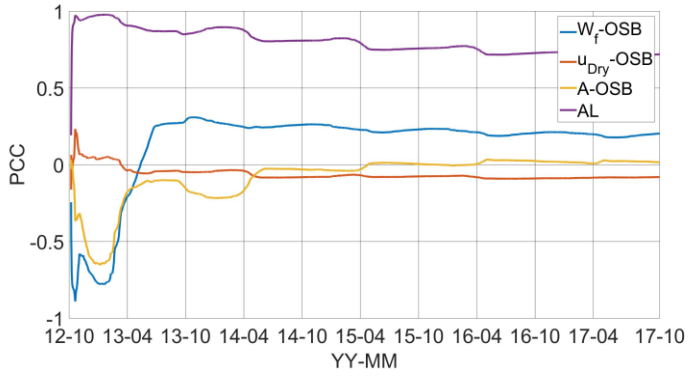

b) Baseline wall _ high load

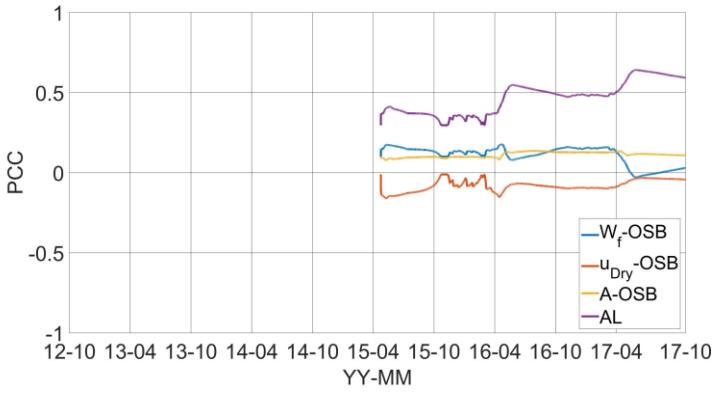

c) I-joist wall _ low load

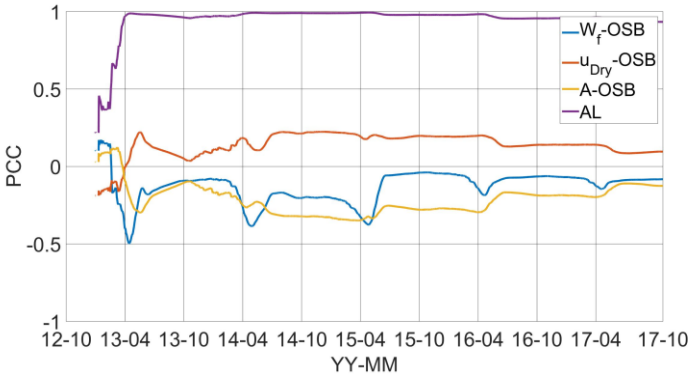

d) I-joist wall _ high load

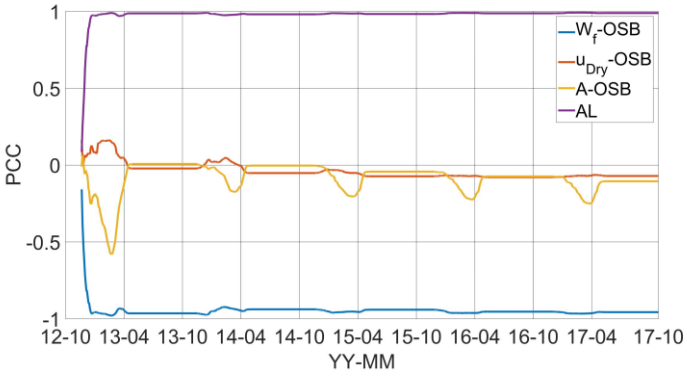

e) Polyisocyanurate wall _high load

Figure 6.17 PCCs of material properties and air leakage rates to mold growth index_north

As shown by Figure 6.17, the PCCs of the parameters to mold growth index does not fluctuate frequently. The air leakage rate always has a strong positive influence on mold growth index for all of the walls have mold growth risk. The influence of material properties is less than air leakage rate.

For baseline wall under low load, the W_f of OSB negatively influence the mold growth index, which means higher moisture storage capacity of the OSB leads to a lower mold growth index. And moisture transport, including vapour and liquid transport, also inhibits the mold growth since PCC of u-value is positive and that of A-value is negative. The influence of u-value is less significant than A-value. Under high internal load condition, the moisture storage function of OSB positively influences the mold growth index, but the influence is less significant than that in low internal load condition. The influence of transport properties of OSB is not significant.

For I-joist wall under low internal load condition, the influence of air leakage rate and material properties are not significant since the mold growth index under this situation is very low. There are no PCCs between mold growth index and the parameters before Apr. 2015 since the mold growth index is zero as shown by Figure 6.13c. For I-joist wall under high internal load condition, the trend of the PCCs is similar with baseline wall.

For plyisocyanurate wall, the air leakage rate always has a positive influence on mold growth index while the W_f always have a negative influence. The A-value negatively influence on mold growth index in the first winter, then the influence disappeared. The u-value has no influence on mold growth index throughout the 5 years.

Since the air leakage rate is the most important parameter influence mold growth index, the relationship between air leakage rate and the highest mold growth index of the walls is presented as scatter plot to figure out the threshold of the air leakage rate which results in mold growth problem.

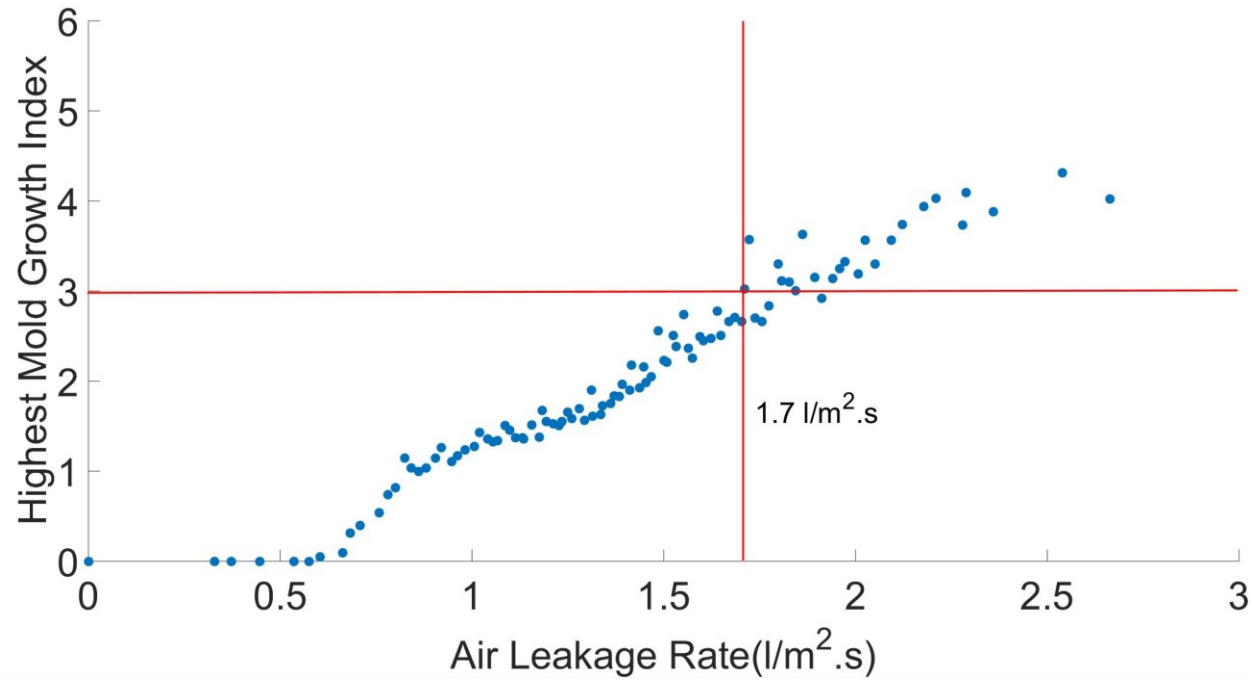

a) Baseline wall_ low load

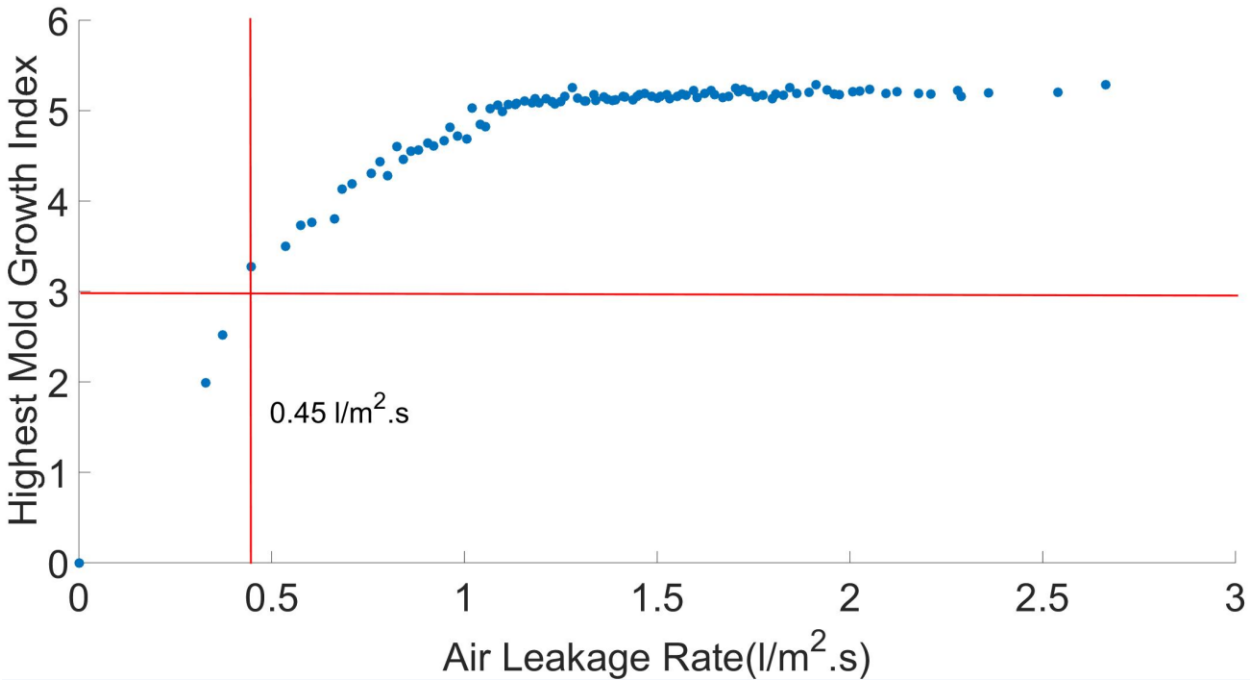

b) Baseline wall _ high load

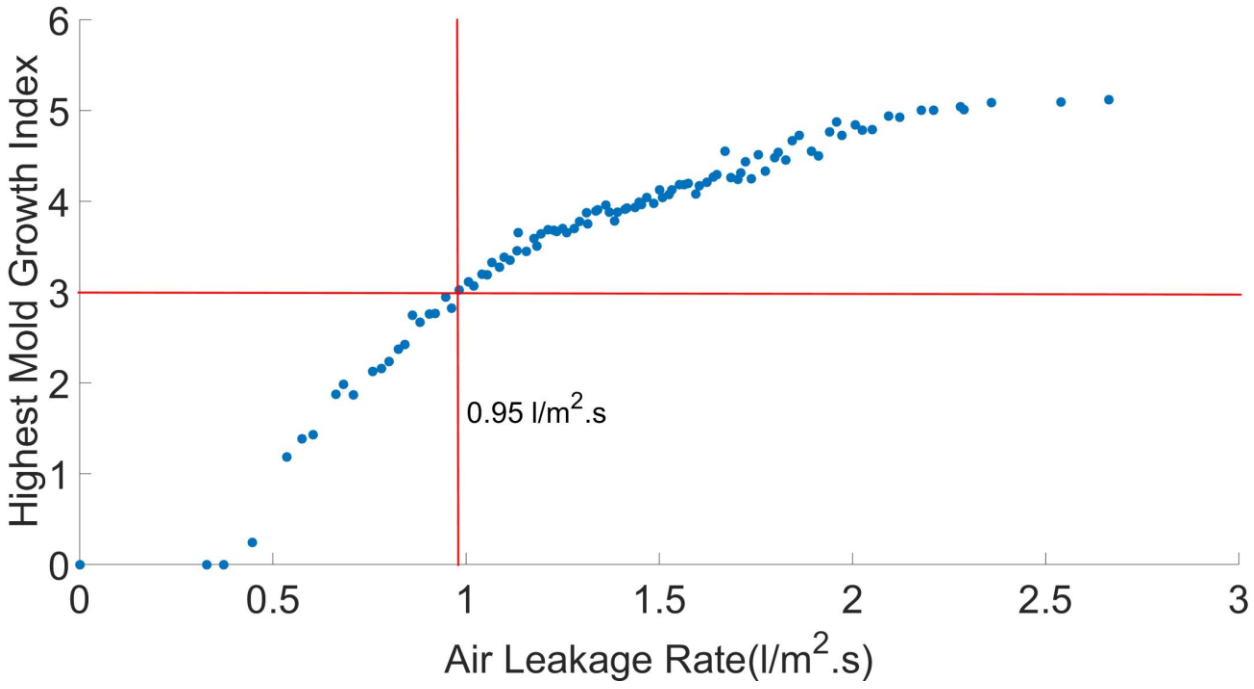

c) I-joist wall _ high load

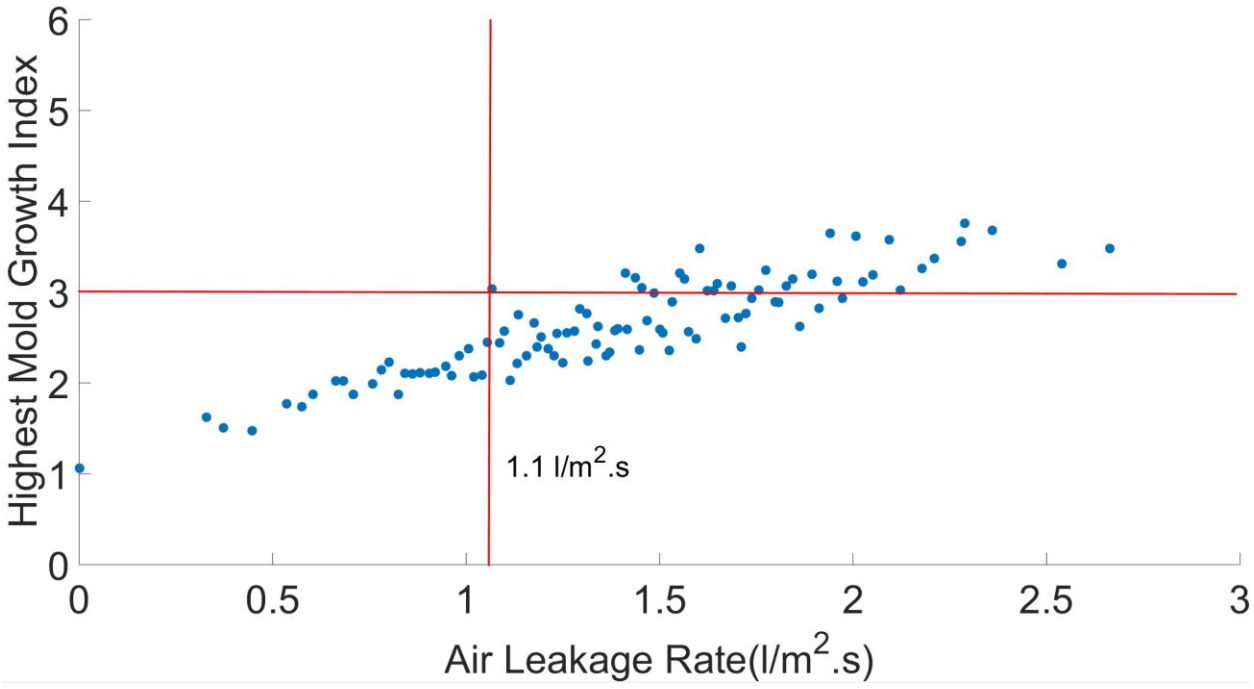

d) Polyisocyanurate wall _ high Load

Figure 6.18 Relationship between air leakage rate and highest mold growth index _ Waterloo

Figure 6.18 shows the relationship between air leakage rate @ 75 Pa and the mold growth index. To minimize the mold growth problem, the air leakage rate of baseline wall should not exceed 1.7 l/m^2·s under low internal load and 0.45 l/m^2·s under high internal load. For I-joist wall and polyisocyanurate wall with low internal load, there is no mold growth risk. Under high internal load, the air leakage rate should not exceed 0.95 l/m^2·s for I-joist wall and 1.1 l/m^2·s for polyisocyanurate wall.

Influence of rain leakage

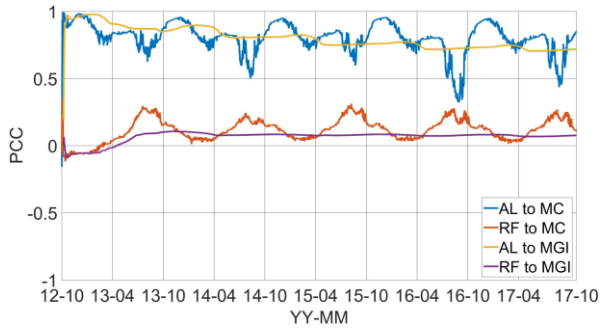

a) Baseline wall

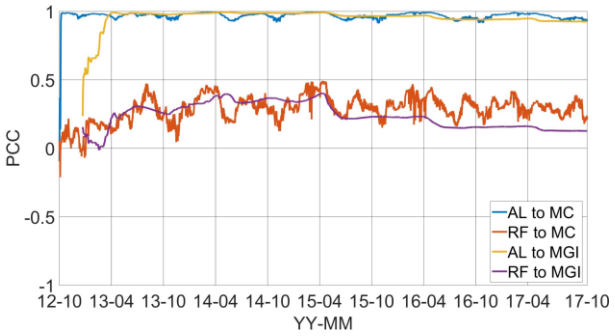

b) I-joist wall

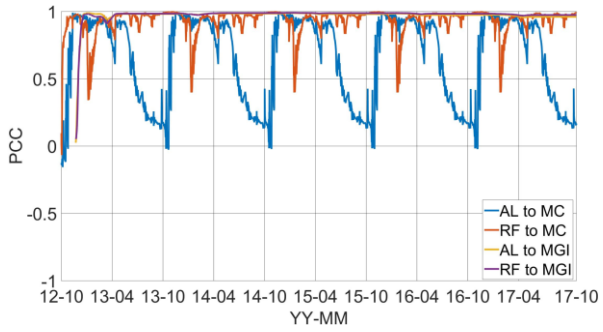

c) Polyisocyanurate wall

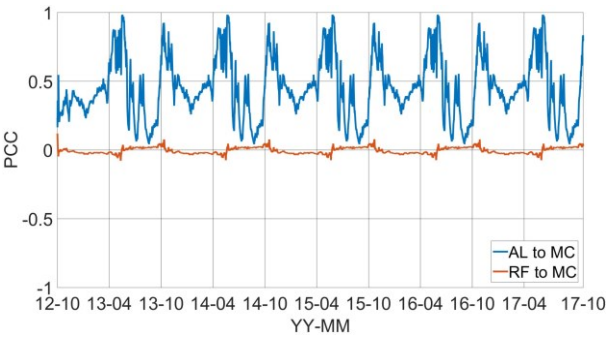

d) Mineral wool wall

Figure 6.19 PCCs of air leakage rates (high load_south) and rain deposition factors (south) _Waterloo

Figure 6.19 shows the PCCs of air leakage and rain deposition factor for scenario 4, both air leakage and rain leakage are taken into account. It can be seen that both air leakage rate and rain deposition factor have positive influence on moisture content and mold growth index. The PCCs of air leakage rate are higher than those of rain deposition factor, which means air leakage has more significant influence on MC and mold growth index than rain leakage. The PCCs against to

MC have seasonal fluctuation while those to mold growth index have no fluctuation. The fluctuation of the PCCs to MC reflects the variation of the strength of air leakage or rain leakage. It can be seen from Figure 6.19a and b that the PCCs of rain deposition factor are lower than 0.5, which means the influence of rain leakage is insignificant compared to air leakage. For polyisocyanurate wall, the influence of rain leakage is more significant than air leakage in summer time, while the influence of air leakage is more significant than rain leakage in winter time. For mineral wool wall, the rain leakage has no significant correlation with the moisture content because of the high exterior permeance allows the moisture drying outward immediately after the rain event.

Figure 6.20 shows the scatter plot of the relationship between air leakage rate and the highest mold growth index, and that between rain deposition factor and the highest mold growth index for the scenario with both air leakage (high load _ south) and rain leakage (south). It can be seen that decreasing of air leakage rate or rain deposition factor does not reduce the highest mold growth index for baseline wall (Figure 6.20 a, b). It is necessary to control both air leakage rate and rain deposition factor to reduce the mold growth risk for baseline wall. For I-joist wall, the highest mold growth index is lower than 3 when the air leakage rate is reduced below 0.75 l/m^2·s, but the stochastic cases with the lowest rain deposition factor still have the mold growth problem (Figure 6.20 c, d). Therefore, controlling air leakage rate is more effective than rain deposition factor in reducing mold growth risk. For polyisocyanurate wall, the mold growth indexes can be reduced below 3 when air leakage rate is lower than 0.75 l/m^2·s or rain deposition factor is lower than 0.57. Therefore, the mold growth risk can be reduced by controlling either air leakage rate or rain deposition factor.

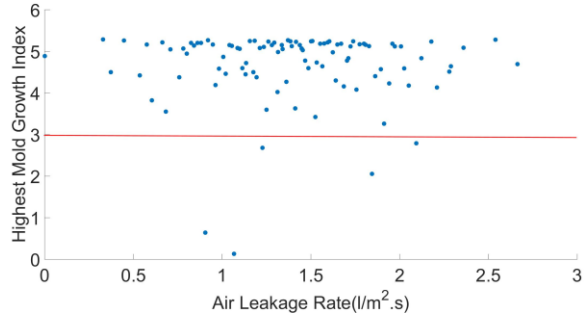

a) Baseline wall _ air leakage rate

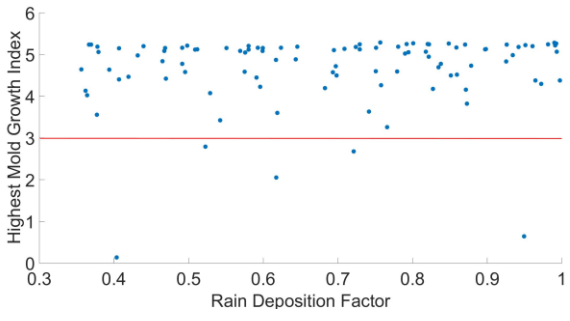

b) Baseline wall _ rain deposition factor

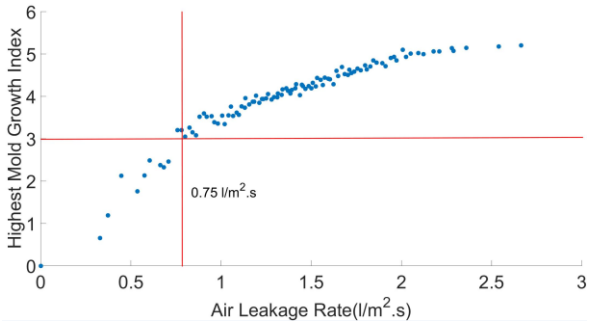

c) I-joist wall _ air leakage rate

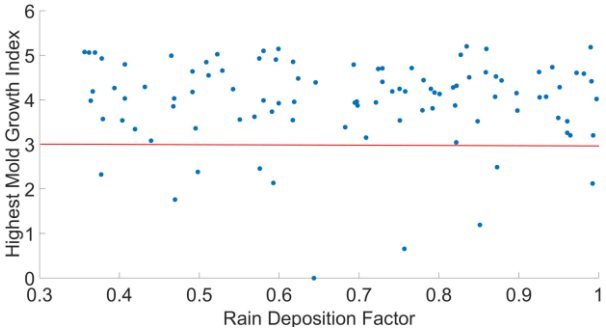

d) I-joist wall _ rain deposition factor

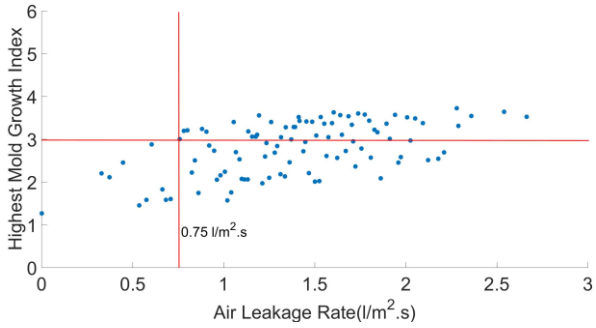

e) Polyisocyanurate wall _air leakage rate

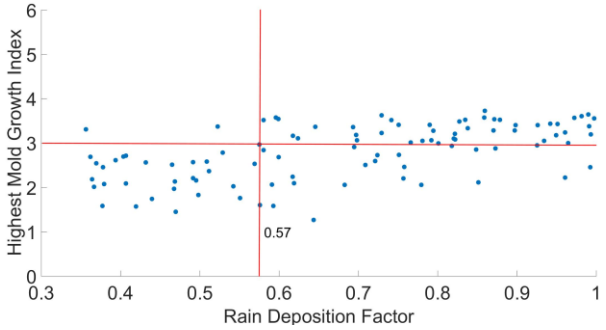

f) Polyisocyanurate wall _ rain deposition factor

Figure 6.20 Relationship between air leakage rates, rain deposition factor and highest mold growth index with air leakage (high load_south) and rain leakage (south) _Waterloo

6.2.3.2 Stochastic analysis for Vancouver

6.2.3.2.1 Stochastic results of moisture content

Scenario group 1: stochastic material properties

It can be seen from Figure 6.21 that the moisture content pattern of the walls in Vancouver are similar with those in Waterloo when there are no air leakage and rain leakage, which means the uncertainties of material properties do not result in a significant uncertainty of the simulation results when there are no air leakage and rain leakage for both Waterloo and Vancouver.

For baseline wall and I-joist wall, the uncertainty of the moisture content in Vancouver (Figure 6.21 a, b, c, d) is higher than in Waterloo (Figure 6.8 a, b, c, d) and the north orientation has higher

moisture content and uncertainty than south orientation. For exterior insulated walls, the MC of polyisocyanurate wall in Vancouver is lower than that in Waterloo, while the mineral wool wall has similar MC with Waterloo. The difference between north orientation and south orientation is more significant in Vancouver because the direct solar radiation in Vancouver is higher than in Waterloo.

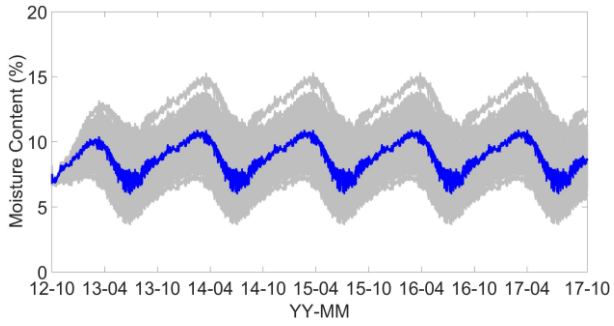

a) Baseline wall _ North

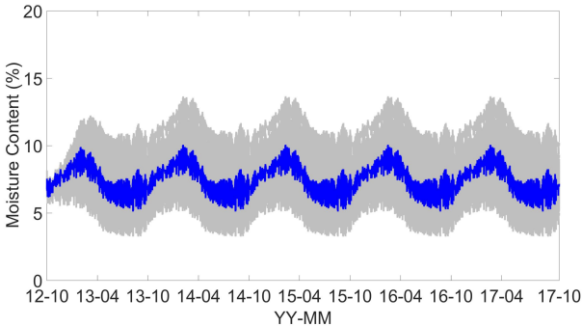

b) Baseline wall _ South

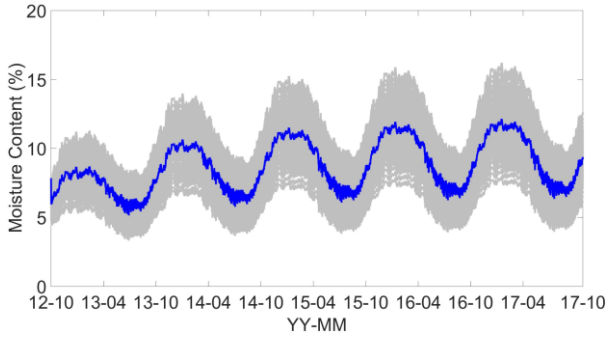

c) I-joist wall _ North

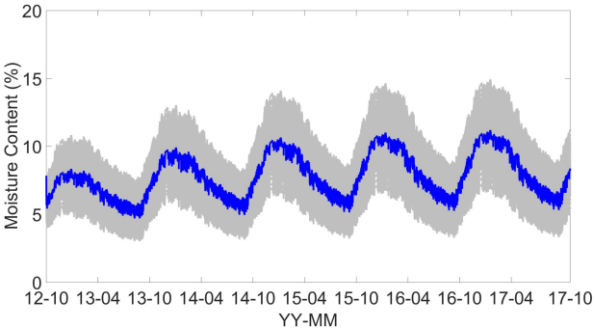

d) I-joist wall _ South

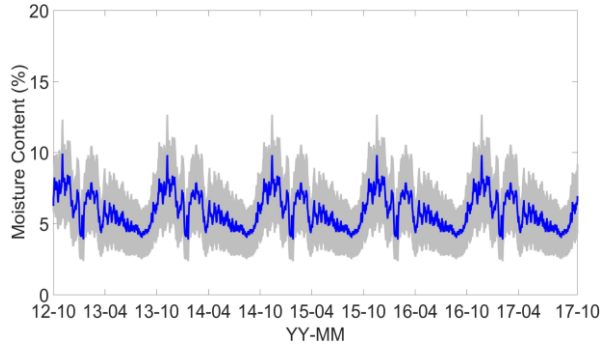

e) Polyisocyanurate wall _North

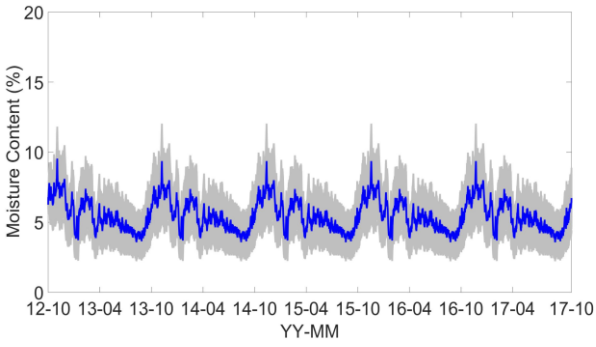

f) Polyisocyanurate wall _ South

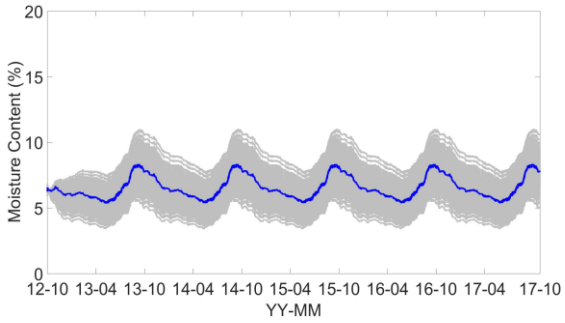

g) Mineral wool wall _ North

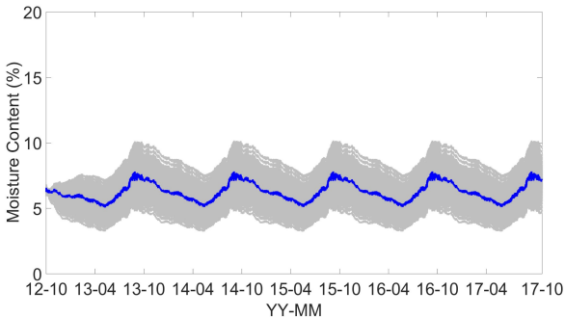

h) Mineral wool wall _ South

Figure 6.21 Stochastic results of MC with variation of material properties _ Vancouver

Scenario group 2: stochastic material properties and air leakage rates

For the scenarios with air leakage under low load condition (Figure 6.22), the moisture content levels of baseline wall and I-joist wall are significantly lower than those in Waterloo (Figure 6.9) because the condensed moisture caused by air leakage in Vancouver is much lower than in Waterloo (Appendix 3). For exterior insulated walls, the air convection method is used to simulate the impact of air leakage since there is no condensation for these walls. The moisture content level of polyisocyanurate wall is almost same as the scenario without air leakage and the mineral wool wall has a similar MC level with scenario without air leakage but different pattern. The reasons are stated in section 6.2.3.1.1

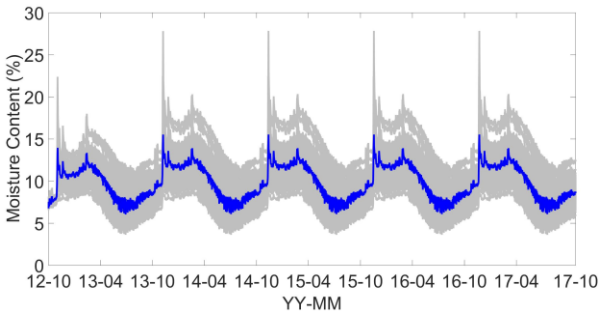

a) Baseline wall _ North

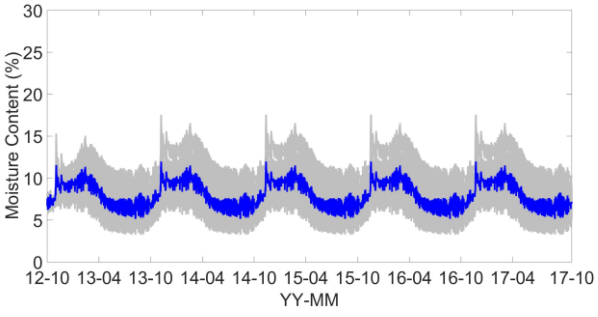

b) Baseline wall _ South

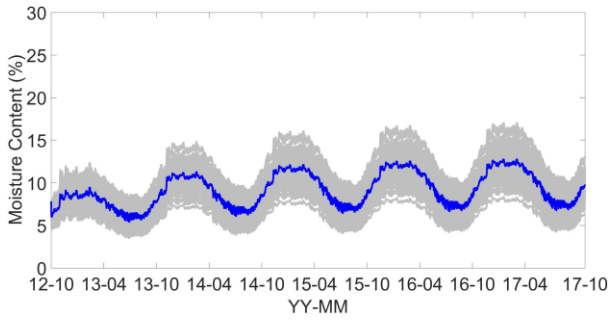

c) I-joist wall _ North

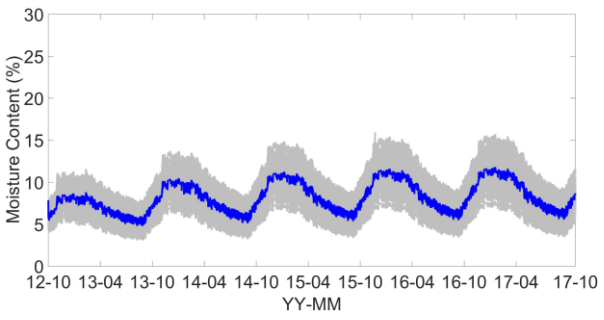

d) I-joist wall _ South

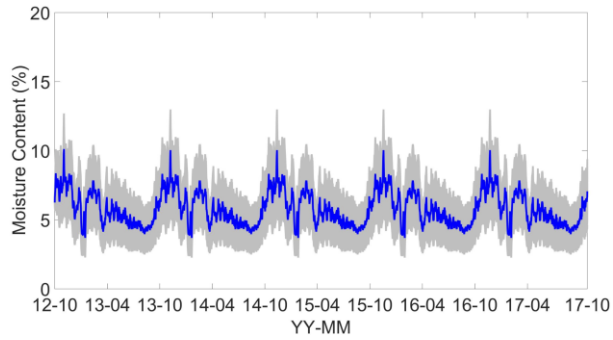

e) Polyisocyanurate wall _North

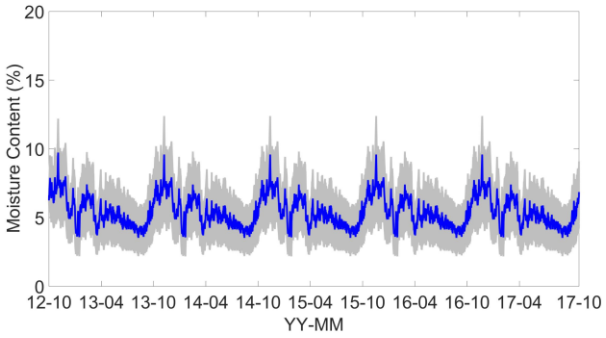

f) Polyisocyanurate wall _ South

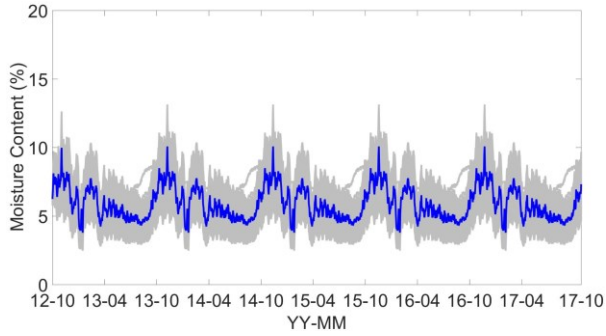

g) Mineral wool wall _ North

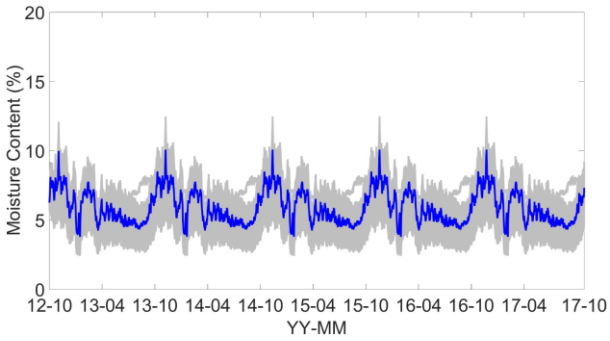

h) Mineral wool wall _ South

Figure 6.22 Stochastic results of MC with variation of material properties and air leakage rates_low load_Vancouver

As shown by Figure 6.23, under the high internal moisture load condition (RH30% to RH50%), the baseline wall has the highest MC increment compare to low load condition (RH20% to RH40%), but the MC level is still lower than the high load condition in Waterloo. The MC increment of I-joist wall is less significant than baseline wall because the cellulose fiber is able to absorb the moisture carried by leaking air, then reduce the MC level of OSB. For exterior insulated

walls, the MC increment of polyisocyanurate wall is more significant than mineral wool wall, because the condensation caused by air leakage in polyisocyanurate wall is higher than in mineral wool wall (Appendix 3). Although condensation is occurred in mineral wool wall, the MC level obtained by air infiltration method is lower than that obtained by air convection method because the condensed moisture is lower than the moisture transported by diffusion. Therefore, air convection method is used to simulate the air leakage impact on mineral wool wall.

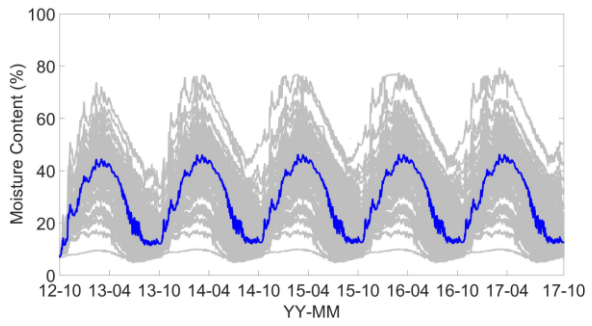

a) Baseline wall _ North

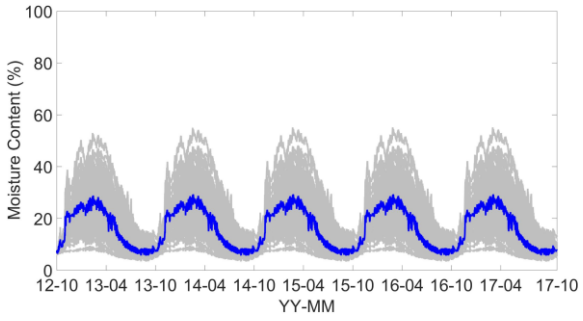

b) Baseline wall _ South

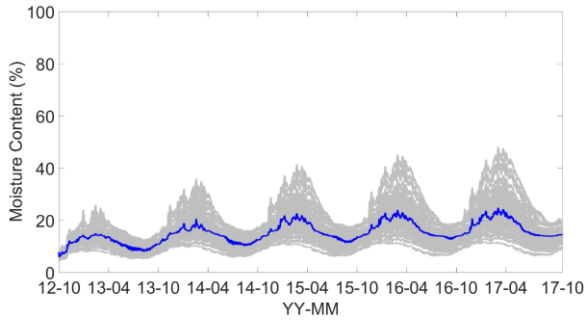

c) I-joist wall _ North

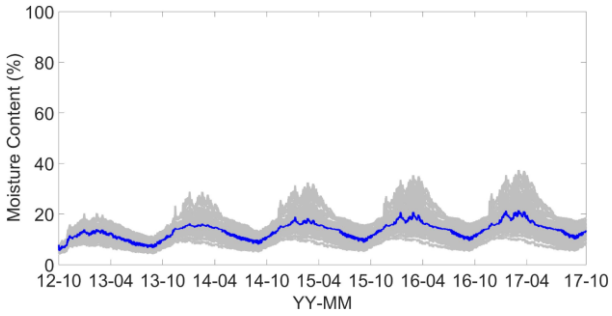

d) I-joist wall _ South

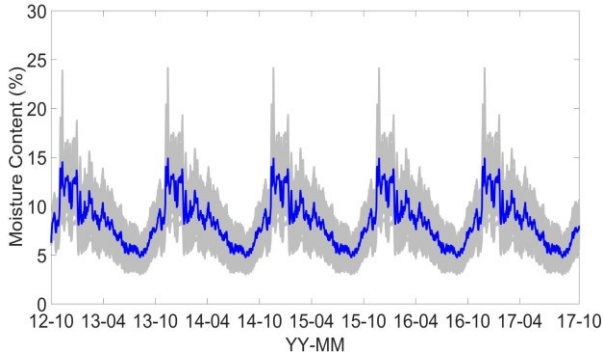

e) Polyisocyanurate wall _North

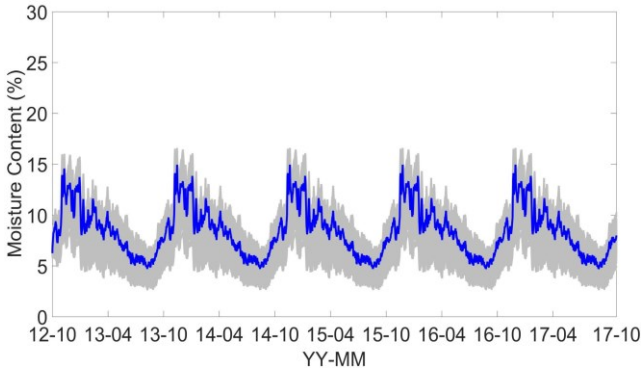

f) Polyisocyanurate wall _ South

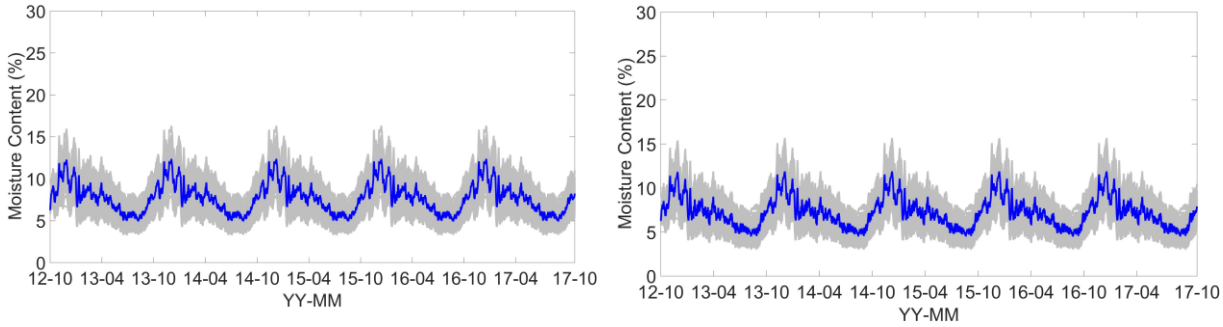

g) Mineral wool wall _ North

h) Mineral wool wall _ South

Figure 6.23 Stochastic results of MC with variation of material properties and air leakage rate_high load_Vancouver

Scenario grope 3: Stochastic material properties and rain deposition factors

For the rain leakage scenario, the simulations are performed for east orientation instead of south orientation because the east orientation receives the highest amount of wind-driven rain. It can be seen from Figure 6.24 that rain leakage almost has no influence on the MCs for north orientation because the north orientation receives the least amount of wind-driven rain. For the walls facing to east orientation, the base cases have almost the lowest moisture content level as they have the lowest rain deposition factor (0.35), which indicates rain deposition factor dominates the moisture content level for the east walls with 1% rain leakage. Baseline wall has higher MC level and uncertainties than I-joist wall because the moisture storage capacity of fiberglass is lower than cellulose fiber. For exterior insulated walls, the mineral wool wall has higher MC level and uncertainties than polyisocyanurate wall because the vapour barrier of mineral wool wall impedes the inward transport of the moisture carried by rain water, while the moisture can be dried inward for polyisocyanurate wall, which has no vapour barrier.

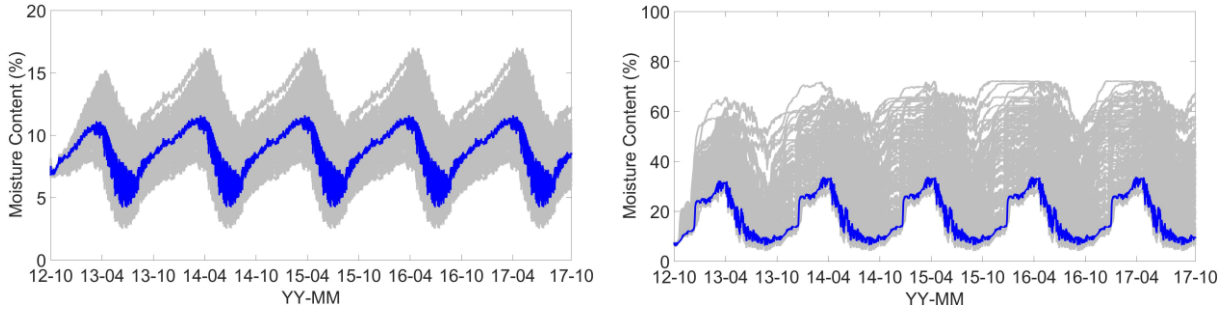

a) Baseline wall _ North

b) Baseline wall _ East

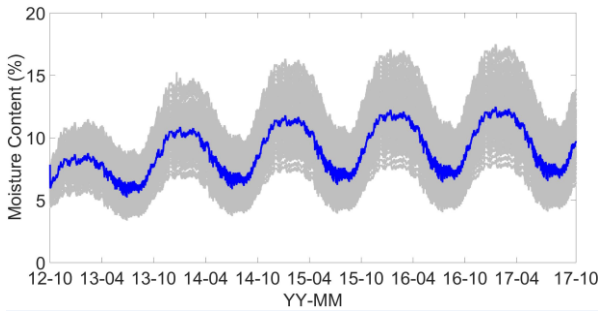

c) I-joist wall _ North

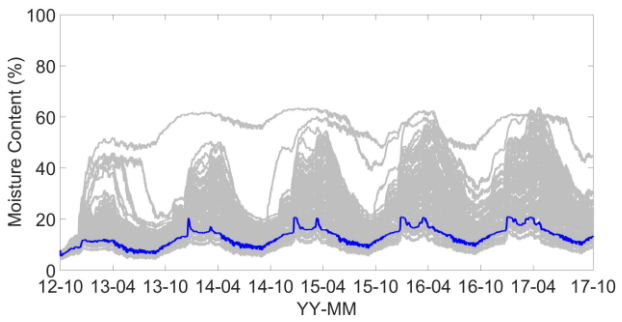

d) I-joist wall _ East

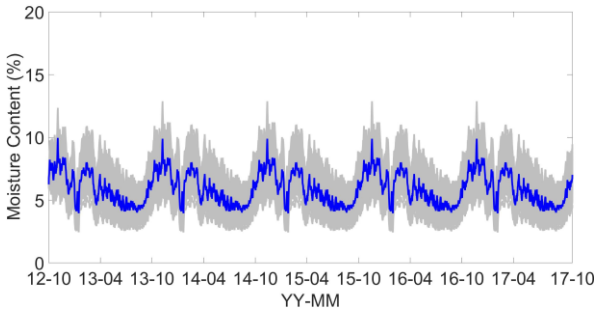

e) Polyisocyanurate wall _North

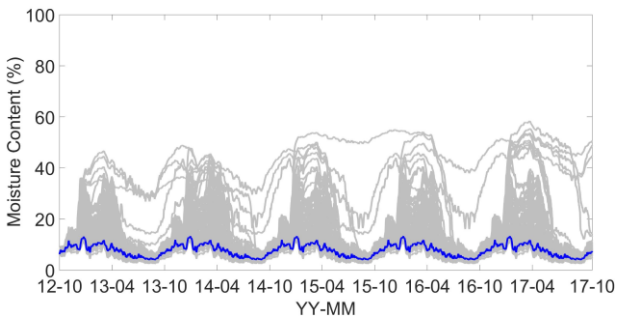

f) Polyisocyanurate wall _ East

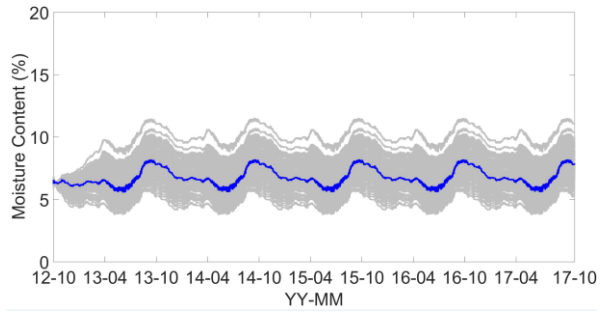

g) Mineral wool wall _ North

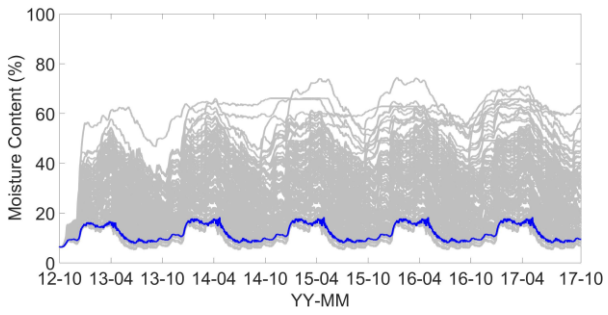

h) Mineral wool wall _ East

Figure 6.24 Stochastic results of MC with variation of material properties and rain deposition factors (1% of wind-driven rain)_Vancouver

For the cases with rain leakage is assumed as 1% of wind-driven rain, the moisture content levels are generally higher than south facing walls in Waterloo because the higher amount of wind-driven rain (Appendix 1). For the cases with rain leakage is set as 0.1% of wind-driven rain, the moisture content of all the walls does not exceed 20% for east orientation (Figure 6.25), which means all the walls are able to handle 0.1% of wind-driven rain penetration. But if the envelopes have a low

water tightness level that causes 1% wind-driven rain penetration, it is necessary to control the amount of the rain water depositing on the exterior surface.

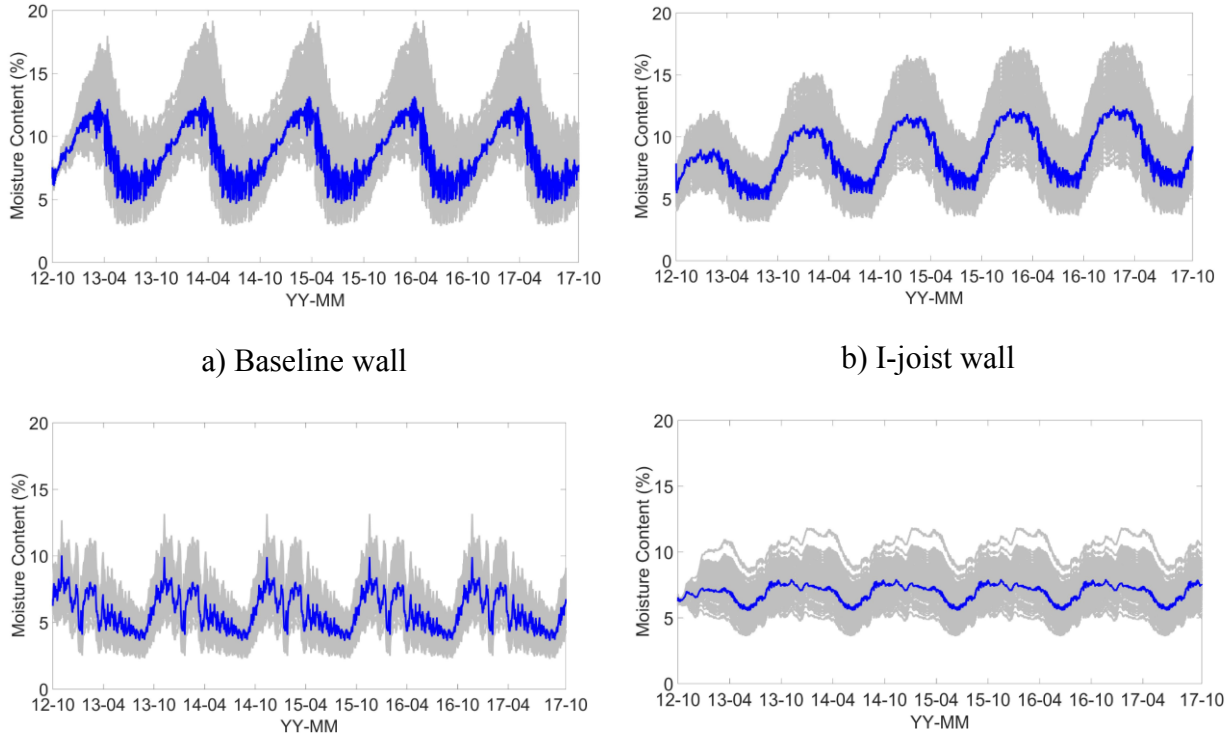

a) Baseline wall

b) I-joist wall

c) Polyisocyanrate wall

d) Mineral wool wall

Figure 6.25 Stochastic results of MC with variation of material properties and rain deposition factors (0.1% of wind-driven rain)_east_Vancouver

Scenario group 4: Stochastic material properties, air leakage and rain leakage

Figure 6.26 shows the stochastic results of MC of the scenario with both rain leakage and air leakage under high internal load. Simulations are only performed for east orientation since east orientation receives the highest amount of wind-driven rain. It can be seen that the moisture content level and uncertainties of the walls are higher than those only rain leakage is introduced except for mineral wool wall. In scenario 3 (the rain leakage scenario), the east facing polyisocyanurate wall has a lower MC level than mineral wool wall because the absent of vapour barrier allows the penetrated rain water to be dried inward, which indicates the indoor air has a drying effect on wetted OSB sheathing. As air convection method is used to simulate the impact of air leakage for

mineral wool wall, a 1 mm air layer with indoor temperature and RH is placed outside of vapour barrier, which allows the wetted OSB sheathing to be dried by the indoor air.

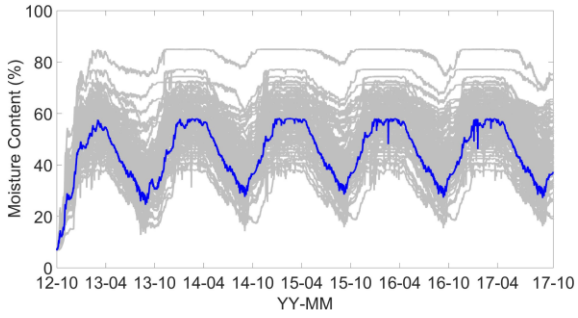

a) Baseline wall

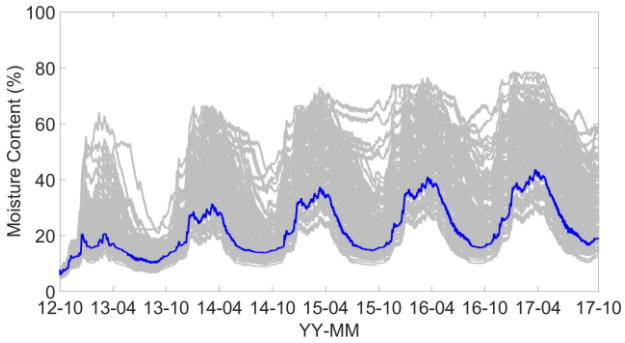

b) I-joist wall

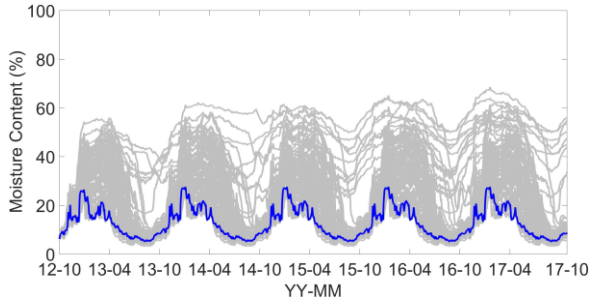

c) Polyisocyanurate wall

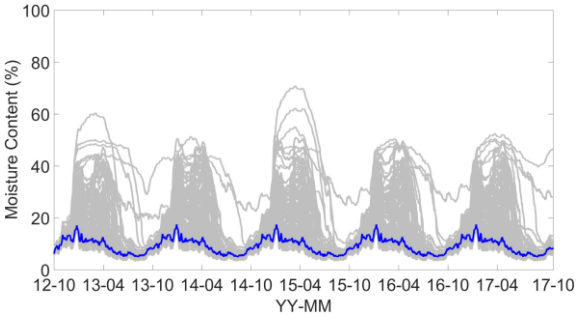

d) Mineral wool wall

Figure 6.26 Stochastic results of MC with variation of material properties, air leakage rates (high load_east) and rain deposition factor (east)_Vancouver

6.2.3.2.2 Mold growth risk analysis

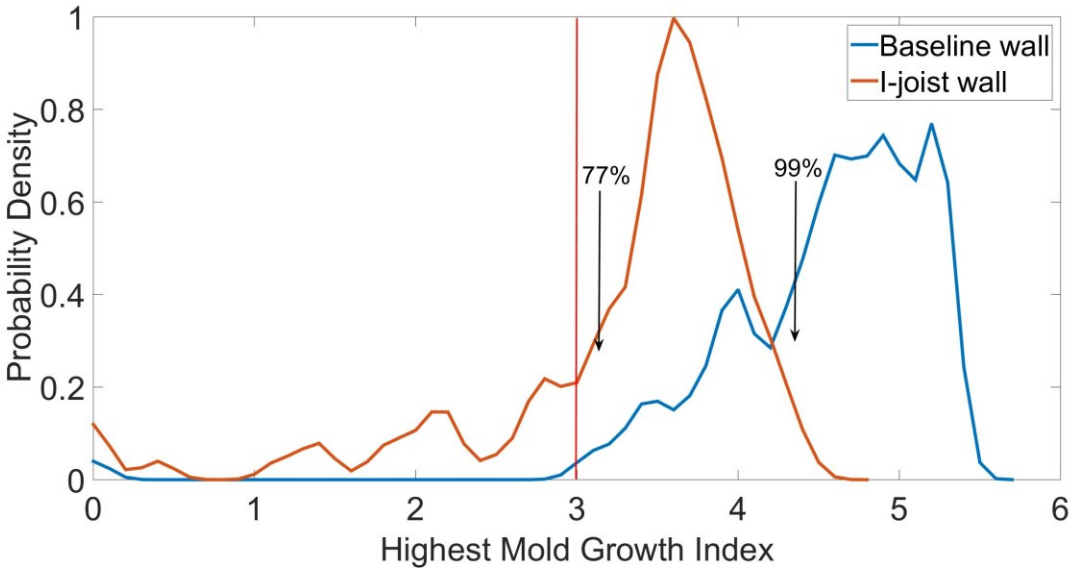

a) With air leakage _ high load

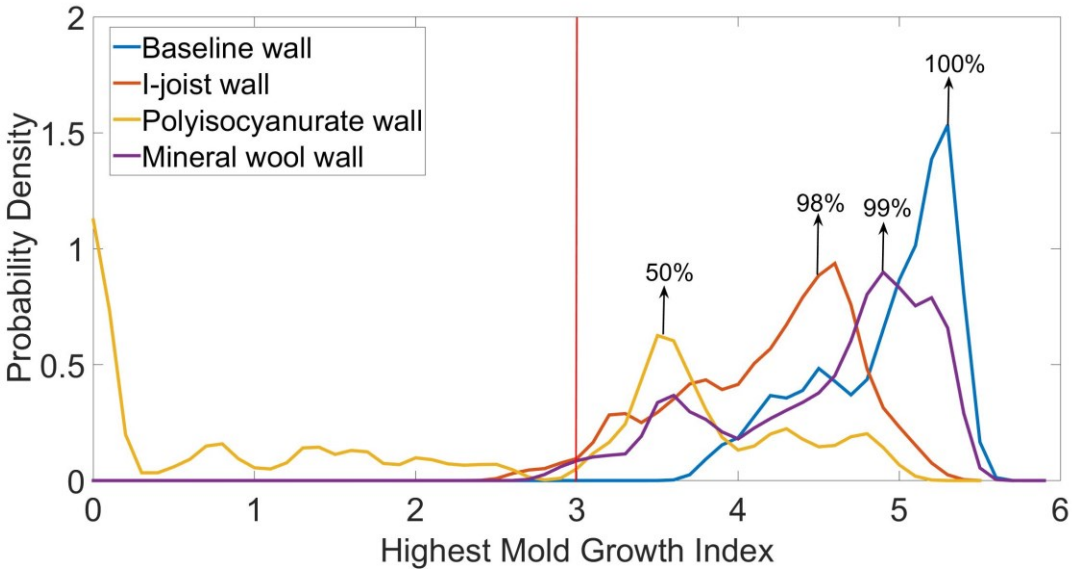

b) With rain leakage _ East

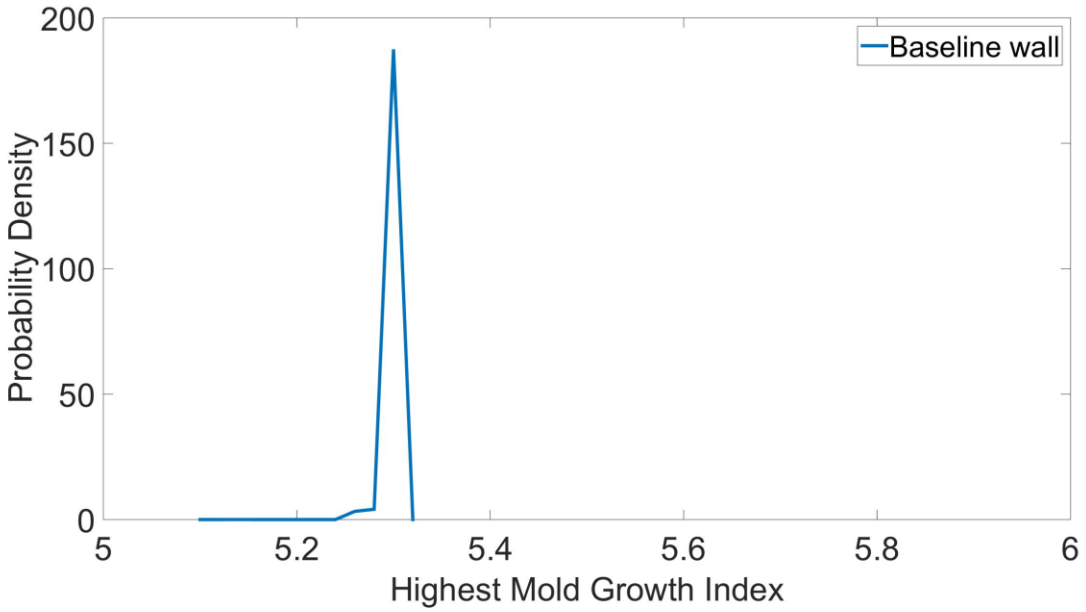

c) With both air leakage (high load _ east) and rain leakage (east) _ Baseline wall

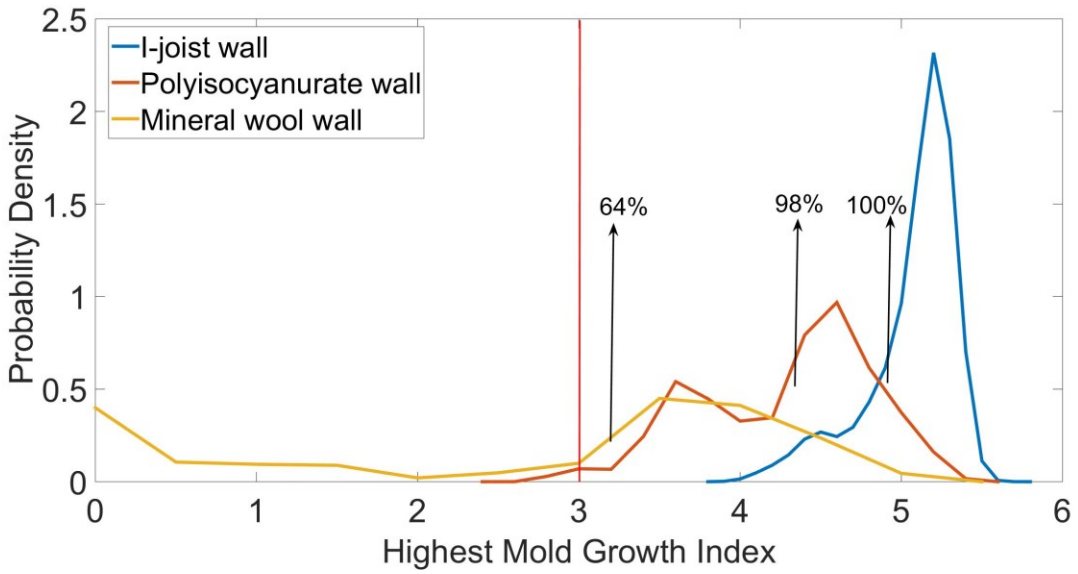

d) With both air leakage (high load _ east) and rain leakage (east) _ highly insulated walls

Figure 6.27 Probability density functions of the highest mold growth index _Vancouver

Figure 6.27 shows the probability density function of the highest mold growth index for the walls under different scenarios. For air leakage with high moisture load scenario, only baseline wall and I-joist wall have mold growth risks, which are comparable to those in Waterloo (Figure 6.14b).

The mold growth risks under rain leakage is much higher than those under air leakage. There is 100% probability of mold growth for baseline wall with 1% rain leakage. For I-joist wall and mineral wool wall with internal vapour barrier, majority of the stochastic cases has mold growth problem. For polyisocyanurate wall, there is 50% probability of mold growth problem. For the worst scenario, under which the walls are exposed to both air leakage with high moisture load and rain leakage of east orientation, the baseline wall has the most serious mold growth problem, which most of the stochastic cases have the highest mold growth index between 5.2 and 5.3. I-joist wall and polyisocyanurate wall have higher mold growth risk than the scenarios only with air leakage or rain leakage, while mineral wool wall has lower mold growth risk than the scenario with only rain leakage. Since the indoor air has a drying effect on the wetted OSB sheathing, removal of vapour barrier helps reducing the mold growth risk of mineral wool wall.

6.2.3.2.3 Sensitivity analysis

Table 6.7 shows the maximum moisture content levels and their uncertainties caused by different factors in Vancouver. It can be seen that the maximum MC level and uncertainties caused by material properties are comparable to Waterloo with a slight increase (Table 6.6). The walls with air leakage have lower maximum MCs and uncertainties than Waterloo as the condensation rates in Vancouver are lower than Waterloo (Appendix 3). The walls facing east with rain leakage have higher MCs and uncertainties than those facing south with rain leakage in Waterloo because of the higher amount of rain leakage (Appendix 1). It can be concluded that the MCs of OSB sheathings are more sensitive to rain leakage than to air leakage under climatic condition of Vancouver.

Table 6.7 The uncertainties caused by different factors- Vancouver

	Material properties	**Moisture loads**		
	(North)	**Air leakage_Low North**	**Air leakage_High North**	**Rain leakage East**
Baseline wall	11±4%	18±10%	44.5±34.5%	50±22%
I-joist wall	12±4%	12.5±4.5%	28±17%	38.6±25%
Polyisocyanurate wall	10±3%	10±3%	15±9%	34.5±24%

Mineral wool wall	8±3%	10±3%	12±4%	44.5±39.5%

Note: the uncertainties are expressed as absolute errors

Figure 6.28 shows the threshold of rain deposition factor to avoid mold growth problem. It can be seen that the rain deposition factor should be lower than 0.35 for I-joist wall and mineral wool wall to avoid mold growth index exceeding 3. For polyisocyanurate wall the rain deposition factor should not be higher than 0.65. For baseline wall, the safest design of rain deposition factor still results in mold growth problem, therefore it is necessary to control the amount of rain leakage to reduce the mold growth risk.

The air leakage with low moisture load will not result in mold growth risk for all the walls. Under high moisture load, the air leakage rate should be restricted to avoid the mold growth problem. As shown by Figure 6.29, the threshold of air leakage rates for baseline wall and I-joist wall are similar to those in Waterloo (Figure 6.18 c, d).

When both rain leakage and air leakage are introduced, all the stochastic cases of baseline wall and I-joist wall have the highest mold growth index exceeding 3, which indicates there is 100% possibility of mold growth problem. It can be observed by Figure 6.30 a, b, c, d that even the cases with lowest level of air leakage rate or rain deposition factor still has mold growth problem, which means the restriction of a single parameter (air leakage rate or rain deposition factor) cannot reduce the mold growth index to a safe level. Therefore, it is necessary to control both of air leakage and rain deposition factor in this scenario to reduce the mold growth risk. For polyisocyanurate wall, the reduction of air leakage rate is not able to control the mold growth index to a safe level, but the when the rain deposition factor is lower than 0.38, the highest mold growth index may be decreased to below 3 (Figure 6.30 e, f). For mineral wool wall, the air leakage has an insignificant negative (higher air leakage rate, lower mold growth index) influence on mold growth index, while the rain deposition factor has a significant positive influence on mold growth index (Figure 6.30 g, h). When the rain deposition factor is lower than 0.62, most of the stochastic cases have the highest mold growth index lower than 3.

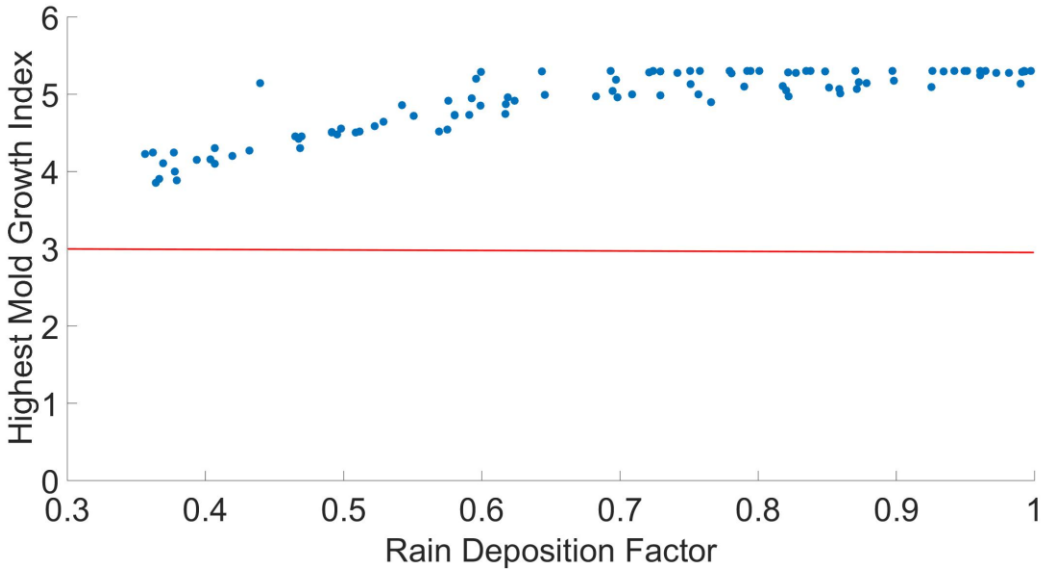

a) Baseline wall

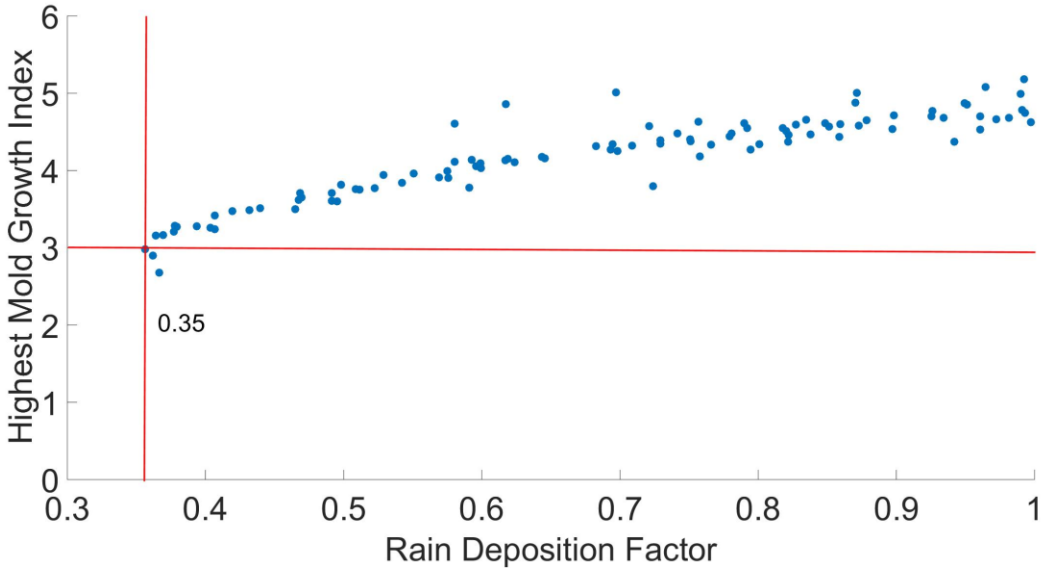

b) I-joist wall

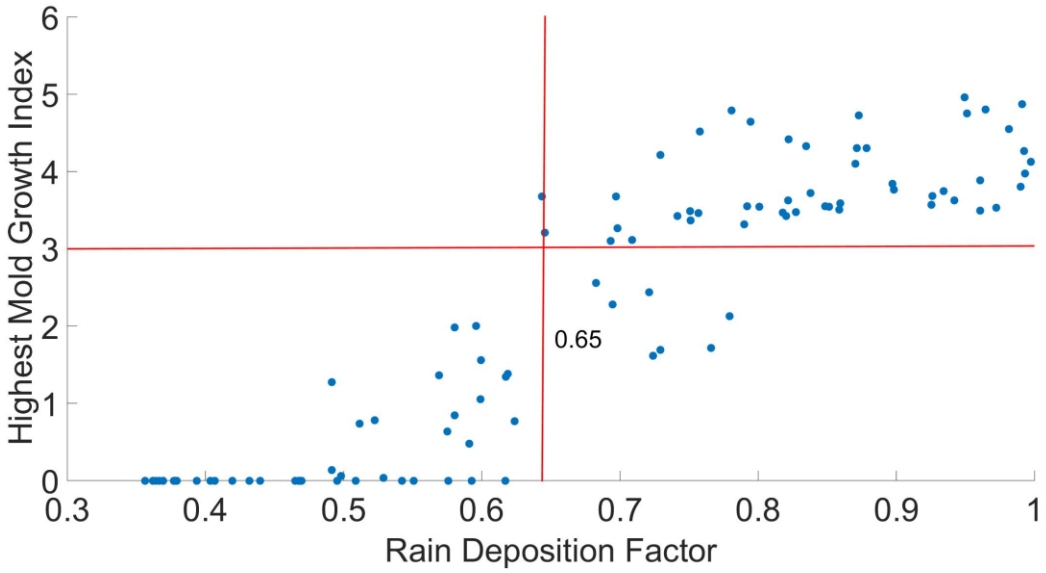

c) Polyisocyanurate wall

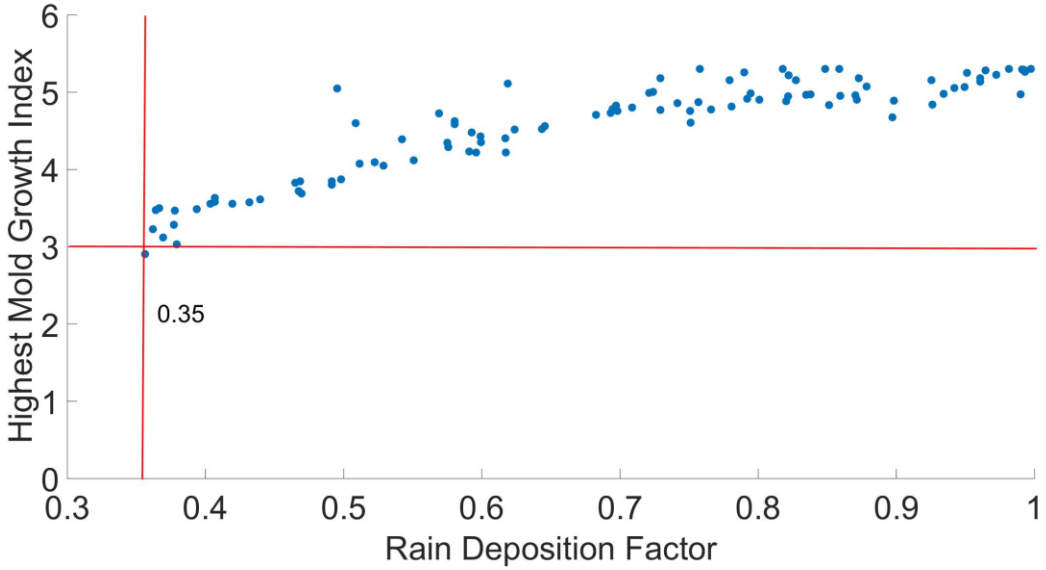

d) Mineral wool wall

Figure 6.28 Relationship between rain deposition factor and highest mold growth index_east_Vancouver

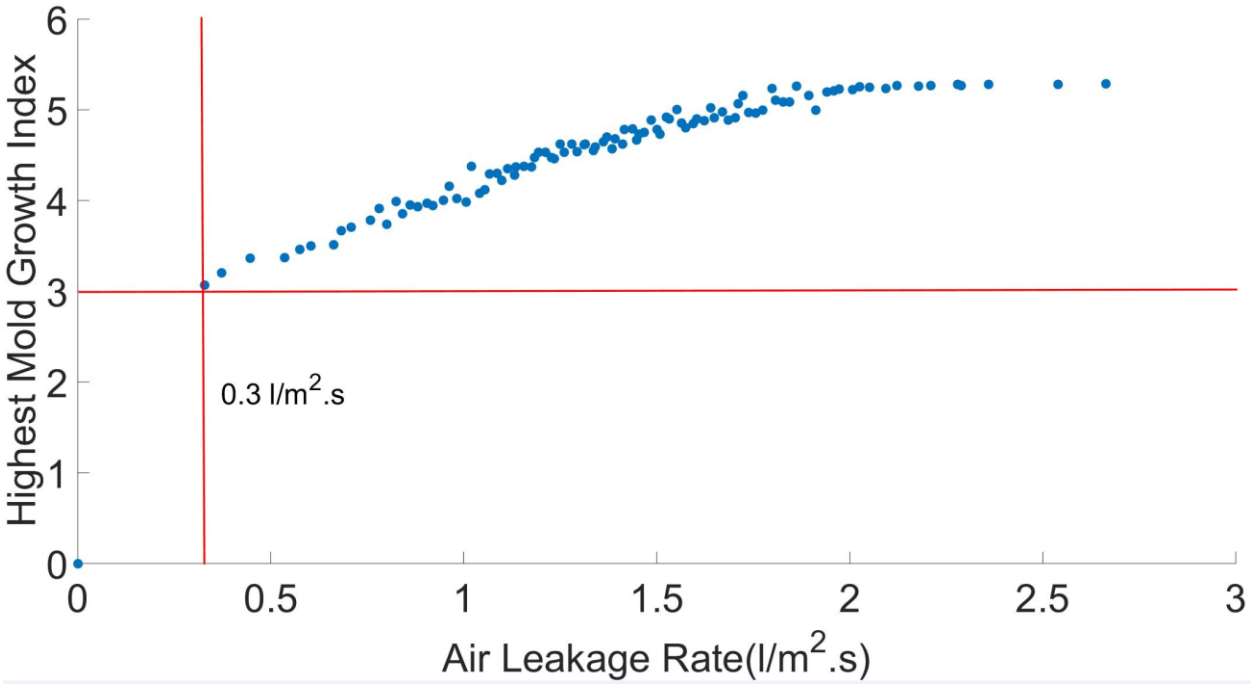

a) Baseline wall

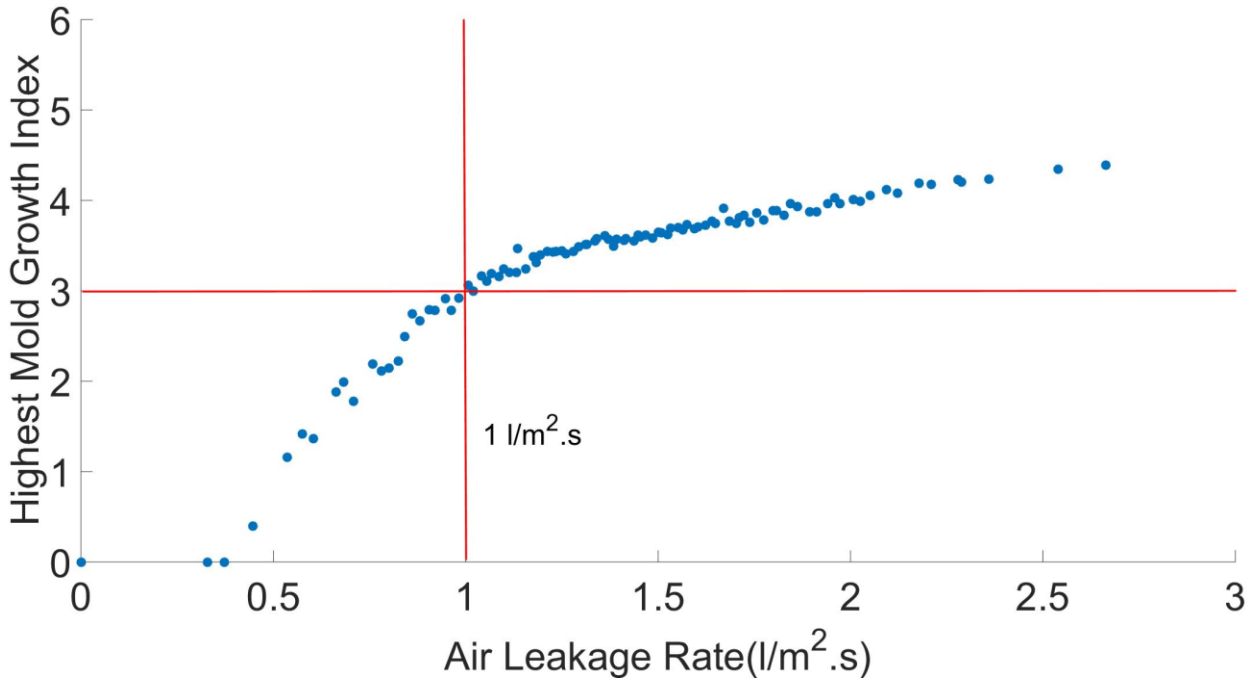

b) I-joist wall

Figure 6.29 Relationship between air leakage rate and highest mold growth index under high load_Vancouver

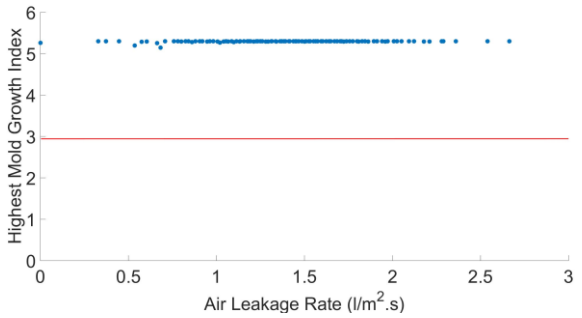

a) Baseline wall _ air leakage rate

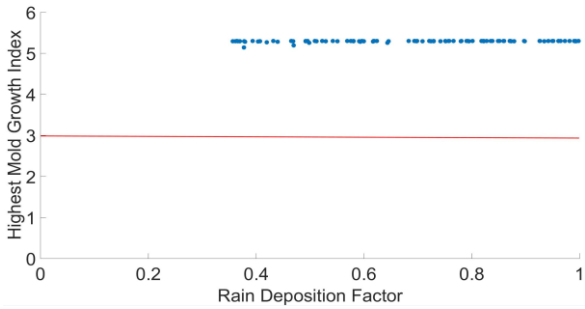

b) Baseline wall _ rain deposition factor

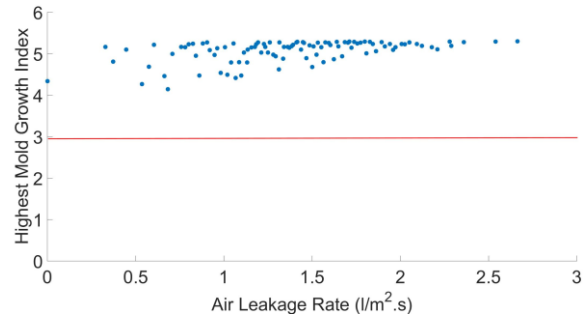

c) I-joist wall _ air leakage rate

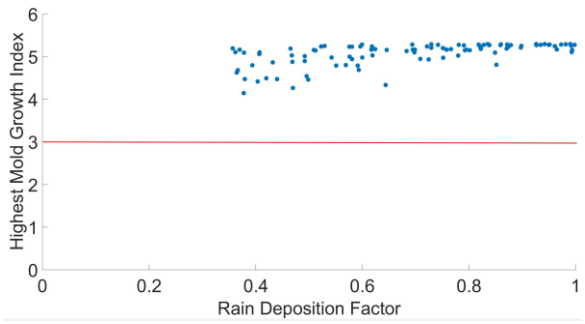

d) I-joist wall _ rain deposition factor

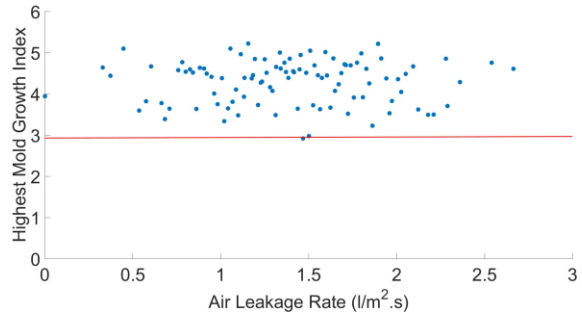

e) Polyisocyanrate wall _ air leakage rate

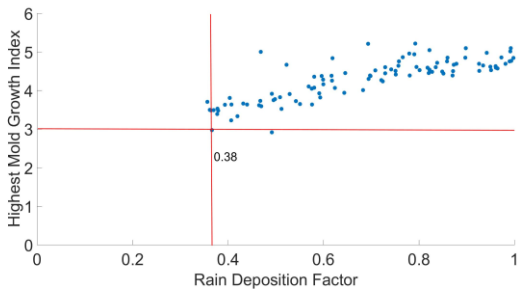

f) Polyisocyanrate wall _ rain deposition factor

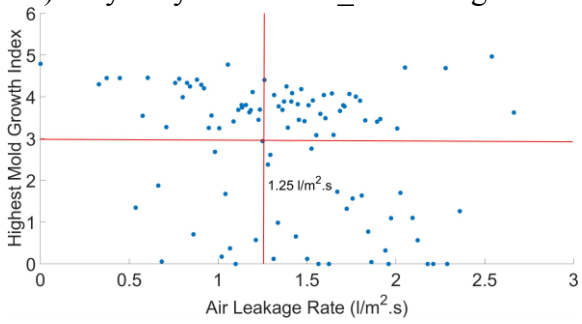

g) Mineral wool wall _ air leakage rate

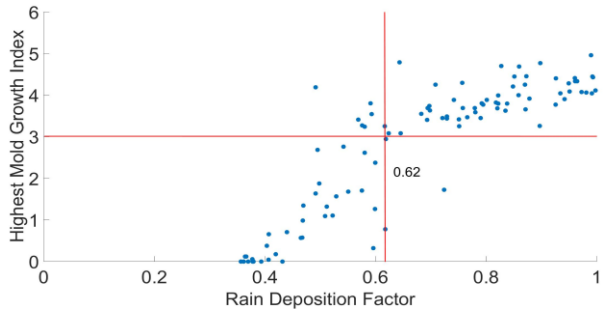

h) Mineral wool wall _ rain deposition factor

Figure 6.30 Relationship between air leakage rate, rain deposition factor and highest mold growth index with air leakage (high load_east) and rain leakage (east)_Vancouver

6.2.4 Conclusions for case study 2

- The uncertainties of material properties will not result in mold growth risk for all the walls when there are no air leakage and rain leakage. The OSB moisture content of I-joist wall and polyisocyanurate exterior insulated wall (low exterior vapour permeance) have higher uncertainties than baseline wall and mineral wool exterior insulated wall (high exterior vapour permeance) when only the uncertainties of material properties are taken into account.

Under climatic condition of Waterloo:

- The OSB moisture content of the baseline wall with fiberglass insulation is more sensitive to air leakage than the I-joist wall with cellulose fiber. The mold growth risk of the baseline wall is higher than the I-joist wall with air leakage. The air leakage does not result in mold growth risk under low internal load condition for exterior insulated walls since there is no condensation caused by air leakage. Under high load condition, the air leakage will result in mold growth problem for polyisocyanurate wall with lower risk than baseline wall and I-joist wall, but the mineral wool wall has no mold growth risk.
- For the baseline wall and I-joist wall, the rain leakage has less influence than air leakage under climatic condition of Waterloo because the moisture source caused by rain leakage is less than that caused by air leakage. The OSB moisture content of polyisocyanurate wall has higher uncertainty than mineral wool wall. All the walls have no mold growth risks caused by rain leakage.

Under climatic condition of Vancouver

- The air leakage will not result in mold growth risk for exterior insulated walls (polyisocyanrate wall and mineral wool wall), but will lead to mold growth risks for baseline wall and I-joist wall under high internal moisture load condition, and the mold growth risks are similar with those in Waterloo.
- The rain leakage has more influence than air leakage. For east orientation, which receives the highest amount of wind-driven rain, the baseline wall, I-joist wall and mineral wool wall have almost 100% probability for mold growth. The polyisocyanurate wall have lower mold growth risk (50% probability for mold growth) than baseline wall, I-joist wall and mineral wool wall.

- In the scenario with both air leakage (high moisture load) and rain leakage (east), baseline wall and I-joist wall have 100% probability of mold growth problem, polyisocyanurate wall has a much higher mold growth risk (98%) than the scenario only with rain leakage (50%). For mineral wool wall the mold growth risk is lower than only with rain leakage (64% compare to 99%).

Mold growth risk evaluation of the walls

- The mold growth risks (the probability of the highest mold growth index exceeding 3) of the walls under different moisture loads and climatic conditions (Waterloo and Vancouver) are listed in Table 6.8.

Table 6.8 Mold growth risks of the walls under different moisture loads and climatic conditions

Climatic condition	**Scenarios**	**Baseline wall**	**I-joist wall**	**Polyisocyanurate wall**	**Mineral wool wall**
Waterloo	Air leakage _ low load	22%	0%	0%	0%
	Air leakage _ high load	97%	79%	28%	0%
	Rain leakage _ south	0%	0%	0%	0%
	Air leakage (high load) and rain leakage (south)	95%	90%	46%	0%
Vancouver	Air leakage _ low load	0%	0%	0%	0%
	Air leakage _ high load	99%	77%	0%	0%
	Rain leakage _ east	100%	98%	50%	99%
	Air leakage (high load) and rain leakage (east)	100%	100%	98%	64%

Thresholds for avoiding mold growth problem

- The thresholds for air leakage rates and rain deposition factors that to avoid mold growth problem depends on the types of the walls, moisture loads and climatic conditions. These thresholds are listed in Table 6.9.

Table 6.9 Threshold of air leakage rates and rain deposition factors under different moisture loads and climatic conditions

Climatic condition	**Parameters**	**Baseline wall**	**I-joist wall**	**Polyisocyanurate wall**	**Mineral wool wall**
Waterloo	Air leakage rate _ low load ($l/m^2 \cdot s$)	1.7	NR	NR	NR
	Air leakage rate _ high load ($l/m^2 \cdot s$)	0.45	0.95	1.1	NR
	Rain deposition factor _ south	NR	NR	NR	NR
Vancouver	Air leakage rate _ low load ($l/m^2 \cdot s$)	NR	NR	NR	NR
	Air leakage rate _ high load ($l/m^2 \cdot s$)	0.3	1	NR	NR
	Rain deposition factor _ east	0.35	0.35	0.65	0.35

NR: No Risk.

Chapter 7 Conclusions and future work

7.1 Conclusions

This thesis developed a stochastic methodology to investigate the mold growth risks of highly insulated wood framed walls, and a software platform which is based on DELPHIN and MATLAB is developed to implement the methodology. The moisture performance of the CLT wall assemblies with high and low exterior permeance and two types of highly insulated wall assemblies: deep cavity wall and exterior insulated wall are evaluated by using the developed methodology. The main conclusions of this thesis can be categorized into two aspects: 1) conclusions regarding stochastic simulation methodology; 2) conclusions regarding to hygrothermal performance and design strategies of CLT walls and highly insulated walls.

7.1.1 Conclusions regarding stochastic simulation methodology

- In most cases, DLPHIN and WUFI have comparable accuracy for simulating hygrothermal performance of wood framed walls. DELPHIN has a higher resolution than WUFI at higher RH levels because it uses moisture retention curve, which interprets the relationship between moisture content and capillary pressure, to describe the moisture storage property.
- Parametric study provides a ranking of the significance of influential parameters for specific situation because it only changes one parameter at a time with keeping other parameters fixed. Therefore, it is not suitable for risk assessment which should consider the combined effect of influential parameters on simulation results. Stochastic approach changes influential parameters simultaneously, which takes the combined effect of the parameters into account. Therefore, stochastic approach is more proper for risk assessment.
- The one-dimensional air leakage modelling methods: air infiltration method and air convection method are used to simulate the effect of air leakage on highly insulated wood framed walls. For air infiltration method, the total amount of the leaking air should be reduced by multiplying a percentage to reflect the actual amount of the air reaching OSB sheathing. For air convection method, the location of the 1mm air layer should be able to reflect cavity depth that the leaking air can reach. The actual amount of the air reaching OSB and the position of the 1mm air layer can be calibrated by comparing the simulated moisture content of OSB with that obtained from field measurement.

7.1.2 Conclusions regarding hygrothermal performance and design strategies for CLT walls and highly insulated wood framed walls

- For a given wall configuration, the hygrothermal performance of wood framed walls is more sensitive to the variability of moisture loads than that of material properties. The uncertainties of the material properties do not result in mold growth risk when the moisture loads such as air leakage and rain leakage are not taken into account. The uncertainties of moisture loads such as internal moisture production, air leakage rate and rain leakage rate are the main factors lead to mold growth risk.
- The moisture content of the wood sheathing is more sensitive to moisture storage property than moisture transport property. The influence of moisture transport properties has a seasonal variation.
- For CLT walls, the wall with low exterior permeance is less responsive to the variation of ambient conditions, including the wind-driven rain and cladding ventilation, than that with high exterior permeance. Therefore, the moisture performance is relatively stable and not prone to moisture problem as long as there is no rain water penetration. However, if there is a defect of the water resistive barrier, the moisture problem risk will be higher than the wall with high exterior permeance. Therefore, for the wall with low exterior permeance, it is critical to control the rain penetration to avoid the moisture problem.
- The CLT wall with high exterior permeance is more sensitive to the ambient conditions than that with low exterior permeance. However, the CLT panel is easier to be dried after the rain event even there is a rain penetration. Therefore, the wall with high exterior permeance is safer than that with low exterior permeance in terms of moisture problem.
- For deep cavity wall, cellulose fiber insulation is able to absorb the ambient moisture, thereby, reduce the moisture content level of OSB. Although the deep cavity wall has higher condensation potential than conventional 2x6 framed wall, the mold growth risk for deep cavity wall with cellulose fiber insulation is lower than conventional 2x6 framed wall with fiberglass insulation because the higher moisture storage capacity of cellulose fiber.
- For the exterior insulated walls, the high exterior permeance is beneficial to reduce the moisture content of wood sheathing, since the moisture is able to be transferred outward. However, the interior vapour barrier reduces the chance of drying inward, and increases

the mold growth risk in mild and humid climate zone. In the climatic condition of Vancouver, where the moisture load from rain leakage is higher than that from air leakage, removal of vapour barrier is able to reduce mold growth risk.

- The significance of the moisture loads depends on the climatic conditions. In cold climate zone like Waterloo, air leakage plays a more important role than rain leakage, and it is the dominant factor that leads to mold growth. In mild and humid climate zone such as Vancouver, rain leakage is more important than air leakage, and it leads to a higher mold growth risk than air leakage.
- The thresholds of the air leakage rate and rain deposition factor, which should not be exceeded to avoid mold growth problem, depends on the types of wall configuration and climatic conditions.

7.2 Future work

- The air leakage modelling methods used in this thesis are one-dimensional methods, which take the leaking air as an equivalent moisture source in the wall assembly. Two dimensional air leakage modeling methods can be applied in future study to investigate the air distribution through the wall assembly.
- The ASHRAE empirical model is used to determine the amount of the wind-driven rain deposited on the wall surface, and rain deposition factor is used as a stochastic variable to reflect the variability of rain leakage. The rain water impinged on the wall surface can also be obtained from CFD modelling, which is more precise than empirical model. The combination of CFD wind-driven rain modelling and hygrothermal modelling can be applied in future study to investigate the moisture performance of the wall assemblies and the catch ratio can be used as a stochastic variable to reflect the uncertainty of the impinged rain water.
- The penetrated rain water is assumed as 1% of wind-driven rain according to the prescription in ASHRAE 160 (2016). However, there are few studies supporting the reasonability of the 1% rain leakage. More field measurement study should be conducted to obtain a proper range of the penetrated rain water.

- The mold growth risks of the highly insulated walls are evaluated under cold climatic condition (Waterloo) and mild/humid climatic condition (Vancouver). The applicability of the wall assemblies should be evaluated under more climatic conditions.
- This thesis only focuses on moisture performance of the wood framed walls. Multi-objective analysis which considering both moisture and energy performance should be performed for a comprehensive evaluation of energy efficiency and durability of the wall assemblies. The combination of hygrothermal modelling and energy modelling can be a powerful tool to achieve the synthesized evaluation.
- The developed stochastic simulation methodology can also be applied for other moisture damage risk analysis such as wood decay and the damage caused by freeze/thaw cycle.

References

Alev, U., Uus, A., Teder, M., Miljan, M.J., & Kalamees, T. (2014). Air leakage and hygrothermal performance of an internal insulated log house. The 10th Nordic Symposium on Building Physics. Lund, Sweden.

Alsayegh, G., Mukhopadhyaya, P., Wang, J., Zalok, E., & van Reenen, D. (2013) Preliminary characterization of physical properties of cross-laminated-timber (CLT) panels for hygrothermal modelling. Advances in Civil Engineering Materials, 2(1), 472-484.

Armstrong, M., Maref, W., Rousseau, M.Z., Lei, W., & Nicholls, M. (2010). Effect of the air and vapour permeance of exterior insulation on the flow of moisture in wood frame walls in a cold climate. International Conference on Building Envelope Systems and Technologies. Vancouver, Canada.

Arena, L., Owens, D., & Mantha, P. (2013). Measured performance of an R-40 Double-Stud wall in climate zone 5A. Thermal Performance of the Exterior Envelopes of Whole Buildings XIII International Conference. Clearwater Beach, Florida, USA.

Arnaut, L. R. (2008). Measurement uncertainty in reverberation chambers-I. Sample statistics. (NPL Report TQE 2). London, UK: National Physical Laboratory.

ASHRAE. (2013). Fundamentals Handbook. Atlanta, GA: American Society of Heating Refrigerating and Air Conditioning Engineers Inc.

ASHRAE. (2016). ANSI/ASHRAE Standard 160-2016 Criteria for moisture-control design analysis in buildings. Atlanta, GA: American Society of Heating Refrigerating and Air Conditioning Engineers Inc.

ASTM E779-10. (2010). Standard test method for determining air leakage rate by fan pressurization. West Conshohocken, PA: ASTM International.

Beaulieu, P., Cornick, S. M., Dalgliesh, W. A., Kumaran, M. K., & Lacasse, M. A. (2001). MEWS methodology for developing moisture management strategies: Application to stucco-clad wood frame walls in North America. (No. NRCC-45213). Ottawa, Canada: National Research Council Canada.

Bedford, T., & Cooke, R. (2001). Probabilistic risk analysis: Foundations and methods. Cambridge, UK: Cambridge University Press.

Belleudy, C., Kayello, A., Woloszyn, M., & Ge, H. (2015). Experimental and numerical investigations of the effects of air leakage on temperature and moisture fields in porous insulation. Building and Environment, 94 (2), 457-466.

Bomberg, M., Pazera, M., & Plagge, R. (2005). Analysis of selected water absorption coefficient measurements. Journal of Building Physics, 28(3), 227-243.

Burch, D. M., & Chi, J. (1997). Moisture-A PC program for predicting heat and moisture transfer in building. Gaithersburg, MD: National Institute of Standards and Technology.

Campolongo, F., & Rossi, A. (2002). Sensitivity analysis and the delta hedging problem. The 6th International Conference on Probabilistic Safety Assessment and Management. San Juan, Puerto Rico, USA.

Carmeliet, J., Hens, H., Roels, S., Adan, O., Brocken, H., Cerny, R., &Pel, L. (2004). Determination of the liquid water diffusivity from the transient moisture transfer experiments. Journal of Building Physics, 27(4), 277-305.

Carmeliet, J., & Roels, S. (2002). Determination of the moisture capacity of porous building materials. Journal of Building Physics, 25(3), 209-237.

CGSB. (1996). CAN/CGSB-149.15-96. Determination of the overall envelope airtightness of buildings by the fan pressurization method using the building's air-handling system. Canada: Canadian General Standards Board.

Chakhunashvili, A., Johansson, P. M., & Bergman, B. L. S. (2004). Variation mode and effect analysis. 2004 Reliability and Maintainability Annual Symposium-RAMS. Los Angeles, CA, USA.

Chan, K. (2016). Design revealed: 18 storey UBC residence to be world's tallest wooden building. Retrieved from http://www.vancitybuzz.com/2016/02/ubc-tall-wood-building-brock-residence/

Chen, W., Francois R, C., Novak, J., Litvak, A., Richieri, F., Solche, O., Pan, W., & Emmerich, S. (2012). Building air leakage database in energy conservation policies: analysis of selected initiatives in 4 European countries and the USA. (Technical Note AIVC 66). Berkeley, CA: TightVent Europe.

Cornick, S., Dalgliesh, W.A. & Maref, W. (2009). Sensitivity of hygrothermal analysis to uncertainty in rain data. Journal of ASTM International, 6(4), 1-17.

Cornick, S. M., Maref, W., & Tariku, F. (2009). Verification and validation: Establishing confidence in hygrothermal tools. (No. IRC-RR-278). Ottawa, Canada: National Research Council of Canada.

Corrado, V. & Mechri, H.E. (2009). Uncertainty and sensitivity analysis for building energy rating. Journal of Building Physics, 33(2), 125-156.

Craven, C., & Garber-Slaght, R. (2014). Exterior insulation envelope retrofits in cold climates: Implications for moisture control. HVAC&R Research, 20(4), 384-394.

Cunningham, M. E., Hann, C. R., & Olsen, A. R. (1980). Uncertainty analysis and thermal stored energy calculations in nuclear fuel rods. Nuclear Technology, 47(3), 457-467.

Defraeye, T., Blocken, B., & Carmeliet, J. (2013). Influence of uncertainty in heat-moisture transport properties on convective drying of porous materials by numerical modelling. Chemical Engineering Research and Design, 91(1), 36-42.

Delgado, J.M.P.Q., Barreira, E., Ramos, N.M.M., & de Freitas, V.P. (2013). Hygrothermal numerical simulation tools applied to building physics. Berlin, Germany: Springer.

DELPHIN. Version 5.8.3. (2015). PC-Program for calculating the coupled heat and moisture transfer in building components. Dresden, Germany: Dresden University of Technology.

Derome, D. (2005). Moisture accumulation in cellulose insulation caused by air leakage in flat wood frame roofs. Journal of Building Physics, 28 (3), 269-287.

Desmarais, G. (2000). Impact of added insulation on the hygrothermal performance of leaky exterior wall assemblies. (Master's Thesis). Concordia University, Montreal, Canada.

De Wit, M.S. (2001). Uncertainty in predictions of thermal comfort in buildings. (Ph.D. Thesis). Delft University of Technology. Delft, Netherlands.

DIN EN ISO 13788. (2012). Hygrothermal performance of building components and building elements – Internal surface temperature to avoid critical surface humidity and interstitial condensation – Calculation methods. Berlin, Germany: German Institute for Standardization.

DIN EN 15026. (2007). Hygrothermal performance of building components and building elements. Assessment of moisture transfer by numerical simulation. Berlin, Germany: German Institute for Standardization.

Durner, W. (1994). Hydraulic conductivity estimation for soils with heterogeneous pore structure. Water Resources Research, 30(2), 211-223.

Emmerich, S., & Persily, A. (2014). Analysis of U.S. commercial building envelope air leakage database to support sustainable building design. International Journal of Ventilation, 12(4), 331-344.

EPA. (2013). Moisture control guidance for building design, construction and maintenance. USA: United States Environmental Protection Agency.

Finch, G., Wang, J., & Ricketts, D. (2013). Guide for designing energy-efficient building enclosures. British Columbia, Canada: FPInnovations.

Fox, M. J. (2014). Hygrothermal performance of highly insulated wood frame walls with air leakage: field measurements and simulations. (Master's Thesis). Ryerson University, Toronto, Canada.

FPInnovation, NEWBuilds (2014). Application of analysis tools from NEWBuilds research network in design of a high-rise wood building. Vancouver, Canada: FPInnovation.

Gagnon, S., & Pirvu, C. (2011). CLT handbook: Cross-Laminated Timber. (Special Publication SP528-E. Canadian Ed.). Quebec, Canada: FPInnovation.

Gibson, S. (2010). Can exterior foam insulation cause mold and moisture problem. Retrieved from http://www.greenbuildingadvisor.com/blogs/dept/qa-spotlight/can-exterior-foam-insulation-cause-mold-and-moisture-problems

Glass, S. V., Kochkin, V., Drumheller, S. C., & Barta, L. (2015). Moisture performance of energy-efficient and conventional wood-frame wall assemblies in a mixed-humid climate. Buildings, 5, 759-782.

Goto, Y., Ghazi Wakili, K., Ostermeyer, Y., Frank, T., Ando, N., & Wallbaum, H. (2011). Preliminary investigation of a vapour- open envelope tailored for subtropical climate. Building and Environment, 46(3), 719-728.

Grunewald, J., Haupl, P., & Bomberg, M. (2003). Towards an engineering model of material characteristics for input to HAM transport simulations-Part1: An approach. Journal of Building Physics, 26(4), 343-366.

Gummerson, R.J., Hall, C., Hoff, W.D., Hawkes, R., Holland, G.N. & Moore, W.S. (1979). Unsaturated water flow within porous materials observed by NMR imaging. Nature, 281, 56-57.

Hagentoft, C. E. (2002a). HAMSTAD - Final report: Methodology of HAM modelling. (No. Report R-02:8). Gothenburg, Denmark: Chalmers University of Technology.

Hagentoft, C. E. (2002b). HAMSTAD-WP2 modelling, version 4. (No. Report R-02:9). Gothenburg, Denmark: Chalmers University of Technology.

Hagentoft, C.E., & Harderup, E. (1996). Moisture conditions in a north facing wall with cellulose loose fill insulation: constructions with and without vapor retarder and air leakage. Journal of Building Physics, 19 (3), 228-243.

Hagentoft, C.E., Kalagasidis, A.S., Adl-Zarrabi, B., Roels, S., Carmeliet, J., Hens, H., Grunewald, J., Funk, M., Becker, R., Shamir, D., Adan, O., Brocken, H., Kumaran, K. & Djebbar, R. (2004). Assessment method of numerical prediction models for combined heat, air and moisture transfer in building components: Benchmarks for one-dimensional cases. Journal of Thermal Envelope and Building Science, 27(4), 327-352.

Haglund, M. (2011). Moisture content penetration in wood elements under varying boundary conditions. Wood Science and Technology, 41(6), 477-490.

Hakansson, H. (1998). Retarded sorption in wood. (Ph.D. Thesis). Department of Building Science, Lund Institute of Technology, Lund, Sweden.

Hameury, S. (2005). Moisture buffering capacity of heavy timber structures directly exposed to an indoor climate: A numerical study. Building and Environment, 40(10), 1400-1412.

Harmby, D. M. (1995). A comparison of sensitivity analysis techniques. Health Physics, 68(2), 195-204.

Haupl, P., & Fechner, H. (2003). Hygric material properties of porous building materials. Journal of Thermal Envelope and Building Science, 26(3), 259-284.

Helton, J. C. (1993). Uncertainty and sensitivity analysis techniques for use in performance assessment for radioactive waste disposal. Reliability Engineering and System Safety, 42(2-3), 327-367.

Helton, J. C., & Davis, F. J. (2002). Illustration of sampling-based methods for uncertainty and sensitivity analysis. Risk Analysis, 22(3), 591-622.

Hens, H. (1996). Final report of IEA Annex 24- Task 1: Modelling. Leuven, Belgium: KU Leuven University.

Holm, A. H., & Kunzel, H. M. (2002). Practical application of an uncertainty approach for hygrothermal building simulations- drying of an AAC flat roof. Building and Environment, 37(8–9), 883-889.

Holm, A. H., & Kunzel, H. M. (2001). Uncertainty approaches for hygrothermal building simulations-drying of AAC in hot and humid climates. The 7th International IBPS Conference. Rio de Janeiro, Brazil.

Iman, R. L., & Helton, J. C. (1991). The repeatability of uncertainty and sensitivity analysis for complex probabilistic risk assessment. Risk Analysis, 11(4), 591-606.

Irving, A. D. (1992). Stochastic sensitivity analysis. Applied Mathematical Modelling, 16(1), 3-15.

J.Lomas, K., & Eppel, H. (1992). Sensitivity analysis techniques for building thermal simulation programs. Energy and Buildings, 19(1), 21-44.

Janssen, H. (2013). Monte-Carlo based uncertainty analysis: sampling efficiency and sampling convergence. Reliability Engineering and System Safety, 109, 123-132.

Janssen, H., Blocken, B., & Carmeliet, J. (2007). Conservative modelling of moisture and heat transfer in building components under atmospheric excitation. International Journal of Heat and Mass Transfer, 50(5-6), 1128-1140.

Janssen, H., Roels, S., Gelder, L. V., & Das, P. (2013). Final report of IEA Annex 55- Subtask 2: Probabilistic tools. Gothenburg, Sweden: International Energy Agency.

Janssens, A., & Hens, H. (2003). Interstitial condensation due to air leakage: A sensitivity analysis. Journal of Building Physics, 27(1), 15-29.

Janz, M. (1997). Methods of measuring the moisture diffusivity at high moisture levels. (Report TVBM-3076). Lund, Sweden: Division of Building Materials, LTH of Lund University.

Kalagasidis, A. S. (2004). HAM-tools: An integrated simulation tool for heat, air and moisture transfer analysis in building physics. (Ph.D. Thesis). Chalmers University of Technology, Gothenburg, Sweden.

Kalagasidis, A. S., & Rode, C. (2013). Final report of IEA Annex 55- Subtask 3: Framework for probabilistic assessment of performance of retrofitted building envelopes. Gothenburg, Sweden: International Energy Agency.

Kalamees, T., & Kurnitski, J. (2010). Moisture convection performance of external walls and roofs. Journal of Building Physics, 33 (3), 225-247.

Kalamees, T., &Vinha, J. (2003). Hygrothermal calculations and laboratory tests on timber-framed structures. Building and Environment, 38(5), 689-697.

Kaplan, S., & Garrick, J. (1981). On the quantitative definition of risk. Risk Analysis, 1(1), 11-27.

Karacabeyli, E., & Douglas, B. (2013). Cross-Laminated Timber (CLT) handbook. (Special Publication SP529-E. US Ed.). Quebec, Canada: FPInnovation and Binational Softwood Lumber Council.

Karagiozis, A. (2002). A North American research approach to moisture design by modelling. The 6th Symposium on Building Physics in Nordic Countries. Trondheim, Norway.

Karagiozis, A.N., & Kunzel, H.M. (2009). The effect of air cavity convection on the wetting and drying behavior of wood-frame walls using a multi-physics approach. Journal of ASTM International, 6 (10), 1-15.

Koda, M., Dogru, A. H., & Seinfeld, J. H. (1979). Sensitivity analysis of partial differential equations with application to reaction and diffusion process. Journal of Computational Physics, 30(2), 259-282.

Krus, M., & Holm, A. (1999). Simple methods to approximate the liquid transport coefficients describing the absorption and drying process. Proceedings of the 5th Symposium on Building Physics in the Nordic Countries, Gothenburg. Sweden, August 24-26, 1999, S. 241-248.

Kumaran, M. K. (2006). A thermal and moisture property database for common building and insulation materials. ASHRAE Transactions, 112(2), 1-13.

Kumaran, K., Lackey, J., Normandin, N., van Reenen, D., &Tariku, F. (2002) Summary report from task 3 of MEWS project at the institute for research in construction – hygrothermal properties of several building materials. (NRCC-45369). Ottawa, Canada: National Research Council Canada.

Kumaran, M.K. (1999). Moisture diffusivity of building materials from water absorption measurements. Journal of Building Physics, 22(4), 349-355.

Kunzel, H. M. (1995). Simultaneous heat and moisture transport in building components (Ph.D. Thesis). Fraunhofer Institute of Building Physics. Stuttgart, Germany.

Kunzel, H. M. (1998). The smart vapor retarder: An innovation inspired by computer simulation. ASHRAE Transactions, 104(2), 903-907.

Kunzel, H.M. (2012). Modelling air leakage in hygrothermal envelope simulation. Building Enclosure Science & Technology (BEST3) Conference. Atlanta, USA.

Kunzel, H.M., & Zirkelbach, D. (2008). Influence of rain water leakage on the hygrothermal performance of exterior insulation systems. The 8th Symposium on Building Physics in the Nordic Countries. Copenhagen, Denmark.

Kunzel, H.M., & Zirkelbach, D. (2012). Advances in hygrothermal building component simulation: modelling moisture sources likely to occur due to rainwater leakage. Journal of Building Performance Simulation, 6(5), 346-353.

Langmans, J., Klein, R., & Roels, S. (2012). Hygrothermal risks of using exterior air barrier systems for highly insulated light weight walls: a laboratory investigation. Building and Environment, 56, 192-202.

Lee, S. H., & Chen, W. (2009). A comparative study of uncertainty propagation methods for black-box-type problems. Structural and Multidisciplinary Optimization, 37(3), 239-253.

Lepage, R. T. M. (2012). Moisture response of wall assemblies of cross laminated timber construction in cold Canadian climates. (Master's Thesis). University of Waterloo, Ontario, Canada.

Li, Q., Rao, J., & Fazio, P. (2009). Development of HAM tool for building envelope analysis. Building and Environment, 44(5), 1065-1073.

Li, Q. (2008). Development of a hygrothermal simulation tool (HAM-BE) for building envelope study. (Ph.D. Thesis). Concordia University, Montreal, Canada.

Macdonald, I. A. (2002). Quantifying the effects of uncertainty in building simulation. (Ph.D. Thesis). University of Strathclyde, Glasgow, UK.

Maref, W., Armstrong, M., Rousseau, M., & Lei, W. (2010). A field monitoring investigation of the effect of adding different exterior thermal insulation materials on the hygrothermal response of wood-frame walls in a cold climate. BEST2 Conference (Building Enclosure Science & Technology). Portland, USA.

Maref, W., Manning, M., Lacasse, M. A., Kumaran, M. K., Cornick, S. M., & Swinton, M. C. (2007). Laboratory demonstration of solar driven inward vapour diffusion in a wall assembly. The 11th Canadian Conference on Building Science and Technology. Alberta, Canada.

Marino, S., Hogue, I. B., Ray, C. J., & Kirschner, D. E. (2008). A methodology for performing global uncertainty and sensitivity analysis systems biology. Journal of Theoretical Biology, 254(1), 178-196.

McClung, R., Ge, H., Straube, J., & Wang, J. (2014). Hygrothermal performance of cross-laminated timber wall assemblies with built-in moisture: Field measurements and simulations. Building and Environment, 71, 95-110.

M.M.Ramos, N., & Grunewald, J. (2015). Final report of IEA Annex 55- Subtask1: Stochastic data. Gothenburg, Sweden: International Energy Agency.

Moon, H.J. (2005). Assessing mold risks in buildings under uncertainty. (Ph.D. Thesis). Georgia Institute of Technology. Atlanta, USA.

Morris, M. D. (1991). Factorial sampling plans for preliminary computational experiments. Technometrics, 33(2), 161-174.

Mukhopadhyaya, P., Kumaran, M.K., Lackey, J., Normandin, N, van Reenen, D, &Tariku, F., (2007). Hygrothermal properties of exterior claddings, sheathing boards, membranes and insulation materials for building envelope design. (NRCC-50287). Ottawa, Canada: National Research Council of Canada.

Mundt-Petersen, S. O., & Harderup, L. E. (2013). Validation of a one-dimensional transient heat and moisture calculation tool under real condition. Thermal Performance of the Exterior Envelopes of Whole Buildings XII. Florida, USA.

Nielsen, A. (2002). Use of FMEA-failure modes effects analysis on moisture problems in buildings. Building Physics 2002-6th Nordic Symposium. Trondheim, Norway.

Nielsen, A. (1972). Gamma-Ray attenuation used for measuring the moisture content and homogeneity of porous concrete. Building Science, 7(4), 257-263.

National Research Council (NRC). (2012). Characterization of hygrothermal properties of CLT. (Report to FPInnovation). Ottawa, Canada: National Research Council Canada.

Ochs, F., & Muller-Steinhagen, H. (2005). Temperature and moisture dependence of the thermal conductivity of insulation materials. Izmir, Cesme: NATO Advanced Study Institute on Thermal Energy Storage for Sustainable Energy Consumption (TESSEC).

Ojanen, T., & Kumaran, M.K. (1996). Effect of exfiltration on the hygrothermal behaviour of residential wall assembly. Journal of Building Physics, 19(3), 215-227.

Ojanen, T., Viitanen, H., Peuhkuri, R., Lahdesmaki, K., Vinha, J., & Salminen, K. (2010). Mold growth modeling of building structures using sensitivity classes of materials. Thermal Performance of the Exterior Envelopes of Whole Buildings XI International Conference. Clearwater Beach, Florida, USA.

Ott, S., Tietze, A., & Winter, S. (2015). Wind driven rain and moisture safety of tall timber houses – evaluation of simulation methods. Wood Material Science & Engineering, 10(3), 300-311.

Pallin, S. (2013). Risk assessment of hygrothermal performance-building envelope retrofit. (Ph.D. Thesis). Chalmers University of Technology, Gothenburg, Sweden.

Pallin, S., Hun, D., & Boudreaux, P. (2016). Simulating air leakage in walls and roofs using indoor and outdoor boundary conditions. Thermal Performance of the Exterior Envelopes of Whole Buildings XIII International Conference, Clearwater Beach, Florida, USA.

Pallin, S., Johansson, P., & Shahriari, M. (2011). Development of a risk assessment procedure applied on building physics. Part two-an applicability study. The 12th International Conference on Durability of Building Materials and Components. Porto, Portugal.

Parsons, G., & Lieburn, B. (2013). Comparative energy and wall performance of twelve residential houses constructed in cold climate. Thermal Performance of the Exterior Envelopes of Whole Buildings XII International Conference. Florida, USA.

Pel, L. (1995). Moisture transport in building materials. (Ph.D. Thesis). Technical University of Eindhoven, Eindhoven, Netherlands.

Peuhkuri, R. (2003). Moisture dynamics in building envelopes. (Ph.D. Thesis). Department of Civil Engineering, Technology University of Denmark, Denmark.

Pietrzyk, K., & Hagentoft, C. (2008). Reliability analysis in building physics design. Building and Environment, 43(4), 558-568.

Rode, C. (1990). Combined heat and moisture transfer in building constructions. (Ph.D. Thesis). Technical University of Denmark, Copenhagen, Denmark.

Roels, S., Carmeliet, J., Hens, H., Adan, O., Brocken, H., Cerny, R., Pavlik, Z., Hall, C., Kumaran, K., Pel, L., & Plagge, R. (2004) Inter-laboratory comparison of hygric properties of porous building materials. Journal of Thermal Envelope and Building Science, 27 (4), 207-325.

Rousseau, M. (1999). An overview of the survey of building envelope failures in the coastal climate of British Columbia, performed by Morrisson- Hershfield limited for CMHC (1996). Journal of Thermal Envelope and Building Science, 22(4), 364-367.

Saber, H.H., & Maref, W. (2015). Risk of condensation and mold growth in wood-frame wall systems with different exterior insulations. Building Enclosure Science & Technology Conference (BEST4). Kansas City, Missouri, USA.

Saber, H.H., Maref, W., Elmahdy, A.H., Swinton, M.C., & Glazer, R. (2011). 3D heat and air transport model for predicting the thermal resistance of insulated wall assemblies. Journal of Building Performance Simulation, 5(2), 75-91.

Salonvaara, M. (2004). Development of heat, air, moisture and pollutant transport model, BEESL/EQS quality assurance and project plan for CHAMPS development. Syracuse, NY: Syracuse University.

Salonvaara, M., Karagiozis, A., & Holm, A. (2001). Stochastic building envelope modelling-the influence of material properties. Proceedings for Performance of Exterior Envelope of Whole Building VIII: Integration of Building Envelope. Clearwater Beach, Florida.

Saltelli, A., Chan, K., & Scott, E. M. (2000). Sensitivity analysis: Gauging the worth of scientific models. Chichester, UK: John Wiley & Sons.

Saltelli, A., Tarantola, S., Campolongo, F., & Ratto, M. (2004). Sensitivity analysis in practice: A guide to assessing scientific models. Chichester, UK: John Wiley & Sons.

Scheffler, G.A. (2008). Validation of hygrothermal material modelling under consideration of hysteresis of moisture storage (Ph.D. Thesis). Dresden University of Technology, Dresden, Germany.

Shahriari, M. (2011). Loss prevention & safety-A Practical risk management handbook. Gothenburg, Sweden: Chalmers University of Technology.

Shdid, A.C., & Younes, C. (2015). Validating a new model for rapid multi-dimensional combined heat and air infiltration building energy simulation. Energy and Buildings, 87, 185-198.

Straube, J. (2002). Moisture in Building. ASHRAE Journal, 44(1), 15-19.

Simpson, Y. (2010). Field evaluation of ventilation wetting and drying of rain-screen walls in coastal British Columbia. (Master's Thesis). Concordia University, Montreal, Canada.

Smegal, J., Lstiburek, J., Straube, J., & Grin, A. (2013). Moisture-related durability of walls with exterior insulation in the Pacific Northwest. Thermal Performance of the Exterior Envelopes of Whole Buildings XIII International Conference. Clearwater Beach, Florida, USA.

Svoboda, A. (2007). The effect of leakages in roofs with ventilated air layers - a CFD Approach. Proceedings of Building Simulation. Beijing, China.

Tariku, F., & Simpson, Y. (2014). Temperature and humidity distributions in a mid-rise residential building suite. The 14th Canadian Conference on Building Science and Technology. Toronto, Canada.

TenWolde, A., & Rose, W.B. (1996). Moisture control strategies for the building envelope. Journal of Building Physics, 19 (3), 206-214.

Tian, W. (2013). A review of sensitivity analysis methods in building energy analysis. Renewable and Sustainable Energy Reviews, 20, 411-419.

van Genuchten, M. T. (1980). A closed-form equation for predicting the hydraulic conductivity of unsaturated soils. Soil Science Society of America Journal, 44(5), 892-898.

Wadso, L. (1994). Describing non-fickian water-vapour sorption in wood. Journal of Material Science, 29(9), 2367-2372.

Wang, J., Mukhopadhyaya, P., & Morris, P. (2014). Sorption and capillary condensation in wood and moisture content of red pine at high relative humidity. Journal of Building Physics, 37(4), 327-347.

Wikipedia. (2015). Uncertainty quantification. Retrieved from https://en.wikipedia.org/wiki/Uncertainty_quantification#cite_note-10

Wu, Y. (2007). Experimental study of hgrothermal properties of building materials. (Master's Thesis). Concordia University, Montreal, Canada.

WUFI Pro. Version 5.3. (2014). PC-Program for calculating the coupled heat and moisture transfer in building components. Stuttgart, Germany: Fraunhofer Institute for Building Physics.

Younes, C., & Shdid, A.C. (2013). A methodology for 3-D multi-physics CFD simulation of air leakage in building envelopes. Energy and Buildings, 65, 146-158.

Zhao, J. (2012). Development of a novel statistical method and procedure for material characterization and a probabilistic approach to assessing the hygrothermal performance of building enclosure assemblies (Ph.D. Thesis). Syracuse University, Syracuse, USA.

Zhao, J., Plagge, R., Nicolai, A., Grunewald, J., & Zhang, J. S. (2011). Stochastic study of hygrothermal performance of a wall assembly-the influence of material properties and boundary coefficients. HVAC&R Research, 17(4), 591-601.

Zhong, H., Lei, B., & Feng, Y. (2010). The comparison of different moisture storage functions in the porous materials. Mechanic Automation and Control Engineering 2010 International Conference. Wuhan, China. 1529-1532.

Appendices

Appendix 1 Amount of rain leakage deposited at OSB sheathing for Waterloo and Vancouver

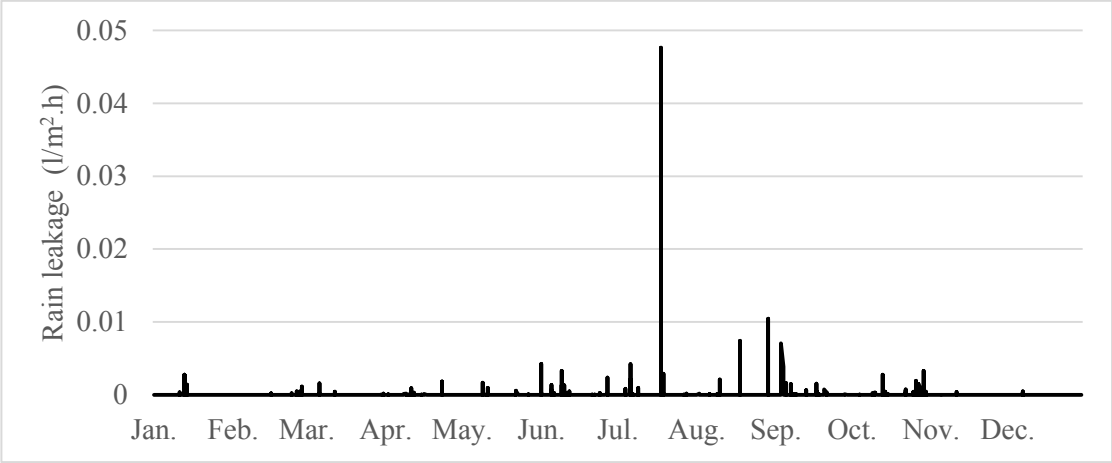

a) Waterloo _ North

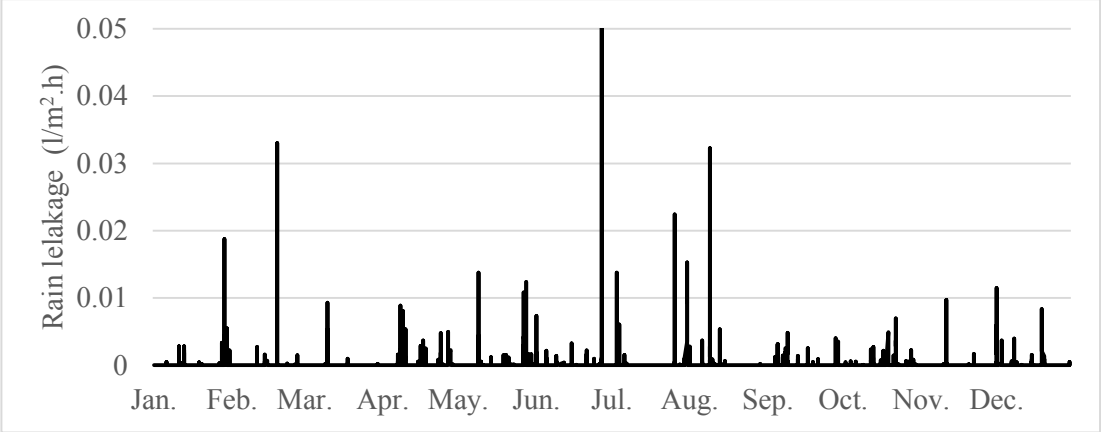

b) Waterloo _ South

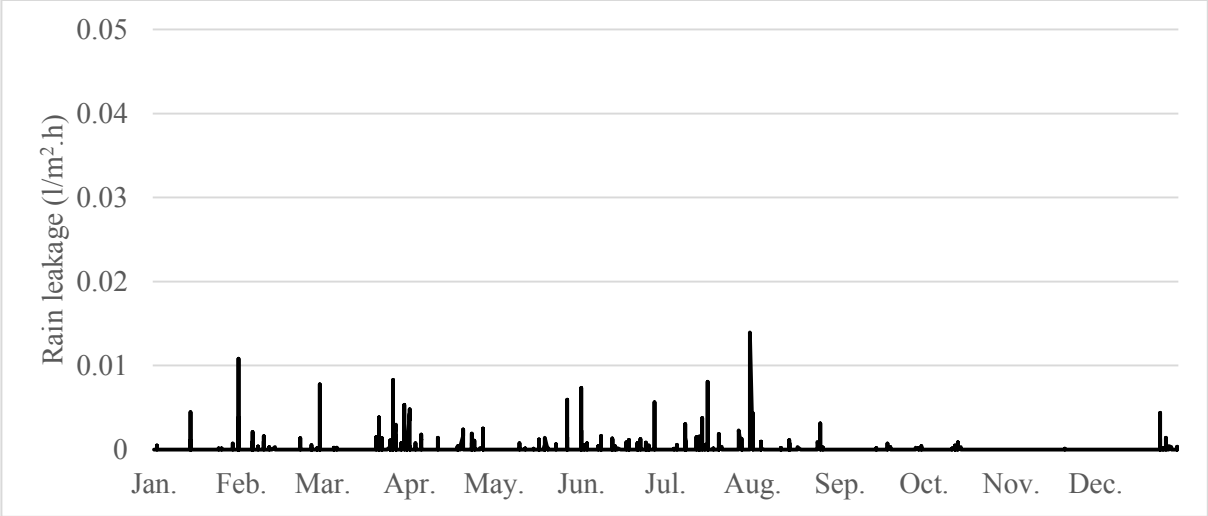

c) Vancouver _ North

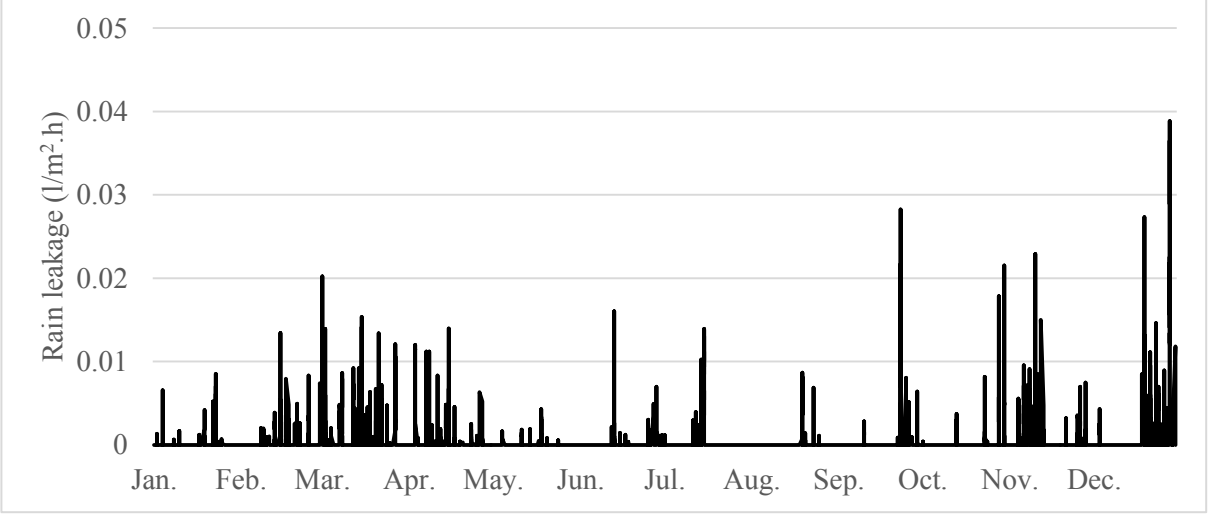

d) Vancouver _ East

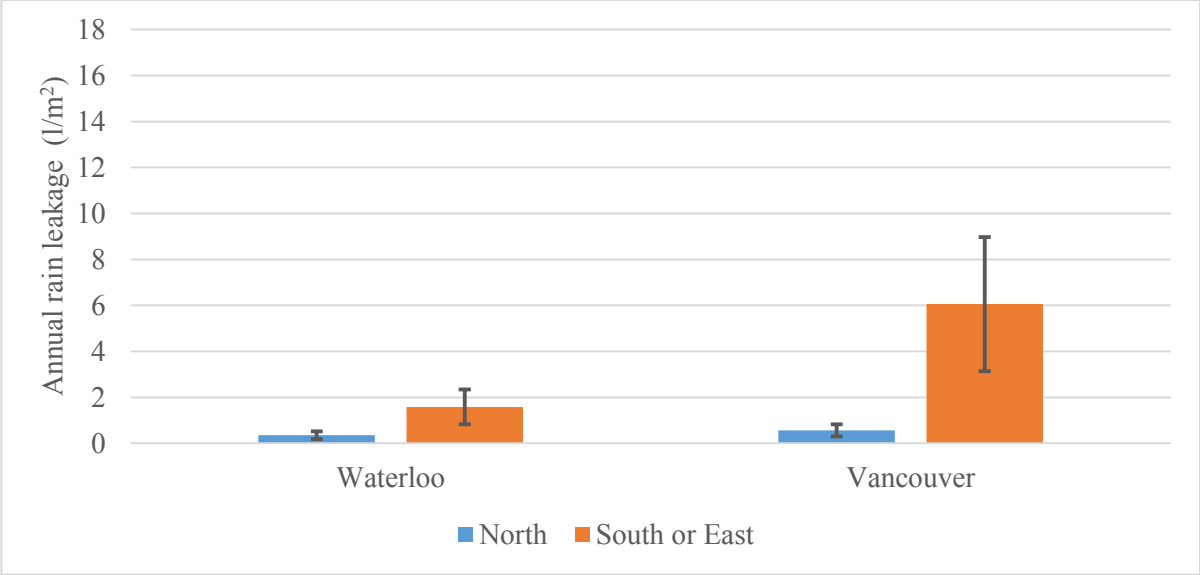

e) Comparison between Waterloo and Vancouver

Appendix 2 Comparison of indoor RH, temperature and moisture excess between low and high internal moisture load

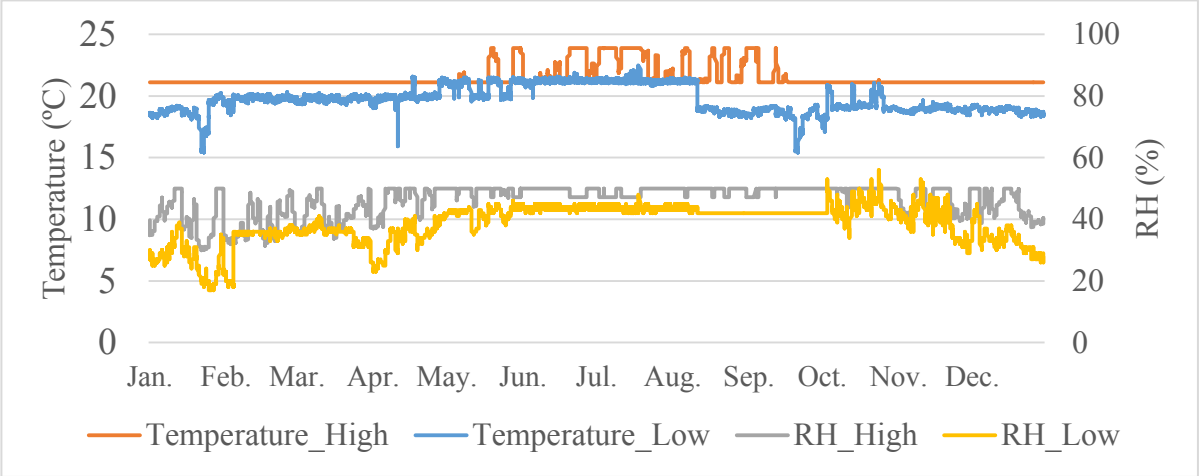

a) Indoor temperature and RH _ Waterloo

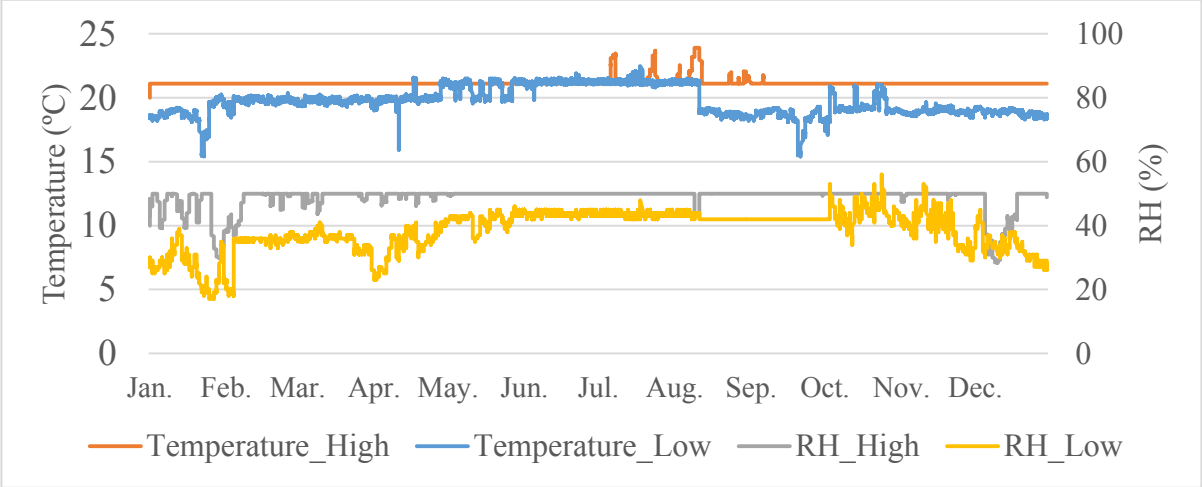

b) Indoor temperature and RH _ Vancouver

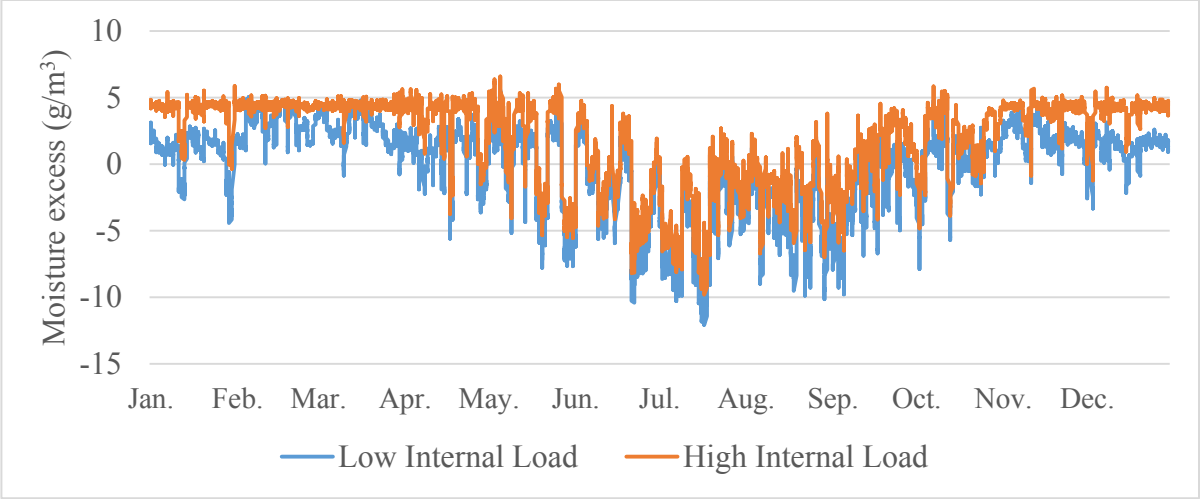

c) Moisture excess _ Waterloo

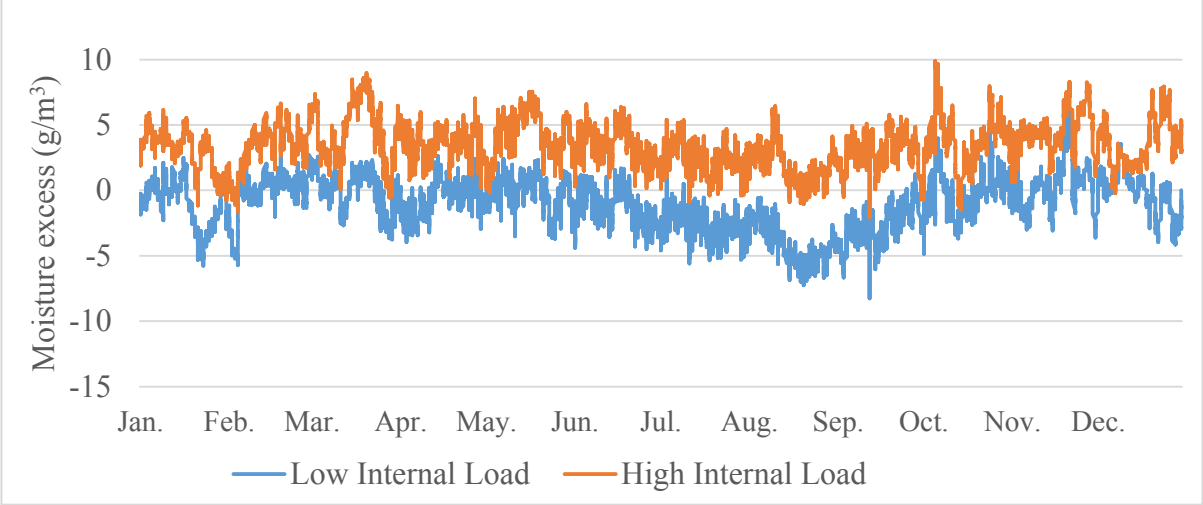

d) Moisture excess _ Vancouver

Appendix 3 Condensation rate calculated at the interior surface of OSB of the highly insulated walls

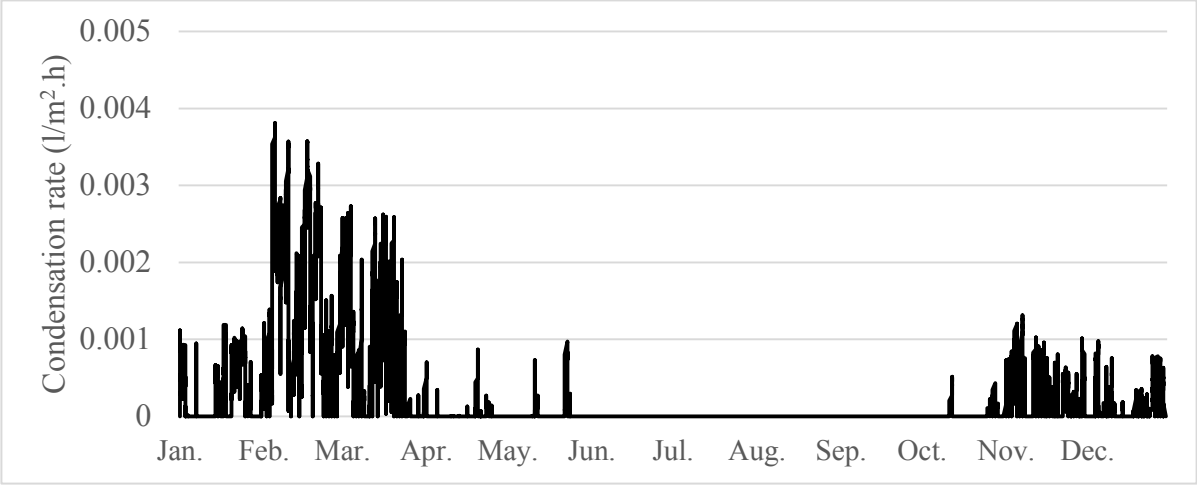

a) Baseline wall _ low internal load

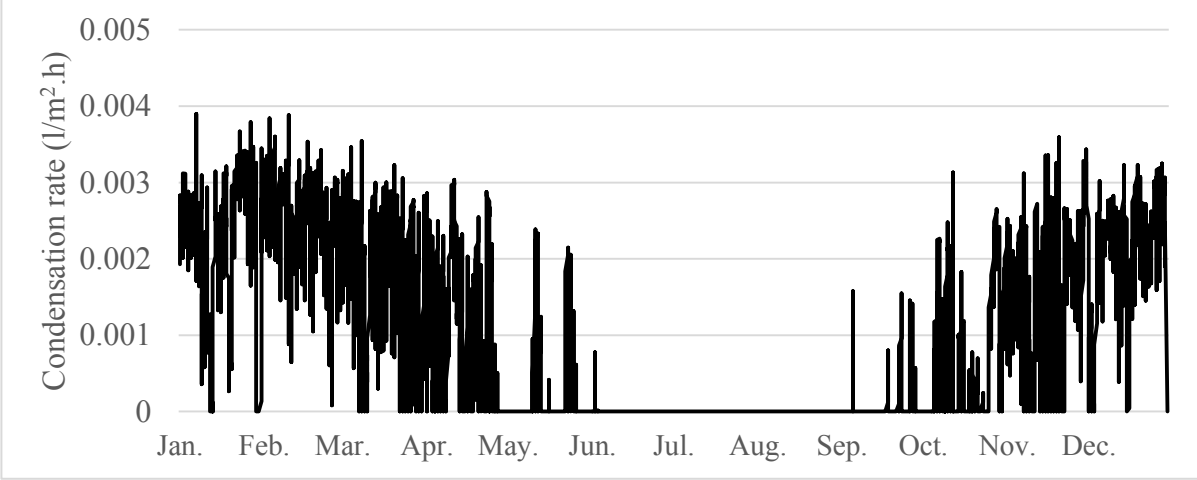

b) Baseline wall _ high internal load

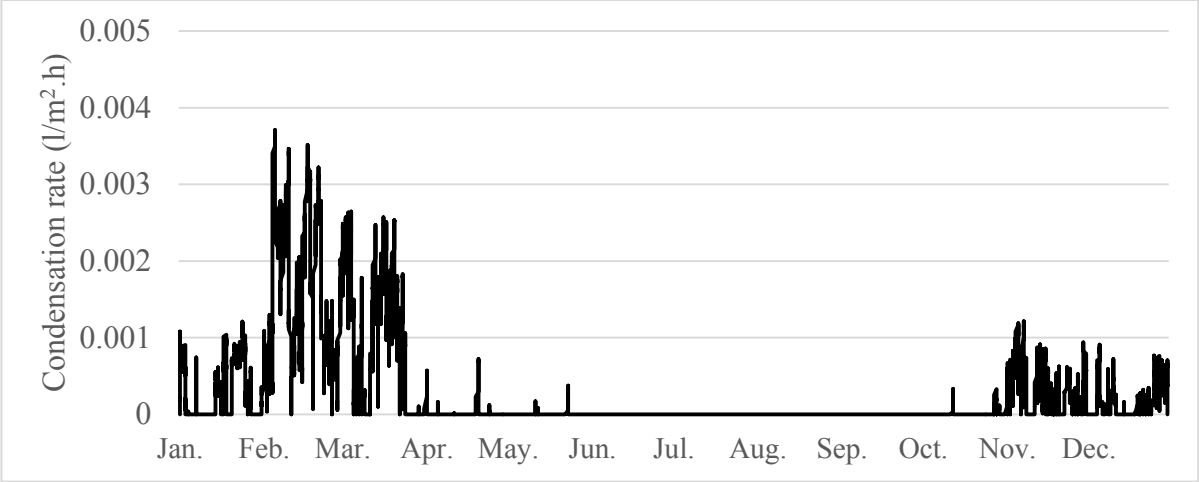

c) I-joist wall _ low internal load

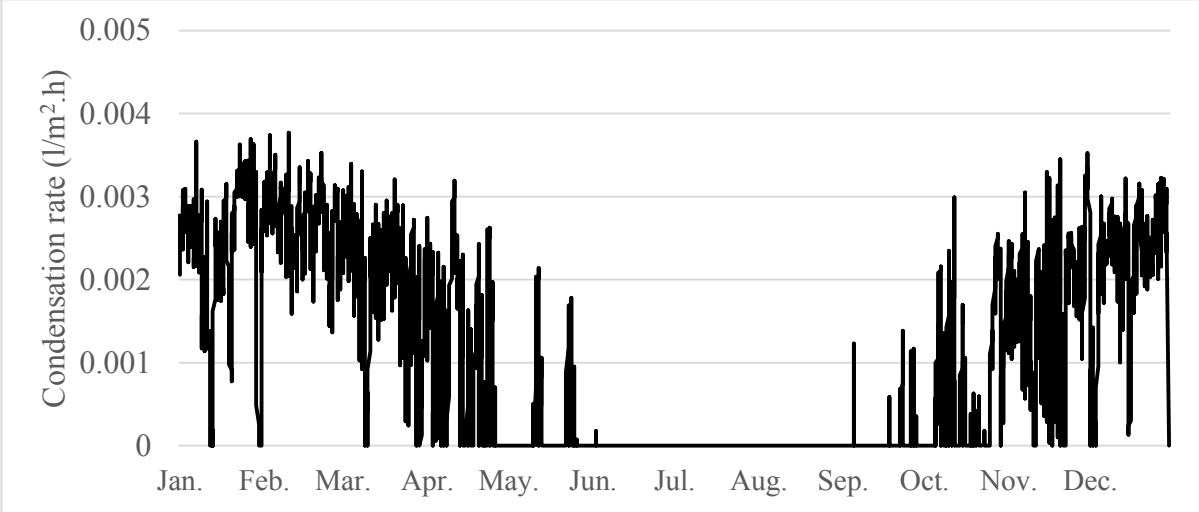

d) I-joist wall _ high internal load

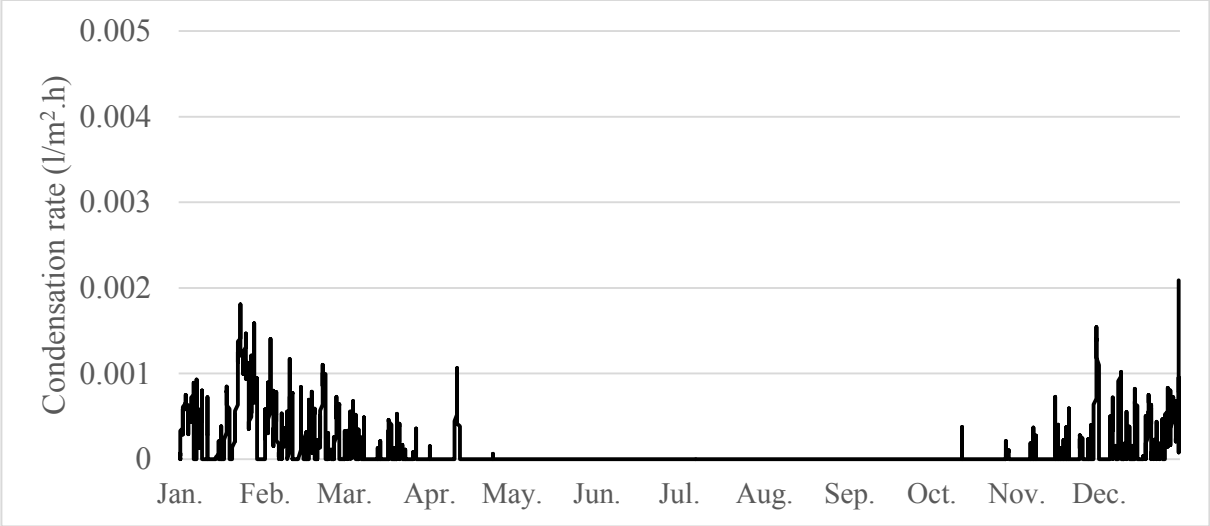

e) Polyisocyanurate wall _ high internal load

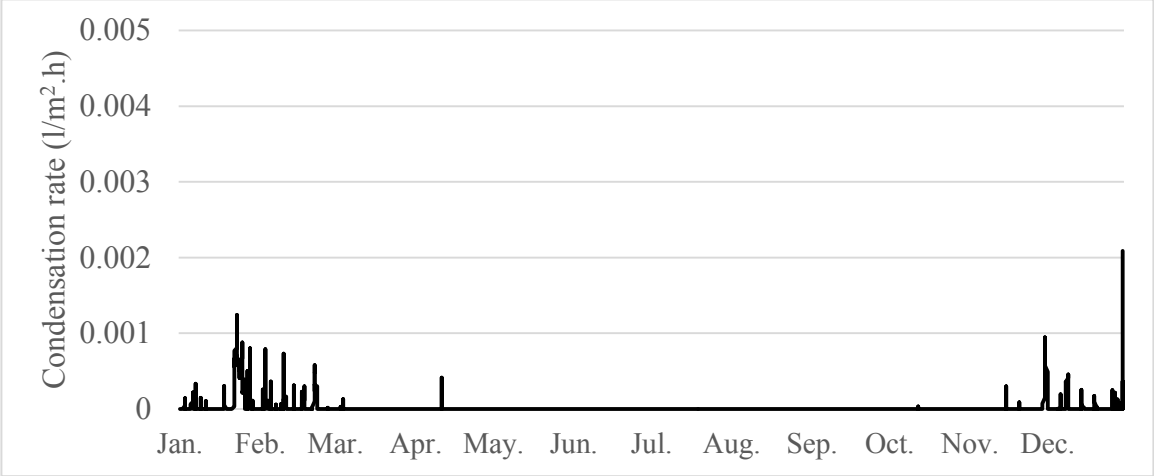

f) Mineral wool wall _ high internal load

Waterloo

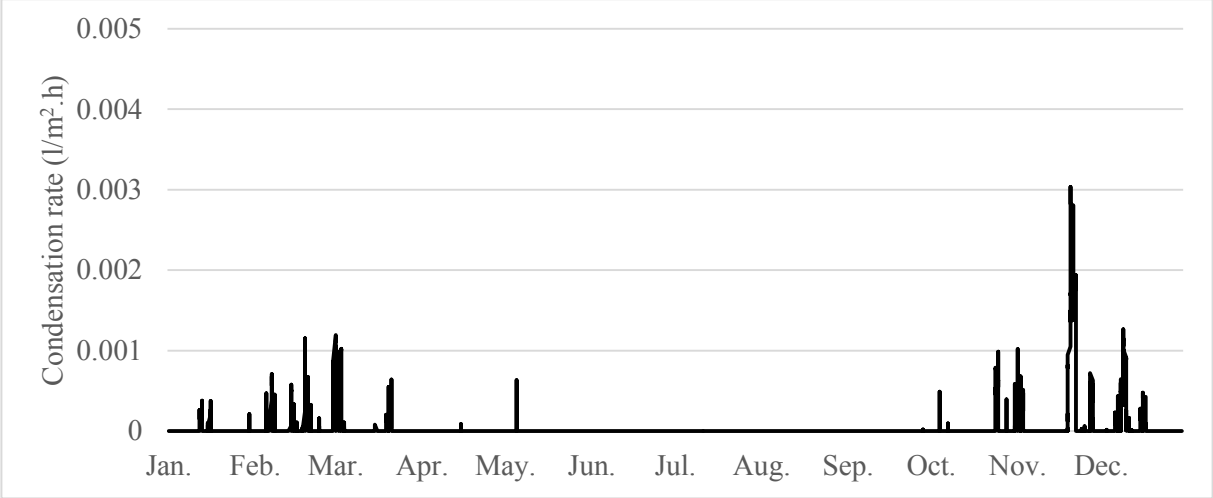

a) Baseline wall _ low internal load

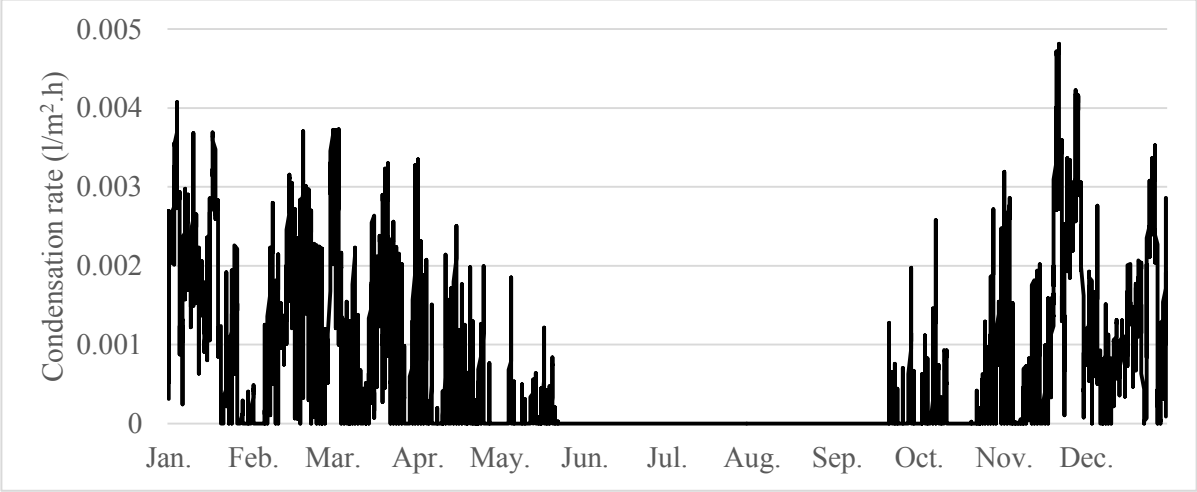

b) Baseline wall _ high internal load

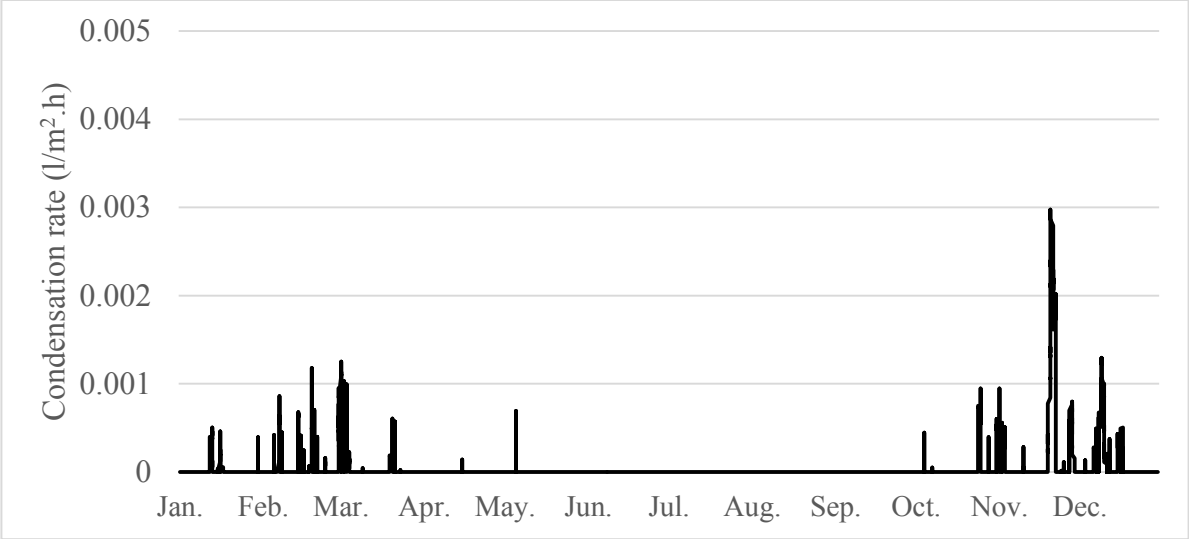

c) I-joist wall _ low internal load

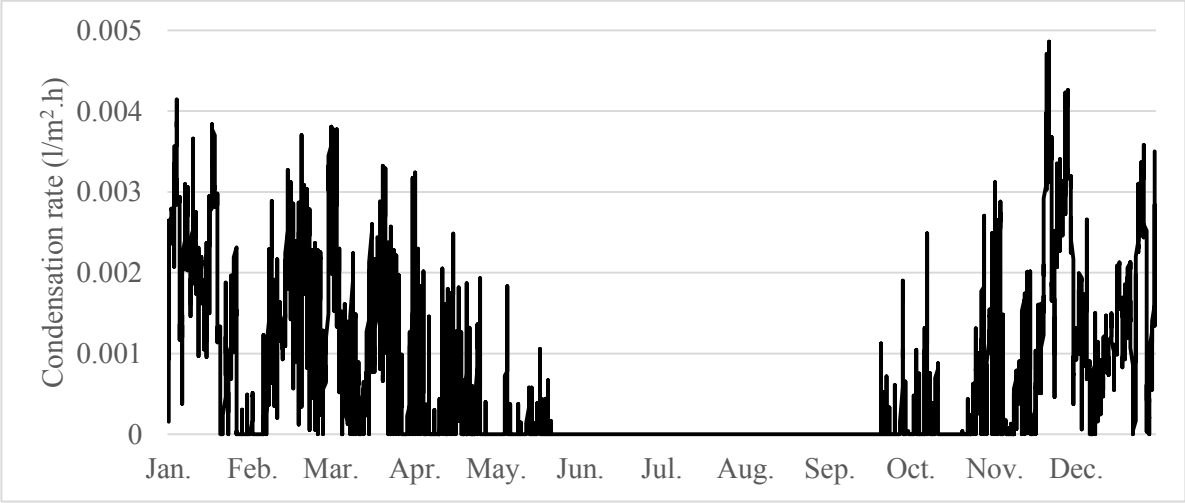

d) I-joist wall _ high internal load

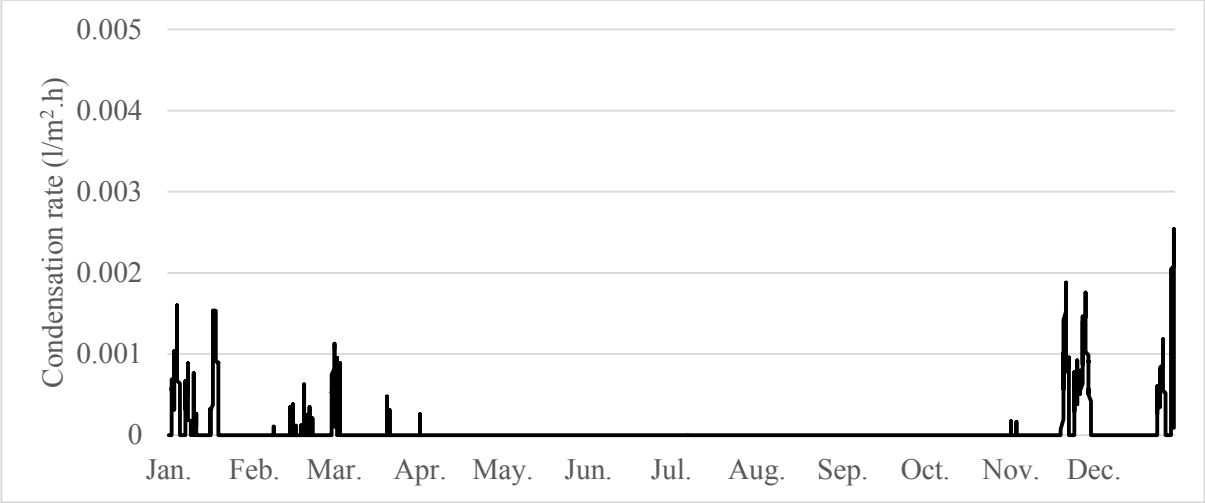

e) Polyisocyanurate wall _ high internal load

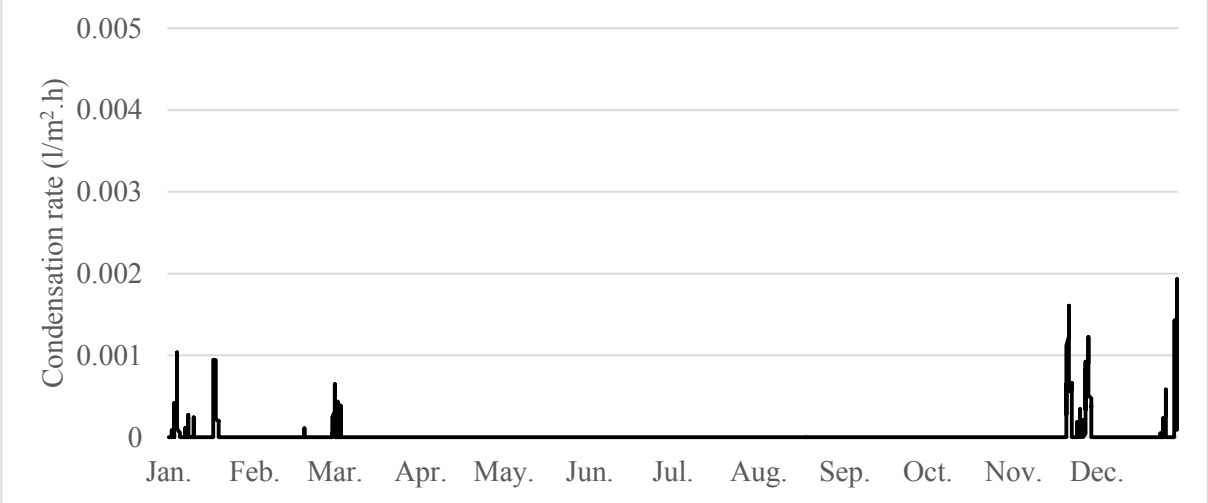

f) Mineral wool wall _ high internal load

Vancouver

Appendix 4 Annual condensation amount at interior surfaced of OSB caused by air leakage

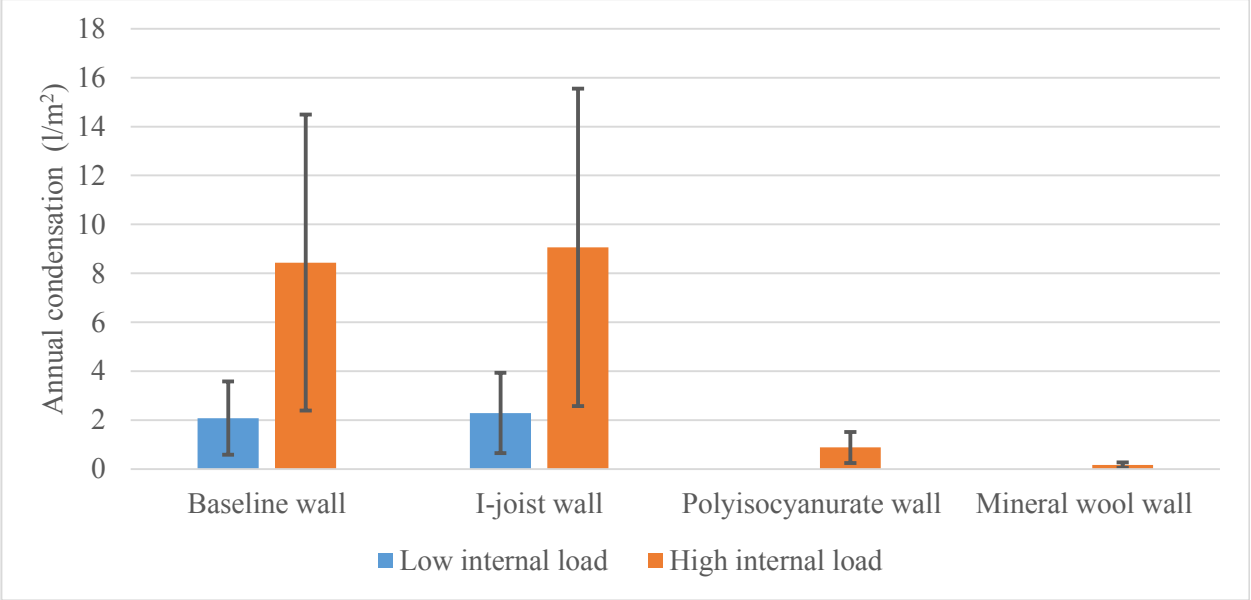

Waterloo

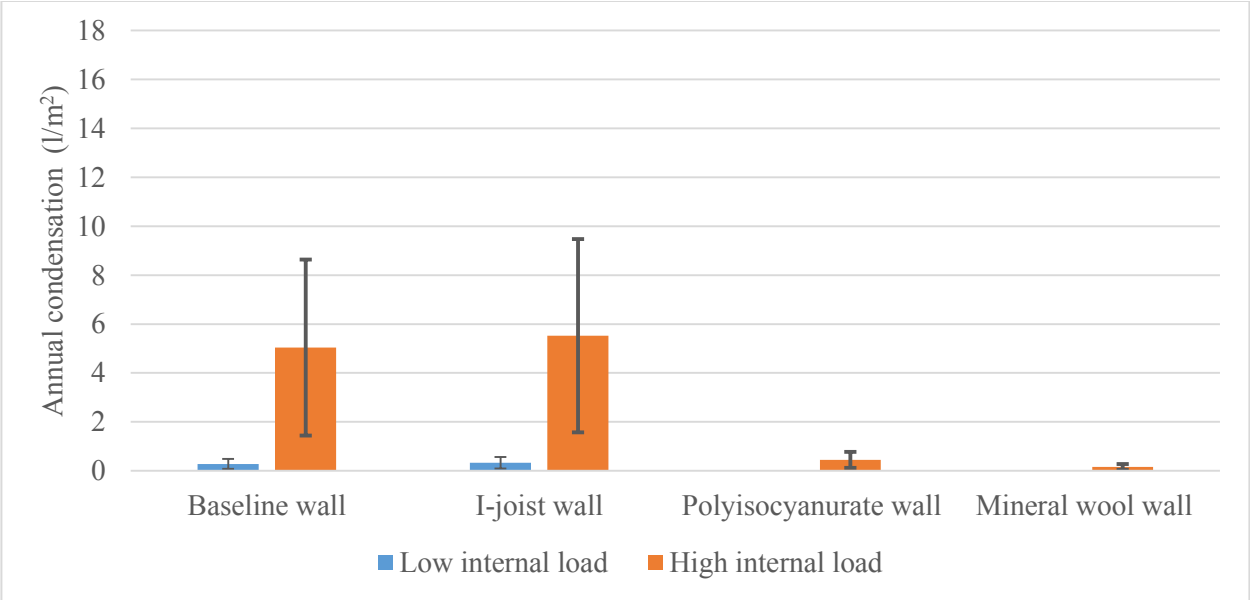

Vancouver